The Dissertation Committee for William Blaine Liechty Certifies that this is the approved version of the following dissertation:

Tunable, responsive nanoscale hydrogels for intracellular delivery of small interfering RNA

Committee:

Nicholas A. Peppas, Supervisor

Hal Alper

Lydia Contreras

Christopher Ellison

Krishnendu Roy

Tunable, responsive nanoscale hydrogels for intracellular delivery of small interfering RNA

by

William Blaine Liechty, B.S.Eng.

Dissertation

Presented to the Faculty of the Graduate School of

The University of Texas at Austin

in Partial Fulfillment

of the Requirements

for the Degree of

Doctor of Philosophy

The University of Texas at Austin

May 2013

Dedication

To Emily and Jackson.

Acknowledgements

I am sincerely grateful for the opportunities that I have enjoyed at the University of Texas at Austin. I must credit my parents for supporting me throughout this journey; my mother and father have been fantastic role models my entire life. My sisters have always kept me humble and I consider myself lucky to be their big brother. My wife, Emily, has been a steadfast beacon of love and patience. I could not ask for a better companion. Thank you. Our son Jackson is my proudest achievement.

I would like to thank my advisor, Dr. Nicholas Peppas, for an immensely rewarding graduate experience. His relentless enthusiasm, encyclopedic knowledge, and vast experience were a constant source of motivation. His ardent and enduring support of his students, young, old, near, and far, was truly an inspiration. I consider myself extremely fortunate to be aligned with such a fantastic leader, scientific mentor, and lifelong advocate. A particularly large thank you is due for indulging the naïve excitement of a young graduate student with a newfound passion for RNA interference.

My early scientific mentors played a pivotal role in my development as a researcher. Special thanks to Dr. Allan Guymon and Dr. Tim White for introducing me to photopolymers. Dr. Nigel Slater was instrumental in helping me realize the simultaneously exciting and frustrating nature of intracellular drug delivery. I am forever grateful to Dr. Rongjun Chen, whose gentle guidance helped set me on the path to becoming an independent researcher.

I was fortunate to benefit from the efforts of several excellent undergraduate researchers. In order of tenure – Rebekah Scheuerle, Amy Bergeron, Grace Fletcher,

Andrea LeBlanc, Ludovic Pao, and Andrew Wong. Their considerable efforts enhanced the quality and scope of this thesis.

It was a great pleasure to work alongside so many wonderful scientists and engineers during my time in the laboratory: Adam Ekenseair, Amey Puranik, Ana Fernandez-Olleros, Brandon Slaughter, Brenda Carillo-Conde, Carolyn Bayer, Cody Schoener, David Kryscio, Diane Forbes, Jenny Knipe, Jonathan Peters, Maggie Phillips, Marty Gran, Mary Caldorera-Moore, Michael Koetting, Stephanie Steichen, and Steve Marek. It was been pleasures to travel with you, learn from you, struggle with you, and grow with you. I will always value our enthusiastic discussions (some academic, some not), and our regular lunches of tacos and chicken nuggettes.

I would like to give special acknowledgement to Dr. Hal Alper for allowing me to work in his laboratory to develop a custom, luciferase-expressing cell line for (future) siRNA studies and Dr. Jeanne Stachowiak for her time and expertise in developing the GUV imaging studies. I would also like to acknowledge the many people that keep the core facilities in top shape, particularly Dwight Romanovicz and Richard Salinas of the Institute for Cellular and Molecular Biology Core. Their help and guidance was crucial to several of the studies described in this thesis.

Lastly, I would like to acknowledge the generous financial support that funded this work: National Science Foundation Graduate Research Fellowship, National Science Foundation Grant 1033746, the William “Tex” Moncrief, Jr. Foundation, and the Pratt Foundation. I would also like to thank the University Coop, George Mitchell, and Michael Granof for sponsoring the Graduate School awards of which I was a grateful recipient.

Tunable, responsive nanoscale hydrogels for intracellular delivery of small interfering RNA

William Blaine Liechty, PhD

The University of Texas at Austin, 2013

Supervisor: Nicholas A. Peppas

Responsive, polybasic nanoscale hydrogels were synthesized using photoemulsion polymerization. The nanoscale hydrogels (nanogels) are approximately 50 nm in diameter and consist of a pH-responsive poly(2-(diethylaminoethyl methacrylate)) core with a poly(ethylene glycol) corona. The nanogels undergo a volume phase transition in response to environmental pH, and possess tunable physicochemical properties based on the copolymer composition. Aqueous solution properties of the nanogels were investigated using dynamic light scattering, pyrene fluorescence spectroscopy, and zeta potential measurements. Nanogel-mediated disruption of biological membranes was investigated with erythrocytes, giant unilammelar vesicles, and live cells to evaluate the potential of these nanogels to act as endosomolytic carriers for intracellular delivery of small interfering RNA. Selective membrane disruption was achieved by increasing nanogel hydrophobicity via copolymerization with tert-butyl methacrylate (TBMA). Nanogels with TBMA possessed an additional advantage of increased cytocompatibility owing to their reduced cationic charge density.

These nanogels are able to efficiently entrap siRNA in the nanogel core and enhance cellular internalization of siRNA in model cell lines. The cell-line dependent mechanism of nanogel internalization and uptake and intracellular distribution of fluorescent nanogel/siRNA complexes was investigated with imaging flow cytometry. Functional activity of delivered siRNA was assessed using gene silencing assays.

Modifications to the polymer chemistry were also explored to enhance the biological activity. A disulfide-containing crosslinker was synthesized, characterized and incorporated into nanogels. This crosslinker enabled the rapid nanogel degradation in response to reductive environments. A functional phenylalanine-derivative monomer (MAPA) was synthesized and characterized to serve as a bio-inspired substitute for TBMA. Nanogels copolymerized with MAPA demonstrate comparable siRNA delivery efficiency to its TMBA analogue.

The ability to exert control over physicochemical properties and biological interactions of these nanogels by tuning polymer composition is a facile strategy to tailor material properties for specific applications. The hydrophobically-modified nanogels possess great potential as delivery vehicles to enhance the cellular internalization and endosomal escape of siRNA cargoes.

Table of Contents

List of Tables

List of Figures

Chapter 1: Introduction

Recent in vivo successes in knockdown of disease targets indicate that siRNA technology is worthy of serious attention from the scientific and medical communities. Although much effort has been directed toward synthetic polymer carriers for siRNA, there remains a paucity of data on the development of oral delivery systems. From a drug delivery standpoint, the oral route of administration is advantageous because it increases patient compliance and comfort over injection, provides a simple, repeatable administration, and large surface area for absorption [1]. Oral delivery of fragile biological molecules, such as proteins, peptides, and nucleic acids is one of the most compelling and difficult problems in drug delivery. Successful development of an oral delivery system for small interfering RNA could revolutionize the treatment of many diseases by providing patients a powerful therapeutic in a convenient and accessible form.

The challenges of advancing this promising therapeutic to the clinical stage are significant and need to be met with innovative solutions. This project presents immense opportunity to develop the next generation of drug delivery systems by enabling the efficient delivery of a potent, highly specific therapeutic via a non-invasive, patient friendly route. Efficient delivery of fragile biotherapeutics, such as peptides, proteins, and nucleic acids has long been considered the "Holy Grail" of drug delivery [2]. As most biotherapeutics are administered via intravenous, intraperitoneal, or local injection, an ingestible drug formulation capable of providing therapeutically-relevant

concentrations in the local environment and/or transport of the drug from the intestinal lumen to the bloodstream would be of significant scientific and medical importance.

This proposal emphasizes a unique and innovative approach to develop new carrier systems for oral delivery of siRNA. In this work, we propose to use a facile photoemulsion polymerization to synthesize polycationic nanoscale hydrogels for oral delivery of small interfering RNA. This synthesis, unlike many current polycationic siRNA delivery agents, does not rely on specialized chemistry or controlled polymerization techniques and is conducted on a relatively short time-scale. Furthermore, the oral delivery of siRNA for disease treatment is largely unexplored. Innovation in this area represents a departure from current thrusts in siRNA delivery, which rely on painful intravenous or impractical intraperitoneal injections. The central aim of this proposal is of great medical significance, as advances in this area could significantly improve the ease and availability of siRNA therapy to patients. The final result of this proposal will be a platform technology for drug delivery; a safe, efficient polymer carrier capable of delivering manifold siRNA cargoes to the epithelial cells in the small intestine. Successful development of this system will pave the way for improved treatment of gastrointestinal diseases where current treatment is sub-optimal, such as Crohn's disease, ulcerative colitis, celiac disease, and gastrointestinal carcinomas.

Current efforts in oral delivery of small interfering RNA [3-5] utilize a two-phase delivery system to navigate the extracellular and intracellular barriers posed by oral administration. Similarly, this ultimate goal of this thesis work is to contribute to the development of a novel, two-phase platform delivery system for oral siRNA. The work described in this thesis is intended to provide a carefully engineered delivery system to

circumvent the *intracellular* barriers of siRNA delivery. The full realization of a platform delivery system will required continued development and ultimately integration of a complementary delivery system carefully engineered to circumvent the *extracellular* barrier to siRNA delivery.

CHAPTER GUIDE

The research described in this body of work is divided into several chapters.

- Chapter 2 offers a detailed background and critical review of synthetic polymers and biomaterials used in drug delivery applications. Particular emphasis is placed on responsive nanomaterials with applications in disease detection or treatment.
- Chapter 3 outlines the objectives of this thesis and the specific aims guiding the work.
- Chapter 4 describes the use of a photoemulsion polymerization to created nanoscale hydrogels, or nanogels, from methacrylate building blocks. In this chapter, the synthesis, purification, and characterization of aqueous solution properties are described.
- Chapter 5 investigates the role of nanogel composition on in vitro physicochemical properties. Nanogel-mediated membrane destabilization is described in three model systems and a relationship between acute toxicity and nanogel composition is described.
- Chapter 6 investigates the mechanism of cellular uptake in target cell lines using imaging flow cytometry
- Chapter 7 leverages the insight from Chapters 4 and 5 to select the most promising formulation for intracellular delivery of siRNA. This chapter also describes the efforts to create a degradable analogue of the most promising formulation. The

siRNA delivery efficiency of these degradable nanogels is assessed with imaging and conventional flow cytometry.

- Chapter 8 details the synthesis and purification of a custom, functional phenylalanine-derived monomer. This monomer was used in responsive nanogels to modulate hydrophobicity. The resulting nanogels were compared to the most promising formulation as determined in Chapter 5.
- Chapter 9 provides overall conclusions and recommendations for future work.

APPENDIX GUIDE

Additional pertinent information is contained in several appendices.

- Appendix A is a guide to nanogel nomenclature
- Appendix B describes relevant theoretical considerations in dynamic light scattering measurements, including a framework for the Cumulants analysis employed in this thesis. Preliminary experiments to optimize sample preparations for dynamic light scattering are also described.
- Appendix C explains the gating strategy, relevant nomenclature, and analysis parameters used in the imaging flow cytometry experiments.
- Appendix D describes the development and classroom implementation of a drug delivery experiment using a facile ionic crosslinking of sodium alginate. This experiment is a core component of an NSF-sponsored high school research program in the laboratory of Prof. Nicholas Peppas and also the Principles of Biomedical Engineering Design Laboratory (BME 102L) course.

REFERENCES

1. Torres-Lugo M and Peppas NA. Biomaterials 2000;21(12):1191-1196.

2. Peppas NA, Bures P, Leobandung W, and Ichikawa H. European Journal of Pharmaceutics and Biopharmaceutics 2000;50(1):27-46.

3. Wilson DS, Dalmasso G, Wang L, Sitaraman SV, Merlin D, and Murthy N. Nature Materials 2010;9(11):923-928.

4. Aouadi M, Tesz GJ, Nicoloro SM, Wang M, Chouinard M, Soto E, Ostroff GR, and Czech MP. Nature 2009;458(7242):1180-1184.

5. Kriegel C and Amiji M. Journal of Controlled Release 2011;150(1):77-86.

Chapter 2: Objectives of Proposed Research

The central goal of this proposal is to synthesize novel polycationic nanomatrices possessing tunable pH-responsive behavior that can encapsulate siRNA, enhance cellular uptake in model cells of the gastrointestinal tract, and facilitate its endosomal escape. Specifically, the aims for this research are:

1. Synthesize nanoscale, intelligent, multi-responsive polycationic polymer networks,
2. Optimize molecular architecture for cellular compatibility, endosomal release, and siRNA encapsulation
3. Rigorously investigate in vitro properties and silencing efficiency using cell models of intestinal epithelia and resident phagocytes in inflamed intestinal tissue.

A representative example of this experimental work flow used to accomplish these aims is seen in Figure 2.1. The novel aspect of this proposal is that it represents the first time that nanoscale hydrogels will be engineered for the oral delivery of siRNA. Local delivery of siRNA to the gastrointestinal tract would be ideal for the treatment of various gastrointestinal and hepatic conditions, including Crohn's disease, ulcerative colitis, celiac disease, gastrointestinal carcinomas, and hepatitis viruses, where non-invasive oral administration would represent a significant improvement over current treatment. Ultimately, we foresee an oral delivery system capable of targeting siRNA therapeutics to any tissue in the body, eliminating the need for injection and enhancing quality of life for the patient.

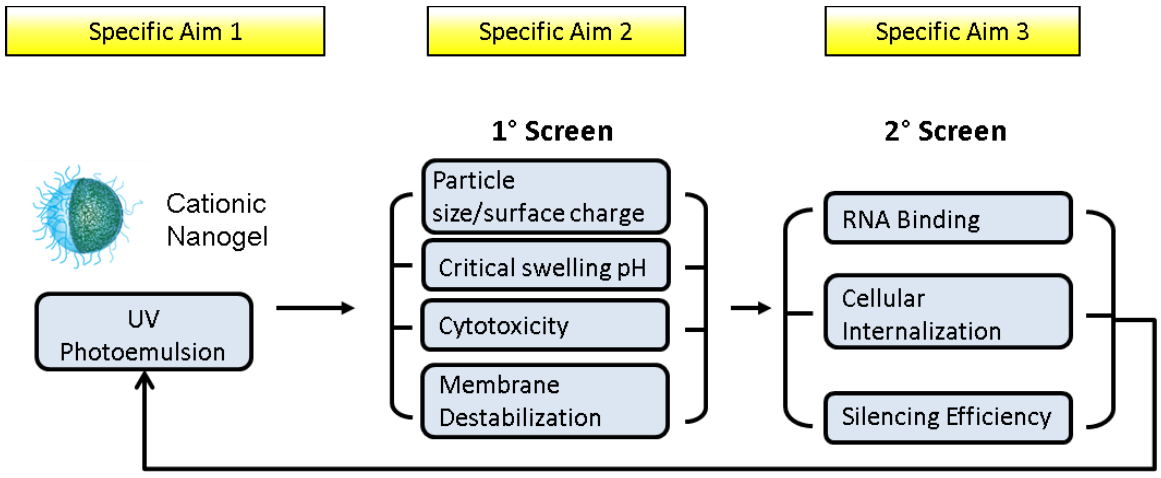

Figure 2.1 – Experimental work flow for outlined specific aims

Chapter 3: Background

Modern advances in science and medicine have brought about the advent of highly specific biological pharmaceutical agents, including proteins (monoclonal antibodies, growth factors, hormones, enzymes, synthetic oligopeptides) and nucleic acids (plasmid DNA, antisense oligonucleotides, siRNA, miRNA) that can be used to treat a variety of diseases[1, 2]. However, a significant obstacle in the emergence of highly specific therapies remains the delivery of these macromolecules to their subcellular site of action. Extracellular and intracellular trafficking barriers represent a significant limitation in the delivery of fragile therapeutics as systemically administered macromolecules are rapidly sequestered by the reticuloendithelial system (RES) and internalized molecules are quickly trafficked to lysosomes for acidic and enzymatic degradation[3].

Many conventional drug delivery modalities indiscriminately distribute drugs throughout the body, frequently exerting effects on both diseased and healthy cells and tissues. Patients stand to benefit from both efficient delivery systems of novel, specific therapeutics and improved, targeted delivery systems for existing therapeutics. Couvreur and colleagues, among others, have provided some of the earliest commentary on the use of nanoparticles for controlled release of therapeutic agents[4, 5]. Recently, the use of polymer-mediated delivery systems, such as polymer-drug conjugates, polymer micelles, polymer-drug polyplexes, and nanoscale hydrogels (Figure 3.1), have been investigated to improve efficacy of these drugs by providing protection from rapid clearance and enzymatic digestion, as well as offering the potential for controlled release [6, 7]. Of particular interest are intelligent systems able to respond to biological cues for tissue

specific targeting or controlled drug release. Molecular design of intelligent delivery systems must consider stability, administration, absorption, metabolism, and bioavailability at target site. By controlling the level and location of biotherapeutics within the body, lower doses are needed and potentially harmful side effects can be minimized[3, 8, 9].

3.1. RESPONSIVE POLYMER DELIVERY SYSTEMS

Selective delivery of biotherapeutics hinges on a safe, efficient, and accurate delivery vector. In recent years, there has been much attention on the rational design of synthetic polymers for novel treatment modalities because of their facile manufacture, large carrying capacity [1], tunable physicochemical characteristics, and modulation of biological activity through attachment of targeting ligands and poly(ethylene glycol) (PEG)[10]. Interdisciplinary research between polymer chemistry and biomedical science has yielded several promising systems for polymer based drug delivery, including polymer-drug conjugates, polymeric micelles, multi-component polyplexes, and nanoscale hydrogels [11, 12]. In particular, pH-responsive polymers have been investigated as delivery agents to overcome intracellular trafficking barriers. It is well known that diseased tissues, tumors, and sites of inflammation exhibit different pH profiles than normal tissue [13]. Also, intracellular pH varies substantially depending on organelle. Endosomes and lysosomes typically exhibit pH values of 6.8 - 4.5. This pH variation can be exploited to specifically deliver therapeutics to a specific intracellular or extracellular site of action. By judicious materials selection and careful engineering of molecular architecture, polymer nanoparticles can be developed to give well-controlled

pH response and drug release[14, 15]. Many pH-responsive polymer delivery systems rely on acid catalyzed hydrolysis to control drug release or on weakly charged polymer chains to mediate endosomal disruption and enable cytoplasmic release.

Anionic polymers undergo a conformational change from charged open chains to compact, hydrophobically-stabilized structures capable of disrupting the membrane of a maturing endosome through pore formation and disruption of membrane integrity. The mechanism of membrane-destabilization by anionic polymers is thought to be related to their pH-dependent conformational transition [16] and the extent of polymer association with the lipid bilayer and cellular uptake can be enhanced by increased polymer hydrophobicity [17].

Cationic polymers, which are able to electrostatically bind negatively-charged nucleic acids such as DNA and RNA, are thought to promote endosomal rupture through the "proton sponge" mechanism. These polymers, which contain ionizable groups, absorb incoming protons during endosomal acidification. This action causes an accumulation of protons and counter ions, such as Cl-, within the endosome. The high osmotic strength within the endosomal compartment subsequently leads to osmotic swelling and endosomal rupture [18]. The general model for drug delivery through endosomal release has been well described[11]. After endocytosis, the decreasing endosomal pH induces a conformational change in the polymer. pH-responsive polymers can increase membrane permeability through hydrophobic associations or the proton sponge mechanism, releasing the payloads into the cytosol. Lysosomal trafficking is undesirable, as harsh enzymatic conditions will readily degrade therapeutic biomolecules.

Environmentally-responsive polymers, or smart polymers, are a class of materials comprised of a large variety of linear and branched (co)polymers or crosslinked polymer networks. A hallmark of responsive polymers is their ability to undergo a dramatic physical or chemical change in response to an external stimulus. Temperature and pH changes are commonly used to trigger behavioral changes but other stimuli, such as ultrasound, ionic strength, redox potential, electromagnetic radiation, and chemical or biochemical agents can be used. These stimuli can be subsumed into discrete classifications of physical or chemical nature [19]. Physical stimuli (i.e. temperature, ultrasound, light, magnetic and electrical field) directly modulate the energy level of the polymer/solvent system and induce a polymer response at some critical energy level. Chemical stimuli (i.e. pH, redox potential, ionic strength, and chemical agents) induce a response by altering molecular interactions between polymer and solvent (adjusting hydrophobic/hydrophilic balance) or between polymer chains (influencing crosslink or backbone integrity, proclivity for hydrophobic association, or electrostatic repulsion) [19]. Types of behavioral change can include transitions in solubility, hydrophilic-hydrophobic balance, and conformation [20]. These changes are manifested in a number of ways, such as the coil-globule transition of polymer chains [21], swelling/deswelling of covalently crosslinked hydrogels [22], sol-gel transition of physically crosslinked hydrogels [23], and self-assembly of amphiphilic polymers [24] (Figure 3.2). This aim of this section is to review recent developments in temperature and pH-responsive polymers and highlight the emerging area of redox-responsive polymers for drug delivery systems. Several excellent reviews which provide a comprehensive treatment of the subject are available [13, 19, 20, 25-29].

3.1.1. Applications and Examples

The majority of responsive polymers for drug delivery can be broadly categorized as hydrogels, micelles, polyplexes, or polymer-drug conjugates. Hydrogels are hydrophilic (co)polymeric networks capable of imbibing large amounts of water or biological fluids [30]. Physical or covalent crosslinks render hydrogels insoluble in water. Hydrogels can be engineered to respond to various stimuli [25] and have demonstrated utility in the medical and pharmaceutical arenas. Peppas and coworkers have pioneered the use pH-responsive complexation hydrogels of poly(methacrylic acid) grafted with PEG, P(MAA-g-EG) for oral protein delivery. Through interpolymer complexation in acidic conditions, this system has been shown to successfully entrap, protect, and mediate delivery of insulin [31], calcitonin [32], and recently interferon β [33]. Micelle-forming polymers, such as block copolymers of poly(ethylene oxide) and poly(propylene oxide), or Pluronics®, have been thoroughly studied in drug delivery [26]. These polymers exhibit thermally-responsive micellization [34], as do block copolymers of poly(N-isopropylacrylamide) (PNIPAAm) coupled with hydrophilic PEG [24]. Polyplexes formed by cooperative electrostatic interactions between polyethyleneimine (PEI) and DNA are widely studied for gene delivery. Since the seminal paper by Boussif, et al. [35], several facets of PEI-mediated gene delivery have been investigated, including the influence of crosslinking, molecular weight, branching, and biodegradability [36-38].

3.1.1.1. Responsive Systems based on Temperature

Temperature has been widely investigated as a stimulant for responsive polymer systems owing to its ease of modulation and applicability in drug delivery applications

[19]. Tanaka observed temperature-dependent swelling of polymer gels [39] following its theoretical prediction over 40 years ago [40]. One thermo-responsive polymer, PNIPAAm, has been thoroughly investigated for its ability to undergo a reversible, inverse (or negative) temperature-dependent phase transition [25]. Below its lower critical solution temperature (LCST) near 32°C, PNIPAAm exists as a hydrophilic coil while above the LCST, PNIPAAm chains collapse sharply into a hydrophobic globule [41]. The nature of this volume phase transition stems from the hydrophilic/hydrophobic balance of polymer chains [42], which is modulated by continual establishment and disruption of intra- and intermolecular electrostatic and hydrophobic interactions. Below the LCST, water molecules exist in an ordered state in the local environment of polymer chains [43]. As temperature rises above the LCST, polymer-polymer hydrophobic interactions dominate [41]. Consequently, polymer chains collapse and water molecules are released to the bulk, resulting in a net entropic gain for the polymer/solvent system [44].

For drug delivery applications, it may be desirable to shift the critical temperature for volume phase transition to specific temperatures. This can be accomplished through the inclusion of hydrophobic or hydrophilic moieties in the polymer chain. Polymers with a larger hydrophobic hydration area possess stronger hydrophobic interactive forces and undergo collapse at a lower temperature[21, 45]. Conversely, increasing the hydrophilic content of the polymer chain will increase the LCST. Polymers that exhibit positive temperature-dependent swelling behavior, i.e. globule-to-coil transition with increasing temperature, possess upper critical solution temperature (UCST) behavior.

These materials, such as poly(acrylic acid) and polyacrylamide interpenetrating networks (IPNs), are discussed in more detail elsewhere [46].

Physically crosslinked gels, such as methoxy-substituted cellulose derivatives, PNIPAAm copolymers, and various Pluronics can undergo a sol-gel phase transition near their LCST [26]. These materials are attractive candidates for in situ implants, in which thermoreversible gelation is exploited for the facile implantation of solid drug-depot preparations [47]. In these systems, a liquid drug/polymer solution is injected to a target site at ambient temperature. As the solution temperature warms to body temperature, the polymer gels, entrapping the drug in the physically crosslinked matrix. Diffusion of drug from the solid gel allows for sustained-release formulations. This approach was used in a study describing the release of model protein bovine serum albumin (BSA) from temperature-responsive chitosan grafted with PEG (PEG-g-chitosan) [48]. PEG-g-chitosan containing 45 and 55 wt% grafted PEG were loaded with BSA and incubated at 37°C to evaluate release kinetics. Both gels demonstrated initial burst release of BSA during the first 5 hours followed by sustained, diffusion-driven release until approximately 70 hours. Crosslinking the gels with genipin resulted in prolonged release of BSA for up to 40 days.

Novel polymerization techniques, such as controlled radical polymerizations and click chemistry reactions, offer superior control over molecular architecture and present the opportunity to create novel materials highly tailored for specific responsive behavior. This approach was employed by Sumerlin and colleagues to produce folate-conjugated temperature-responsive block copolymers of N,N-dimethylacrylamide (DMAAm) and PNIPAAm with RAFT polymerization [49]. Above the LCST (34°C) of this polymer

system, PNIPAAm blocks collapsed into hydrophobic globules while DMAAm blocks remained hydrophilic. Ensuing aggregation resulted in particles of approximately 46 nm, postulated to be micelles with PNIPAAm cores and DMAAm shells. Surface decoration of the polymer chains with folate enable the system to be actively targeted to certain tissues via receptor-mediated endocytosis. Self-assembled folate-conjugated polymers provided controlled release of a model hydrophobic drug, dipyridamole over the course of 12 days.

3.1.1.2. Responsive Systems based on Redox Potential

Polymers containing labile linkages present an attractive opportunity to develop biodegradable or bioerodible delivery devices. Much of the early work in this field focused on acid labile linkages of polyanhydrides [50, 51], poly(lactic/glycolic acid) [52], and more recently poly(β-amino esters) [53, 54]. However, intracellular cues are now being investigated as a means to trigger cytoplasmic degradation of polymer carriers incorporating advanced therapeutics like siRNA and anticancer drugs. Disulfide linkages are well known to be unstable in a reductive environment as the disulfide bond is readily cleaved in favor of corresponding thiol groups. Polymers with disulfide cross-links have been synthesized as polymersomes [55], nanogels [56], and core-cross-linked polyplexes [57] and degrade when exposed to cysteine or glutathione, reductive amino-acid based molecules present at intracellular concentrations 50 - 1000 fold greater than that of the extracellular milieu [57].

The Hubbell group [55] has used amphiphilic copolymers of PEG and poly(propylene sulfide) (PPS) to form vesicular compartments. Rather than relying on hydrolytic linkages, which may respond too slowly to avoid non-productive lysosomal

accumulation of the polymer carrier, they have incorporated a disulfide linkage between the hydrophilic PEG and hydrophobic PPS portions of the polymer, imparting a high degree of reductive sensitivity to the polymersomes.

In another study, glutathione-degradable nanogels were prepared by inverse emulsion ATRP [56]. Upon exposure to 10 wt% glutathione, half of the polymer degraded in nearly 6 hours. Exposing polymers to 20 wt% glutathione resulted in 85% degradation within 1 hour. Doxorubicin was efficiently incorporated into the polymer matrix at 16 wt% of the polymer with over 50% loading efficiency and the authors demonstrated in vitro release of fluorescent dye Rhodamine G6 and doxorubicin. Dox-loaded nanogels displayed negligible toxicity toward HeLa cells in the absence of glutathione while causing approximately 40% reduction in cell viability following introduction of exogenous glutathione to the cellular media. It remains to be determined if this polymer system is capable of degrading and releasing drug upon exposure to intracellular glutathione concentrations or if the time-scale for degradation in the presence of endogenous glutathione will allow efficient cytoplasmic delivery of incorporated therapeutics.

In a more recent investigation, Kataoka and colleagues [57] synthesized and thoroughly characterized a core-cross-linked polyplex comprised of iminothiolane-modified PEG-block-poly(L-lysine), or [PEG-b-(PLL-IM)], for intracellular siRNA delivery. The use of a block copolymer affords modular functionality; the polycationic poly(L-lysine) segment serves to bind siRNA and provide endosomal buffering capacity [58] while the hydrophilic PEG segment prolongs circulation time, prevents aggregation, and reduces opsonization [59]. Lysine groups of the PEG-b-PLL copolymer were reacted

with 2-iminothiolane and subsequently oxidized to form disulfide cross-links. Introducing crosslinks to the micelle core confers stability to the system, as crosslinked polymers maintained micellar structure in physiological salt conditions while their non-crosslinked counterparts could not. The resulting polyion complex micelles were approximately 60 nm in diameter, a particle size well within the accepted limits (20 - 100 nm) for avoiding uptake by the RES and renal exclusion [60]. Not surprisingly, micellar stability exerted strong influence over the ultimate siRNA transfection efficiency. The authors observed a narrowly defined N/P RATIO at which stable micellization occurred. Interestingly, this optimum N/P ratio shifted to higher values with increased crosslinking. Highly efficient (over 80%) knockdown of a reporter gene was detected at the optimum N/P ratio, however, a considerable decrease in transfection efficiency was observed upon slight departure from this critical value.

3.1.1.3. Responsive Systems based on pH

Physiological pH varies systematically in the body, particularly along the gastrointestinal (GI) tract, where harsh pH and enzymatic conditions in the stomach (pH ~ 2) degrade macromolecules. The small intestine is substantially more alkaline, with pH ~ 6.2 - 7.5. Physiological pH profile will also change amongst cellular compartments. Endosomes typically exhibit pH values of 5.0 - 6.8 and lysosomes 4.5 - 5.5 [61, 62]. Also, it is well known that diseased tissues and sites of inflammation exhibit different pH profiles than normal tissue [13]. Tumors have been widely reported to produce acidic conditions (pH ~ 6.5) in the extracellular milieu [63]. Thus, it is no surprise that scientists and engineers have devoted considerable effort toward the rational design of polymers capable of exploiting these pH variations to selectively deliver valuable

therapeutics to specific intracellular or extracellular sites of action. By judicious materials selection and careful engineering of molecular architecture, pH-responsive polymer delivery systems can be developed to give well-controlled pH response and drug release.

Recently, we have synthesized polycationic nanomatrices capable of well-defined hydrophilic-hydrophobic transition near physiological pH [64, 65]. Relatively uniform particles of poly[2-(diethylamino)ethyl methacrylate-co-t-butyl methacrylate-g-PEG] (PDBP) measuring 51 nm were synthesized using a novel photoemulsion polymerization technique [64]. Relevant properties of the system, such as swelling ratio, critical swelling pH, surface charge, and biocompatibility were tailored by tuning polymer composition, crosslinking density, and the incorporation of hydrophobic moieties to the hydrogel core. Ongoing work aims to optimize these systems for intracellular siRNA delivery.

Promising work by Hu et al. [66] describes the development of pH-responsive core-shell hydrogels for intracellular delivery of ovalbumin to dendritic cells, a class of cells intimately involved with adaptive immunity. Emulsion polymerization was used to create crosslinked PDEAEMA core - PAEMA shell nanoparticles measuring 205 nm in diameter. The authors hypothesized that PDEAEMA would exhibit pH-responsive behavior while PAEMA would remain constitutively ionized throughout the physiological pH range. Interestingly, the authors used the cationic PAEMA shell to adsorb and protect a model ovalbumin protein, rather than the archetypal practice of loading therapeutics to the hydrogel core. Subsequent studies demonstrated the versatility of this approach through intracellular delivery of siRNA and influenza A particles [67]. This strategy of using a charged, pH-insensitive shell distinct from the pH-

responsive domain represents an intriguing departure from the current paradigm of using a neutral, hydrophilic shell, such as PEG, to shield surface charges. However, several drawbacks may limit the feasibility of this design in vivo. First, charged particles have a much higher opsonization rate than neutral particles [59] and the cationic PAEMA shell may attract opsonin proteins or promote adsorption of anionic serum proteins, resulting in rapid clearance by the RES. Secondly, the slow dissociation of electrostatically bound cargo from polymer shell may provide a kinetic barrier to therapeutic efficacy.

Bae and colleagues [68-70] have recently reported polymer micelles possessing dynamic, multi-functional behavior for drug delivery. Self-assembling amphoteric polyamine-based block copolymers were functionalized with folate [68], biotin [70], and HIV peptide TAT ligands [69], demonstrating robust applicability in targeted delivery. Folate or biotin ligands enhance cellular uptake via receptor mediated endocytosis [71] and TAT is a well-known peptide transduction domain [72]. By conjugating the cell-penetrating peptide TAT, particles of up to 200 nm gain direct access to the cell [73], effectively circumventing the intracellular trafficking pathway. The polymer system, a mixture of two block copolymers 1) poly(L-histidine)-b-PEG (polyHis-b-PEG) and 2) poly(L-lactic acid)-b-PEG-b-polyHis-ligand (pLLA-b-PEG-b-polyHis-ligand), self-assembled into mixed micelles capable of ligand exposure, micelle destabilization, and endosomal disruption in response to pH [69, 70]. A short polyHis block preceding the ligand serves to anchor the ligand at the core-shell interface, effectively shielding its presentation on the micelle surface at neutral pH. Upon exposure to slightly acidic ($6.5 < pH < 7.0$) environment, the short polyHis anchor ionizes and PEG-b-polyHis arm unfurls, exposing the ligand on the micellar surface. This response is expected to confer

tumor specificity to the micelle carrier as the ligand will be unavailable to promote receptor mediated endocytosis or cellular transduction in normal (pH 7.4) tissue. Further acidification (pH < 6.5) induced micelle dissociation by ionization of the His residues in the micelle core. Breast adenocarcinoma cells exposed to doxorubicin-loaded mixed micelles displayed prominent intracellular distribution and nuclear localization of Dox after 30 minutes and experienced ~60% reduction in cell viability of after 48 hours.

3.2. POLYMER-DRUG CONJUGATES

The use of synthetic polymer-drug conjugates for drug delivery was first proposed in 1975 [74]. Generally, these entities are composed of a reactive drug conjugated to a water soluble polymer backbone through a biodegradable linkage [75]. Common pH-responsive linkages include anhydrides, cis-aconityl, hydrazones, and acetals [11]. Targeting ligands, such as transferrin, can also be conjugated to the polymer backbone. The transferrin receptor is typically over-expressed in rapidly proliferating and cancer cells [76], providing an attractive opportunity for tumor-targeting.

Covalent conjugation of anticancer drugs to a polymer backbone via a pH-sensitive linkage has been explored as an option to liberate compounds such as doxorubicin in the local tumor environment. This type of delivery requires a conjugate that is stable in circulation and normal tissue but releases a fully active drug at the target site. Mayumi and colleagues have synthesized a copolymer of vinylpyrrolidone and dimethylmaleic anhydride, where the dimethylmaleic anhydride serves as the pH-responsive linker [77]. The dimethylmaleic anhydride is able to bind amine groups at pH > 8.0 and reverts back to anhydride form at pH < 7.0, releasing the bound drug. The copolymer showed negligible toxicity to cells at concentrations as high as 1 mg/mL.

Typical concentrations of polymer drug delivery systems are near 200 μg/mL . The polymer-drug conjugate was demonstrated to have increased circulatory half-life and enhanced anti-tumor activity compared to doxorubicin alone. In fact, intravenously injected polymer-doxorubicin conjugates were able to completely inhibit tumor growth in murine sarcoma models, confirming that the released drug was indeed fully active.

Doxorubicin has also been conjugated to a N-(hydroxypropyl)methacrylamide (HPMA) polymer via degradable hydrazone linkages [78]. Covalent attachment was stable at physiological pH, as less than 10% of doxorubicin was released from the polymer at pH 7.4. However, at pH 5.0, nearly 50% was released after 5 hours. Intravenous injection in mice significantly slowed tumor growth lasting 60 days and prolonged survival for 30 days over control treatments.

3.3. POLYMER MICELLES

Many polymer micelles are formed by amphiphilic block copolymers. These supramolecular structures self-assemble to form particles with hydrophobic interior and a hydrophilic corona. Hydrophobic or water-insoluble drugs can be encapsulated in the hydrophobic core. The thermodynamic and kinetic stability of micelle structures allow them to retain integrity, even after extreme dilution (e.g. intravenous injection) or extended circulation time [79]. Typical micelle size (20 - 100 nm) is large enough to avoid renal clearance yet small enough to avoid rapid uptake by the RES [60]. Physical encapsulation of hydrophobic drugs within micelles may be a more favorable approach than conjugation as covalent attachment of drugs to a polymer carrier may negatively affect their bioavailability or require conjugation to the drug's active site [79].

Kataoka and colleagues [80] have developed pH-sensitive micelles demonstrating release of adriamycin. Adriamycin was conjugated to poly(aspartate) through an acid-labile hydrazone linker. Following acid-catalyzed hydrolysis, the micellar structure was disrupted, releasing free drug. A recent study by Geng, et al. describes the formation of cylindrical micelles, or filomicelles, from copolymers of poly(ethylene glycol) and poly(caprolactone) (PCL) [81]. These particles, owing to their extended shape, were not readily taken up by the RES and achieved circulation times of over one week after systemic administration. Acid catalyzed degradation of PCL promotes micellar fragmentation and subsequent extravasation and cellular uptake. In vivo studies in tumor-bearing mice confirmed the benefit of prolonged circulation. Paclitaxel-loaded filomicelles caused significant increase in tumor apoptosis and decrease in tumor volume relative to free drug. Additionally, the magnitude of apoptotic response and tumor size reduction increased with filomicelle length (i.e. longer filomicelles delivered paclitaxel more efficiently than did short filomicelles). Long-circulating, pH degradable structures such as this could have significant utility in cancer therapy. Chemotherapeutic agents, such as paclitaxel or doxorubicin, could be administered less frequently, decreasing the intensity of conventional chemotherapy and improving quality of life for the patient.

pH-responsive micelles based on acetal polymers have shown promise in controlled release of doxorubicin [82]. The acetal block forms a hydrophobic core able to efficiently encapsulate doxorubicin (12 wt%). Upon exposure to mildly acidic conditions, the acetal core begins to hydrolyze, exposing polar groups in the micelle core. This alters solubility of the core block and disrupts the micelle, releasing free doxorubicin to the surrounding environment. This system releases 50% of doxorubicin content after 5

hours in pH 4.0 and 40 hours in pH 5.0, while the release rate at pH 7.4 is negligible. Thus, the time scale of doxorubicin release suggests this system would be applicable for sustained release to the acidic interstitial fluid surrounding tumors. As intracellular trafficking from endosomes to lysosomes occurs on the order of minutes, a carrier designed to enhance intracellular delivery through endosomal rupture should possess a comparable response time.

3.4. POLYMER-DRUG POLYPLEX

Polyplexes are formed by electrostatic or hydrophobic interactions between polymers and nucleic acids, proteins, or low molecular weight drugs. These structures are thought to have increased mechanical stability over micelles due to chain entanglements and hydrophobic interactions [83]. For example, polycations such as polyethyleneimine are routinely used to bind negatively-charged plasmid DNA for gene therapy. These systems contain DNA-binding amines, and may contain targeting ligands to direct cell-specific delivery and receptor-mediated endocytosis [18]. In some cases, the addition of pH-responsive polyanions or hydrophobic comonomers may aid in the endosomal release of multi-component polyplexes [84-86]. In fact, DNA transfer has been increased up to three orders of magnitude by introduction of a membrane-lytic peptide [18].

Work by Shenoy and Amiji [53, 54, 87] has focused on using poly(β-amino esters) as pH-responsive polyplexes for delivery of chemotherapeutic agents. Copolymers of poly(ethylene oxide) and poly(propylene oxide) were blended with poly(β-amino ester) to form spherical nanoparticles of 150 - 200 nm. These polymers can be formulated to efficiently deliver small molecular weight drugs or polynucleotides

in the form of oligonucleotides or plasmid DNA. Cytotoxicity studies have demonstrated that poly(β-amino esters) are significantly less toxic than conventional polymers used for nucleic acid delivery, such as poly(ethyleneimine) or poly(L-lysine) [53]. Paclitaxel was efficiently loaded into these nanoparticles, achieving 20 wt% drug in polymer concentration. The particles exist in a stable, insoluble form at physiological pH but undergo a rapid dissolution at pH < 6.5, releasing drug to the surrounding environment in a sudden burst. When injected intravenously to tumor-bearing mice, paclitaxel-loaded nanoparticles significantly inhibited tumor growth relative to paclitaxel injection alone [87]. Moreover, body weight and blood count measurements indicated little to no adverse toxicity in mice injected with poly(β-amino ester).

In an effort to explore synergistic advantage of both pH- and temperature-responsive behavior, Kang, et al. have prepared a series of graft copolymers based on temperature-responsive N-isopropylacrylamide and pH-responsive sulfamethoxypyridazine [83]. Doxorubicin was loaded into the polyplex at 10 wt % drug in polymer and released from the matrix by inducing a hydrophobic to hydrophilic phase transition. As expected, the release rate of doxorubicin was highest when the temperature-sensitive and pH-sensitive blocks were simultaneously converted to the hydrophilic state.

3.5. NANOSCALE HYDROGELS

Nanoscale hydrogels, or nanogels, are materials with diverse biomedical applications. Because of their inherent mechanical integrity and biocompatibility, hydrogels have utility in imaging, biosensing, molecular recognition, and therapeutic delivery [65, 88]. Nanoscale hydrogels are of particular interest in drug delivery because

of their tunable nanoscale dimensions (i.e. large enough to avoid renal clearance and small enough to evade RES), drug loading capacity, colloidal stability, and large surface area for conjugation of active targeting moieties [88]. Furthermore, the nanoscale dimensions ensure a rapid response to pH changes, an attractive attribute in drug delivery applications. The pH response of hydrogels can be modulated by the pKa of polymer chains and choice of monomer.

Cationic monomers with pKa > 7, such as poly(dimethylaminoethyl methacrylate) (PDMAEMA), will exist in an ionic state at physiological pH. The positively charged amino groups will repel each other and permit the osmotically-driven flux of water into the polymer matrix. However, increasing the pH above the nanogel pKa will deprotonate the amino groups and hydrophobic interactions will collapse the gel, excluding water. Polymers based on anionic monomers (pKa < 7), such as methacrylic acid, will behave in the opposite manner. At pH below the pKa, pendant carboxyl groups are protonated and hydrophobic interactions maintain the gel in the collapsed state. Increasing the pH above the pKa will deprotonate the carboxyl groups, swelling the gel through electrostatic repulsions and influx of water.

Nanogels are being explored as drug delivery agents for a variety of therapeutic agents due to their ability to efficiently encapsulate therapeutics through simple equilibrium partitioning or electrostatic interactions. Using a cationic chitosan-based nanogel (180 nm diameter), researchers have delivered antitumor therapeutic metotrexate disodium to tumor cells [88]. Blanchette and Peppas have explored the use of methacrylic acid and ethylene glycol nanogels for oral delivery of chemotherapeutic agents [89]. Bleomycin was encapsulated in the hydrogel during polymerization and

release studies demonstrated favorable release kinetics. The therapeutic agent was well protected in the hydrogel at low pH and nearly 100% of bleomycin was released after 1 hour at pH 7.4.

Recently, Peppas and coworkers described the synthesis of polycationic nanogels capable of well-defined hydrophilic-hydrophobic transitions near physiological pH[15, 64, 65] and successfully demonstrated loading of biological therapeutics (e.g. insulin) and imaging agents (e.g. gold nanoparticles). Akiyoshi and colleagues recently completed a Phase I clinical trial using a self-assembled, cholesterol-modified pullulan nanogel to deliver a HER2 protein fragment for vaccination against cancer [90]. HER2 protein has been implicated in increased aggressiveness of tumors, particularly in breast cancer[71]. Their results indicate that administration of the protein fragment successfully initiated an innate immune response against HER2.

3.6. TARGETED DELIVERY

3.6.1. Barriers to targeted delivery

Though localized delivery represents an attractive method for achieving a high concentration of biotherapeutics, most tissues are not accessible for localized treatment. Thus, systemic and oral administrations are commonly employed to introduce therapeutics to the circulatory system. However, before reaching their site of action, biomacromolecular drugs face a series of extracellular obstacles which threaten to reduce bioavailability and therapeutic benefit. The mononuclear phagocytic system (MPS), or reticuloendothelial system (RES), presents a major barrier to prolonged circulation of polymer nanoparticles [59]. Macrophages and monocytes of the MPS play an important physiological role by clearing foreign material, such as bacteria, viruses, and fungi, from

the body. However, they are also highly efficient at removing unprotected polymer nanoparticles. Present in bloodstream and extracellular matrix of tissues, these phagocytic bodies are not able to recognize circulating material directly, but must do so through the presence of opsonin proteins [59]. The association of opsonin proteins, termed opsonization, can occur within seconds after entering the bloodstream as complement proteins and immunoglobulins bind to the surface of the polymer particle [59]. Bound opsonins stimulate phagocytosis of the associated particle, ultimately resulting in its degradation or removal from the bloodstream. Particle aggregation with serum proteins such as serum albumin can also result in phagocytosis and clearance by the RES [91]. Typically, this process occurs through non-specific hydrophobic or electrostatic interactions between polymer particles and serum proteins [18, 59]. In addition to avoiding removal by the RES, polymer therapeutics must also escape filtration by the renal system. Current calculations, based on the sieving coefficient of the glomerular capillary wall, estimate that a polymer nanoparticle should be at least 10 nm in diameter to avoid first-pass renal filtration [60]. Extravasation, or escape from the blood vessels, poses a problem because molecules larger than 2 nm in diameter do not easily cross the capillary epithelia [60]. Once outside the capillaries, proteins and polysaccharides that comprise the extracellular matrix hinder diffusion of nanoparticles, increasing opportunity for phagocytosis by macrophages in the interstitial space [92].

Further obstacles face polymer therapeutics delivered through the oral route (Figure 3.3). The stomach, lumen of the small intestine, mucus layer, and the intestinal epithelial cell membrane must be successfully traversed [93]. Ingested formulations quickly encounter the harsh environment of the stomach, where digestive enzymes and

low pH (pH ~ 2) contribute to the rapid degradation of unprotected therapeutics, particularly proteins and nucleic acids. Though the pH is less extreme in the small intestine (pH 5 - 7.4), digestive enzymes in the intestinal lumen threaten to break down therapeutics before they cross the epithelium. The mucus lining, a dense network of glycoproteins, coats epithelial cells along the GI tract and provides resistance to macromolecular transport [94]. At the luminal surface of the epithelial cell layer, macromolecules are largely precluded from paracellular transport due to the presence of tight junctions. These junctions limit the paracellular space to approximately 10 - 50 Å [95], defending the body from entry of viruses and toxins through the GI tract. Additionally, intestinal motility reduces the residence time for release and absorption by the intestine.

Intracellular trafficking barriers represent a significant obstacle in the delivery of biotherapeutics to their subcellular site of action. Most therapeutics must localize in the cytosol to exert functional activity. After passive or receptor-mediated endocytosis, macromolecules are rapidly delivered to early endosomes, where the vesicular pH is lowered by the action of ATP-dependent proton pumps [62]. Acidification is an important characteristic of endosomal trafficking, serving primarily to dissociate ligands from receptors. Although free receptors are recycled back to the cell surface, the early endosome contents are transferred to late endosomes and ultimately lysosomes for degradation [61]. The transit from early endosomes to late endosomes is fairly rapid, on the order of 2 – 3 minutes [62]. The luminal pH is progressively lowered throughout the pathway by ATP-dependent proton pumps. Typically the pH of early endosomes is 6.8 – 5.9, pH of late endosomes is 6.0 – 5.0, and pH of lysosomal compartments reaches 5.5 –

4.5 [61, 62]. Degradative enzymes populate the lysosome and readily break down foreign material. After successively protecting its cargo through numerous extracellular and intracellular barriers, a delivery vehicle must then release the therapeutic in functional form [18]. Therefore, enabling efficient translocation of cargo from endosome to cytoplasm is an essential feature of any polymer-mediated drug delivery system.

3.6.1.1. Passive Targeting

Cellular barriers present formidable obstacles in the delivery of biotherapeutics. Researchers in cancer treatment have fortunately been able to exploit certain aspects of cancer physiology to achieve passive targeting to tumor sites. Rapid growth of tumors leads to aberrant angiogenic vasculature. The newly formed blood vessels are often disorganized and discontinuous, resulting in increased permeability to macromolecules. Moreover, lymphatic drainage systems are often poorly developed or non-existent in tumor sites, enabling accumulation of therapeutics [96]. This phenomenon, called the enhanced permeation and retention (EPR) effect [96], has increased the tumor concentration of anticancer agents up to 70-fold in some cases [11].

Since the pioneering work of Couvreur [97], nanoscale systems have been aggressively investigated for their utility in drug delivery applications. Nanoparticle size is known to play a critical role in achieving passive targeting. Nanoparticles above 10 nm in diameter are generally able to avoid filtration by the kidneys, while less well understood, the upper size limit for passively targeted nanoparticles is thought to be approximately 150 nm [60, 98]. Extravasation and diffusional barriers limit nanoparticle access to tumors when particle size is over 200 nm [60]. Additionally, previous studies

have shown that nanoparticle clearance rate increases with size [99]. One such investigation demonstrated that the blood clearance of 80 nm nanoparticles was half as fast as the clearance of 170 and 240 nm particles [100]. Presumably, this effect is due to non-specific protein adsorption on the surface of larger nanoparticles, leading to opsonization and subsequent clearance by the RES [99].

Clearly, particles with longer circulation times have superior ability to reach the tumor site through passive targeting. As opsonization is an integral step in the removal of foreign macromolecules by the RES, many efforts for increasing serum stability and extending circulation time have focused on blocking absorption of opsonins onto the nanoparticle surface [59]. Hydrophobic and charged nanoparticles associate readily with opsonins and serum proteins. Attachment of polyethylene glycol (PEG), or PEGylation, has been a popular approach for conferring "stealth" properties to circulating nanoparticles. PEG is highly flexible, hydrophilic, non-degradable, and non-toxic [101]. PEGylation helps shield hydrophobic or charged nanoparticles and slows the process of opsonization through steric hindrance [59].

3.6.1.2. Active targeting

The primary goal of a targeted therapeutic is to eliminate diseased cells while leaving normal cellular activities unimpaired. Therefore, it is highly advantageous for a polymer delivery system to preferentially localize in the disease tissue rather than normal tissue in the body. Through careful engineering of polymer nanoparticles, various targeting ligands can be displayed to enhance selective delivery to a disease sites, thereby decreasing the preferential localization in the liver and spleen [2, 102]. Similar to leaky

tumor sites, these organs allow passage of macromolecules, generally up to 200 nm in size. Unchecked accumulation of non-degradable compounds may lead to undesired toxicity. Attachment of antibody fragments has been explored as a potential strategy to enhance tumor targeting due to their high binding specificity. By incorporating a fragment, specificity is retained and the antibody region responsible for eliciting an immune response is not present [71]. Despite some early success in antibody targeting [103], more recent attention has been focused on exploiting transport receptors upregulated in tumors, such as transferrin and folate. In normal cells, transferrin receptors exist to facilitate the endocytosis of transferrin, an iron-binding glycoprotein. Folate receptors function to allow transport of folic acid, a vitamin required for synthesis of purines and pyrimidines [71]. Transferrin and folate receptors are constitutively over expressed in many tumor cell types due to their increased metabolic demand. Active targeting continues to command significant attention because many cancer-cell types display tumor-specific receptor upregulation. Strategies are being developed to specifically target breast, colorectal, lung, and prostate cancer by way of tumor-specific ligands [71]. As new genetic and physiological anomalies in cancer cells are discovered, incorporation of active targeting agents will play an important role in the local delivery of specialized therapeutic agents.

Targeted, functional delivery of therapeutic agents is a significant unmet need in drug delivery. Despite tremendous effort in targeted carriers and directed drug delivery systems, true targeting remains elusive. While surface conjugation of various peptide sequences, proteins, antibodies, and other small molecules can effectively enhance the preferential uptake of nanocarriers at disease sites, this enhancement is largely

probabilistic (i.e., more receptors per unit area increases the chance of receptor–ligand interaction and subsequent internalization). Given adequate circulation time, the current generation of nanoparticles will ultimately traffic to highly perfused tissue such as the liver, lungs, pancreas, kidneys, tumors, and sites of angiogenesis. The next generation of intelligent delivery systems should be deterministic rather than probabilistic; capable of tunable pharmacokinetics and biodistribution whereby the carriers will localize at, and only at, the intended disease targets and in response to the diseased environment will release their therapeutic payload. In addition, they should be able to seek, find, and persist in disease sites while providing concomitant treatment and noninvasive monitoring.

3.7. RNA INTERFERENCE

The landmark discovery of RNA mediated interference (RNAi) in 1998 has sparked a massive research effort in all fields of biological science and redefined our understanding of gene regulation mechanisms[104, 105]. RNAi pathways are guided by the presence of small interfering RNA (siRNA), short strands of duplex RNA capable of selective, potent, and reversible silencing of target genes3. These nucleotide strands are part of an endogenous regulatory pathway present in a variety of eukaryotic organisms to control gene expression. RNA interference pathways have been demonstrated in protozoa, plants, fungi, and animals, indicating a conserved pathway which serves to protect the genome from viral pathogens, transposons and aberrant messenger RNA (mRNA)[106]. Theoretically, siRNA could be used as a powerful and versatile therapeutic to treat nearly any disease resulting from aberrant gene expression. Furthermore, recent advances in genomics, bioinformatics, and increased understanding

of the molecular and genetic nature of disease enable siRNA technology to be rapidly adapted for disease treatment. Owing to its remarkable potency and low therapeutic dosage, siRNA holds extraordinary promise as a new biological therapeutic[107, 108]. Inefficient delivery and immunostimulation concerns have been implicated as the major hurdles to its widespread clinical implementation[92, 109].

3.7.1. Mechanism of RNAi

siRNAs are formed by cleavage of long double-stranded RNA into 21 - 23 nucleotide fragments by the enzyme Dicer, a member of the Ribonuclease III family[110]. In most therapeutic applications, siRNA is produced synthetically and presented directly to the cell. This method mitigates the possibility of an innate immune interferon response as previous reports have indicated that cytoplasmic dsRNA > 30 nucleotides triggers interferon synthesis in mammalian cells[111]. siRNA subsequently associates with a multi-protein complex termed RNA induced silencing complex (RISC) after which the duplex is unwound through the action of RISC protein Argonaute 2 (Figure 3.4)[112, 113]. Following unwinding, the sense strand is cleaved while the anti-sense strand directs the activated RISC complex to selectively target and degrade complementary mRNA[114]. Each activated RISC complex can catalyze degradation of multiple target mRNA strands, making RISC-mediated mRNA degradation a prolific gene-silencing mechanism. Recent reports have demonstrated the sustained potency of siRNA silencing. Bartlett and Davis observed knockdown of a luciferase reporter gene lasting 4 - 7 days in rapidly dividing cells and over 3 weeks in non-dividing cells[107], and a study by Elbashir showed that 21 nt synthetic siRNA effectively mediated gene silencing at nanomolar concentrations[108].

Because of its broad therapeutic potential and sustained, sequence-specific gene silencing, siRNA has been identified as a treatment modality for a variety of diseases, including many viruses and cancers. Following a pioneering study by Song, et al., which demonstrated the first in vivo evidence of siRNA efficacy[115], many investigations have shown successful knockdown of disease targets. More recently, Davis and colleagues reported evidence of nanoparticle-mediated delivery of functional siRNA in humans[116]. Many RNAi-based therapeutics are currently undergoing clinical trials, predominantly for indications in ophthalmology and oncology (Figure 3.5).

3.7.2. Key Challenges and Opportunities in siRNA therapeutics

Although siRNA should not be considered a panacea for all disease, its broad therapeutic applicability and promising success both in vitro and in vivo cannot be ignored. Many disease treatments stand to benefit from the clinical implementation of siRNA therapeutics. However, translating this therapeutic value into a clinical reality is hampered by the lack of an efficient delivery system. This is due primarily to the combination of extracellular and intracellular barriers which limit the access of exogenous siRNA to the cytoplasm of target cells.

Interference with viral RNA genomes or replicative intermediates has proven effective, particularly with hepatitis viruses[117]. Several groups have demonstrated significant siRNA-mediated inhibition of hepatitis B virus replication in vivo[118-121] and in vitro studies indicate that siRNA may be an attractive antiviral therapy for hepatitis C (HCV) [122, 123]. Targeted siRNA holds promise in the treatment of other liver conditions. For example, recent efforts have explored lipid nanoparticle siRNA-

based treatments for hypercholesterolaemia[124], a formulation for which Alnylam Pharmaceuticals has applied to initiate Phase I clinical trials.

siRNA has been hypothesized as a potential treatment strategy for several types of cancer. Numerous studies present compelling evidence for siRNA as a novel therapeutic approach, but work remains to be done to elucidate the precise anti-tumor activity of siRNA. Reports have indicated siRNA may induce off-target effects, activating immune responses and stimulating production of cytokines and interferons, which could enhance innate anti-tumor activity[125]. Other diseases, such as liver cirrhosis and human papillomavirus have shown promising response to siRNA treatment in vivo[92].

The development of RNAi technologies has largely been driven by innovation in small biotechnology and pharmaceutical companies, like Alnylam, Marina, Tekmira, Isis, Rxi, Calando, and others. Prior to 2008, much of the news around RNAi focused on lucrative acquisitions and development partnerships. Traditional large pharmaceutical companies invested heavily in RNAi, with $500M from Roche, $200M from Pfizer, and $1.5B+ from Merck. Since then, these announcements have been followed by a series of high-profile realignments, with both Roche (November 2010) and Pfizer (February 2011) abandoning internal RNAi efforts.

This model is expected to continue as traditional pharmaceutical companies shy away from lengthy and expensive exploratory R&D. Rather, recent trends suggest big pharma companies are becoming more conservative with their research efforts; content to acquire technical expertise and intellectual property through acquisition of companies with promising clinical data. Thus, big pharma is able to leverage its expertise in

marketing and distribution of new drug candidates, shifting the onus for innovation to smaller companies.

In many ways, the future for RNAi, for scientists, funding agencies, and private investors, has never been brighter. The recent announcements by Roche and Pfizer served to deflate what was perhaps an RNAi bubble from 2006 – 2008. It should be noted, however, that both Merck and Novartis continue to quietly invest in RNAi development programs. Furthermore, recent clinical data from the recent meeting of the American Society for Clinical Oncology in June 2011 indicate that meaningful clinical progress is being made with siRNA-based therapies. Both Atu027 (advanced solid cancer, Silence Therapeutics) and ALN-VSPO2 (liver cancer, Alnylam) achieved important safety endpoints in Phase I clinical trials. These developments, combined with recent advances in RNA chemistry that significantly reduce immunostimulation, suggest that RNAi remains a clinically viable therapeutic strategy.

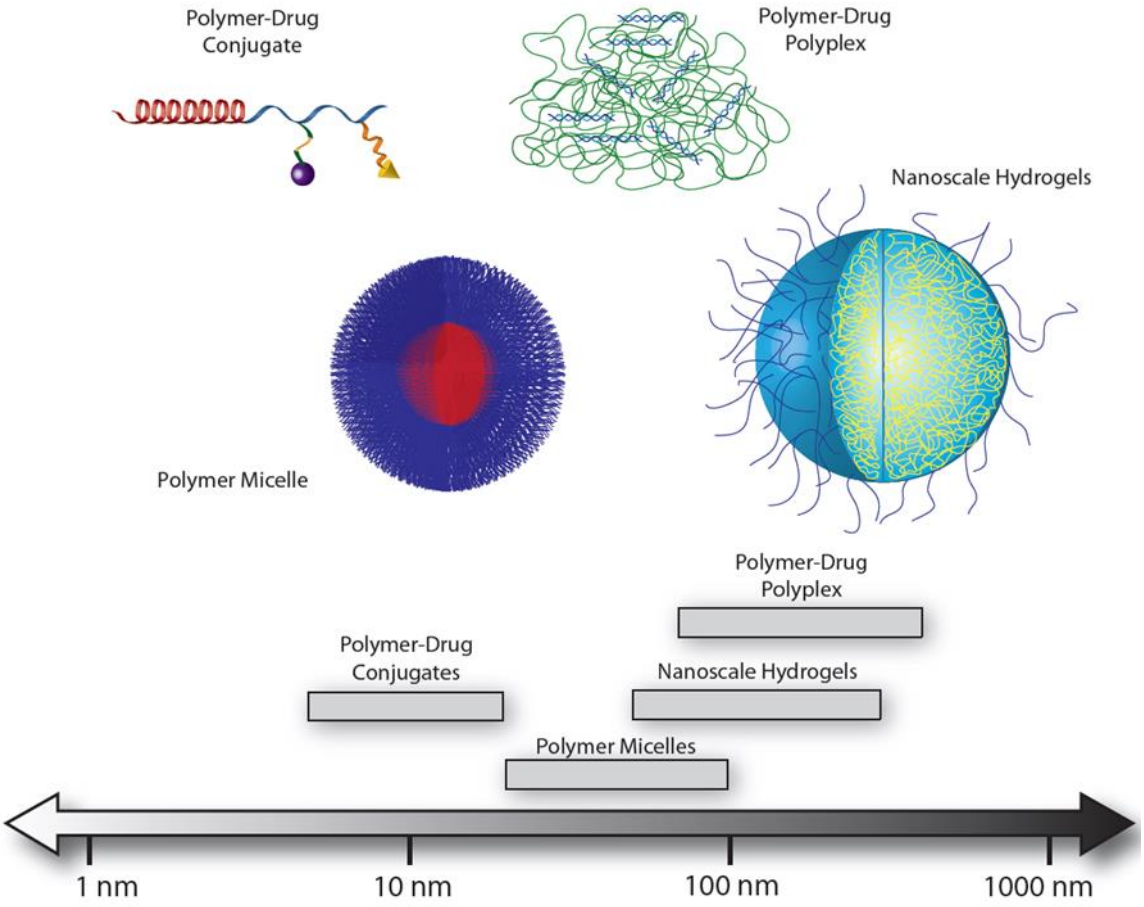

Figure 3.1 - Typical length scales of responsive nanoscale drug delivery systems

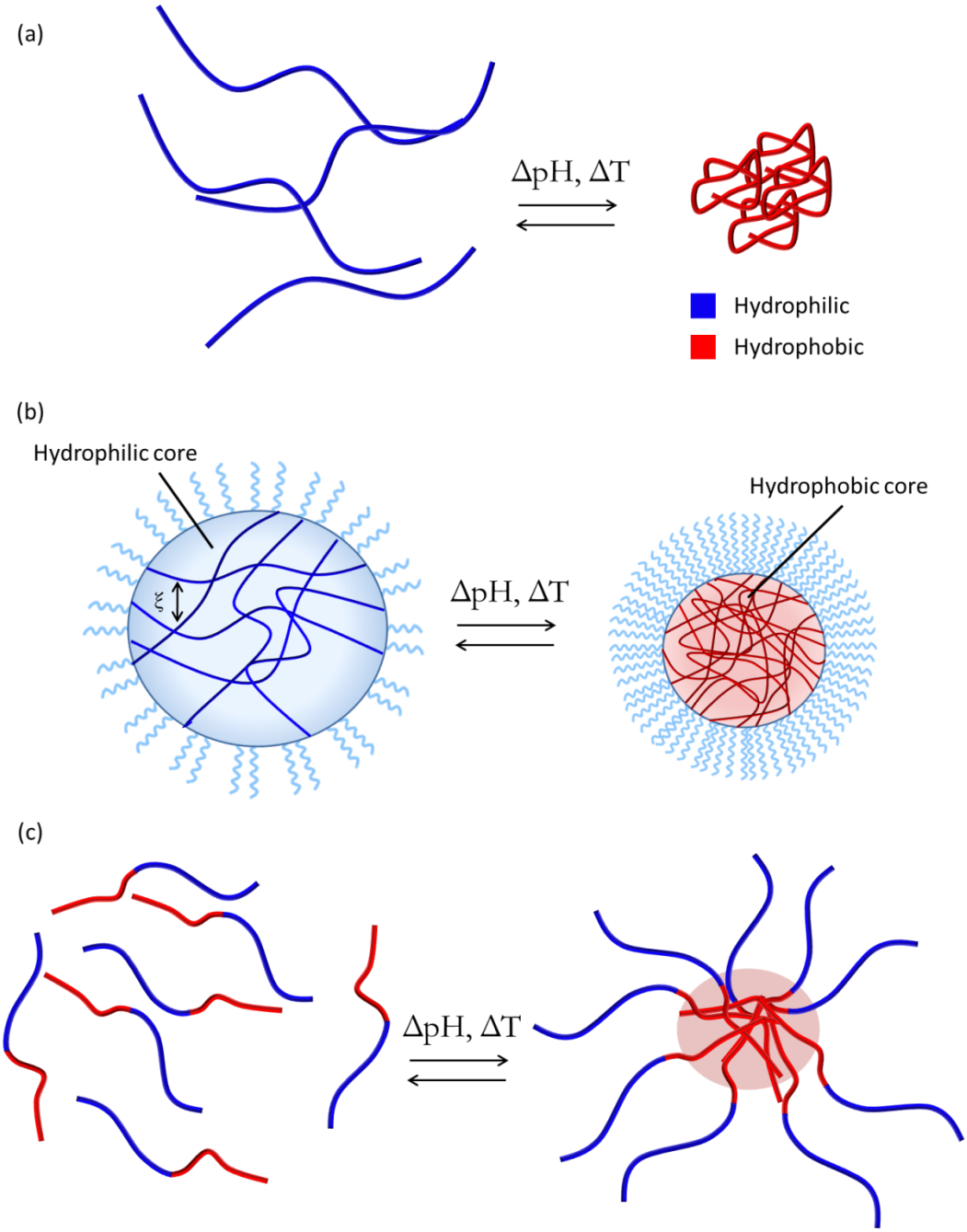

Figure 3.2 - Illustrative examples of responsive behavior. (a) Coil-to-globule transition of a linear polymer chain in solution. (b) Responsive swelling/deswelling of a surface-grafted crosslinked hydrogel particle. (c) Stimuli-responsive micellization of amphiphilic block copolymers

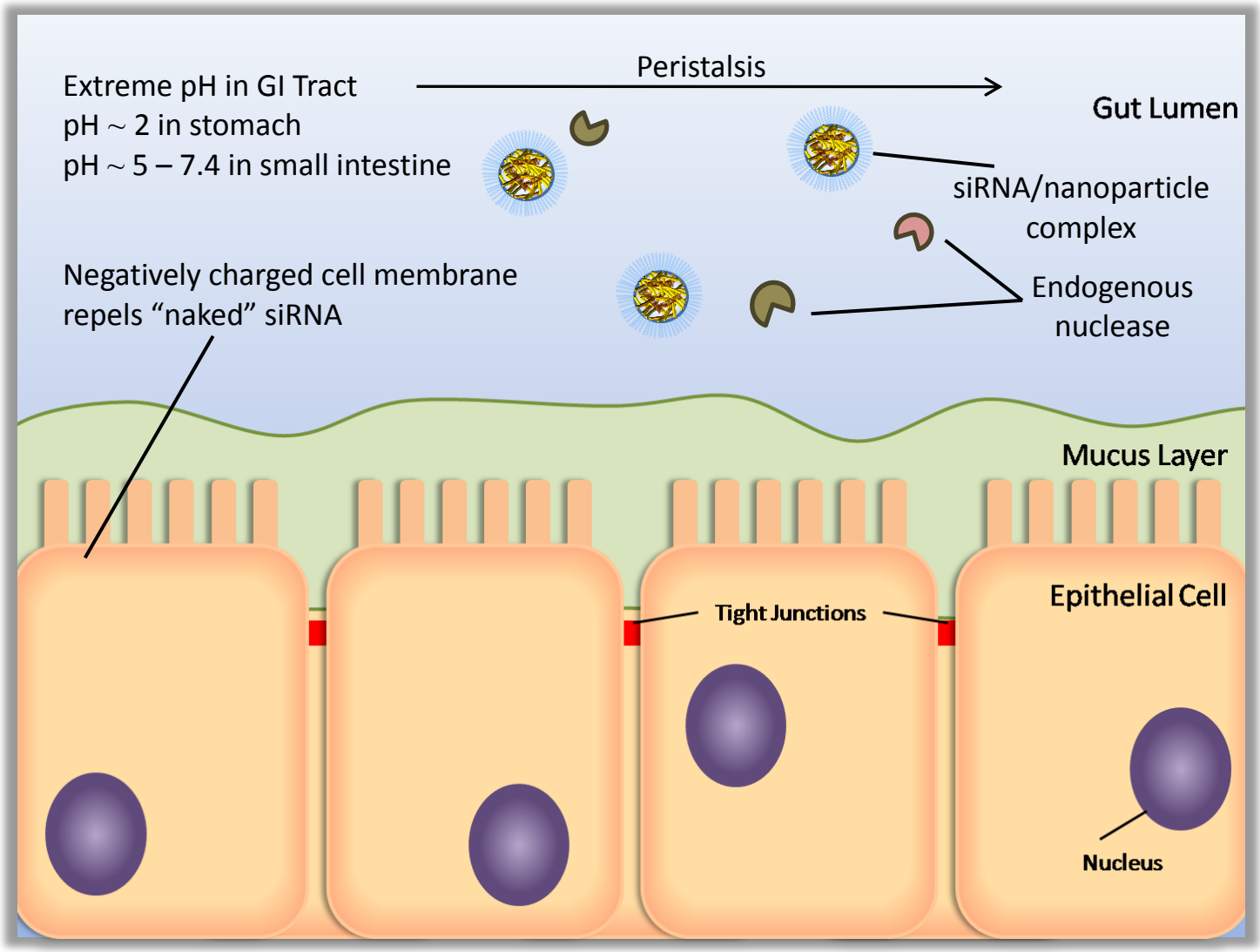

Figure 3.3 - Extracellular barriers to oral siRNA delivery

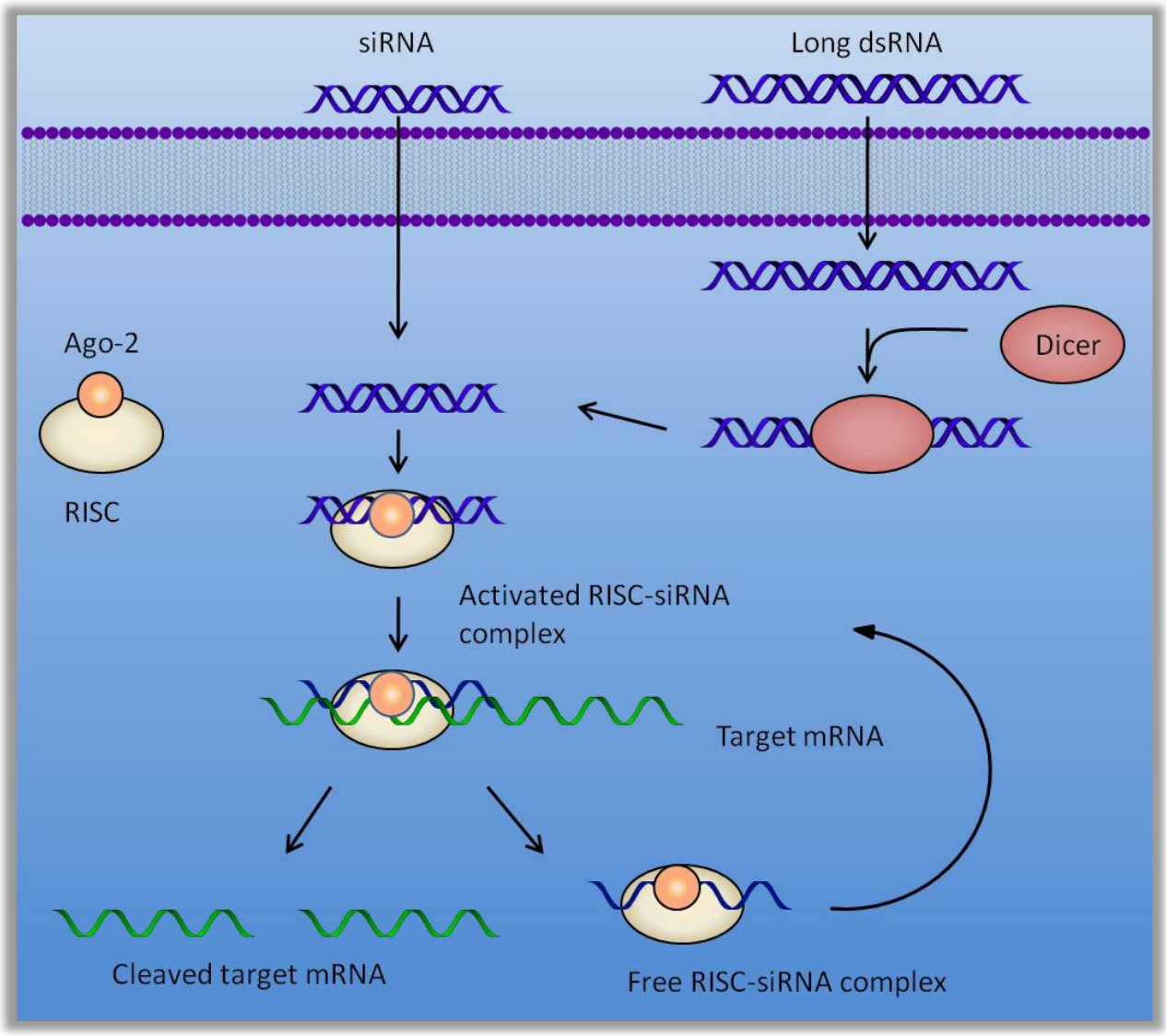

Figure 3.4 - Mechanism of siRNA-mediated RNA interference [92]

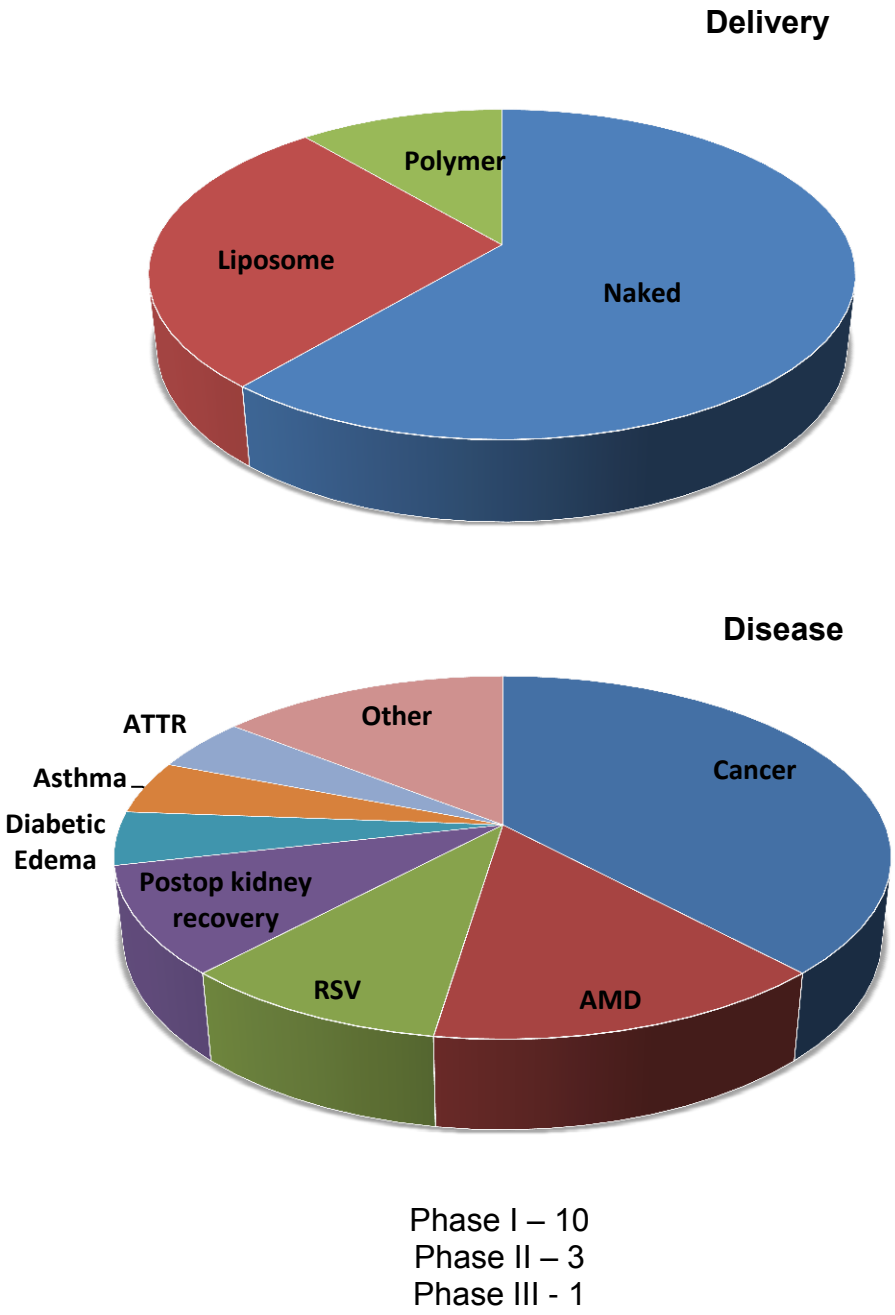

Figure 3.5 - Delivery vehicles and disease indication for RNAi products in clinical trials. Data adapted from ref. [126]. Abbreviations: AMD: Age-related macular degeneration; RSV: respiratory syncytial virus; ATTR: transthyretin amyloidoses

REFERENCES

1. Dincer S, Turk M, and Piskin E. Gene Therapy 2005;12:S139-S145.

2. Couvreur P, Brigger I, and Dubernet C. Advanced Drug Delivery Reviews 2002;54(5):631-651.

3. Langer R and Peppas NA. Aiche Journal 2003;49(12):2990-3006.

4. Couvreur P and Puisieux F. Advanced Drug Delivery Reviews 1993;10(2-3):141-162.

5. Couvreur P, Dubernet C, and Puisieux F. European Journal of Pharmaceutics and Biopharmaceutics 1995;41(1):2-13.

6. Langer R. Nature 1998:5-10.

7. Duncan R. Nature Reviews Cancer 2006;6:688-701.

8. Langer R. Nature 1998;392(6679):5-10.

9. Peppas NA. Advanced Drug Delivery Reviews 2004;56(11):1529-1531.

10. des Rieux A, Fievez V, Garinot M, Schneider YJ, and Preat V. Journal of Controlled Release 2006;116(1):1-27.

11. Duncan R. Nature Reviews Drug Discovery 2003;2(5):347-360.

12. Liechty WB, Kryscio DR, Slaughter BV, and Peppas NA. Annual Review of Chemical and Biomolecular Engineering, Vol 1 2010;1:149-173.

13. Ganta S, Devalapally H, Shahiwala A, and Amiji M. Journal of Controlled Release 2008;126(3):187-204.

14. Leobandung W, Ichikawa H, Fukumori Y, and Peppas NA. Journal of Applied Polymer Science 2003;87(10):1678-1684.

15. Liechty WB, Caldorera-Moore M, Phillips MA, Schoener C, and Peppas NA. Journal of Controlled Release;In Press, Corrected Proof.

16. Yessine M-A and Leroux J-C. Advanced Drug Delivery Reviews 2004;56(7):999-1021.

17. Lloyd JB, Pratten MK, Duncan R, Kooistra T, and Cartlidge SA. Biochemical Society Transactions 1984;12(6):977-978.

18. Pack DW, Hoffman AS, Pun S, and Stayton PS. Nature Reviews Drug Discovery 2005;4(7):581-593.

19. Gil ES and Hudson SA. Progress in Polymer Science 2004;29(12):1173-1222.

20. Schmaljohann D. Advanced Drug Delivery Reviews 2006;58(15):1655-1670.

21. Schild HG. Progress in Polymer Science 1992;17(2):163-249.

22. Khare AR and Peppas NA. Biomaterials 1995;16(7):559-567.

23. Malmsten M and Lindman B. Macromolecules 1992;25(20):5440-5445.

24. Topp MDC, Dijkstra PJ, Talsma H, and Feijen J. Macromolecules 1997;30(26):8518-8520.

25. Qiu Y and Park K. Advanced Drug Delivery Reviews 2001;53(3):321-339.

26. Ruel-Gariépy E and Leroux J-C. European Journal of Pharmaceutics and Biopharmaceutics 2004;58(2):409-426.

27. Alarcon CDH, Pennadam S, and Alexander C. Chemical Society Reviews 2005;34(3):276-285.

28. Hoare TR and Kohane DS. Polymer 2008;49(8):1993-2007.

29. Kost J and Langer R. Advanced Drug Delivery Reviews 2001;46(1-3):125-148.

30. Peppas NA, Bures P, Leobandung W, and Ichikawa H. European Journal of Pharmaceutics and Biopharmaceutics 2000;50(1):27-46.

31. Lowman AM, Morishita M, Kajita M, Nagai T, and Peppas NA. Journal of Pharmaceutical Sciences 1999;88(9):933-937.

32. Torres-Lugo M and Peppas NA. Macromolecules 1999;32(20):6646-6651.

33. Kamei N, Morishita M, Chiba H, Kavimandan NJ, Peppas NA, and Takayama K. Journal of Controlled Release 2009;134(2):98-102.

34. Alexandridis P, Holzwarth JF, and Hatton TA. Macromolecules 1994;27(9):2414-2425.

35. Boussif O, Lezoualch F, Zanta MA, Mergny MD, Scherman D, Demeneix B, and Behr JP. Proceedings of the National Academy of Sciences of the United States of America 1995;92(16):7297-7301.

36. Mok H and Park TG. Macromolecular Bioscience 2009;9(8):731-743.

37. Gosselin MA, Guo WJ, and Lee RJ. Bioconjugate Chemistry 2001;12(6):989-994.

38. Godbey WT, Wu KK, and Mikos AG. Journal of Biomedical Materials Research 1999;45(3):268-275.

39. Tanaka T. Physical Review Letters 1978;40(12):820-823.

40. Duscaronek K and Patterson D. Journal of Polymer Science Part A-2: Polymer Physics 1968;6(7):1209-1216.

41. Heskins M and Guillet JE. Journal of Macromolecular Science, Part A: Pure and Applied Chemistry 1968;2(8):1441 - 1455.

42. Bae YH, Okano T, and Kim SW. Journal of Polymer Science Part B-Polymer Physics 1990;28(6):923-936.

43. Shibayama M and Tanaka T. Advances in Polymer Science 1993;109:1-62.

44. Kopecek J. European Journal of Pharmaceutical Sciences 2003;20(1):1-16.

45. Inomata H, Goto S, and Saito S. Macromolecules 1990;23(22):4887-4888.

46. Katono H, Maruyama A, Sanui K, Ogata N, Okano T, and Sakurai Y. Journal of Controlled Release 1991;16(1-2):215-227.

47. Klouda L and Mikos AG. European Journal of Pharmaceutics and Biopharmaceutics 2008;68(1):34-45.

48. Bhattarai N, Ramay HR, Gunn J, Matsen FA, and Zhang M. Journal of Controlled Release 2005;103(3):609-624.

49. De P, Gondi SR, and Sumerlin BS. Biomacromolecules 2008;9(3):1064-1070.

50. Mathiowitz E, Jacob JS, Jong YS, Carino GP, Chickering DE, Chaturvedi P, Santos CA, Vijayaraghavan K, Montgomery S, Bassett M, and Morrell C. Nature 1997;386(6623):410-414.

51. Leong KW, Brott BC, and Langer R. Journal of Biomedical Materials Research 1985;19(8):941-955.

52. Cohen S, Yoshioka T, Lucarelli M, Hwang LH, and Langer R. Pharmaceutical Research 1991;8(6):713-720.

53. Shenoy D, Little S, Langer R, and Amiji M. Molecular Pharmaceutics 2005;2(5):357-366.

54. Shenoy D, Little S, Langer R, and Amiji M. Pharmaceutical Research 2005;22(12):2107-2114.

55. Cerritelli S, Velluto D, and Hubbell JA. Biomacromolecules 2007;8(6):1966-1972.

56. Oh JK, Siegwart DJ, Lee H-i, Sherwood G, Peteanu L, Hollinger JO, Kataoka K, and Matyjaszewski K. Journal of the American Chemical Society 2007;129(18):5939-5945.

57. Matsumoto S, Christie RJ, Nishiyama N, Miyata K, Ishii A, Oba M, Koyama H, Yamasaki Y, and Kataoka K. Biomacromolecules 2009;10(1):119-127.

58. Dufresne MH, Elsabahy M, and Leroux JC. Pharmaceutical Research 2008;25(9):2083-2093.

59. Owens DE and Peppas NA. International Journal of Pharmaceutics 2006;307(1):93-102.

60. Davis ME, Chen Z, and Shin DM. Nature Reviews Drug Discovery 2008;7(9):771-782.

61. Mukherjee S, Ghosh RN, and Maxfield FR. Physiological Reviews 1997;77(3):759-803.

62. Mellman I. Annual Review of Cell and Developmental Biology 1996;12:575-625.

63. Vaupel P, Kallinowski F, and Okunieff P. Cancer Research 1989;49(23):6449-6465.

64. Fisher OZ and Peppas NA. Macromolecules 2009;42(9):3391-3398.

65. Fisher O, Kim T, Dietz S, and Peppas N. Pharmaceutical Research 2009;26(1):51-60.

66. Hu Y, Litwin T, Nagaraja AR, Kwong B, Katz J, Watson N, and Irvine DJ. Nano Letters 2007;7(10):3056-3064.

67. Hu Y, Atukorale PU, Lu JJ, Moon JJ, Um SH, Cho EC, Wang Y, Chen J, and Irvine DJ. Biomacromolecules 2009;10(4):756-765.

68. Lee ES, Na K, and Bae YH. Journal of Controlled Release 2005;103(2):405-418.

69. Lee ES, Gao Z, Kim D, Park K, Kwon IC, and Bae YH. Journal of Controlled Release 2008;129(3):228-236.

70. Lee ES, Na K, and Bae YH. Nano Letters 2005;5(2):325-329.

71. Byrne JD, Betancourt T, and Brannon-Peppas L. Advanced Drug Delivery Reviews 2008;60(15):1615-1626.

72. Guelen L, Paterson H, Gaken J, Meyers M, Farzaneh F, and Tavassoli M. Oncogene 2003;23(5):1153-1165.

73. Sethuraman VA and Bae YH. Journal of Controlled Release 2007;118(2):216-224.

74. Ringsdorf H. Journal of Polymer Science Part C Polymer Symposium 1975;51:135-153.

75. Duncan R, Vicent MJ, Greco F, and Nicholson RI. Endocrine-Related Cancer 2005;12:S189-S199.

76. Cassidy J and Schätzlein AG. Expert Reviews in Molecular Medicine 2004;6(19):1-17.

77. Kamada H, Tsutsumi Y, Yoshioka Y, Yamamoto Y, Kodaira H, Tsunoda S-i, Okamoto T, Mukai Y, Shibata H, Nakagawa S, and Mayumi T. Clin Cancer Res 2004;10(7):2545-2550.

78. Etrych T, Jelínková M, Říhová B, and Ulbrich K. Journal of Controlled Release 2001;73(1):89-102.

79. Lavasanifar A, Samuel J, and Kwon GS. Advanced Drug Delivery Reviews 2002;54(2):169-190.

80. Bae Y, Fukushima S, Harada A, and Kataoka K. Angewandte Chemie-International Edition 2003;42(38):4640-4643.

81. Geng Y, Dalhaimer P, Cai SS, Tsai R, Tewari M, Minko T, and Discher DE. Nature Nanotechnology 2007;2(4):249-255.

82. Gillies ER and Frechet JMJ. Bioconjugate Chemistry 2005;16(2):361-368.

83. Kang SI, Na K, and Bae YH. Colloids and Surfaces a-Physicochemical and Engineering Aspects 2003;231(1-3):103-112.

84. Chen R, Khormaee S, Eccleston ME, and Slater NKH. Biomaterials 2009;30(10):1954-1961.

85. Chen RJ, Eccleston ME, Yue ZL, and Slater NKH. Journal of Materials Chemistry 2009;19(24):4217-4224.

86. Liechty WB, Chen R, Farzaneh F, Tavassoli M, and Slater NKH. Advanced Materials 2009;21(38-39):3910-3914.

87. Devalapally H, Shenoy D, Little S, Langer R, and Amiji M. Cancer Chemotherapy and Pharmacology 2007;59(4):477-484.

88. Raemdonck K, Demeester J, and De Smedt S. Soft Matter 2009;5(4):707-715.

89. Blanchette J and Peppas NA. Annals of Biomedical Engineering 2005;33(2):142-149.

90. Shinichi Kageyama SK, Michiko Hirayama, Yasuhiro Nagata, Hiroshi Imai, Taizo Shiraishi, Kazunari Akiyoshi, Andrew M. Scott, Roger Murphy, Eric W. Hoffman, Lloyd J. Old, Naoyuki Katayama, Hiroshi Shiku,. Cancer Science 2008;99(3):601-607.

91. Vauthier C and Couvreur P. Pharmaceutical Research 2006;23(7):1417-1450.

92. Whitehead KA, Langer R, and Anderson DG. Nature Reviews Drug Discovery 2009;8(2):129-138.

93. Yamanaka YJ and Leong KW. Journal of Biomaterials Science-Polymer Edition 2008;19(12):1549-1570.

94. Bhavsar MD, Shenoy, Dinesh B., Amiji, Mansoor M. Polymeric Nanoparticles for Delivery in the Gastro-Intestinal Tract. In: Torchilin VP, editor. Nanoparticulates as Drug Carriers. London: Imperial College Press, 2006.

95. Morishita M and Peppas NA. Drug Discovery Today 2006;11(19-20):905-910.

96. Matsumura Y and Maeda H. Cancer Research 1986;46(12):6387-6392.

97. Couvreur P, Kante B, Roland M, Guiot P, Bauduin P, and Speiser P. Journal of Pharmacy and Pharmacology 1979;31(5):331-332.

98. Brannon-Peppas L and Blanchette JO. Advanced Drug Delivery Reviews 2004;56(11):1649-1659.

99. Alexis F, Pridgen E, Molnar LK, and Farokhzad OC. Molecular Pharmaceutics 2008;5(4):505-515.

100. Fang C, Shi B, Pei Y-Y, Hong M-H, Wu J, and Chen H-Z. European Journal of Pharmaceutical Sciences 2006;27(1):27-36.

101. Tong R and Cheng JJ. Polymer Reviews 2007;47(3):345-381.

102. Phillips MA, Gran ML, and Peppas NA. Nano Today 2010;5(2):143-159.

103. Maruyama K, Takahashi N, Tagawa T, Nagaike K, and Iwatsuru M. Febs Letters 1997;413(1):177-180.

104. Fire A, Xu S, Montgomery MK, Kostas SA, Driver SE, and Mello CC. Nature 1998;391(6669):806.

105. de Fougerolles AR. Human Gene Therapy 2008;19(2):125-132.

106. Tijsterman M, Ketting RF, and Plasterk RHA. Annual Review of Genetics 2002;36(1):489-519.

107. Bartlett DW and Davis ME. Nucl. Acids Res. 2006;34(1):322-333.

108. Elbashir SM, Harborth J, Lendeckel W, Yalcin A, Weber K, and Tuschl T. Nature 2001;411(6836):494-498.

109. Cun D, Jensen LB, Nielsen HM, Moghimi M, and Foged C. Journal of Biomedical Nanotechnology 2008;4(3):258-275.

110. Bernstein E, Caudy AA, Hammond SM, and Hannon GJ. Nature 2001;409(6818):363-366.

111. Stark GR, Kerr IM, Williams BRG, Silverman RH, and Schreiber RD. Annual Review of Biochemistry 1998;67:227-264.

112. Hammond SM, Bernstein E, Beach D, and Hannon GJ. Nature 2000;404(6775):293-296.

113. Hammond SM, Boettcher S, Caudy AA, Kobayashi R, and Hannon GJ. Science 2001;293(5532):1146-1150.

114. Ameres SL, Martinez J, and Schroeder R. Cell 2007;130(1):101-112.

115. Song E, Lee S-K, Wang J, Ince N, Ouyang N, Min J, Chen J, Shankar P, and Lieberman J. Nat Med 2003;9(3):347-351.

116. Davis ME, Zuckerman JE, Choi CHJ, Seligson D, Tolcher A, Alabi CA, Yen Y, Heidel JD, and Ribas A. Nature 2010;464(7291):1067-1070.

117. Sklan EH and Glenn JS. Gastroenterology 2007;132(7):2291-2295.

118. Giladi H, Ketzinel-Gilad M, Rivkin L, Felig Y, Nussbaum O, and Galun E. Molecular Therapy 2003;8(5):769-776.

119. Klein C, Bock CT, Wedemeyer H, Wustefeld T, Locarnini S, Dienes HP, Kubicka S, Manns MP, and Trautwein C. Gastroenterology 2003;125(1):9-18.

120. Peng JL, Zhao YG, Mai JH, Pang WK, Wei XH, Zhang PZ, and Xu YH. Journal of General Virology 2005;86:3227-3234.

121. Xuan BQ, Qian ZK, Hong J, and Huang WD. Virus Research 2006;118(1-2):150-155.

122. Yokota T, Sakamoto N, Enomoto N, Tanabe Y, Miyagishi M, Maekawa S, Yi L, Kurosaki M, Taira K, Watanabe M, and Mizusawa H. Embo Reports 2003;4(6):602-608.

123. Randall G, Grakoui A, and Rice CM. Proceedings of the National Academy of Sciences of the United States of America 2003;100(1):235-240.

124. Frank-Kamenetsky M, Grefhorst A, Anderson NN, Racie TS, Bramlage B, Akinc A, Butler D, Charisse K, Dorkin R, Fan Y, Gamba-Vitalo C, Hadwiger P, Jayaraman M, John M, Jayaprakash KN, Maier M, Nechev L, Rajeev KG, Read T, Rohl I, Soutschek J, Tan P, Wong J, Wang G, Zimmermann T, de Fougerolles A, Vornlocher HP, Langer R, Anderson DG, Manoharan M, Koteliansky V, Horton JD, and Fitzgerald K. Proceedings of the National Academy of Sciences of the United States of America 2008;105(33):11915-11920.

125. Judge AD, Robbins M, Tavakoli I, Levi J, Hu L, Fronda A, Ambegia E, McClintock K, and MacLachlan I. Journal of Clinical Investigation 2009;119(3):661-673.

126. Rossi JJ, Lares MR, and Ouellet DL. Trends in Biotechnology 2010;28(11):570-579.

Chapter 4: Tunable, responsive nanogels containing tert-butyl methacrylate and 2-(tert-butylamino)ethyl methacrylate

4.1. INTRODUCTION

Responsive polymers are a class of functional materials capable of undergoing a discrete behavioral change when subjected to chemical (pH, redox potential, ionic strength) or physical (temperature, light, ultrasound, electrical field) stimuli. Distinct transitions in solubility, hydrophilic/hydrophobic balance, and physical conformation result from these stimuli and are commonly manifested as coil-globule transitions; network swelling and deswelling; sol-gel transitions; and self-assembly [1, 2]. Tailoring these critical phenomena and resultant physicochemical properties of polymers by tuning copolymer composition is an attractive strategy that has been routinely employed for materials in drug delivery [3-7], tissue engineering [8-10], diagnostics and sensing [11, 12], and "smart" optical [13, 14] applications.

A particularly well-studied example of the influence of copolymer composition on critical phenomena is in the thermoresponsive polymer poly(N-isopropyl acrylamide) (PNIPAAm). Temperature has been widely used to induce phase transitions in polymer networks because of its ease of modulation and applicability in biomedical applications [15] and PNIPAAm is capable of undergoing a reversible, temperature-dependent phase transition near 32°C [16]. This lower solution critical temperature (LCST) can be depressed through the inclusion of hydrophobic moieties in the polymer chain as demonstrated by copolymerizing NIPAAm with t-butyl acrylamide (TBAm) [17], n-butyl methacrylate (BMA) [18], and 5,6-benzo-2-methylene-1,3-dioxepane [19]. Conversely, the LCST can be raised by copolymerizing thermoresponsive polymers with hydrophilic

[20] or ionic monomers such as 2-(dimethylamino)ethyl methacrylate (DMAEMA) [21] or (meth)acrylic acid (MAA) [22].

Inclusion of hydrophobic or hydrophilic moieties in pH-responsive polymers has been explored in analogous fashion. Monomers containing ionizable tertiary amine groups, such as DMAEMA or 2-(diethylaminoethyl) methacrylate (DEAEMA), are typically used in pH-responsive polymers. Armes and co-workers [23-25] created a variety of DEAEMA-based polymers through several polymerization methods; synthesizing responsive microgels via emulsion polymerization [23], diblock copolymers via group transfer polymerization [25], and triblock copolymer micelles via atom transfer radical polymerization (ATRP)[24]. Stayton and collaborators [6, 26, 27] employed a polymerization to create well-controlled block copolymers of DEAEMA and BMA to create responsive micelles for delivery of plasmid DNA [27] or small interfering RNA [6]. These copolymer micelles possess tunable pH-responsiveness and membrane-disruptive activity depending on polymer composition and block length.

Siegel and Cornejo-Bravo [28] examined copolymerization of PDEAEMA gels with BMA or 2-hydroxyethyl methacrylate (HEMA) and resultant impact on buffering range. As the hydrophobic character of the polymer increased (via inclusion of BMA), the buffering pH was depressed. This observation can be explained by relative strength of polymer/polymer interactions to that of polymer/solvent/ion interaction. In addition to directly impacting critical phenomena and physical properties like size and surface charge, copolymer composition also influences circulation time [29, 30], protein binding [31], cellular internalization [32], cytocompatibility [33, 34], and drug loading and release [35].

Recent focus on biomedical applications of responsive hydrogels has prompted examination of these bulk critical phenomena in nanoscale systems [36-38]. Nanoscale hydrogels, or nanogels, are particularly attractive as drug delivery agents owing to their facile manufacture, tunable physicochemical characteristics, and repeatable release [39]. Furthermore, their covalent crosslinking endows them with mechanical integrity not available in their self-assembled counterparts. Several recent efforts have explored the utility of responsive nanoscale hydrogel carriers in drug delivery [33, 40, 41], demonstrating release of biological therapeutics such as insulin and imaging agents such as gold.

We have previously reported the development of a UV-initiated, oil-in-water photoemulsion polymerization [33, 42] that allows for the facile synthesis of sub-100 nm hydrogel particles without specialized conditions requisite for RAFT or ATRP. Analogous work in thermal-initiated emulsion polymerizations of DEAEMA has resulted in sub-50 nm nanogels [43]. We have used the UV-initiated photoemulsion method as a robust synthesis for a panel of tunable, responsive polymer networks. As mentioned in the preceding text, BMA, both n-butyl methacrylate and t-butyl methacrylate, have been used in conjunction with tertiary amine methacrylates to modulate physicochemical properties. TBAEMA, a secondary amine methacrylate, is less well studied. Morse, et al. [44] recently provided a thorough characterization of TBAEMA latex particles and highlighted their applicability as Pickering emulsifiers. Previously, TBAEMA was evaluated in copolymer coatings for surgical instruments and orthopedic implants because of its antibacterial activity and low human toxicity [45].

In the present study, we examine the influence of TMBA and TBAEMA on the aqueous solution properties of poly(ethylene glycol) methyl ether methacrylate (PEGMA)-grafted DEAEMA nanogels. This represents, to the best of our knowledge, the first known examples of P(DEAEMA-co-TBAEMA-g-PEGMA) nanogels synthesized via aqueous photoemulsion polymerization. We also provide a direct comparison of physicochemical properties with a P(DEAEMA-co-TMBA-g-PEGMA) nanogel system. This polymerization method represents a platform from which abundant combinations of methacrylate-based hydrogels could be produced to create responsive hydrogels with nanoscale dimensions and tunable physicochemical properties (Figure 4.1).

4.2. MATERIALS AND METHODS

4.2.1. Polymer synthesis

Hydrogel particles of nanoscale dimensions were synthesized via UV-initiated free radical photoemulsion polymerization/crosslinking according to previous reports from our laboratory [33, 42]. Briefly, 2-(diethylamino) ethyl methacrylate (DEAEMA, Sigma-Aldrich, St. Louis, MO), 2-(tert-butylamino)ethyl methacrylate (TBAEMA, Polysciences, Inc., Warrington, PA), tert-butyl methacrylate (TBMA, Sigma-Aldrich, St. Louis, MO), and tetra(ethylene glycol) dimethacrylate (TEGDMA, Sigma-Aldrich, St. Louis, MO) were passed through a column of basic alumina powder to remove inhibitor prior to use. Poly(ethylene glycol) methyl ether methacrylate (PEGMA), Mn ~ 2080, (Sigma-Aldrich, St. Louis, MO) was used as received. DEAEMA, TEGDMA, and TBMA or TBAEMA were added to an aqueous solution containing 5 wt% PEGMA,

Irgacure 2959 (Ciba Geigy, Tarrytown, NY) at 0.5 wt% of total monomer, 4 mg mL-1 Brij-30 (Acros Organics, Fair Lawn, NJ) and 1.16 mg mL-1 (3.4 mM) ionic surfactant myristyltrimethylammonium bromide (MyTAB, Sigma-Aldrich, St. Louis, MO). The reaction pH was routinely pH 8.5. The mixture was emulsified using a Misonix Ultrasonicator (Misonix, Inc., Newtown, CT). The emulsion was purged with nitrogen gas and exposed to a UV source for 2.5 hr with constant stirring.

4.2.2. Polymer Purification

MyTAB, Brij 30, and unreacted monomers were removed by repeatedly inducing polymer-ionomer collapse, separating particles by centrifugation for 10 min at 3,200×g, and resuspending in 0.5 N HCl. Polymer particles were dialyzed against ddH_2O for at least 7 days in 12 – 14 kDa molecular weight cutoff dialysis tubing (Spectrum Labs, Rancho Dominguez, CA) with water changes twice daily. Following dialysis, polymers were flash frozen in liquid N_2 and lyophilized for 5 days.

4.2.3. ^{1}H- NMR Spectroscopy

The composition of uncrosslinked polymer formulations and purification fractions were investigated using a Varian (Palo Alto, CA) DirectDrive 400 MHz nuclear magnetic resonance spectrometer equipped with automatic sampler. Deuterium oxide (D_2O, 99.9%) was obtained from Cambridge Isotope Laboratories (Andover, MA). Deuterium chloride (DCl, 100.0%) and methyl sulfoxide-d6 (DMSO, 99.5%) with 0.03% tetramethyl silane (TMS) were obtained from Acros Organics (Fairlawn, NJ). All glassware, including NMR Tubes (Wilmad Lab Glass, Vineland, NJ), 2 mL sample vials, and Pasteur pipettes were dried overnight in a vacuum oven. Uncrosslinked polymer

samples of approximately 50 mg were weighed directly in sample vials and D_2O was added to bring the final polymer concentration to 25 mg mL-1. Samples were briefly sonicated in a sonic bath and transferred to NMR tubes for subsequent analysis. Aliquots of the purification supernatants were frozen at -80°C and lyophilized with a Labconco FreeZone -105°C benchtop lyophilizer (Kansas City, MO) for 48 hours. The resulting dry residue was dissolved in 0.75 ml deuterated DMSO and transferred to NMR tubes. All NMR Spectra were analyzed using SpinWorks 3™ software.

4.2.4. Dynamic Light Scattering Analysis

The hydrodynamic diameter in aqueous suspension of the polymer networks was measured using a measured using a Brookhaven ZetaPlus instrument (Brookhaven Instruments Corp.) operating with a 659 nm diode laser source. Dynamic light scattering (DLS) measurements of particle size and its response to dynamic pH were conducted by resuspending lyophilized particles in PBS at 0.75 mg mL^{-1}. The suspension pH was adjusted to 10.5 using 1 N NaOH and gradually lowered to pH 3.5 using 1 N HCl. Measurements of the z-average particle size were collected at 23°C. Subsequent studies employed a Malvern Zetasizer NanoZS (Malvern Instruments Corp., Malvern, UK) operating with a 633 nm laser source equipped with MPT-2 Autotitrator. DLS measurements of particle size and pH-responsive behavior were conducted by resuspending lyophilized particles in PBS at 0.5 mg mL^{-1}. The suspension pH was adjusted to 10.5 using 1 N NaOH and gradually lowered to pH 3.5 using 1 N HCl. Measurements of the z-average particle size were collected at 25°C and pH intervals of 0.5.

4.2.5. Transmission Electron Microscopy

Transmission electron micrographs were collected using a FEI Tecnai (Hillsboro, OR) Transmission Electron Microscope (80 kV) at magnifications from 16,500× to 160,000×. Lyophilized particles were diluted in ddH_2O and stained with 2% uranyl acetate immediately prior to imaging. Typically, 5 µL of 0.02 w/v% of particle suspension was dropped onto a 400-mesh Formvar-coated copper TEM grid (Electron Microscopy Sciences, Hatfield, PA) and excess liquid wicked off using filter paper. An equivalent volume of 2 w/v% uranyl acetate was then added to the grid and allowed to stain for 60 seconds before excess liquid was wicked away with filter paper. Particle volume in the dry state was taken as the cube of mean diameter from TEM images. Particle diameters were calculated from the particle area as determined by an ImageJ particle sizing algorithm. Reported values represent the mean ± standard deviation ($n > 50$).

4.2.6. Electrophoretic Light Scattering

The effective surface ζ-potential of the polymer networks was measured using a Brookhaven ZetaPlus instrument (Brookhaven Instruments Corp.) operating with a 659 nm diode laser source. Measurements of ζ-potential as a function of pH were conducted by resuspending lyophilized particles in 5 mM phosphate buffer at 0.5 mg mL^{-1}. The suspension pH was adjusted to 10.5 using 1 N NaOH and gradually lowered to pH 3.5 using 1 N HCl. Electrophoretic light scattering measurements of the surface ζ-potential were collected at 22°C with nanogels suspended in 5 mM sodium phosphate.

4.2.7. Fluorescence Spectroscopy

Pyrene (Puriss grade, >99.0%, Sigma-Aldrich, St. Louis, MO) was used without further purification. Disodium phosphate heptahydrate ($Na_2HPO_4 \bullet 7H_2O$) and sodium phosphate monohydrate ($NaH_2PO_4 \bullet H_2O$) were purchased from Fisher Chemical. Phosphate buffer solutions from pH 5.8 – pH 8.0 were prepared by combining solutions of 0.2M $NaH_2PO_4 \bullet H_2O$ and 0.2M $Na_2HPO_4 \bullet 7H_2O$. Polymer solutions were prepared by suspending dry nanoparticles in ultrapure DI water at a concentration of 1 mg mL^{-1}. These preceding two solutions were then mixed in equal volumes to give a final concentration of nanoparticles at 0.5 mg mL^{-1} in 100 mM phosphate buffer. Pyrene was dissolved in methanol at 1 mM. Fluorescence spectra were collected on a Fluorlog-3 Spectrofluorometer (Jobin Yvon, Horiba Scientific, Edison, NJ). Emission spectra were collected with λ_{ex} = 339 nm, 1 nm increments, 1.5 nm slit with for excitation, 1 nm slit width for emission, and 0.8 s integration time. Excitation spectra were collected with λ_{em} = 390 nm, 1 nm increments, 1 nm slit for excitation, and 1.5 nm for emission, and 0.8 s integration time.

4.3. RESULTS AND DISCUSSION

4.3.1. Polymer Synthesis

A series of tunable, polycationic nanoscale hydrogels comprised of a crosslinked core of PDEAEMA surface grafted with PEG was synthesized using photoemulsion polymerization. Polymer composition was varied from 0 ~ 25 mol% TBMA or TBAEMA in the copolymer to determine the effect of core hydrophobicity on

physicochemical properties. A methoxy-terminated poly(ethylene glycol) methacrylate (PEGMA, MW ~ 2080) was employed as an emulsion stabilizer and to provide grafted PEG chains on the nanogel surface. PEGMA is commercially available and routinely used as a reactive stabilizer in the aqueous emulsion polymerization of methacrylate copolymers [23, 44] The MW 2080 PEGMA was chosen because previous work has indicated a minimum PEG graft size of 2 kDa was needed to minimize nonspecific protein adsorption [46].

As this polymerization method is a UV-initiated free radical polymerization, the copolymer could be optimally assumed to be random, whereby monomers are incorporated into the copolymer based on their relative feed concentrations and reactivities in no preferential order. This assumption can be evaluated by examining the reactivity ratios (r_1, r_2) for constituent monomer pairs (M_1 and M_2). Generally, copolymerizations with $r_1r_2 = 0.5 – 2$ can be considered to obey moderate ideal behavior [47]. To estimate the reactivity ratios between monomer pairs, the Q-e scheme [47, 48] was used to calculate r_1 and r_2 values. Reported Q-e values and resulting reactivity ratios are tabulated in Table 4.2.

From these data, it can be seen that all estimated values for r_1 and r_2 lie between 0.4 – 2.0, suggesting that the resultant copolymer can be described as ideal, with copolymer compositions closely related to the feed concentration. For the purpose of this analysis, the ratio between hydrophobic (TBMA or TBAEMA) and ionizable (DEAEMA) monomer was considered to be the key ratio in modulating network hydrophobicity and its influence on resultant physicochemical properties, such as dynamic swelling/deswelling, zeta potential, etc. It is well known that adjusting polymer

composition and altering polymer-solvent interactions can impact various critical phenomena, including temperature (LCST/UCST) or pH at which polymer chains undergo phase transitions [15, 49]. For this reason, polymer formulation nomenclature was established such that the numerical suffix on the polymer name (e.g. PDETB30 or PDETBA20) refers to the moles of hydrophobic monomer (TBMA or TBAEMA) per 100 moles of DEAEMA.

4.3.2. Polymer Purification

As described in our previous reports [33, 42], purification was achieved by repeatedly inducing a polyelectrolyte-ionomer transition. Following polymerization, 1 N HCl was added directly to the reaction flask at 1:1 (vol/vol) ratio with the reaction mixture to protonate DEAEMA pendant groups. Following this step, the acidified reaction mixture was added to acetone to bring the final acetone concentration to 80 vol%. The addition to an organic solvent was used to lower the dielectric strength (ε) of the suspension and facilitate the transition from polyelectrolyte regime to ionomer regime [50]. In the polyelectrolyte regime, counterions diffuse freely through polymer networks, while in the ionomer regime, counterions are bound to ionized groups on the polymer network in ion pairs. This transition is shown schematically in Fig. The energy gain (E) from electrostatic attraction of ions can be described by the equation:

$$E = \frac{e^2}{\varepsilon \cdot a} \tag{4.1}$$

where e is the charge of the ion species, ε is the dielectric strength, and a is the distance between charges in the ion pair [50].

The ionomer regime is rare in solvents with a sufficiently high dielectric constant (e.g. water, $\varepsilon = 81$). As the solvent dielectric strength is lowered, however, the formation of ion pairs decreases the concentration of mobile counterions and concomitantly the gel osmotic pressure. Moreover, these ion pairs attract one another through dipole-dipole interactions and form multiplets. These mutliplets act as additional physical crosslinks in the gel and support gel collapse. By using the polymer-ionomer transition, these nanogels can be simultaneously collapsed and ionized, a state that resulted in rapid flocculation and sedimentation. The ionomer phase was then separated from the solvent by centrifugation. Surfactant removal was monitored by analyzing the supernatant from each purification cycle via ^{1}H-NMR. A purification cycle is defined as (1) protonation of DEAEMA with 0.5 N HCl, (2) ionomer phase transition by addition of 4 vol. equivalents of acetone (80 vol% acetone total), and (3) centrifugation of ionomer/solvent mixture. The progressive removal of surfactant from the purification supernatant can be seen in Figure 4.4 and Table 4.3.

In Figure 4.4, the peaks at 3.3 ppm and 2.5 ppm can be attributed to the solvent residual peak and HDO, respectively. The strong peak near 3.5 ppm disappears rapidly following the Cycle 1, signifying the loss of unreacted PEGMA and/or Brij-30, both of which possess oxyethylene protons ($-CH_2-CH_2-O-$) with $\delta = 3.50$ in DMSO. Additionally, the peaks near $\delta = 1.15 - 1.30$ diminished significantly following Cycle 1. This likely indicates the loss of Brij-30 and MyTAB, both of which possess aliphatic protons ($-CH_2-CH_2-$) near 1.2 ppm. Following purification cycle 6, any residual surfactants or unreacted monomers were removed by dialysis.

The uncrosslinked polymer chains were purified in a similar fashion, albeit with much higher relative centrifugal force (RCF). Sedimentation of uncrosslinked polymer chains following polyelectrolyte-ionomer transition required RCF of 30,000×g or greater. The absence of a oxyethylene peak (δ = 3.6 ppm) in the polymer synthesized without PEGMA, P(DEAEMA-co-TBMA) (PDB30), serves as additional evidence that Brij-30 was successfully removed during the purification process.

4.3.3. ^{1}H-NMR Spectroscopy

To verify polymer composition, the ^{1}H NMR spectra of uncrosslinked nanoscale hydrogels were collected and analyzed (Figure 4.5 and Figure 4.6). The results are summarized in Table 4.4. The resultant copolymer ratio of t-butyl (either from TBMA or TBAEMA) to DEAEMA closely mirrors that of the comonomer ratio in the feed. This result is expected given the reactivity ratios of constituent comonomers, all containing methacrylate groups, are relatively similar, as previously shown in Table 4.2. Furthermore, the pairwise products of reactivity ratios (r_1r_2) lie within the region described by ideal radical polymerizations, resulting in a random copolymer.

The peak assignments and spectra for both TBMA- and TBAEMA-containing copolymers are shown in Figure 4.5 and Figure 4.6. For this analysis, the [-N-(C***H*****$_2$**-$CH_3)_2$-] (peak *d,* 3.1 ppm) was selected as the basis for determining the relative molar quantity of DEAEMA, the [-C-(C***H*****$_3$**$)_3$-] (peak *h*, 1.3 ppm) for determining the relative molar quantities of TBMA (Figure 4.5) and TBAEMA (Figure 4.6), and the [-O-C***H*****$_2$**-C***H*****$_2$**-] (peak *f*, 3.6 ppm) for determining the relative molar quantity of PEGMA.

A notable observation of the data in Table 4.4 is the poor efficiency with which PEGMA was incorporated into the copolymer; below 10% of PEGMA in the feed was detected in the copolymer. PEGMA is a large (MW ~ 2,080) and highly hydrophilic macromonomer and consequently may not partition into the oil phase of the emulsion, where DEAEMA, TBMA, and TBAEMA reside. Rather, it is far more likely that the PEG macromonomer adsorbed to the oil droplet surface along with Brij®-30 and MyTAB, serving to reduce interfacial tension at the oil-water boundary. Based on the relative molar compositions determined in Table 4.4, the copolymer contains approximately 5 wt% PEG. Other reports involving emulsion-based polymerizations of DEAEMA/PEGMA to form microgels [23] or nanogels [42] have reported PEG incorporation of 5 - 7 wt% polymer. A consequence of the PEG macromonomer's preferential association with the emulsion interface and water phase is that it will predominantly graft to the particle surface, with incorporated PEG chains protruding in the surrounding aqueous media. . Indeed, ^{1}H-NMR studies of crosslinked nanogels (Figure 4.7) revealed a strong peak at 3.6 ppm (peak *a*), indicative of oxyethylene protons from PEG. Protons from the ethlyamino groups of DEAEMA (peak *c,* 3.2 ppm and peak *d*, 1.25 ppm) are also present, although suppressed relative to their uncrosslinked spectra (Figure 4.5 and Figure 4.6). Similar observations were reported by Fisher et al. [42] in our initial reports of crosslinked nanogels synthesized via photoemulsion polymerization. These results suggest that the vast majority of DEAEMA and TBMA/TBAEMA protons are sequestered in the network core, unavailable for solvation and detection by ^{1}H-NMR. This PEG coating may serve to impart colloidal stability and minimize opsonization potential in biomedical applications [51].

4.3.4. Electron Microscopy

Nanoscale hydrogels of varying composition were initially subjected to TEM and DLS measurements to confirm nanoscale dimensions and pH-responsive behavior. Analysis of TEM micrographs revealed successful formation of nanoscale hydrogel networks. Nearly all preparations appear to have a narrow particle size distribution with a mean diameter of approximately 50 nm, as seen in Figure 4.8. Diameters of the dry nanogels are tabulated in Table 4.5.

The particle area was determined using ImageJ software to identify particles based on relative contrast between particle and background. This measurement was then used to obtain the dry diameter of nanoscale hydrogels. Images obtained at 26,500× and 43,000× magnification were used most frequently to construct the number-average particle size distribution, as they offered to best combination of particle number, typically 40 – 50 particles/image, and resolution. In practice, however, images obtained at magnifications of 16,500× – 60,000× could be used with little variation in the calculated diameter and standard deviation. Both PDETBA20 (Figure 4.8, Panel F) and PDETBA30 (Figure 4.8, Panel G) exhibit a mean particle size greater than that of the other formulations, 63 nm and 66 nm. This can perhaps be ascribed to the staining procedure. A staining time of 1 minute was determined sufficient for uranyl acetate to penetrate nanogels of TEGDMA-crosslinked P(DEAEMA-co-TBMA-g-PEGMA) (PDETB30), providing homogenous staining and high contrast. However, this staining time was not sufficient for copolymers with 20 mol% TBAEMA (PDETBA20) and 30 mol% TBMA (PDETBA30) and is most evident in Figure 4.8, Panel G, where a hazy ring outlines the particle perimeter. This is present, albeit more subtly, in Figure 4.8,

Panel F. This blurred boundary made identification of particle perimeter more inaccurate and likely resulted in an overestimation of the true particle area. In all cases, the number-average particle size distribution was roughly Gaussian, an example of which is seen in Figure 4.9.

4.3.5. Dynamic Light Scattering

Dynamic light scattering was used to probe physicochemical properties of the nanoscale hydrogels, including their hydrodynamic diameter, swelling ratio, and critical swelling pH. The latter is of particular interest in hydrogel-mediated intracellular drug delivery because this parameter is an indication of when the network swells and will permit drug efflux to the surrounding milieu.

In the pH-dependent phase transitions described in the following text, nanogels were first adjusted to pH 10.5 and titrated to progressively lower pH values using HCl, as described in the Materials and Methods. The justification is that acidification (via the action of endosomal ATP-dependent proton pumps) is the most prevalent pH-dependent pathway an intracellular drug delivery carrier would experience. In our tests, the pH-dependent swelling response was completely reversible with no evidence of hysteresis upon titrating from pH 10.5 to pH 3.5 and back to pH 10.5. No salt induced flocculation was observed in these studies over the course of two titration cycles.

The hydrodynamic diameter and polydispersity index reported represent those determined by Cumulant analysis as outlined in ISO 13321 [52]. Other analysis algorithms exist, such as CONTIN and NNLS, but the cumulant analysis is the readily accepted and has been widely adopted by industry and academia. The limiting

assumption of this method is a single distribution of spherical particles. The method returns a single z-average particle size, which represents a hydrodynamic diameter based on the intensity-weighted particle size distribution. Figure 4.10 shows representative distributions for nanoscale hydrogels in the swollen and collapsed state, suggesting the Cumulant analysis is applicable for these measurements. It should be noted that both CONTIN and NNLS are mathematically equipped to describe multimodal particle distributions.

The colloidal stability of nanoparticle dispersions is a function of both surface charge [53] and/or any steric stabilization [23, 54] from adsorbed or bound molecules protruding from the surface. A net surface charge, or ζ-potential, of ± 30 mV is generally regarded as the minimum for purely electrostatic stabilization. PEG has been widely used as a steric stabilizer [55, 56] in biomaterials to impart colloidal stability and prevent protein adsorption in biological applications [51]. The resistance to particle-particle aggregation was tested in a copolymer containing a hydrophobic co-monomer, TBMA, after 4 weeks and 8 weeks in aqueous suspension. The TBMA was incorporated to increase network core hydrophobicity, and as such, these nanoparticles should display the highest propensity for aggregation or flocculation. According to DLVO theory [57], this process in colloidal suspensions is driven largely by Van der Waals attractions between approaching particles undergoing Brownian motion. The results, shown in Figure 4.11 demonstrate that the nanogels are able to resist aggregation for at least 8 weeks in aqueous suspension. The hydrodynamic diameter remains at approximately 93 – 96 nm in the deswollen state (pH > 7.5) and 119 – 122 nm in the swollen state (pH < 6.0). The pH_c is also unchanged from 4 to 8 weeks in aqueous suspension.

The polydispersity index (PdI), is given by a ratio of the second (μ_2) and first moment (Γ) of the Cumulants analysis (μ_2/Γ^2)[1] and describes the apparent width of the size distribution [52] . It should be noted that this PdI, as defined in the Cumulants analysis, does not describe a true particle size distribution, but rather the width of an assumed Gaussian distribution around a single exponential fit of the generated autocorrelation function. Little variation is seen in the PdI between 4 weeks and 8 weeks in aqueous suspension. Moreover, nearly all PdI values, except measurements in the hydrophobic to hydrophilic phase transition around pH 7.0, lie below 0.2. These data suggest our nanogels are stable in aqueous suspension and are able to resist significant particle aggregation over the course of at least 8 weeks. In a previous report [42], we replaced reactive PEGMA (MW ~ 2080) with a non-reactive PEG monomethyl ether (MW ~ 1900) in the photoemulsion reaction mixture. The resultant nanogels (w/o PEG graft) demonstrated poor stability and underwent visible flocculation and sedimentation within 1 h. As a result, we infer that the PEG graft is important to conferring colloidal stability to these nanogels.

Figure 4.12 illustrates the influence of hydrophobic moiety incorporation on pH-dependent volume swelling of the nanogel formulations. Swelling in ionizable hydrogel systems is driven by a balance of thermodynamic and physical forces; namely the free energy of polymer and solvent interactions, osmotic pressure generated by mobile counterions inside the gel, and elastic contractile response to gel deformation [58]. As hydrophobic content increases, greater proton activity or greater ionization (i.e. lower pH) is required to promote polymer/solvent/ion interaction over polymer/polymer

[1] See Appendix B: Practical Considerations in Light Scattering for a more detailed description of the Cumulants analysis.

interaction. As expected, this effect also leads to a decrease in the onset of pH-dependent gel swelling [33, 59].

The addition of TBMA (Figure 4.12A) clearly shifts the onset of pH-dependent swelling from ~ pH 7.8 to pH 7.0. The critical swelling pH can be defined by fitting a hyperbolic tangent or sigmoidal function to the measured hydrodynamic diameter (D_H) and determining the inflection point. In this case, data were fit to a hyperbolic tangent function of the form [60]

$$D_H = A + B \cdot tanh(C \cdot pH + D) \tag{4.2}$$

Taking the second derivative of Equation 1 yields the inflection point of the curve, which is taken to represent the critical swelling pH, pH_c.

$$\boldsymbol{pH_c = -\frac{D}{C}} \tag{4.3}$$

In networks containing TBMA, the pH_c trend decreased as follows: PDET (pH_c = 7.37) ~ PDETB20 (pH_c = 7.36) ~ PDETB10 (pH_c = 7.31) > PDETB30 (pH_c = 6.65). Additionally, PDET, PDET10, and PDET20 have reached maximum swelling volume by ~ pH 6.8, while PDETB30 reaches maximum volume swelling near pH 6.0. This pH is characteristic of the early endosomes in mammalian cells, suggesting these networks may have utility as vehicles for intracellular drug delivery.

The degree of volume swelling is decreased as the gel concentration of TBMA is increased. Both PDETB10 and PDETB20 exhibit a lower volume swelling ratio than the base formulation PDETB, while PDETB30 exhibits a markedly reduced capacity for

network expansion. This observation may be ascribed to two effects, (1) the persistence of hydrophobic associations in the polymer network that resist solvation and limit elastic deformation of the network, and (2) a reduction in ionizable amine content and consequent decrease in osmotic pressure generated by salts migrating into the network core.

In order to maintain the total monomer concentration constant throughout various formulations, an increase in TBMA concentration required a concomitant decrease in DEAEMA concentration. Simply, the PDETB30 contains less tertiary amines than PDETB, and therefore, the capacity for electrostatic repulsion and osmotic swelling decreases proportionally with decreasing DEAEMA content. These data suggest that there may be a critical [TBMA]:[DEAEMA] ratio, below which hydrophobic TBMA groups are not present in sufficient concentration to segregate into hydrophobic domains and counterbalance the effects of amine-group ionization and osmotic swelling.

Incorporation of TBAEMA (Figure 4.12B) also lowers the onset of pH-dependent swelling, though the effect is less pronounced. In these copolymers, the decrease in pH_c does not follow any particular compositional trend: PDET (pH_c = 7.37) > PDETBA30 (pH_c = 7.13) > PDETBA10 (pH_c = 7.01) ~ PDETBA20 (pH_c = 6.98). These formulations also display similar capacity for volumetric swelling. As TBAEMA contains a secondary amine, the network charge density (and resultant osmotic pressure) should remain relatively constant between PDET, PDETBA10, PDETBA20 and PDETBA30. Moreover, this suggests the ionizable secondary amine group in TBAEMA likely precludes the formation of discrete domains of hydrophobic t-butyl groups. Hydrophobic domains in polyelectrolyte gels have been shown to increase the effective crosslinking density and

reduce volumetric swelling [61]. These data suggest that the presence of a *t*-butyl-R group is not necessary and sufficient to depress pH_c, but rather a more general, hydrophobic effect governs the modification of phase change behavior.

4.3.6. Electrophoretic Light Scattering

Measurements of the effective surface ζ-potential reveal insignificant differences between the various formulations. These data are consistent with the expectation that the PEG-grafted surface of these nanoscale hydrogels are very similar and that the modifications in monomer composition primarily affect the network core. All formulations possess a reversible surface charge, with an isoelectric point (IEP) at approximately pH 8.0, slightly positive ζ-potential at pH 7.4, and a maximum ζ-potential of 25 - 30 mV at pH 3.50 (Figure 4.13). These observations are consistent with those by Amalvy, et al. [23], who noted the nature of grafted stabilizer was more important in determining IEP than the nature of core particles in PDEAEMA microgels.

At physiological pH, the slightly positive ζ-potential may help facilitate non-specific cell-uptake. The negative ζ-potential observed from pH 10.5 to ~ pH 8.0 can be ascribed to the adsorption of negatively charged hydroxyl ions on the PEG-coated surface [62] and has been noted previously in similar DEAEMA-based materials [23, 41]. Likewise, the positive ζ-potential can be ascribed the surface adsorption of hydronium ions and protonation of amine-containing groups in the network core, which serve to establish an electrical double layer around the particles. While the measured ζ-potential for all formulations fall outside the limits for electrostatically-driven colloidal stability (± 30 mV), no flocculation or aggregation was observed throughout the pH range, even that

where nanoscale hydrogels possessed a net surface charge of ± 5 mV. This provides additional evidence of the steric stabilization afforded by PEG surface grafts. Moreover, previous work [41] has estimated the ζ-potential of neat PDEAEMA nanogels to be approximately -45 mV at pH 10 and 75 mV at pH 4. Thus, the surface layer of PEG was indeed effective at shielding surface charge.

4.3.7. Pyrene Fluorescence Spectroscopy

The ratio of the first to third vibronic peak (I_1/I_3) in the fluorescence emission spectra of pyrene was used to study the pH-dependent conformational transition of responsive nanoscale hydrogels. The fluorescence spectra of pyrene undergoes a characteristic shift depending on the polarity of pyrene microenvironment. When dissolved in highly polar, aqueous solvents the I_1/I_3 ratio in the emission spectra is approximately 1.59 while this ratio decreases to 0.61 in nonpolar, aliphatic hydrocarbons such as *n*-hexane or dodecane [63]. Therefore, a decrease in the emission I_1/I_3 ratio indicates pyrene is preferentially partitioned in hydrophobic domains. Figure 4.14 shows a representative change in pyrene fluorescence in aqueous suspensions of PDETB30 between collapsed hydrophobe (pH 8.0) and swollen hydrophile (pH 6.0). Consequently, the fluorescence spectra of pyrene can be used to probe the polarity of aqueous suspensions of nanoscale hydrogels and determine the influence of polymer composition on relative network hydrophobicity and the critical pH required to induce a conformational transition. Figure 4.15A clearly demonstrates that inclusion of TBMA causes, in a composition-dependent fashion, a decrease in the pH required to induce a conformational transition.

This value decreases from approximately pH 7.5 in PDET to below pH 7.0 in PDETB30, with both PDETB10 and PDETB20 exhibiting intermediate values. Additionally, whereas PDET displays a rather abrupt transition from hydrophobe to hydrophile, the networks containing TBMA transition over a substantially wider pH range. In previous investigations of hydrophobic polybasic gels, Siegel and Firestone [59] postulated increasing chain stiffness served to increase the breadth of the pH-dependent swelling transition. In bulk gels of similar monomeric composition P(DMAEMA-co-TBMA) to our polymer system P(DEAEMA-co-TBMA-g-PEGMA), the persistence of hydrophobic microdomains resulted in 35% increase in shear modulus at 20% TBMA content and a 245% increase at 40% TBMA content [61]. In the present study, a similar stiffening effect could be imparted by TBMA in DEAEMA-based nanogels and result in a more broad swelling transition. These studies also provide additional insight into the relative hydrophobicity of the network core. For example, at pH 8.0, the I_1/I_3 ratio for collapsed PDET is 1.15 whereas the I_1/I_3 ratio for collapsed PDETB30 is approximately 1.09. Upon suspension in pH 5.8 buffers, these ratios increased to 1.58 and 1.49 for PDET and PDETB30, respectively. These values for I_1/I_3 correspond well with previous reports of pyrene fluorescent probes in DEAEMA-based polymeric materials [64].

Our understanding of the impact of TBAEMA on pH-dependent swelling transition is less clear, however. Nanoscale hydrogels containing TBAEMA did not exhibit the same type of composition-dependent phase transition displayed by the TBMA copolymers (Figure 4.15B). When copolymerized in DEAEMA-based nanogels at low concentrations (PDETBA10), TBAEMA decreases the critical swelling pH in both light

scattering (Figure 4.12B) and pyrene (Figure 4.15B) studies. The breadth of the transition remains relatively constant when compared to PDET, which contains neither TBAEMA nor TBMA. When copolymerized with DEAEMA at 20 mol% and 30 mol% (PDETBA20 and PDETBA30), TBAEMEA raises the pH_c as determined by DLS and significantly increases the breadth of the hydrophobe-hydrophile phase transition as determined by pyrene fluorescence. This observation is seemingly inconsistent with the chain stiffness argument applied to TBMA-containing nanogels. If chain stiffness and mobility were the dominant factors governing the breadth of the hydrophobe-hydrophile phase transition, one would expect PDET, PDETBA10, PDETBA20, and PDETBA30 to have phase transitions of similar breadth. DEAEMA and TBAEMA have identical molecular weights and similar end-group bulkiness. We therefore expect that TBAEMA will have little impact on the chain stiffness. One possible explanation for the broad nature of the TBAEMA-induced hydrophobe-hydrophile phase transition may be the heterogeneous distribution of ionizable amine species in the network core. PTBAEMA has pKa ~7.6 - 8.0 [44] while PDEAEMA has pKa ~ 7.0 – 7.3 [23]. Thus, PDETBA30 should possess a greater network charge density at elevated pH and create an increasingly polar environment (indicated by increasing I_1/I_3 in Figure 4.15B) that is distributed over the pKa range of the multiple ionizable species. This effect is less notable in PDETAB20 and nearly absent in PDETBA10.

4.4. CONCLUSIONS

Nanoscale, pH-responsive polycationic networks were successfully synthesized using a photoemulsion polymerization. Copolymer composition and incorporation of

hydrophobic moieties, TBMA and TBAEMA, was verified using ^{1}H-NMR. Hydrogel nanoparticles exhibit a dry diameter of approximately 50 - 65 nm as determined by TEM and a collapsed, yet hydrated, diameter of approximately 90 nm. Dynamic light scattering reveals a single distribution of particle sizes that remain stable in aqueous suspension for at least 8 weeks. In P(DEAEMA-g-PEGMA) copolymers, the onset of pH-dependent swelling occurs ~ pH 7.8 - 8.0 and networks have reached maximum volume swelling ~ pH 6.7 - 7.0. In P(DEAEMA-co-TBMA-g-PEGMA) copolymers, the onset of pH-dependent swelling decreasing with increasing TBMA content, reaching ~ pH 7.2 with maximum volume swelling ~ pH 5.50 in PDETB30. Moreover, TBMA broadens the transition from collapsed hydrophobe and swollen hydrophile in light scattering and pyrene fluorescence spectroscopy studies. In P(DEAEMA-co-TBAEMA-g-PEGMA) copolymers, the compositional dependence is less obvious and may be complicated by the presence of multiple ionizable species in TBAEMA and DEAEMA. The polymerization described in this report and in our previous work [33, 42] permits the reliable formation of hydrogel nanoparticles with utility in diverse applications that require tailoring material properties. In particular, PDETB30 possesses size (d_H ~ 100 nm) responsive characteristics (pH_c ~ 6.6) well-suited for intracellular drug delivery applications. Our future efforts will focus on evaluating the safety and efficacy of PDETB30 in intracellular delivery of therapeutics.

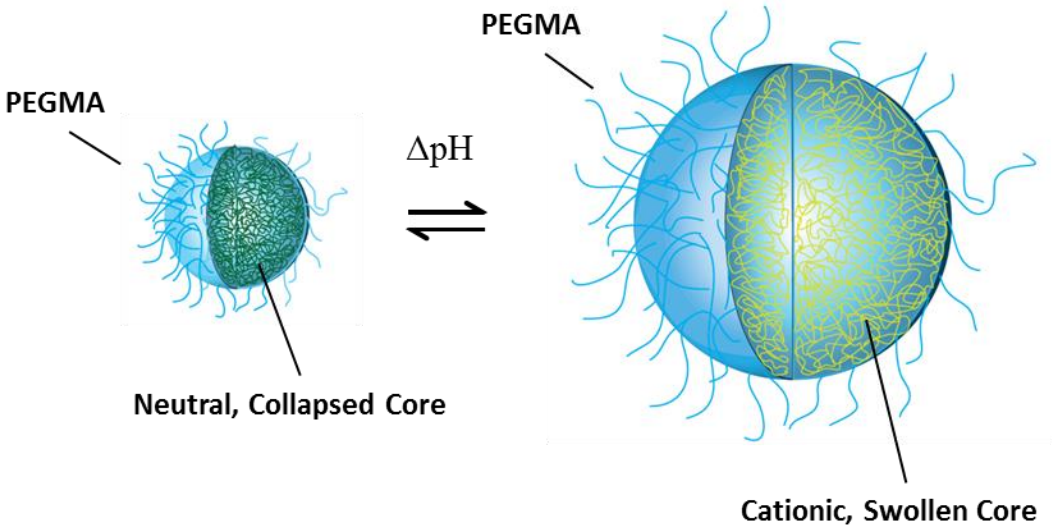

Figure 4.1 - Schematic of pH-responsive nanogel

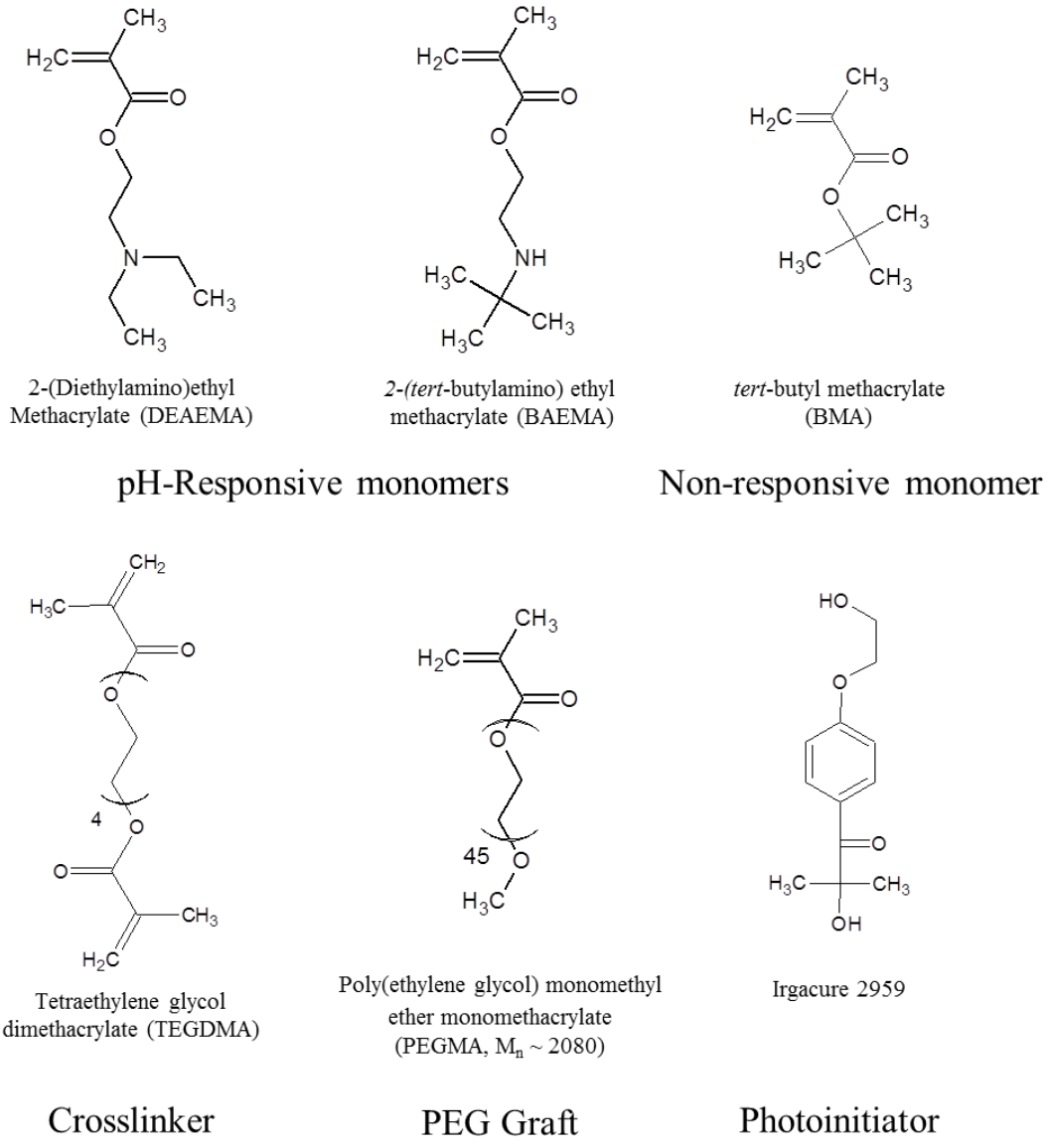

Figure 4.2 - Methacrylate monomers and initiator used in synthesis of pH-responsive nanoscale hydrogels

Table 4.1 - Reagents used for nanoscale hydrogel synthesis

Name	Crosslinked copolymer	mol *t*-butyl/100 mol DEAEMA	DEAEMA (g)	PEGMA (g)	TBMA (g)	TBAEMA (g)	TEGDMA (g)	Water (mL)	Monomer Fraction in Water (w/v)
PDETB	P(DEAEMA-g-PEGMA)	0	2.500	5.000	-	-	0.121	50	0.1
PDETB10	P(DEAEMA-co-TBMA-g-PEGMA)	10	2.322	5.000	0.178	-	0.124	50	0.1
PDETB20	P(DEAEMA-co-TBMA-g-PEGMA)	20	2.168	5.000	0.332	-	0.126	50	0.1
PDETB30	P(DEAEMA-co-TBMA-g-PEGMA)	30	2.033	5.000	0.467	-	0.128	50	0.1
PDETBA10	P(DEAEMA-co-TBAEMA-g-PEGMA)	10	2.273	5.000	-	0.227	0.121	50	0.1
PDETBA20	P(DEAEMA-co-TBAEMA-g-PEGMA)	20	2.084	5.000	-	0.416	0.121	50	0.1
PDETBA30	P(DEAEMA-co-TBAEMA-g-PEGMA)	30	1.924	5.000	-	0.576	0.121	50	0.1

Table 4.2 - Reactivity data of comonomers in photoemulsion polymerization for fixed M1 of DEAEMA

		Q^t	e^t	r_1	r_2	r_1r_2
M2	DEAEMA	2.08	0.42	1.0	1.0	1.0
	TBMA	1.18	-0.35	1.28	0.43	0.55
	TBAEMA	0.98	0.17	1.91	0.49	0.94

[t]Tabulated data

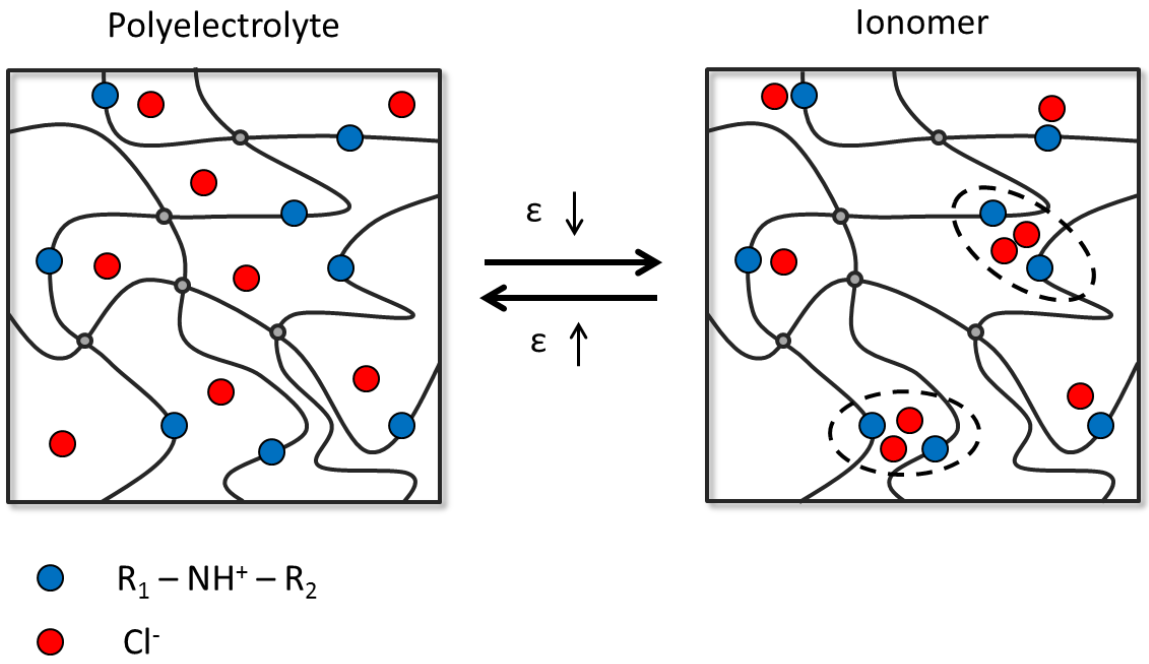

Figure 4.3 - Polyelectrolyte to ionomer transition in tertiary amine-containing gels. Hashed ovals indicate the formation of ion pair multiplets. Adapted from ref [50].

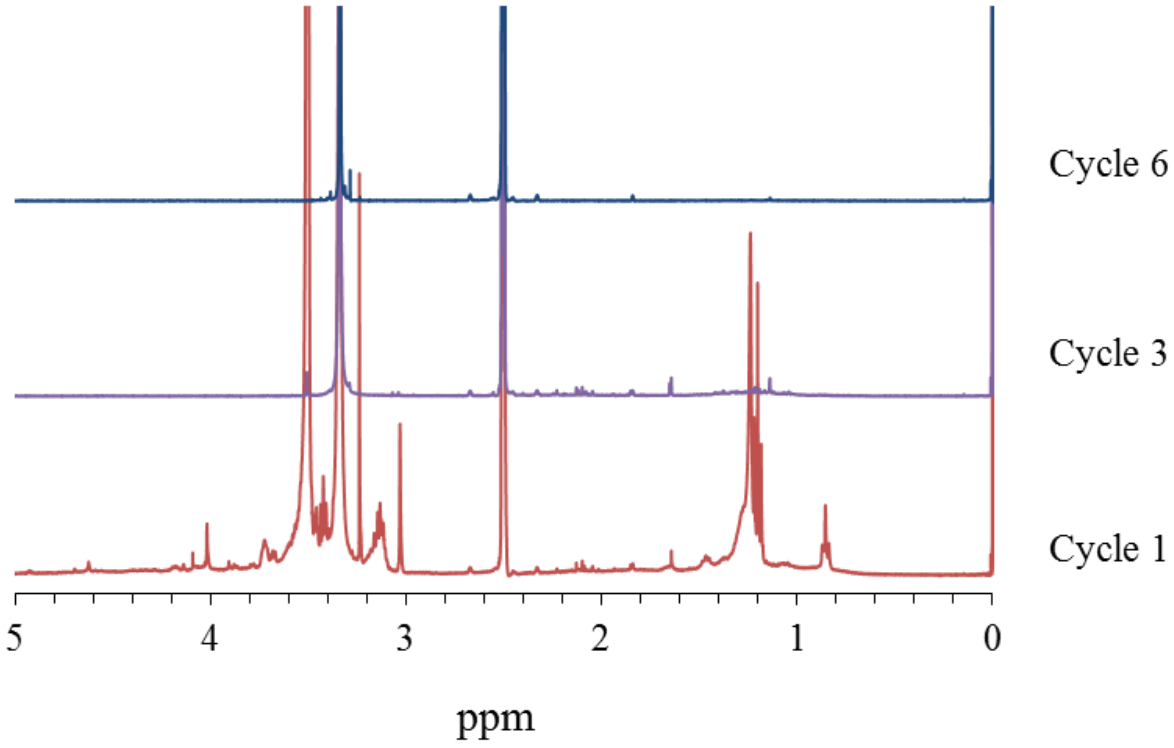

Figure 4.4 - ^{1}H-NMR Analysis of nanogel purification supernatants. Purification aliquots were analyzed following 1, 3, or 6 cycles of polyelectrolyte-ionomer transition and centrifugation. Supernatant samples were frozen, lyophilized, and dissolved in DMSO-d6.

Table 4.3 – Relative area of contaminant peaks in the supernatant following a purification cycle of (1) protonation of DEAEMA with 0.5 N HCl, (2) ionomer phase transition by addition of 4 vol. equivalents of acetone (80 vol% acetone total), and (3) centrifugation of ionomer/solvent mixture. Supernatant aliquots from each cycle were frozen, lyophilized, and dissolved in DMSO-d_6 for ^{1}H-NMR analysis.

Purification Cycle	Peak Area[1] (δ = 3.40 - 3.65)	Peak Area[1] (δ = 1.15 - 1.35)
1	42.6	10.3
2	3.3	1.7
3	0.7	1.4
4	0.8	1.5
5	1.3	1.9
6	0.7	0.5

[1]Relative to TMS at 0.03% (v/v) in DMSO-d6

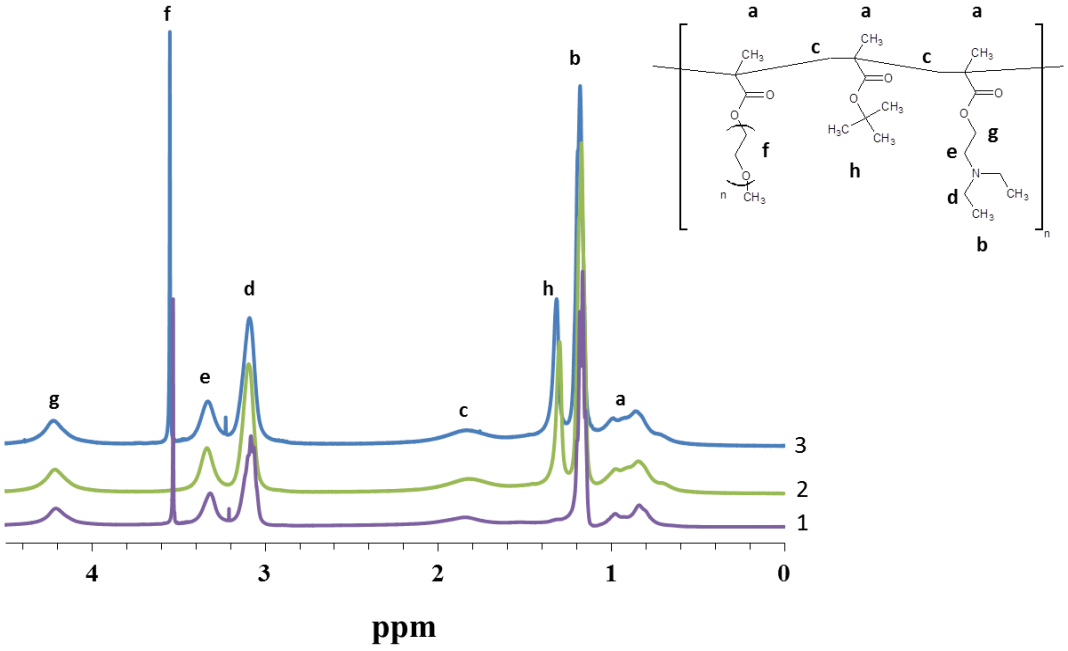

Figure 4.5 - NMR Spectra of uncrosslinked copolymers containing TBMA in D_2O. (1) P(DEAEMA-g-PEGMA) (PDE), (2) P(DEAEMA-co-TBMA) (PDB30) and (3) P(DEAEMA-co-TBMA-g-PEGMA) (PDEB30). Inclusion of TBMA is verified by the presence of the t-butyl proton peak at 1.3 ppm. Inclusion of PEGMA is verified by the presence of the oxyethylene peak at 3.6 ppm.

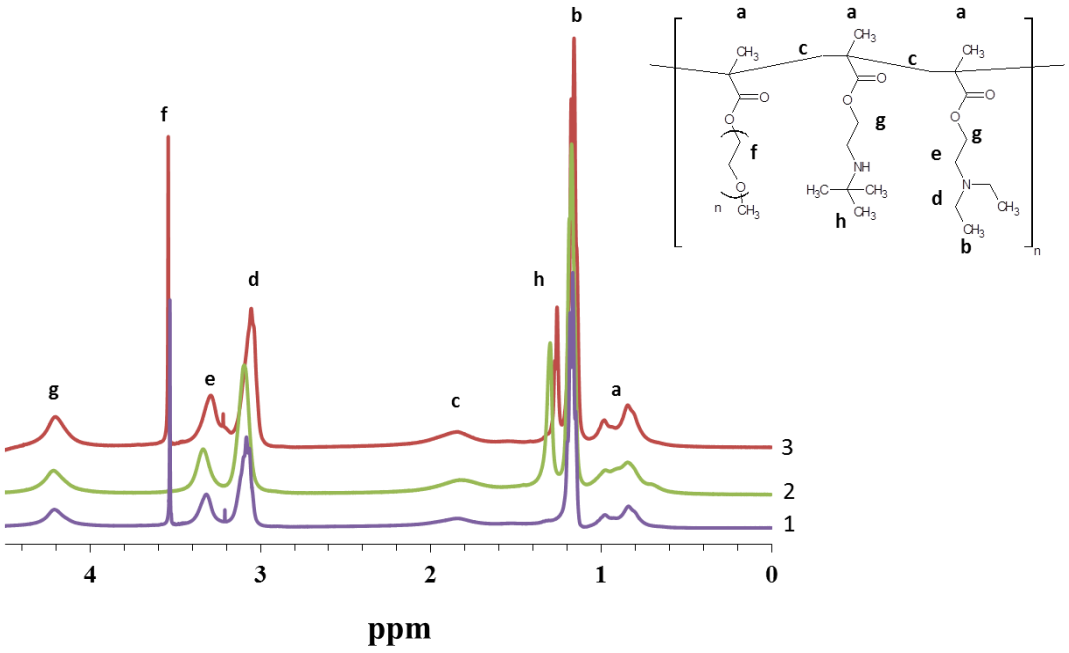

Figure 4.6 - NMR Spectra of uncrosslinked copolymers containing TBAEMA in D_2O. (1) P(DEAEMA-g-PEGMA) (PDE), (2) P(DEAEMA-co-TBMA) (PDB30) and (3) P(DEAEMA-co-TBAEMA-g-PEGMA) (PDEBA20). Inclusion of TBMA is verified by the presence of the t-butyl proton peak at 1.3 ppm. Inclusion of PEGMA is verified by the presence of the oxyethylene peak at 3.6 ppm.

Table 4.4 - Polymer composition as determined by ^{1}H-NMR for linear copolymers containing t-butyl methacrylate (TBMA) or t-butylaminoethyl methacrylate (TBAEMA)

		t-butyl (TBMA or TBAEMA)		DEAEMA		PEGMA	
Linear copolymer	mol *t*-butyl/100 mol DEAEMA	mol% in feed	mol% in polymer[a]	mol% in feed	mol% in polymer[a]	mol% in feed	mol% in polymer[a]
P(DEAEMA-g-PEGMA)	0	-	-	91.8	99.5	8.2	0.48
P(DEAEMA-co-TBMA)	30	23.1	24.6	76.9	75.4	-	-
P(DEAEMA-co-TBMA-g-PEGMA)	30	21.6	21.4	72	78.1	6.4	0.45
P(DEAEMA-co-TBAEMA-g-PEGMA)	20	15.5	13.5	77.6	86.1	6.9	0.38

[a]Determined by ^{1}H-NMR

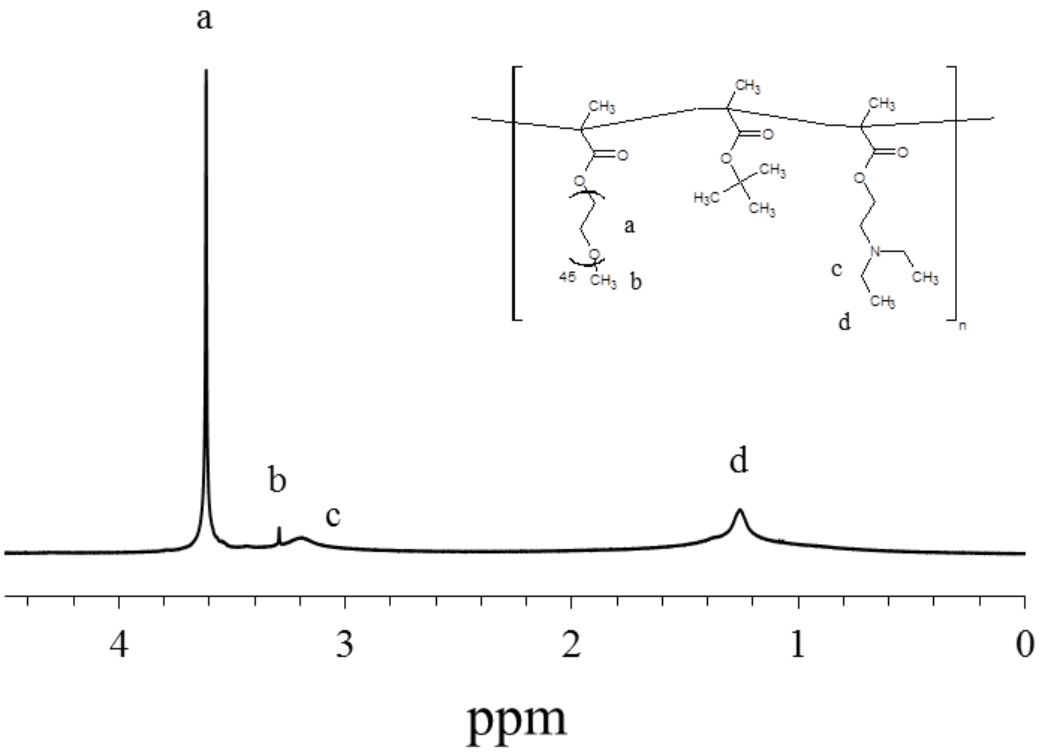

Figure 4.7 – ^{1}H-NMR Analysis of crosslinked P(DEAEMA-co-TBMA-g-PEGMA) (PDETB30) in 0.1 N DCl/D_2O.

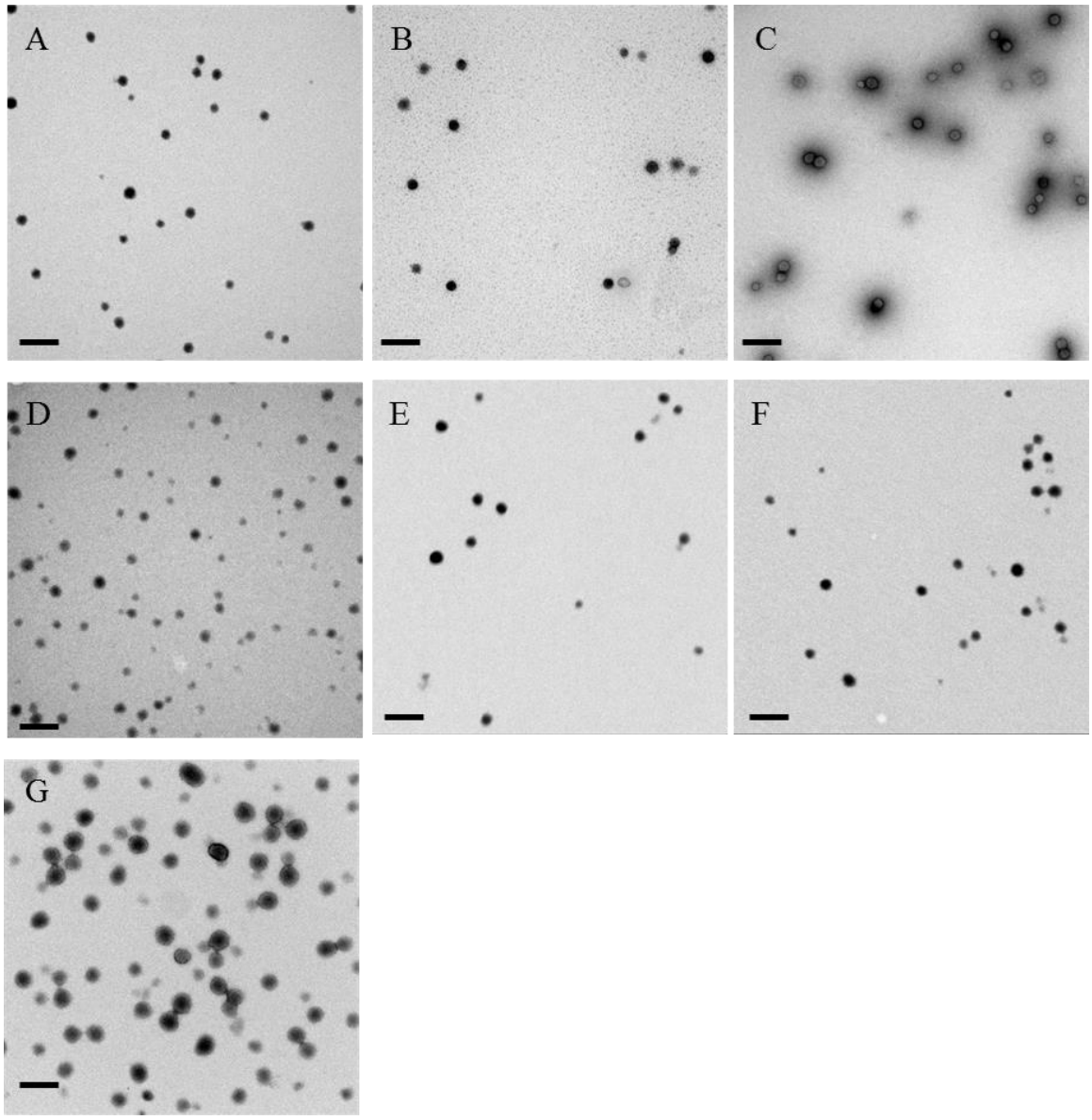

Figure 4.8 - Representative transmission electron microscopy images of TEGDMA-crosslinked nanogels. PDET (A), PDETB10 (B), PDETB20 (C) PDETB30 (D), PDETBA10 (E), PDETBA10 (F), PDETBA30 (G). Particles stained with uranyl acetate and images collected at 43,000×. Scale bar represents 200 nm.

Table 4.5 - Calculated dry diameters of nanogels from TEM micrographs. Reported values represent the mean ± s.d. ($n > 150$).

Name	Calculated diameter (nm)
PDET	47 ± 13
PDETB10	60 ± 26
PDETB20	50 ± 22
PDETB30	52 ± 17
PDETBA10	50 ± 18
PDETBA20	63 ± 21
PDETBA30	66 ± 25

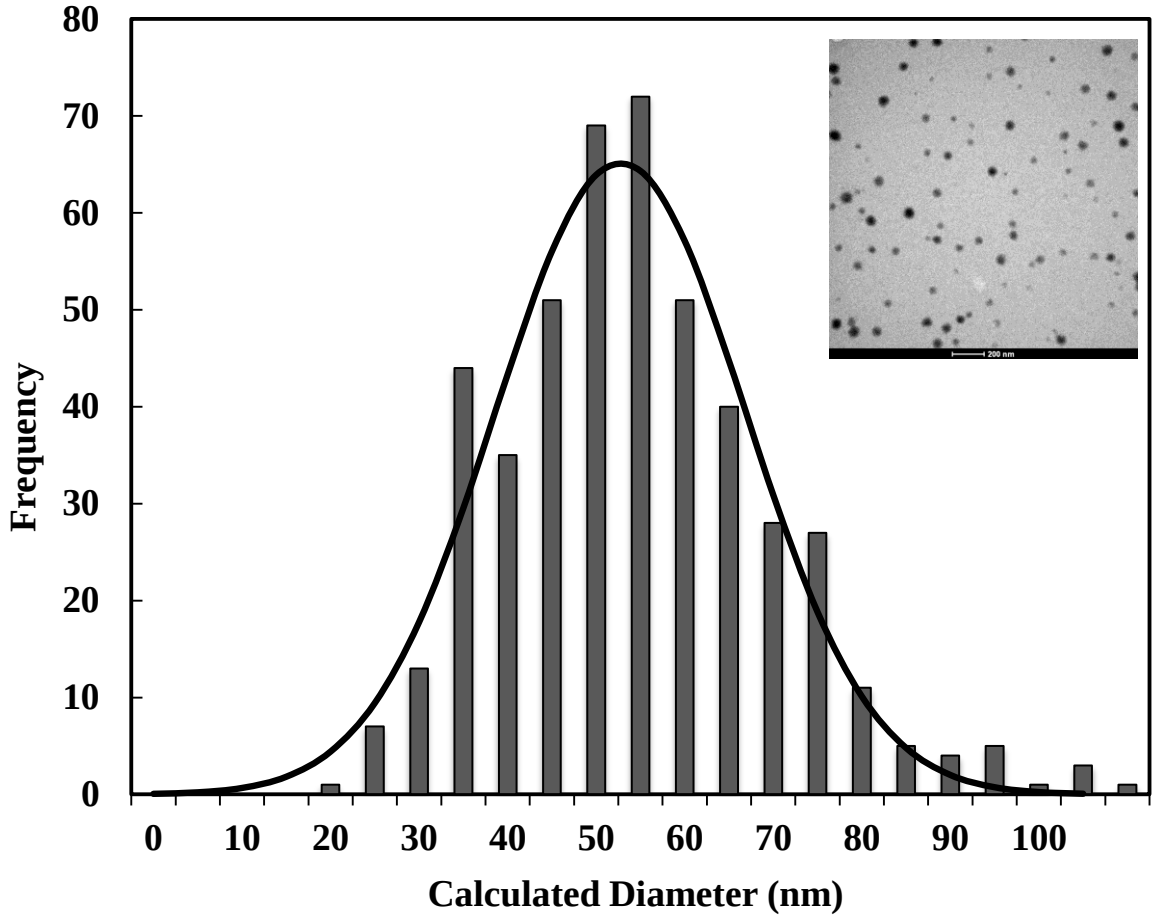

Figure 4.9 - Sample number-average particle size distribution of dry P(DEAEMA-co-TBMA-g-PEGMA) (PDETB30) generated by quantitative particle sizing from TEM micrographs. Distribution mean = 52.0, Std Dev = 17.3, n = 200. Bars represent observed data and line represents best fit Gaussian distribution (R2 = 0.982).

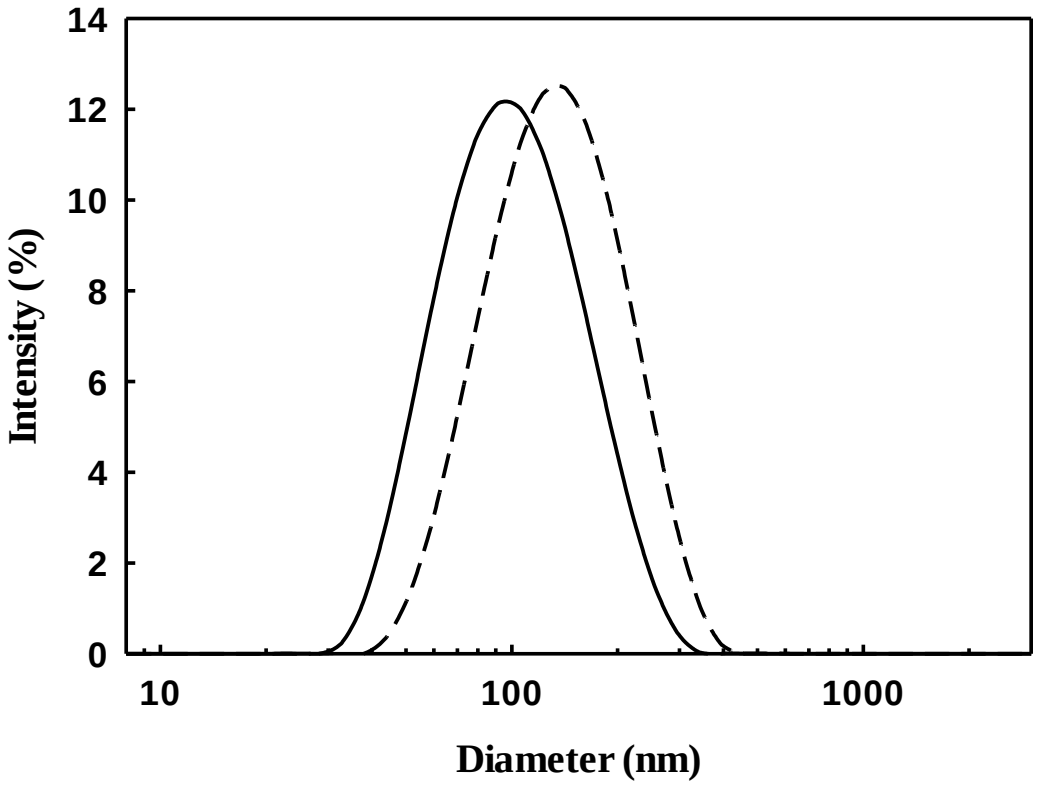

Figure 4.10 – Representative intensity-weighted particle size distribution for P(DEAEMA-co-TBMA-g-PEGMA) crosslinked with 2.5 mol% TEGDMA (PDETB30) in the collapsed (solid) and swollen (dashed) state.

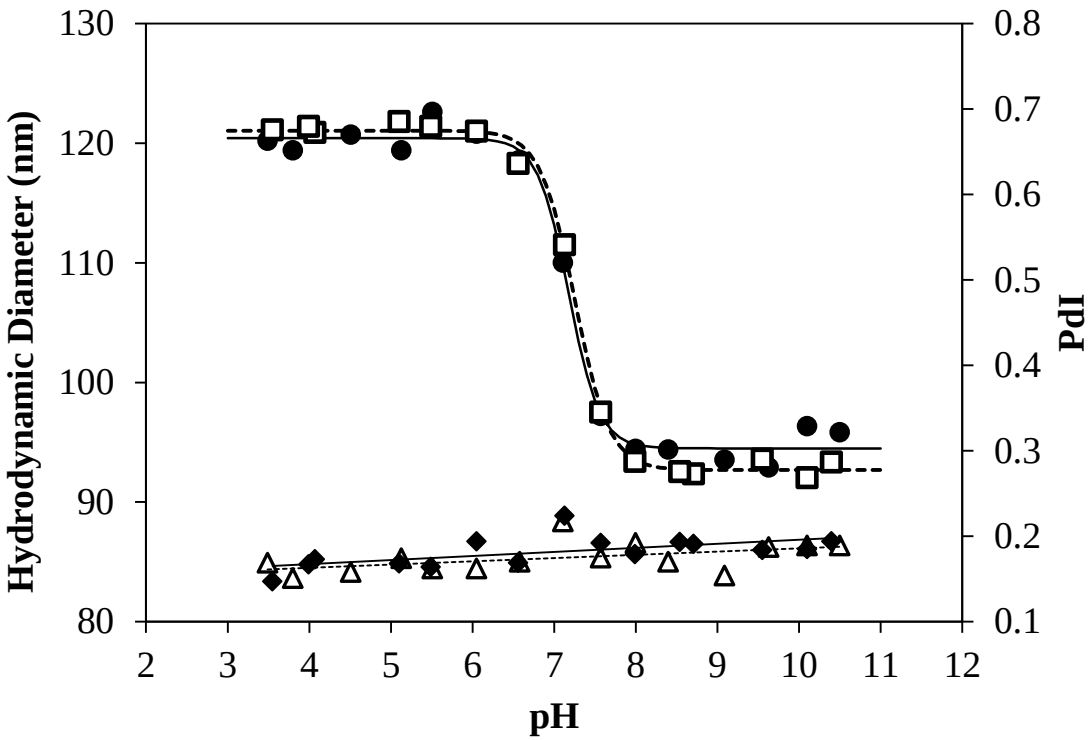

Figure 4.11 – Colloidal stability of nanoscale hydrogels. Hydrodynamic diameter (left axis) and polydispersity index (right axis) of P(DEAEMA-co-TBMA-g-PEGMA) networks crosslinked with 2.5 mol% TEGDMA after 4 weeks (filled symbols) and 8 weeks (empty symbols) in aqueous suspension. Data points represent mean of 12 measurements and lines represent a best fit to the data. A hyperbolic tangent fit was applied to the measurements of hydrodynamic diameter and a linear fit was applied to the measurements of polydispersity index.

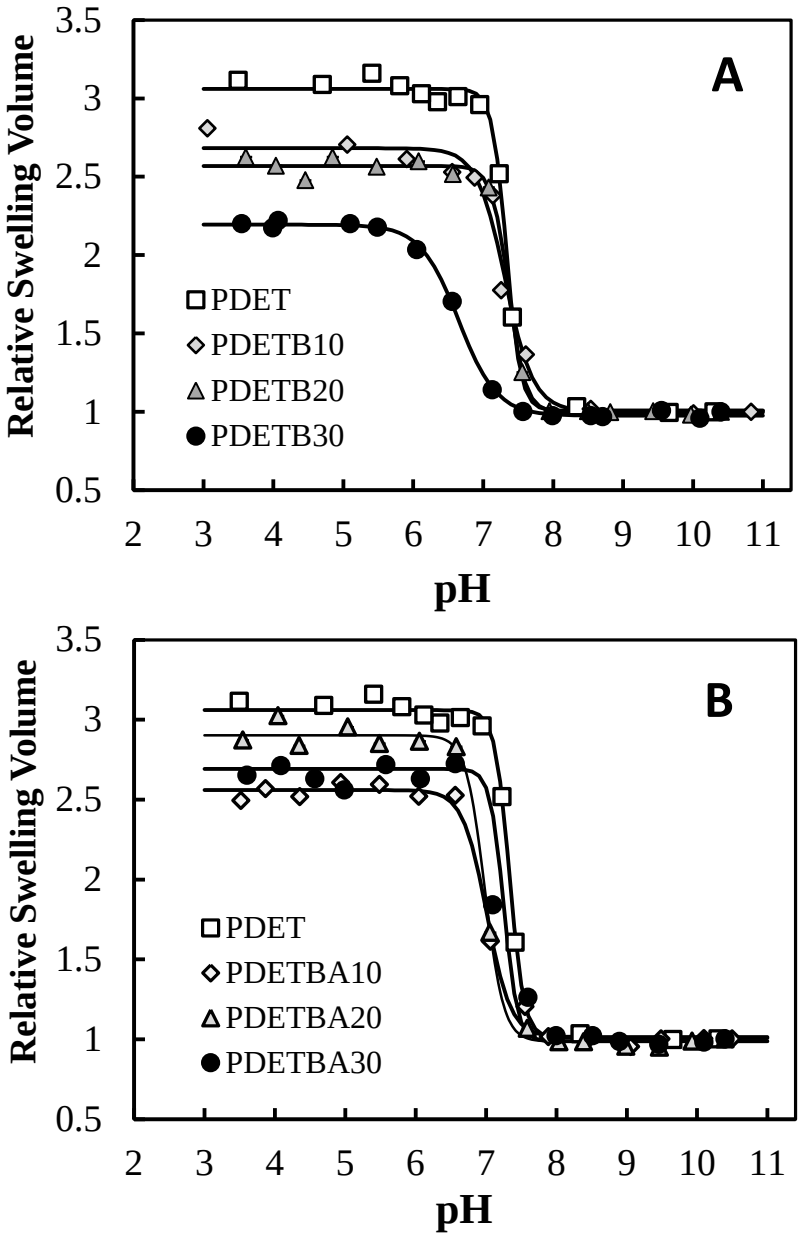

Figure 4.12 - Influence of hydrophobic moiety incorporation on pH-dependent swelling properties in nanoscale hydrogels containing TBMA (A) or TBAEMA (B). Symbols indicate 0 mol% (□), 10 mol% (◊), 20 mol% (Δ), or 30 mol% (●) comonomer based on DEAEMA. Data points represent mean of 12 measurements and lines represent a hyperbolic tangent best fit to the data.

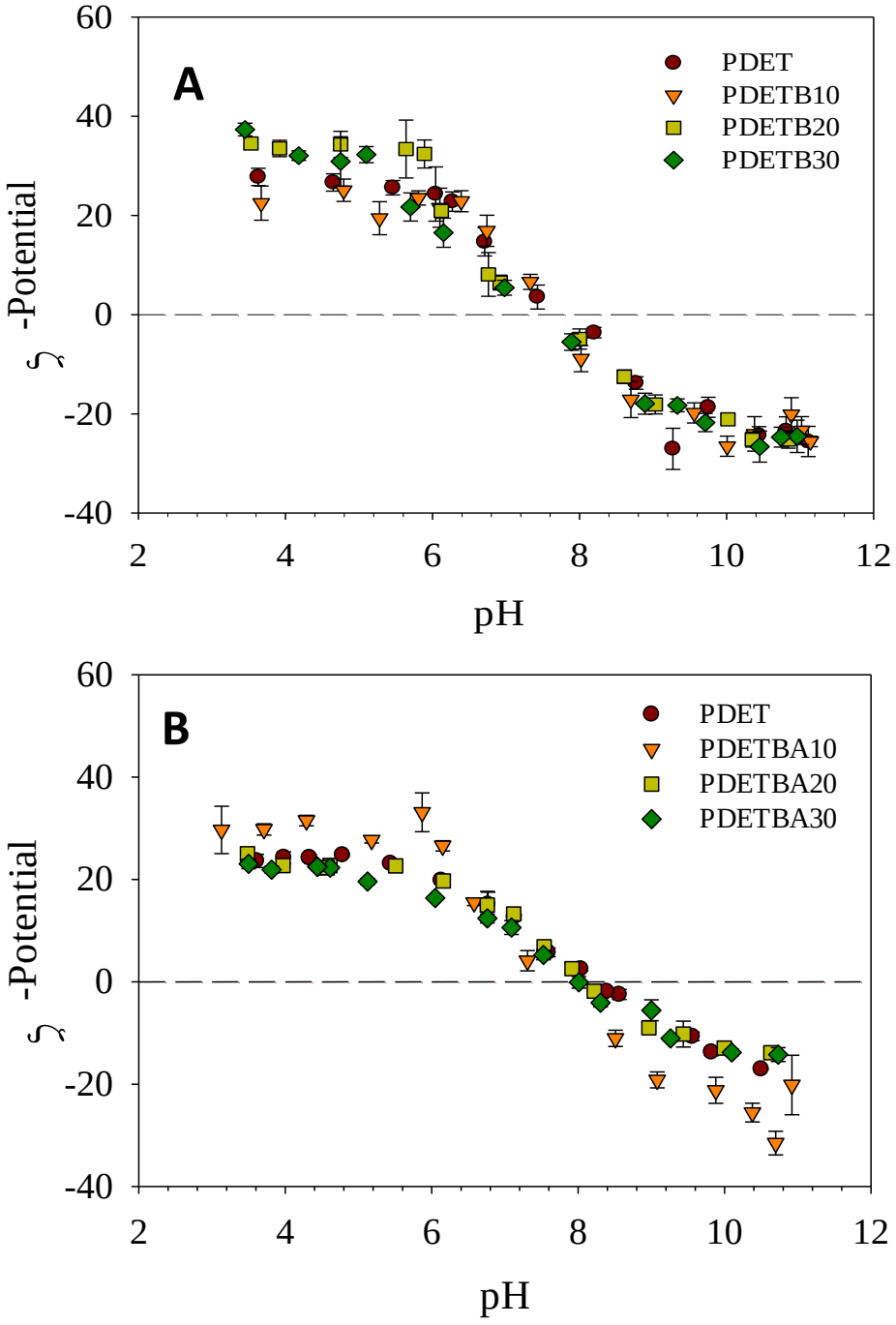

Figure 4.13 - Effective surface zeta-potential of polymer formulations synthesized with varying TBMA (A) and TBAEMA (B). Data points represent the mean of 10 measurements ± SD.

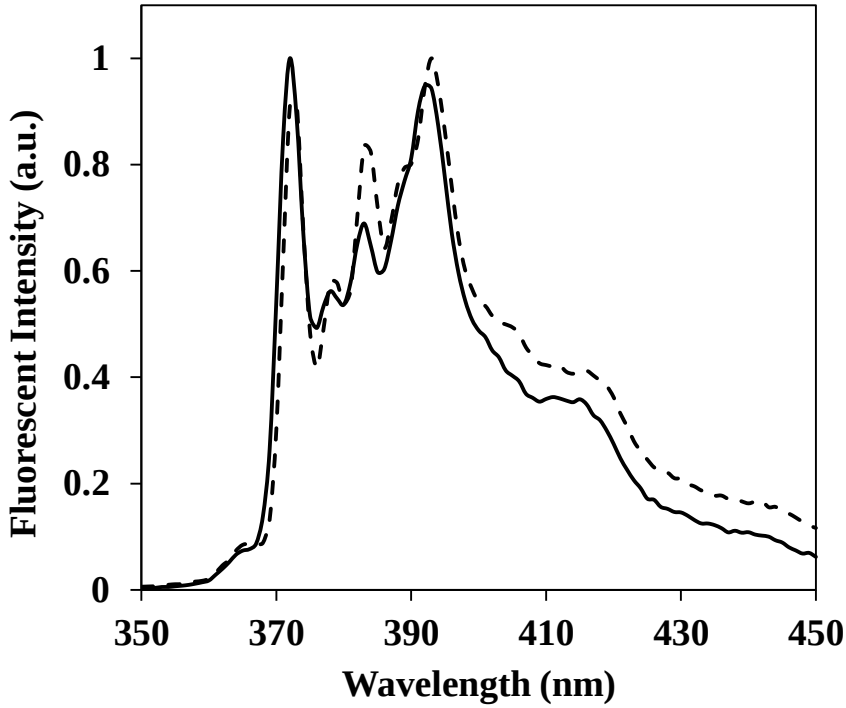

Figure 4.14 – Normalized fluorescent emission spectra of pyrene in 100 mM phosphate buffer and 0.5 mg mL^{-1} PDETB30 at pH 8.0 (solid) and pH 6.0 (dashed).

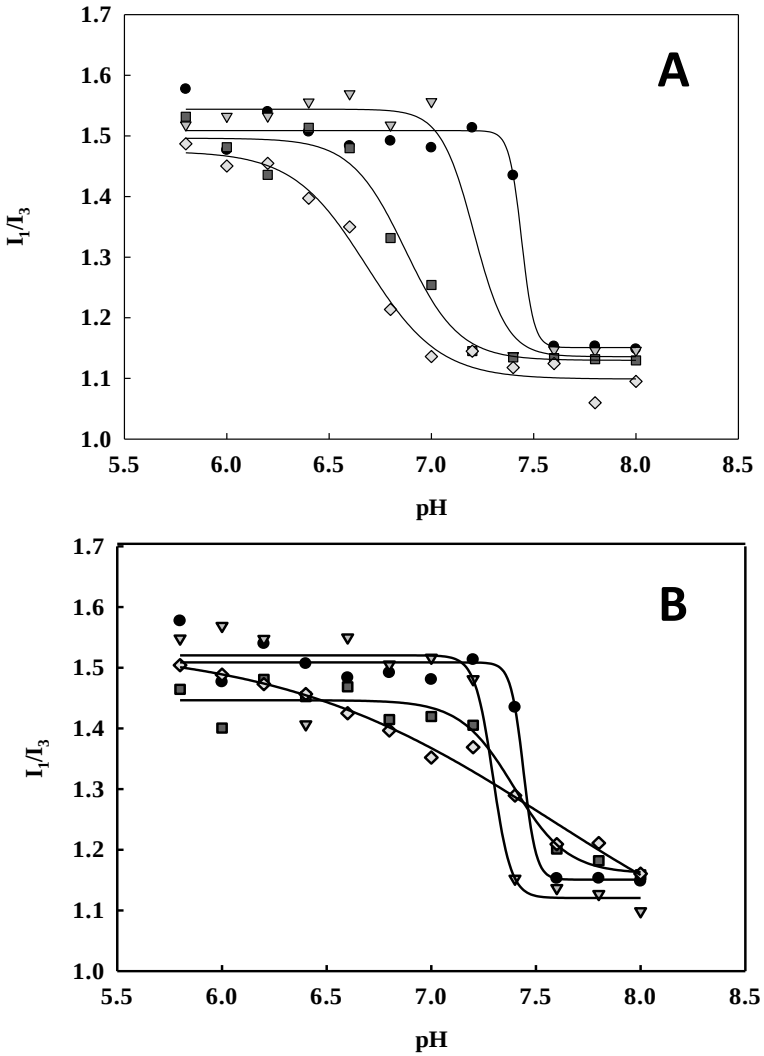

Figure 4.15 - Influence of t-butyl incorporation on fluorescence emission spectra of nanogels synthesized with TBMA (A) or TBAEMA (B). Nanogels suspended at 0.5 mg mL^{-1} and pyrene dissolved at 6×10^{-7} M in 100 mM phosphate buffers. Symbols designate PDET (●), PDETB10 (▼), PDETB20 (■), or PDETB30 (◊) in (A) and PDET (●), PDETBA10 (▼), PDETBA20 (■), or PDETBA30 (◊) in (B). Points represent measured data and lines represent best-fit sigmoidal curves.

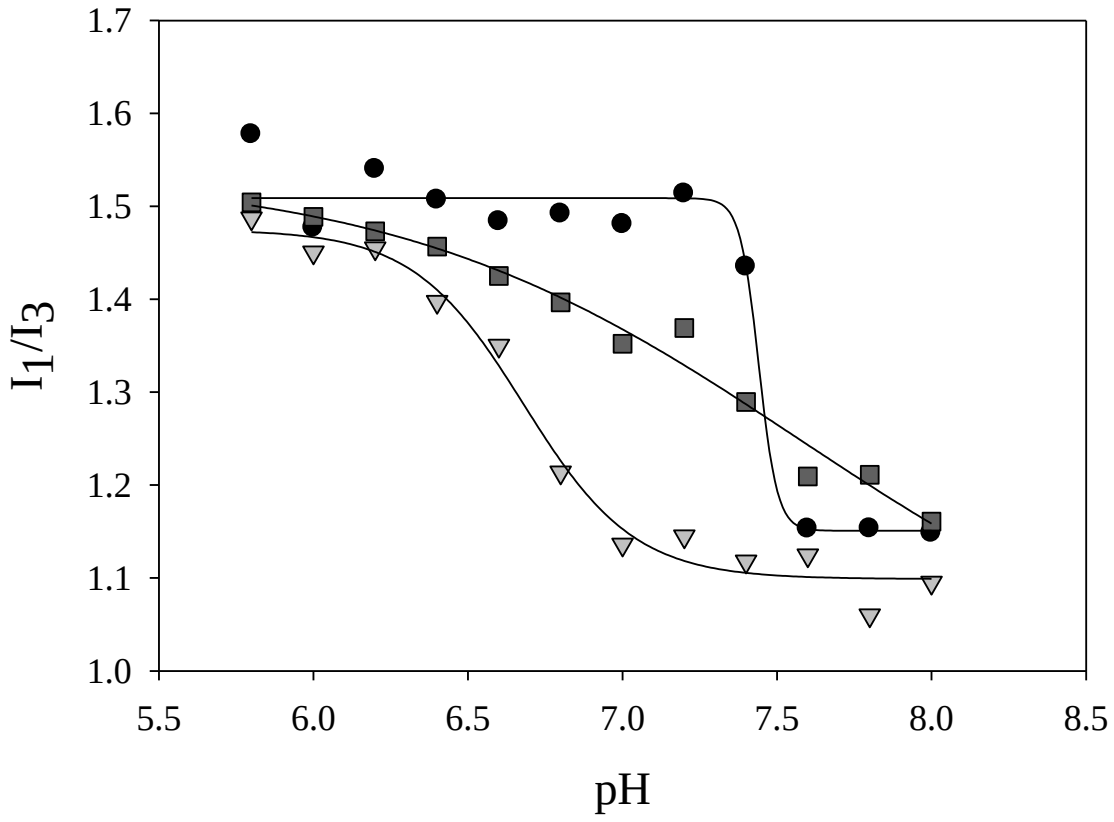

Figure 4.16 - Influence of hydrophobic moiety on fluorescence emission spectra of pyrene. Pyrene dissolved at 6×10^{-7} M in 100 mM phosphate buffers with PDET (●), PDETB30 (▼), or PDETBA30 (■) at 0.5 mg mL^{-1}. Points represent measured data and lines represent best-fit sigmoidal curves.

REFERENCES

1. Stuart MAC, Huck WTS, Genzer J, Muller M, Ober C, Stamm M, Sukhorukov GB, Szleifer I, Tsukruk VV, Urban M, Winnik F, Zauscher S, Luzinov I, and Minko S. Nature Materials 2010;9(2):101-113.

2. Liechty WB, Kryscio DR, Slaughter BV, and Peppas NA. Annual Review of Chemical and Biomolecular Engineering, Vol 1 2010;1:149-173.

3. Chen R, Khormaee S, Eccleston ME, and Slater NKH. Biomaterials 2009;30(10):1954-1961.

4. Santos AF, Murthy N, Stayton PS, Press OW, Tirrell D, and Hoffman AS. Journal of Investigative Medicine 1998;46(1):91a-91a.

5. Murthy N, Robichaud JR, Tirrell DA, Stayton PS, and Hoffman AS. Journal of Controlled Release 1999;61(1-2):137-143.

6. Convertine AJ, Benoit DSW, Duvall CL, Hoffman AS, and Stayton PS. Journal of Controlled Release 2009;133(3):221-229.

7. Dufresne MH and Leroux JC. Pharmaceutical Research 2004;21(1):160-169.

8. Du Y, Lo E, Ali S, and Khademhosseini A. Proceedings of the National Academy of Sciences 2008;105(28):9522-9527.

9. Slaughter BV, Khurshid SS, Fisher OZ, Khademhosseini A, and Peppas NA. Advanced Materials 2009;21(32-33):3307-3329.

10. Ekenseair AK, Boere KWM, Tzouanas SN, Vo TN, Kasper FK, and Mikos AG. Biomacromolecules 2012;13(9):2821-2830.

11. Tokareva I, Minko S, Fendler JH, and Hutter E. Journal of the American Chemical Society 2004;126(49):15950-15951.

12. VanBlarcom DS and Peppas NA. Biomedical Microdevices 2011;13(5):829-836.

13. Dong L, Agarwal AK, Beebe DJ, and Jiang HR. Nature 2006;442(7102):551-554.

14. White TJ, Natarajan LV, Tondiglia VP, Bunning TJ, and Guymon CA. Macromolecules 2007;40(4):1112-1120.

15. Gil ES and Hudson SA. Progress in Polymer Science 2004;29(12):1173-1222.

16. Schild HG. Progress in Polymer Science 1992;17(2):163-249.

17. Debord JD and Lyon LA. Langmuir 2003;19(18):7662-7664.

18. Bae YH, Okano T, Hsu R, and Kim SW. Makromolekulare Chemie-Rapid Communications 1987;8(10):481-485.

19. Siegwart DJ, Bencherif SA, Srinivasan A, Hollinger JO, and Matyjaszewski K. Journal of Biomedical Materials Research Part A 2008;87A(2):345-358.

20. Pich A, Tessier A, Boyko V, Lu Y, and Adler HJP. Macromolecules 2006;39(22):7701-7707.

21. Beltran S, Baker JP, Hooper HH, Blanch HW, and Prausnitz JM. Macromolecules 1991;24(2):549-551.

22. Huglin MB, Liu Y, and Velada JL. Polymer 1997;38(23):5785-5791.

23. Amalvy JI, Wanless EJ, Li Y, Michailidou V, Armes SP, and Duccini Y. Langmuir 2004;20(21):8992-8999.

24. Tang Y, Liu SY, Armes SP, and Billingham NC. Biomacromolecules 2003;4(6):1636-1645.

25. Bütün V, Armes SP, and Billingham NC. Polymer 2001;42(14):5993-6008.

26. Bulmus V, Woodward M, Lin L, Murthy N, Stayton P, and Hoffman A. Journal of Controlled Release 2003;93(2):105-120.

27. Manganiello MJ, Cheng C, Convertine AJ, Bryers JD, and Stayton PS. Biomaterials 2012;33(7):2301-2309.

28. Siegel RA and Cornejobravo JM. ACS Symposium Series 1992;480:131-145.

29. Kwon G, Yokoyama M, Okano T, Sakurai Y, and Kataoka K. Pharmaceutical Research 1993;10(7):970-974.

30. Avgoustakis K, Beletsi A, Panagi Z, Klepetsanis P, Livaniou E, Evangelatos G, and Ithakissios DS. International Journal of Pharmaceutics 2003;259(1–2):115-127.

31. Gref R, Lück M, Quellec P, Marchand M, Dellacherie E, Harnisch S, Blunk T, and Müller RH. Colloids and Surfaces B: Biointerfaces 2000;18(3–4):301-313.

32. Zuidam NJ, Posthuma G, de Vries ETJ, Crommelin DJA, Hennink WE, and Storm G. Journal of Drug Targeting 2000;8(1):51-+.

33. Fisher O, Kim T, Dietz S, and Peppas N. Pharmaceutical Research 2009;26(1):51-60.

34. Rimmer S, Wilshaw S-P, Pickavance P, and Ingham E. Biomaterials 2009;30(13):2468-2478.

35. Liechty WB, Caldorera-Moore M, Phillips MA, Schoener C, and Peppas NA. Journal of Controlled Release 2011;155(2):119-127.

36. Liechty WB and Peppas NA. European Journal of Pharmaceutics and Biopharmaceutics 2012;80(2):241-246.

37. Khademhosseini A and Peppas NA. Advanced Healthcare Materials 2013;2(1):10-12.

38. Caldorera-Moore ME, Liechty WB, and Peppas NA. Accounts of Chemical Research 2011;44(10):1061-1070.

39. Pack DW, Hoffman AS, Pun S, and Stayton PS. Nature Reviews Drug Discovery 2005;4(7):581-593.

40. Owens DE, Jian Y, Fang JE, Slaughter BV, Chen Y-H, and Peppas NA. Macromolecules 2007;40(20):7306-7310.

41. Marek SR, Conn CA, and Peppas NA. Polymer 2010;51(6):1237-1243.

42. Fisher OZ and Peppas NA. Macromolecules 2009;42(9):3391-3398.

43. Hayashi H, Iijima M, Kataoka K, and Nagasaki Y. Macromolecules 2004;37(14):5389-5396.

44. Morse AJ, Dupin D, Thompson KL, Armes SP, Ouzineb K, Mills P, and Swart R. Langmuir 2012;28(32):11733-11744.

45. Ignatova M, Voccia S, Gilbert B, Markova N, Cossement D, Gouttebaron R, Jerome R, and Jerome C. Langmuir 2006;22(1):255-262.

46. Moghimi SM, Hunter AC, and Murray JC. Pharmacological Reviews 2001;53(2):283-318.

47. Odian G. Principles of Polymerization, Fourth ed. Hoboken, New Jersey: John Wiley and Sons, 2004.

48. Ham GE. Copolymerization. In: Mark H, editor. High Polymers, vol. 18. New York: Interscience Publishers, 1964.

49. Schmaljohann D. Advanced Drug Delivery Reviews 2006;58(15):1655-1670.

50. Khokhlov AR and Kramarenko EY. Macromolecular Theory and Simulations 1994;3(1):45-59.

51. Owens DE and Peppas NA. International Journal of Pharmaceutics 2006;307(1):93-102.

52. Standardization IOf. ISO 13321: Particle Size Analysis - Photon Correlation Spectroscopy. 1996.

53. Heurtault B, Saulnier P, Pech B, Proust J-E, and Benoit J-P. Biomaterials 2003;24(23):4283-4300.

54. Gref R, Domb A, Quellec P, Blunk T, Müller RH, Verbavatz JM, and Langer R. Advanced Drug Delivery Reviews 1995;16(2–3):215-233.

55. Schwarte LM and Peppas NA. Polymer 1998;39(24):6057-6066.

56. Vinogradov SV, Zeman AD, Batrakova EV, and Kabanov AV. Journal of Controlled Release 2005;107(1):143-157.

57. Verwey EJW and Overbeek JTG. Theory of the Stability of Lyophobic Colloids: Courier Dover Publications, 1999.

58. Brannon-Peppas L and Peppas NA. Chemical Engineering Science 1991;46(3):715-722.

59. Siegel RA and Firestone BA. Macromolecules 1988;21(11):3254-3259.

60. Farmer TG, Edgar TF, and Peppas NA. Industrial & Engineering Chemistry Research 2008;47(24):10053-10063.

61. Emileh A, Vasheghani-Farahani E, and Imani M. European Polymer Journal 2007;43(5):1986-1995.

62. Moriyama K and Yui N. Journal of Controlled Release 1996;42(3):237-248.

63. Kalyanasundaram K and Thomas JK. Journal of the American Chemical Society 1977;99(7):2039-2044.

64. Lee AS, Gast AP, Butun V, and Armes SP. Macromolecules 1999;32(13):4302-4310.

Chapter 5: Membrane Disruptive Properties of Hydrophobic Polybasic Nanoscale Hydrogels

5.1. INTRODUCTION

Compositional considerations, such as the balance between cationic and nonionic, hydrophilic components and ratio of hydrophobic monomers have significant impact on resultant drug delivery properties (i.e. transfection efficiency, complex stability, etc.) [1]. These parameters must be carefully investigated and optimized in the development of polymer drug delivery systems. It is generally understood that increasing cationic content leads to increased nucleic acid condensation. Previous work on the interaction between poly(dimethylaminoethyl methacrylate) (PDMAEMA) or poly(aminoethyl methacrylate) (PAEMA) and DNA showed that PAEMA interacts more strongly with DNA while PDMAEMA exhibited superior buffering capacity [1], which should lead to increased endosomolytic activity. However, excess cationic content in polymer delivery systems can have deleterious effects. High cationic charge density is frequently correlated with toxicity of conventional cationic polymers like poly(ethyleneimine) (PEI) [2] and may host of undesirable consequences in vivo [3].

Thus, hydrophobically-modified polymers with decreased charged density have been investigated as substitutes in polynucleotide (e.g. DNA, siRNA) delivery applications. Hydrophobic modifications to gene-delivery polymers serve to, among others, enhance the physical encapsulation of genetic material, increase non-specific adsorptive endocytosis, facilitate unpacking of gene-polymer complexes, and potentially increase cytocompatibility [4]. High molecular weight polymers with decreased charge density have markedly improved gene transfection efficiency in some systems [5].

Recently, Saltzman and coworkers [6] described a series of lactone-based terpolymers with tunable hydrophobicity based on lactone ring size. The best-performing terpolmyer was susceptible to serum aggregation and subsequently required a surface coat of an RGD-terminated polyglutamic acid to enhance colloidal and in vivo stability. This polymer subsequently enabled the delivery of the pro-apoptotic TRAIL gene to tumor xenografts and slowed tumor growth.

Chapter 4 outlined a facile strategy to tune the polymer hydrophobicity and critical swelling pH by incorporating tert-butyl methacrylate in the nanogel. This synthetic strategy has been employed by Peppas and coworkers [7-9] to decrease critical swelling pH and others to increase endosomolytic [10] and gene transfection [11] efficiency. The previous studies in Chapter 4 compared the pH-dependent aqueous solution behavior of P(DEAEMA-g-PEGMA) and P(DEAEMA-co-TBMA-g-PEGMA) nanogels. TBMA-modified networks exhibited a more tightly collapsed network at elevated pH [7], which could theoretically provide improved protection of encapsulated siRNA. Moreover, a decrease in the pH required to induce a critical transition (as demonstrated by PDETB30) may minimize premature siRNA release before the intended site of action.

However, the optimum balance between hydrophobic and cationic core monomers must be carefully considered. Excessive core hydrophobicity could result in limited siRNA encapsulation, poor buffering capacity, and perhaps inefficient endosomolysis due to lack of cationic core groups. Decreased swelling observed with increased core hydrophobicity may also limit the diffusion of siRNA in to and out of the nanogel below critical swelling pH.

This work builds upon the studies performed in Chapter 4 and seeks to understand the role of hydrophobicity in modulating membrane destabilization. To study this interaction, three model membrane systems were used. Sheep erythrocytes were used to assess the pH- and concentration-dependent membrane destabilization of lipid bilayers, lactate dehydrogenase (LDH) leakage was measured from Caco-2 and RAW 264.7 cells to evaluate the non-specific membrane destabilization in live cells, and giant unilammelar vesicles (GUVs) were used to gain insight into the mechanism of membrane destabilization. Cytotoxicity of each copolymer was also investigated as a function of concentration and exposure time.

5.2. MATERIALS AND METHODS

5.2.1. Polymer synthesis and purification

Polymer synthesis and purification proceeded as described in Section 4.3.1 and Section 4.3.2. Briefly, 2-(diethylamino) ethyl methacrylate (DEAEMA, Sigma-Aldrich, St. Louis, MO), 2-(tert-butylamino)ethyl methacrylate (TBAEMA, Polysciences, Inc., Warrington, PA), tert-butyl methacrylate (TBMA, Sigma-Aldrich, St. Louis, MO), and tetra(ethylene glycol) dimethacrylate (TEGDMA, Sigma-Aldrich, St. Louis, MO) were passed through a column of basic alumina powder to remove inhibitor prior to use. Poly(ethylene glycol) methyl ether methacrylate (PEGMA), Mn ~ 2080, (Sigma-Aldrich, St. Louis, MO) was used as received. DEAMA, TEGDMA, and TBMA or TBAEMA were added to an aqueous solution containing 5 wt% PEGMA, Irgacure 2959 (Ciba Geigy, Tarrytown, NY) at 0.5 wt% of total monomer, 4 mg mL^{-1} Brij-30 (Acros Ogranics, Fair Lawn, NJ) and ionic surfactant myristyltrimethylammonium bromide

(MyTAB, Sigma-Aldrich, St. Louis, MO). The reaction pH was routinely pH 8.5. The mixture was emulsified using a Misonix Ultrasonicator (Misonix, Inc., Newtown, CT). The emulsion was purged with nitrogen gas and exposed to a UV source for 2.5 h with constant stirring. MyTAB, Brij 30, and unreacted monomers were removed by repeatedly inducing polymer-ionomer collapse, separating particles by centrifugation, and resuspending in 0.5 N HCl. Polymer particles were dialyzed against ddH20 for 7 days with the water changed twice daily. Following dialysis, polymers were flash frozen in liquid N2 and lyophilized for 5 days.

5.2.2. Fluorescence Spectroscopy

Pyrene fluorescence measurements were conducted in similar fashion to those described in Section 4.2.7. Pyrene excitation spectra were collected on a Fluorlog-3 Spectrofluorometer (Jobin Yvon, Horiba Scientific, Edison, NJ). Excitation spectra were collected with λ_{em} = 390 nm, 1 nm increments, 1 nm slit for excitation, and 1.5 nm for emission, and 0.8 s integration time.

5.2.3. Cell Culture

Human colorectal adenocarcinoma cells (Caco-2) and murine macrophages (RAW 264.7) were maintained in Dulbecco's Modified Eagles Medium (DMEM) supplemented with 100 U mL^{-1} penicillin, 100 μg mL^{-1} streptomycin, 0.25 μg mL^{-1}Amphotercin B, and 10% FBS. Caco-2 cells were used between passage 34 and 62. RAW 264.7 cells were used between passage 9 and 16. Caco-2 cells were passaged by washing with pre-warmed Dulbecco's phosphate buffered saline (DPBS) and subsequent incubation with 0.25% Trypsin-EDTA at 37°C. Trypsin was neutralized by addition of

fresh, prewarmed DMEM and cells were separated by centrifugation. The resulting pellet was suspended in 10 mL DMEM and cell count was determined using a Scepter Automated Cell Counter (Millipore, Billerica, MA) with 60 μm tips. The cell suspension was diluted as necessary and added to tissue-culture treated flasks or multi-well plates. Caco-2 cells were typically passaged at 1:5 ratio with media replenished every 2-3 days. RAW 264.7 cells were passaged by washing with prewarmed DPBS and replacing the original culture volume with fresh DMEM. Cells were removed from the flask surface by gentle scraping with a 25 cm cell scraper (BD Falcon, Franklin Lakes, NJ). The number of suspended cells was counted using a Scepter Automated Cell Counter and diluted as necessary for addition to tissue culture flasks or multi-well plates. RAW 264.7 cells were typically passaged every 2 days.

5.2.4. Cytocompatibility

In vitro cytocompatibility of polycationic nanoscale hydrogels was evaluated using commercially available cytotoxicity assays. MTS assays were performed using the CellTiter 96 AQueous One Solution Cell Proliferation Assay kit (Promega Corp., Madison, WI) in which the soluble tetrazolium salt [3-[4,5-dimethylthiazol-2-yl]-5-(3-carboxymethoxyphenyl)-2-(4-sulfophenyl)-2H-tetrazolium] (MTS) is reduced to a purple formazan product. The absorbance of the formazan product is proportional to the number of viable cells. Stock solutions of polymer were suspended in PBS and allowed to equilibrate overnight. Caco-2 cells were seeded in 96-well plates at 15,000 cells/well and incubated for 36 hours prior in 200 μL DMEM. RAW 264.7 cells were seeded in 96-well plates at 10,000 cells/well and incubated for 36 hours prior to assay in 200 μL DMEM.

Media was aspirated and cells were washed 2× with DPBS and incubated in 160 µL serum-free DMEM for 90 minutes. Following this incubation period, polymer stock solutions at 5× were added to cells for another designated exposure times. Media and polymer were aspirated and replaced with a DMEM/MTS solution. Absorbance at 490 nm was recorded after 4 hours incubation in the DMEM/MTS solution.

5.2.5. Membrane Destabilization

5.2.5.1. Hemolysis

Sheep blood in sodium citrate was obtained from Hemostat Laboratories (Dixon , CA) and used for up to two weeks after receipt. Phosphate buffers (0.15 M) from pH 5.0 – 8.0 were prepared by dissolving predetermined amounts of monosodium phosphate and disodium phosphate in ultrapure DI water. The buffer pH was adjusted as needed using 1 N HCl or 1 N NaOH. Dry nanoscale hydrogels were suspended in 150 mM phosphate buffer at the desired pH at a concentration of 2.5 mg ml^{-1} and allowed to equilibrate overnight. Erythrocytes were isolated from whole sheep blood by 3 successive washes with freshly prepared 150 mM NaCl. Red blood cells (RBCs) were separated by centrifugation from 10 minutes at 2,000×g. The supernatant and remaining buffy coat were carefully aspirated and discarded. After removing the supernatant following the final wash, RBCs were suspended in a volume of 150 mM phosphate buffer identical to that of the original blood aliquot at the pH matching that of the suspended polymers. This solution was diluted 10-fold in 150 mM phosphate buffer to yield an RBC suspension of approximately 5×10^8 cells/mL. In a typical experiment, 1×10^8 RBCs were exposed to nanogels at specified concentrations while shaking in a bead bath (LabArmor,

Cornelius, OR) pre-equilibrated at 37°C. Following a 60 min incubation period, samples were centrifuged at 14,500 RPM for 5 min to separate cells and membrane fragments. An aliquot of each sample was transferred to a clear 96-well plate and hemoglobin absorbance was measured at 541 nm. Negative controls (0% lysis) consisted of 150 mM phosphate buffer at experimental pH and positive controls (100% lysis) consisted of RBCs incubated in ultrapure DI water.

The pH values tested in this analysis range from pH 5.0 – pH 8.0; experiments performed at pH 5.00, 5.50, 6.00, 6.50, 7.40, 7.60, 7.80, and 8.00. The concentrations tested range from 1 – 2000 μg ml^{-1}; with experiments performed with 2000, 1000, 500, 250, 100, 50, 25, 10, 5, 2.5, and 1 μg ml^{-1} nanogel suspended in 150 mM phosphate buffer at the specified pH.

5.2.5.2. Lactate Dehydrogenase Release

LDH assays were performed using a CytoTox-ONE™ Homogeneous Membrane Integrity Assay (Promega Corp., Madison, WI) to measure release of lactate dehydrogenase (LDH) from cells with damaged membranes. Cells were seeded to 96-well plates and polymer solutions added as previously described. At designated time points, 50 μL aliquots of media was aspirated and combined with 50 μL LDH assay buffer in a black-walled 96-well plate. Following 10 minutes incubation at room temperature, the fluorescence was measured at 530 ex/590 em. Generally, cell culture plates were used for a maximum of two different aliquots.

5.2.5.3. Giant Unilammelar Vesicle Disruption

1-palmitoyl-2-oleoyl-sn-glycero-3-phosphocholine (POPC), 1,2-dihexadecanoyl-sn-glycero-3-phosphoethanolamine (DHPE) labeled with BODIPY® FL, cholesterol, and Texas Red-sucrose were kindly donated by Prof. Jeanne Stachowiak (University of Texas at Austin, Austin, TX). Giant unilammelar vesicles (GUVs) were synthesized via electroformation as previously described [12, 13]. Briefly, lipid/cholesterol solutions were combined in the following ratio: 7:3:0.01 POPC:Cholesterol:Bodipy FL DHPE and drop-cast onto clean glass slides. The lipid solutions were allowed to dry and were then assembled into electroformation chambers. Vesicles were electroformed at 60°C in Texas Red-sucrose (~350 milliosmole(mOsm)) solution.

GUVs were placed in 35 mm glass-bottom petri dishes for real-time confocal microscopy imaging. PDET and PDETB30 were prepared at 2 mg ml^{-1} in 100 mM phosphate buffer adjusted to pH 6.50. The osmolarity of the resulting suspensions was measured and adjusted with sucrose to ~350 mOsm as needed. 1 ml of GUV suspension was transferred to the glass-bottom petri dish and was allowed to sediment for 5 min. 25 μL of the nanogel suspension was carefully injected into the dish so as not to disturb the spatial distribution of focused GUVs. Images were collected every 5 s at a fixed focal plane.

5.3. RESULTS AND DISCUSSION

5.3.1. Pyrene Fluorescence Spectroscopy

Analogous to the pyrene emission studies performed in Section 4.3.7, pyrene excitation spectra were collected to confirm the pH required for phase transition from

hydrophobe to hydrophile. The maximum excitation wavelength of pyrene red-shifts from 333 nm to 338 nm upon transition from polar to nonpolar environment. Therefore, an increase in the excitation I_{338}/I_{333} ratio indicates pyrene is preferentially partitioned in hydrophobic domains. Figure 5.1 shows a representative change in pyrene fluorescence in aqueous suspensions of PDETB30 between collapsed hydrophobe (pH 8.0) and swollen hydrophile (pH 6.0). Consequently, the fluorescence excitation spectra of pyrene can be used to probe the polarity of aqueous nanogel suspensions and determine the influence of polymer composition on nanogel hydrophobicity and the critical pH required to induce a conformational transition.

Increasing the proportion of TBMA causes a clear decrease in the onset for the pH-dependent phase transition, as seen in Figure 5.2. These observations follow the expected trend - increasing TMBA composition progressively lowers the apparent pH (pH_{app}) for the hydrophobic – hydrophilic transition. Moreover, these data corroborate the pH-responsive swelling profiles presented in Figure 4.12A and are in excellent agreement with the pyrene emission studies shown in Figure 4.16A.

Likewise, increasing the proportion of TBAEMA from 0 mol% of DEAEMA to 30 mol% of DEAEMA causes a clear increase in the onset of the pH-dependent phase transition, as seen in Figure 5.3. This trend is also expected, given that TBAEMA contains a secondary amine that should increase the pKa, and thus the onset of pH-dependent phase transition, to higher pH values. The broad transitions observed for PDETBA20 and PDETBA30 for pyrene emission studies (Figure 4.16B) are notably absent in the I_{338}/I_{333} ratio of pyrene excitation spectra. In fact, the breadth of the phase

transition is quite similar for PDET, PDETBA10, PDETBA20, and PDETBA30. A direct comparison of the effects of TBMA and TBAEMA on pH of hydrophobe-hydrophile phase shift can be seen in Figure 5.4

5.3.2. Membrane Destabilization

This series of experiments was constructed to identify nanogels capable of selective membrane destabilization. An optimal nanogel would be relatively inert and non-disruptive under normal physiological conditions. Upon transition to endosomal conditions, this optimal nanogel would undergo a conformational transition to render it capable of potent membrane destabilization. Conversely, a non-optimal nanogel would mediate membrane disruption under physiological conditions and/or be non-disruptive in endosomal conditions.

5.3.2.1. Hemolysis

Hemolysis experiments were used to approximate the endosomolytic ability of these nanogels. The pH- and concentration-dependent hemolysis was determined according to Equation 5.1:

$$\%\,\boldsymbol{Hemolyis} = \frac{\boldsymbol{A_{sample} - A_{blank}}}{\boldsymbol{A_{max} - A_{blank}}} \tag{5.1}$$

Where A_{sample} represents RBCs exposed to polymer at a given pH and concentration, A_{blank} is the absorbance of the supernatant after RBC exposure to phosphate buffer at a given pH, and A_{max} represents maximum lysis following RBC

exposure to DI water. The relative lysis for nanoscale hydrogels containing varying amounts of TBMA or TBAEMA is shown in contour plot form in Figure 5.5. These data demonstrate that polymer composition has a clear impact on membrane-disruptive capabilities. As demonstrated previously with dynamic light scattering studies (Figure 4.12), the simple presence of a t-butyl group alone in the copolymer is not the critical parameter for exerting control over resultant physicochemical properties. Rather, the increased network hydrophobicity of TBMA-containing nanogels seems to govern the interactions with biological membranes.

As seen in Figure 5.5, inclusion of TMBA in the nanogels markedly expands both the pH and concentration range at which these networks effectively disrupt erythrocyte membranes. For example, PDET demonstrates efficient hemolysis at high concentrations (> 0.25 mg mL-1) and between pH 7.0 and pH 7.6. In contrast, PDETB30 demonstrates highly efficient hemolysis in the pH range of early endosomes (pH 5.5 – pH 6.5) at concentrations as low as 1 $\mu g\ mL^{-1}$. The enhanced hemolytic ability of PDETB30 at pH 6.0 is depicted in Figure 5.6, along with that of PDET and PDETBA30. Notably, PDETB30 is 10× more efficient (on a mass basis) than previously reported polycationic block copolymer systems with demonstrated efficacy in in vitro siRNA delivery[10] and 25× more efficient than phenylalanine-grafted pseudo-peptides[14] with demonstrated utility in intracellular protein delivery[15]. These data indicate that the membrane-disruptive properties of these nanogels can be tuned by adjusting hydrophobic monomer incorporation, an observation in accordance with several previous studies [16-20].

5.3.2.2. Lactate dehydrogenase leakage

The influence of polymer composition and exposure time on membrane destabilization in live cells was investigated using an LDH membrane integrity assay. In this assay, the percentage of LDH leakage from permeabilized or damaged cell membranes can be given by an equation analogous to Equation 5.2.

$$\%\ \boldsymbol{LDH\ Release} = \mathbf{100} * \frac{\boldsymbol{RFU_S - RFU_{PBS}}}{\boldsymbol{RFU_{max} - RFU_{PBS}}} \tag{5.2}$$

Where RFU_S is the fluorescent reading from the sample, RFU_{PBS} is the fluorescent reading from cells exposed only to PBS (0% lysis) and RFU_{max} (100% lysis) is the maximum fluorescent reading from the plate. In typical applications, RFU_{max} is given by a commercial lysis buffer. In practice, however, the fluorescent reading generated by the greatest polymer concentration (2 mg/mL) generated fluorescent values that exceeded that of the kit lysis buffer and 1% w/v solutions of Triton-X100. Thus, LDH release is occasionally reported as >100% at polymer concentrations 1 – 2 mg ml^{-1}.

LDH leakage as a function of nanogel concentration and exposure time is shown for PDET (Figure 5.7), PDETB30 (Figure 5.8), and PDETBA30 (Figure 5.9). For PDET (Figure 5.7), the LDH leakage increases with longer exposure time (60 min to 180 min) and remains relatively constant from 180 min to 360 min. For PDETB30 (Figure 5.8), the LDH leakage is negligible at concentrations up to 250 μg ml^{-1} for 60 min and 180 min exposure. However, the leakage increases considerably following 360 min exposure. LDH release following exposure to PDETBA30 (Figure 5.9) follows no clear time dependence and the release values are similar across all time points. These data

underscore the need for careful consideration of incubation time in future cytotoxicity and siRNA delivery experiments to minimize the non-selective disruption of cellular membranes.

The influence of nanogel composition on LDH leakage, shown in Figure 5.10A for TBMA-containing polymers and Figure 5.10B for TBAEMA-containing polymers, show that PDETB30 is less damaging to Caco-2 cell membranes than PDET, PDETB10, and PDETB20. The general trend for inducing LDH membrane leakage is PDET ~ PDETB10 ~ PDETB20 > PDETB30. For the TBAEMA-containing polymers (Figure 5.10B), the general trend is as follows: PDETBA30 > PDETBA20 ~ PDETBA10 > PDET. Notably, these trends are in excellent agreement with the trends in hydrophobic-hydrophilic phase transition shown in Figure 5.2 and Figure 5.3 and summarized in Table 5.1.

Therefore, the pH-responsive transition regime (from collapsed hydrophobe to swollen hydrophile) is critical factor in determining the membrane-disruptive ability of these nanogels. In all cases, nanogels were demonstrated maximum hemolysis at or near the pH_{app} determined by pyrene fluorescence studies (Table 5.1). If this pH_{app} is near physiological pH, this membrane-disruptive effect was obvious in hemolysis (at pH 7.4) and LDH leakage assays. However, if the pH_{app} is decreased through increased polymer hydrophobicity (e.g. PDETB30), the nanogels are less disruptive at physiological conditions and more disruptive at endosomal conditions.

5.3.2.3. Giant Unilammelar Vesicle Disruption

Visualizing a model lipid bilayer during the destabilization can provide some insight into the mechanism of membrane disruption. Prevailing theories for membrane disruptive mechanisms by cationic polymers include reorientation of lipid head groups through ammonium-phosphate interactions [21], transient nanopore formation [22, 23] following electrostatic attraction between polycation and cell membrane, or even catastrophic membrane disruption [24]. Naturally, size, surface charge, and ligand functionalization play important roles in modulating membrane interaction [25]. However, many of these studies rely on biophysical measurements of controlled model systems such as supported lipid bilayers. In reality, mammalian cell membranes are far more complex than these model systems. Mammalian cell membranes typically contain dynamic combinations of surface- and transmembrane proteins, sugar coatings, diverse lipid combinations, and cholesterol. Unfortunately, a mechanistic comprehension of membrane destabilization in mammalian cell membrane is currently underdeveloped.

The micrographs in Figure 5.11 suggest that transient nanopore formation is the predominant mechanism through which PDETB30 exerts a membrane-destabilizing effect. For these initial studies, pH 6.50 was selected to approximate the pH of an early endosomal environment. Based on the hemolysis studies presented in Figure 5.5, PDET should be non-disruptive and PDETB30 should be highly-disruptive at these conditions. Following an injection to bring the PDET to 50 $\mu g\ ml^{-1}$ in the buffered GUV solution, no discernible change was detected in membrane integrity. The sucrose-Texas Red remains entrapped in the GUV for several minutes after injection, confirming the persistence of membrane integrity. The difference in GUV location in Figure 5.11, Panels A and C is

due to a mechanical disturbance displacing the GUVs from the focal plane. Shifting the focal plane revealed that many GUVs had been forced downward by the force of the PDET injection.

In contrast, the micrographs in Figure 5.11, Panels B and D, reveal substantial PDETB30-mediated destabilization of lipid membranes. Exposure to 50 ug ml^{-1} PDETB30 in pH 6.50 buffered solution resulted in a rapid and complete efflux of sucrose-Texas Red from the vesicle interior. These data concur with the hemolysis data for PDETB30 at this concentration and pH, which indicate complete (~100%) disruption of erythrocytes. Further efforts in this area will determine if the mechanism of membrane destabilization exhibits a dependence on polymer concentration. Additionally, the molecular weight of the entrapped fluorescent solute (currently sucrose) will be varied to estimate the average pore size formed by membrane-disruptive nanogels.

5.3.3. Cytocompatibility

The effect of polymer concentration and composition on cellular proliferation was assessed using MTS assays. These data are important to determine the non-toxic polymer doses for future drug delivery experiments. In this assay, the metabolic activity of an experimental population relative to control populations can be given by the ratio:

$$Relative\ Proliferation = \frac{A_S - A_{bkg}}{A_{PBS} - A_{bkg}} \tag{5.3}$$

Where A_s is the absorbance (λ = 490 nm) from sample wells, A_{bkg} is the background absorbance from DMEM/MTS solution, and A_{PBS} is the absorbance from wells in which cells were incubated only with DPBS.

5.3.3.1. Caco-2 Cells

As seen in Figure 5.12, PDETB20 and PDETB30 are non-toxic to Caco-2 cells at concentrations below 0.5 mg mL^{-1}. From 0.05 mg mL^{-1} - 2 mg mL^{-1}, these formulations are significantly less toxic than the base formulation of P(DEAEMA-g-PEG) (PDET). It has been well documented that free amino groups contribute to the untoward cytotoxicity of many polycationic delivery agents and that increased cationic charge density correlates with increased cytotoxicity [2]. As expected, polymers with similar cationic charge densities, e.g. nanogels with 20 mol% and 30 mol% TBAEMA, as well as PDET, exhibit similar toxicity profiles. By nature of the polymer composition, nanogels with 20 mol% and 30 mol% TBMA have less cationic charge density and thus result in decreased toxicity.

5.3.3.2. RAW 264.7 Cells

In order to assess the concentration- and time-dependent toxicity of polymer carriers in model cells of intestinal phagocytes, MTS assays were conducted on murine macrophage cells. As seen in Figure 5.13, the composition-dependent trend in toxicity profile remains consistent with observations in Caco-2 cells, though the magnitude of difference in toxicity was less pronounced. The general trend across the concentration range, in terms of relative toxicity, was PDET > PDETB10 > PDETB20 > PDETB30.

PDETB30 was significantly less toxic ($p < 0.05$) than the base formulation of PDET from 5 – 500 μg mL^{-1}.

Comparison the polymer dose-dependent toxicity between Caco-2 cells and RAW 264.7 cells reveals that the macrophages are more sensitive to the presence of nanogels than are the Caco-2 cells. This disparity may be due to the relative amount of nanogel uptake demonstrated by each cell type. Macrophages are phagocytic cells and will more readily imbibe macromolecules from their environment, thereby amplifying any harmful effects of the nanogels on cellular membranes or processes.

In order to develop a conservative estimate for nontoxic nanogel concentrations in further experiments, RAW 264.7 cells were exposed to nanogels for 24 h and the metabolic activity compared to untreated control cells via MTS assay. This comparison, shown in Figure 5.14 for PDET and PDETB30, reveals that PDETB30 is non-toxic below nanogel concentrations of 50 μg ml^{-1}.

5.4. CONCLUSIONS

Physicochemical properties of nanoscale hydrogel networks, including critical phase transition pH, membrane disruption, and cytocompatibility can be modulated by tuning polymer composition. PDETB30 nanogels exhibit favorable pH-responsive phase transition behavior for intracellular delivery and offer an excellent combination of hemolytic ability and cytocompatibility. Additionally, the breadth of the pH range for maximum membrane disruption is related to the pH range for hydrophobic-hydrophilic transition. PDETB30 is membrane-disruptive over a broader pH range than other nanogels that undergo a more rapid hydrophobic-hydrophilic phase transition (e.g. PDET

and PDETBA30). For these reasons, TBMA-containing nanoscale hydrogels, particularly PDETB30, possess attractive characteristics for intracellular drug delivery vehicles.

Table 5.1 – Comparison of critical pH values for phase transition and pH of maximum hemolysis.

Name	Copolymer	mol *t*-butyl/ 100 mol DEAEMA	pH_c[1]	pH_{app}[1]	pH_{hemo}[3]
PDET	P(DEAEMA-g-PEGMA)	0	7.37	7.39	7.4
PDETB10	P(DEAEMA-co-TBMA-g-PEGMA)	10	7.31	7.24	7.4
PDETB20	P(DEAEMA-co-TBMA-g-PEGMA)	20	7.36	7.04	6.5
PDETB30	P(DEAEMA-co-TBMA-g-PEGMA)	30	6.65	6.78	6.5
PDETBA10	P(DEAEMA-co-TBAEMA-g-PEGMA)	10	7.01	7.30	7.4
PDETBA20	P(DEAEMA-co-TBAEMA-g-PEGMA)	20	6.98	7.54	7.4
PDETBA30	P(DEAEMA-co-TBAEMA-g-PEGMA)	30	7.13	7.66	7.6

[1]Critical swelling pH determined by dynamic light scattering in Chapter 4, Figure 4.12.
[2]pH value for apparent hydrophobe-hydrophile phase transition (pH_{app}) determined by pyrene fluorescence spectroscopy. Determined by calculating the inflection point of sigmoidal fit in Figures 5.2 and 5.3.
[3]pH for maximum hemolysis at polymer concentration of 0.05 mg mL^{-1}

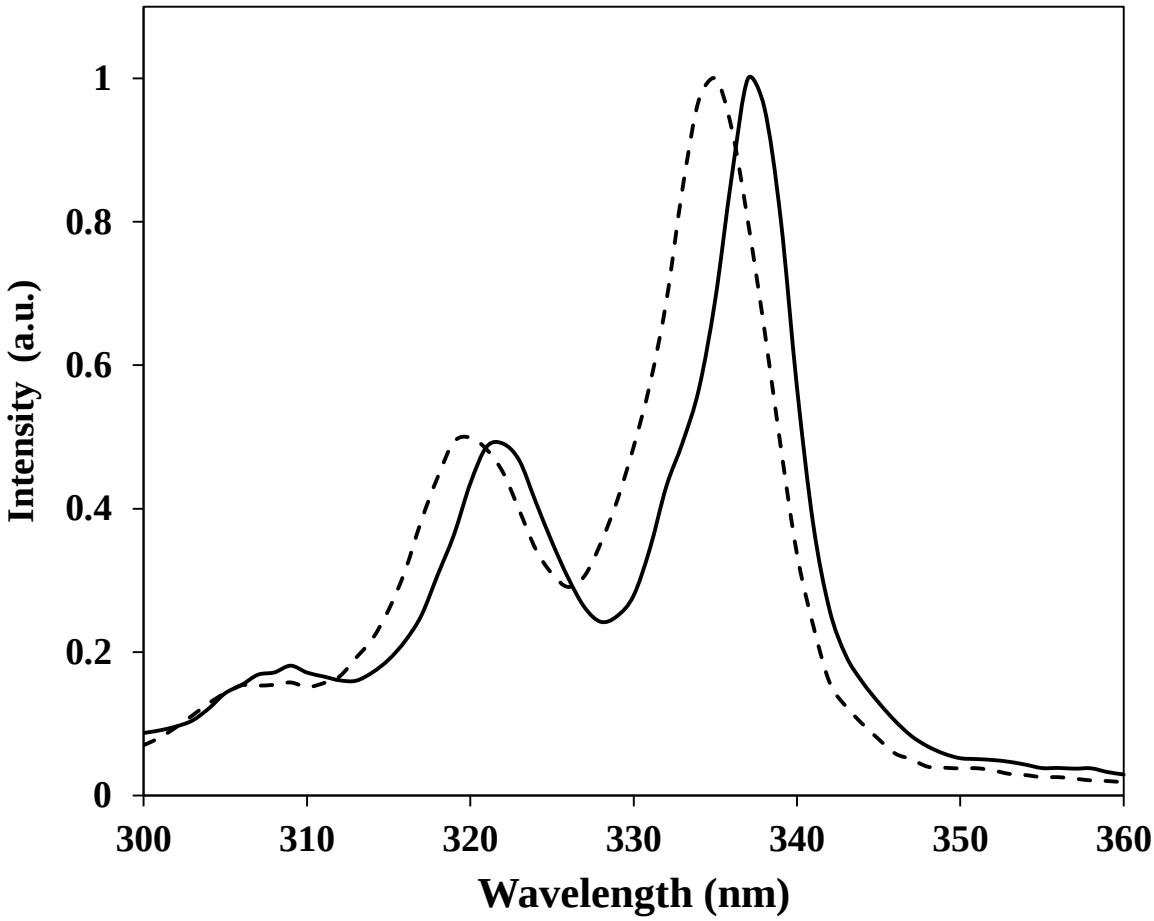

Figure 5.1 - Normalized fluorescent excitation spectra of pyrene in 100 mM phosphate buffer and 0.5 mg mL^{-1} PDET at pH 8.0 (solid) and pH 6.0 (dashed).

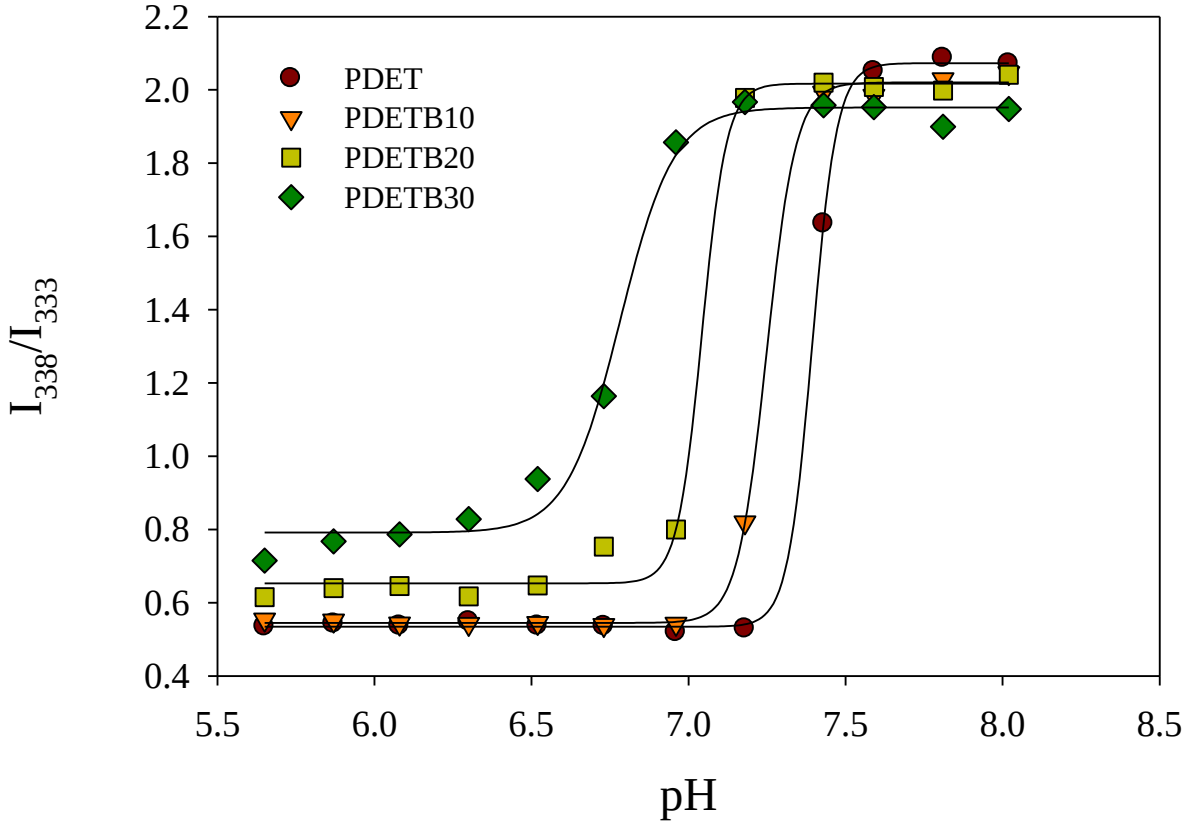

Figure 5.2 – Influence of TBMA incorporation on pyrene excitation (I338/I333 ratio) in P(DEAEMA-co-TBMA-g-PEGMA) nanogels. Nanogels suspended at 0.5 mg mL-1 and pyrene dissolved at 6×10-7 M in 100 mM phosphate buffers at designated pH values. Symbols designate PDET (●), PDETB10 (▼), PDETB20 (■), or PDETB30 (◊).

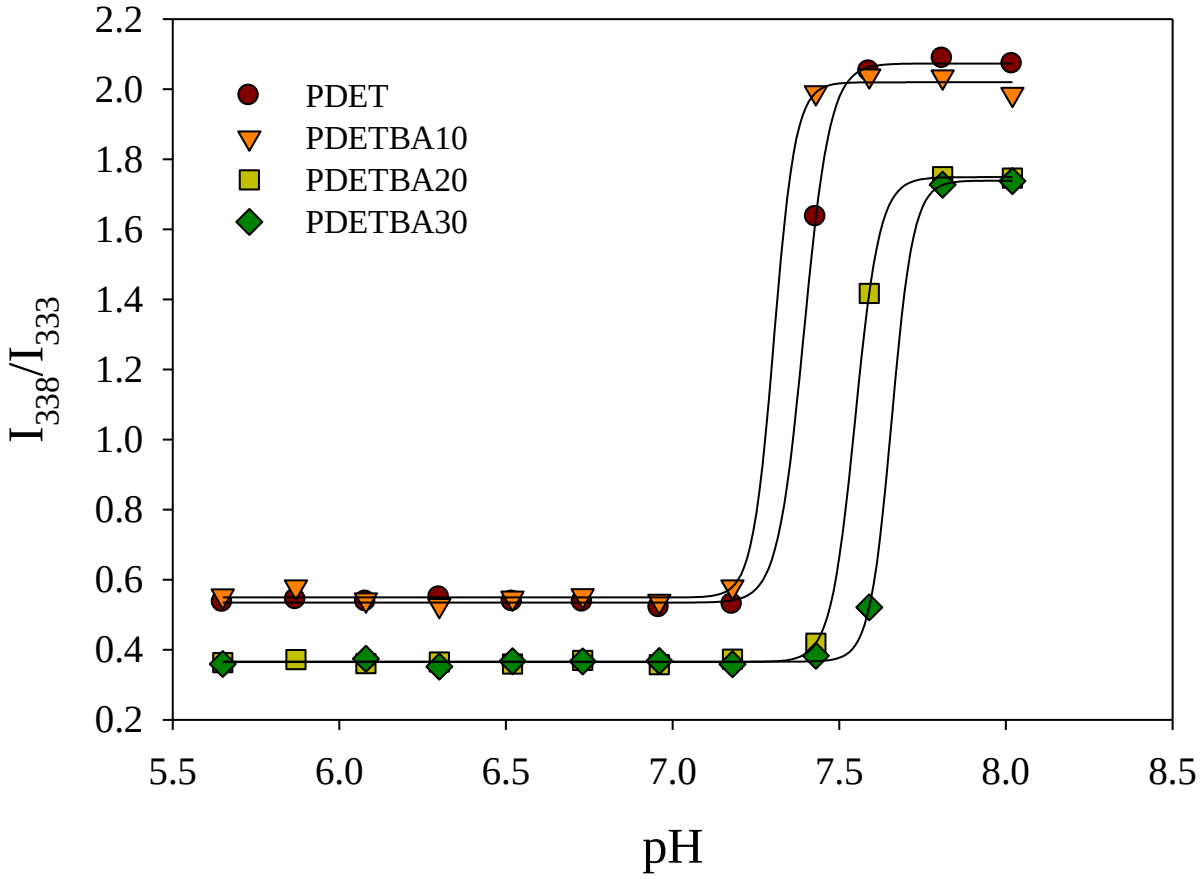

Figure 5.3 – Influence of TBAEMA incorporation on pyrene excitation (I_{338}/I_{333} ratio) in P(DEAEMA-co-TBAEMA-g-PEGMA) nanogels. Nanogels suspended at 0.5 mg mL^{-1} and pyrene dissolved at 6×10-7 M in 100 mM phosphate buffers at designated pH values. Symbols designate PDET (●), PDETB10 (▼), PDETB20 (■), or PDETB30 (◊).

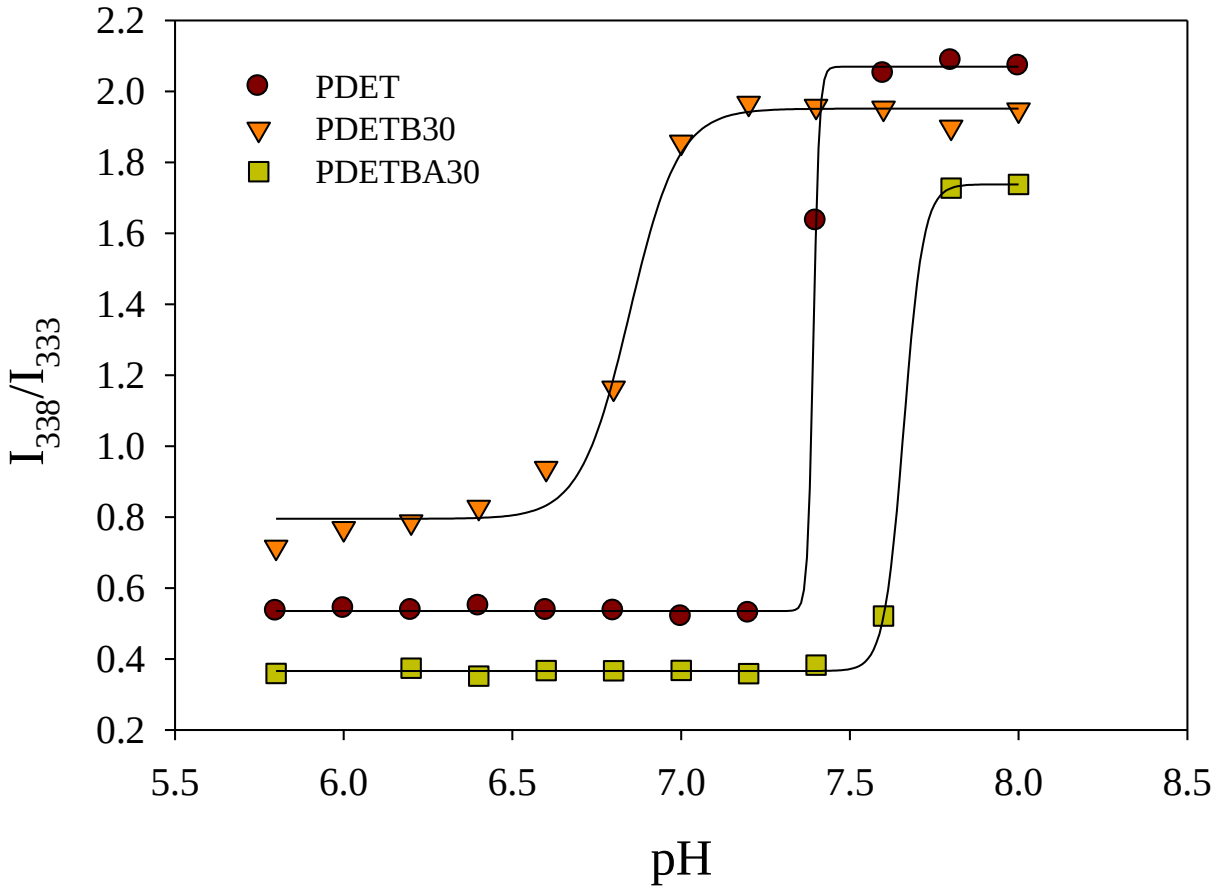

Figure 5.4 - Influence of hydrophobic moiety on fluorescence excitation spectra of pyrene. Pyrene dissolved at 6×10^{-7} M in 100 mM phosphate buffers with PDET (●), PDETB30 (▼), or PDETBA30 (■) at 0.5 mg mL^{-1}. Points represent measured data and lines represent best-fit sigmoidal curves.

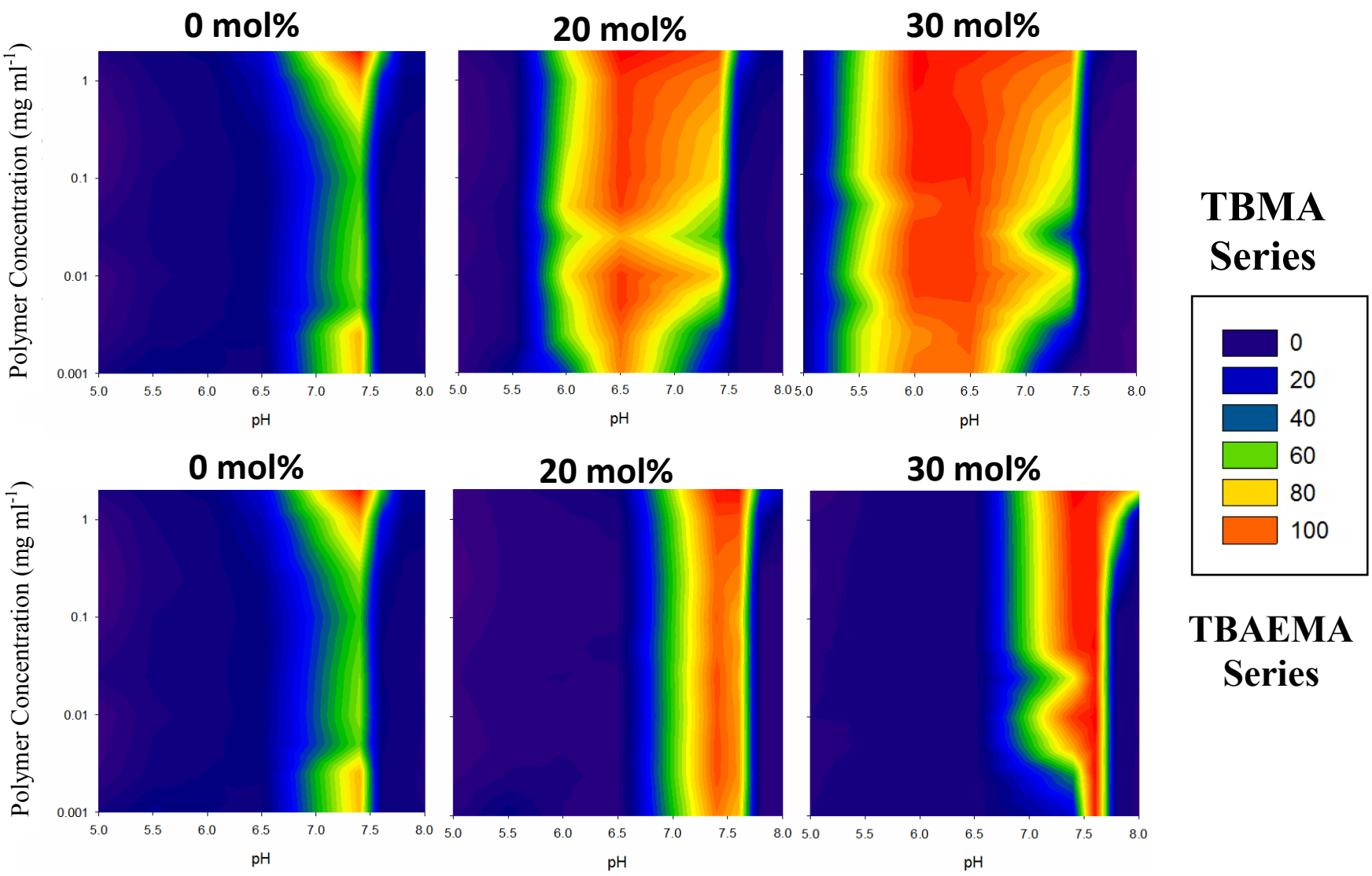

Figure 5.5 – Hemolysis as a function of nanogel concentration and solution pH. Contour plots for PDET, PDETB20 and PDETB30 (top) and PDET, PDETBA20, and PDETBA30 (bottom).

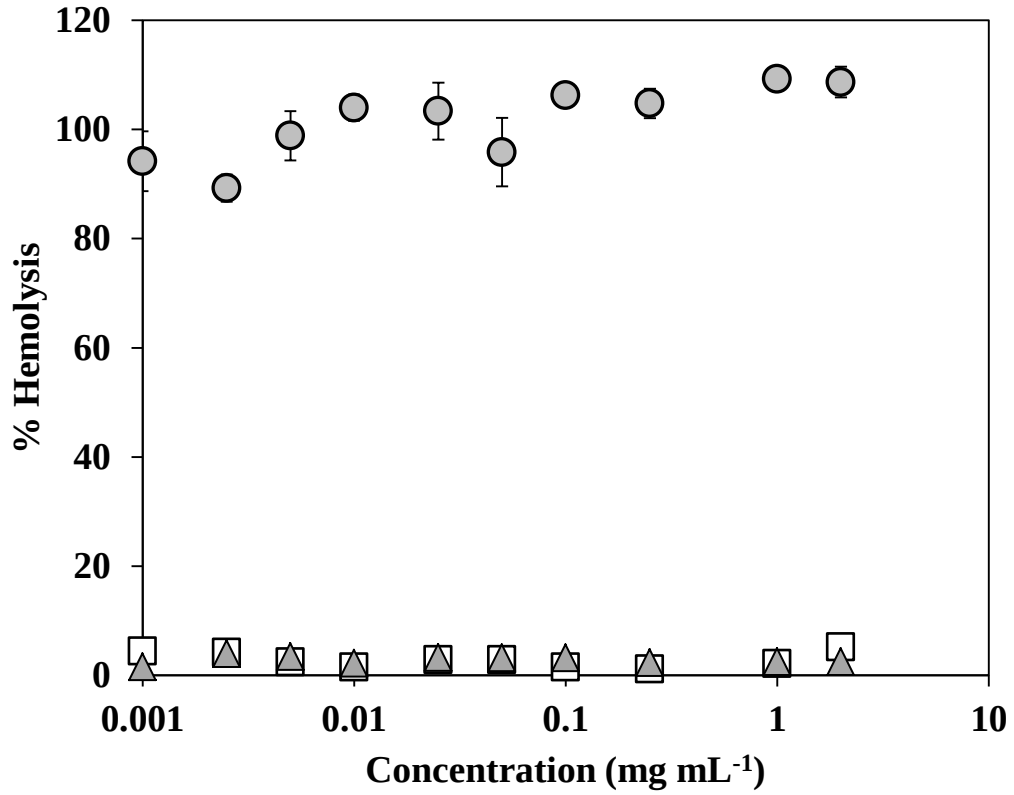

Figure 5.6 – Concentration-dependent hemolytic activity of PDET (□), PDETB30 (●), and PDETBA30 (□) in 150 mM phosphate buffer at early endosomal pH (pH 6.0). Erythrocytes exposed to various polymer concentrations for 60 min at 37°C. Data points represent the mean of triplicate samples ± s.d.

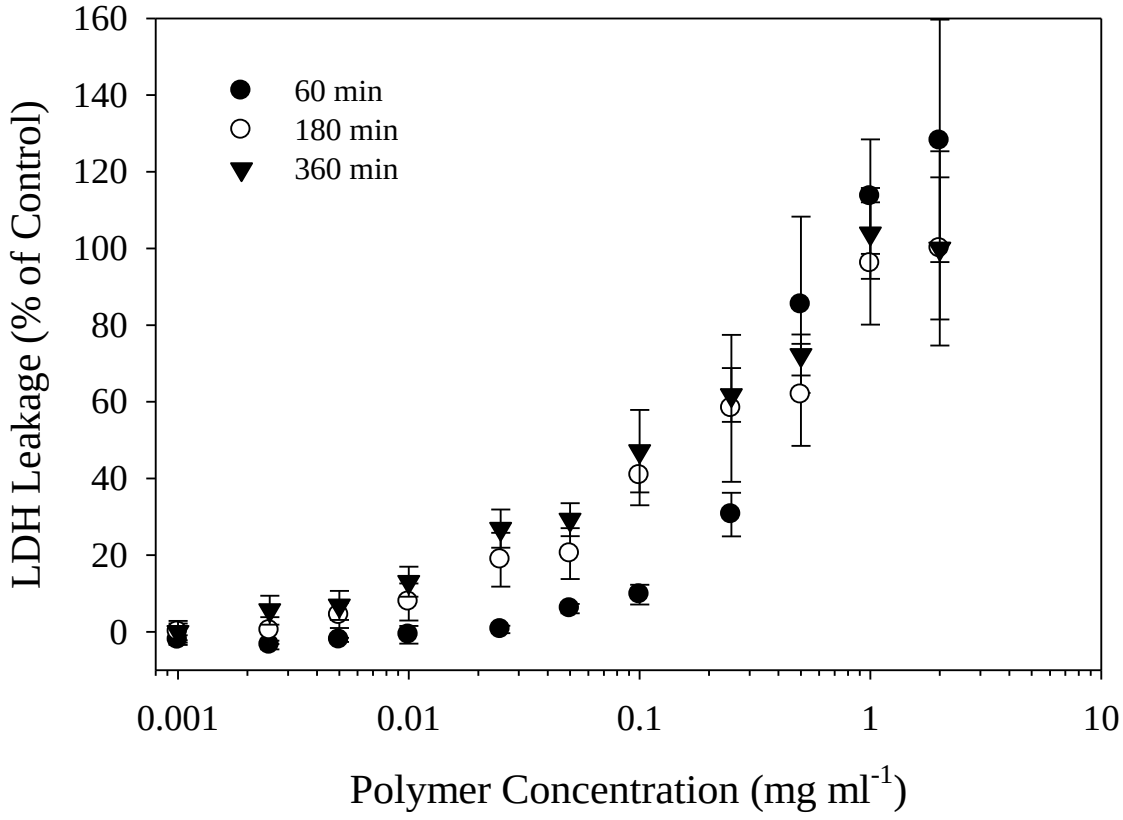

Figure 5.7 – Representative time-dependent LDH leakage from Caco-2 cells following 60 min (●), 180 min (○), or 360 min (▼) exposure to PDET. Data points represent the sample mean ± std error (n=4). LDH leakage calculated relative to untreated cells and surfactant-lysed cells.

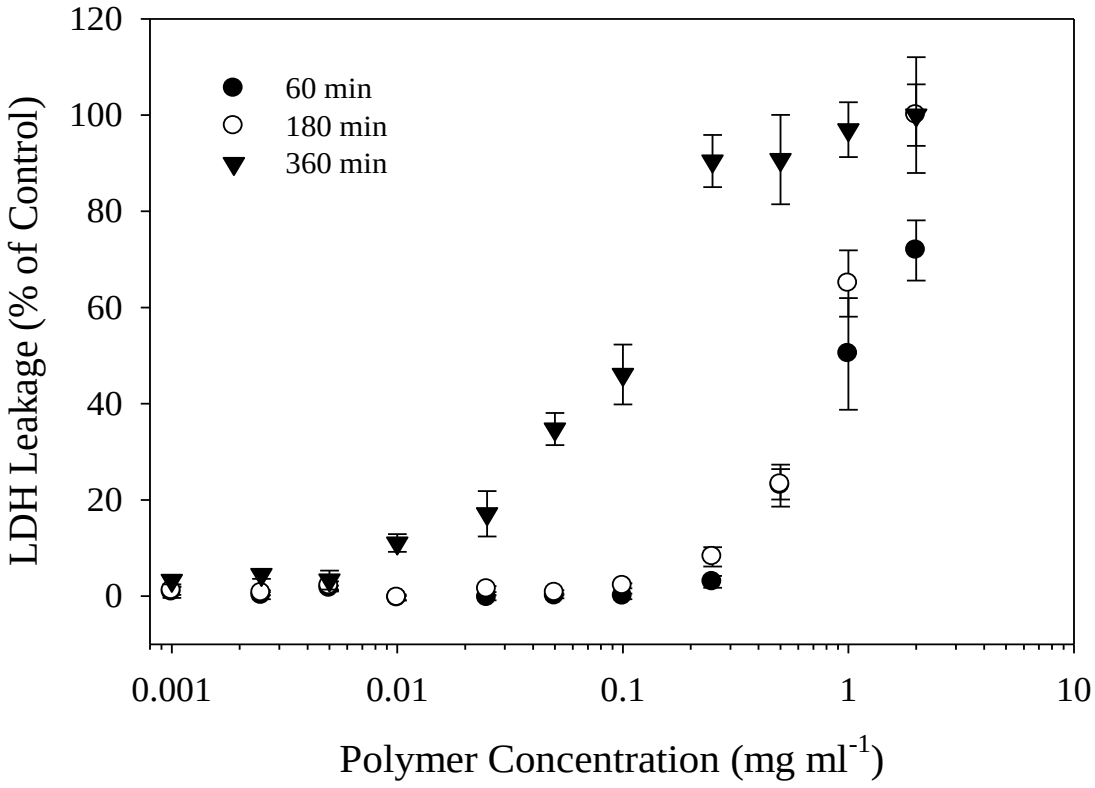

Figure 5.8 - Representative time-dependent LDH leakage from Caco-2 cells following 60 min (●), 180 min (○), or 360 min (▼) exposure to PDETB30. Data points represent the sample mean ± std error (n=4). LDH leakage calculated relative to untreated cells and surfactant-lysed cells.

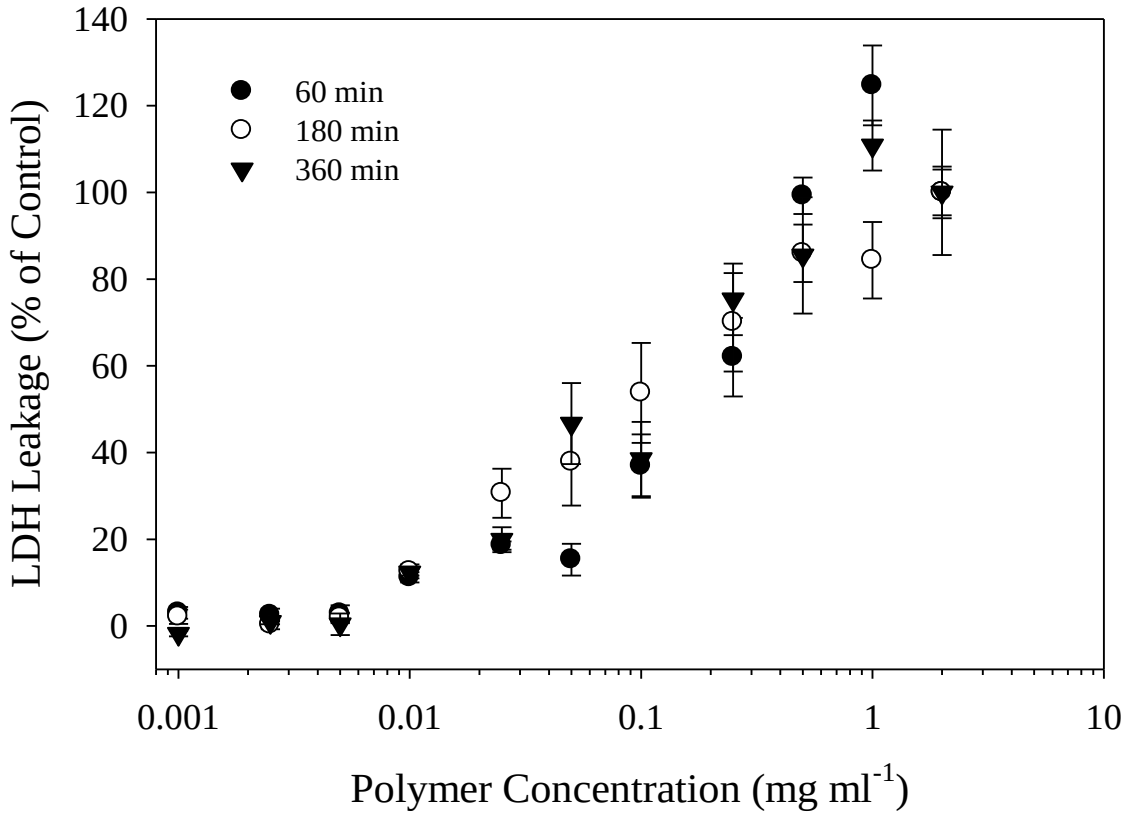

Figure 5.9 – Representative time-dependent LDH leakage from Caco-2 cells following 60 min (●), 180 min (○), or 360 min (▼) exposure to PDETBA30. Data points represent the sample mean ± std error (n=4). LDH leakage calculated relative to untreated cells and surfactant-lysed cells.

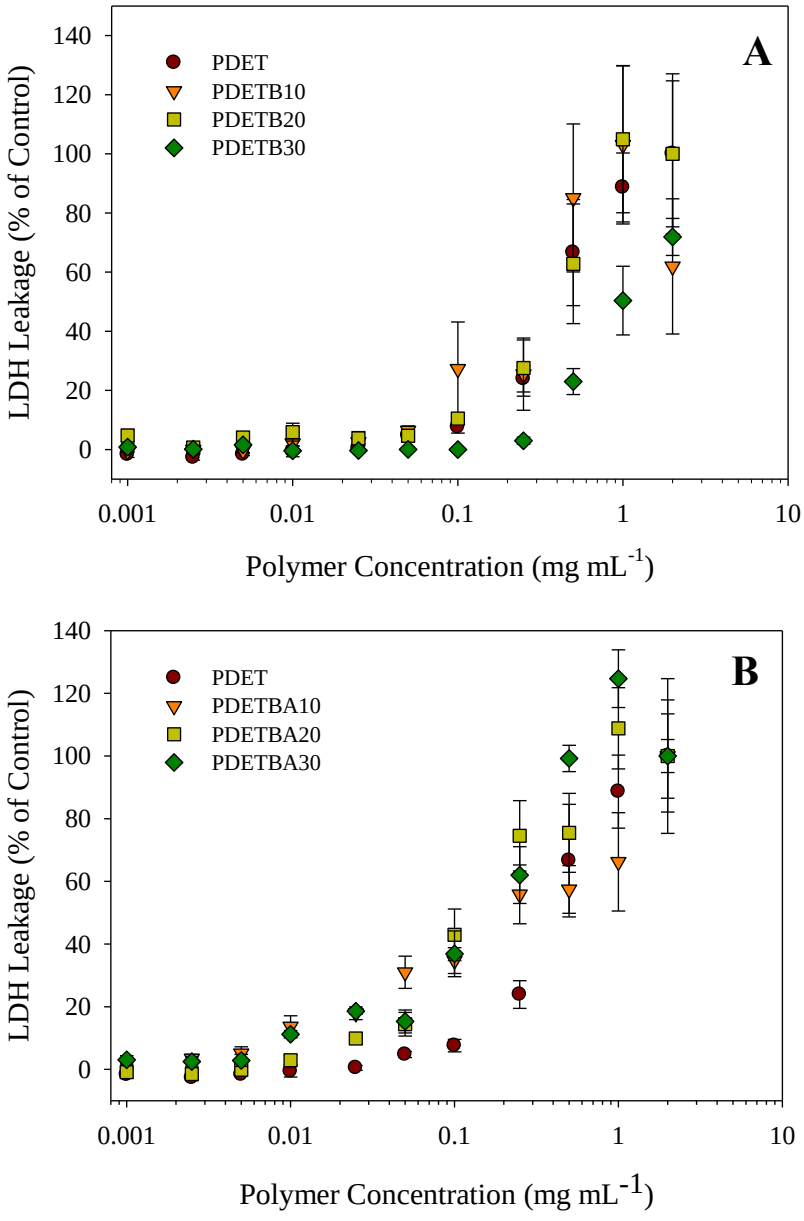

Figure 5.10 – Polymer-mediated LDH leakage from Caco-2 cells following exposure to PDET (●), PDETB10 (▼), PDETB20 (■), or PDETB30 (◊) for 60 min (A) or PDET (●), PDETBA10 (▼), PDETBA20 (■), or PDETBA30 (◊) for 60 min (B).

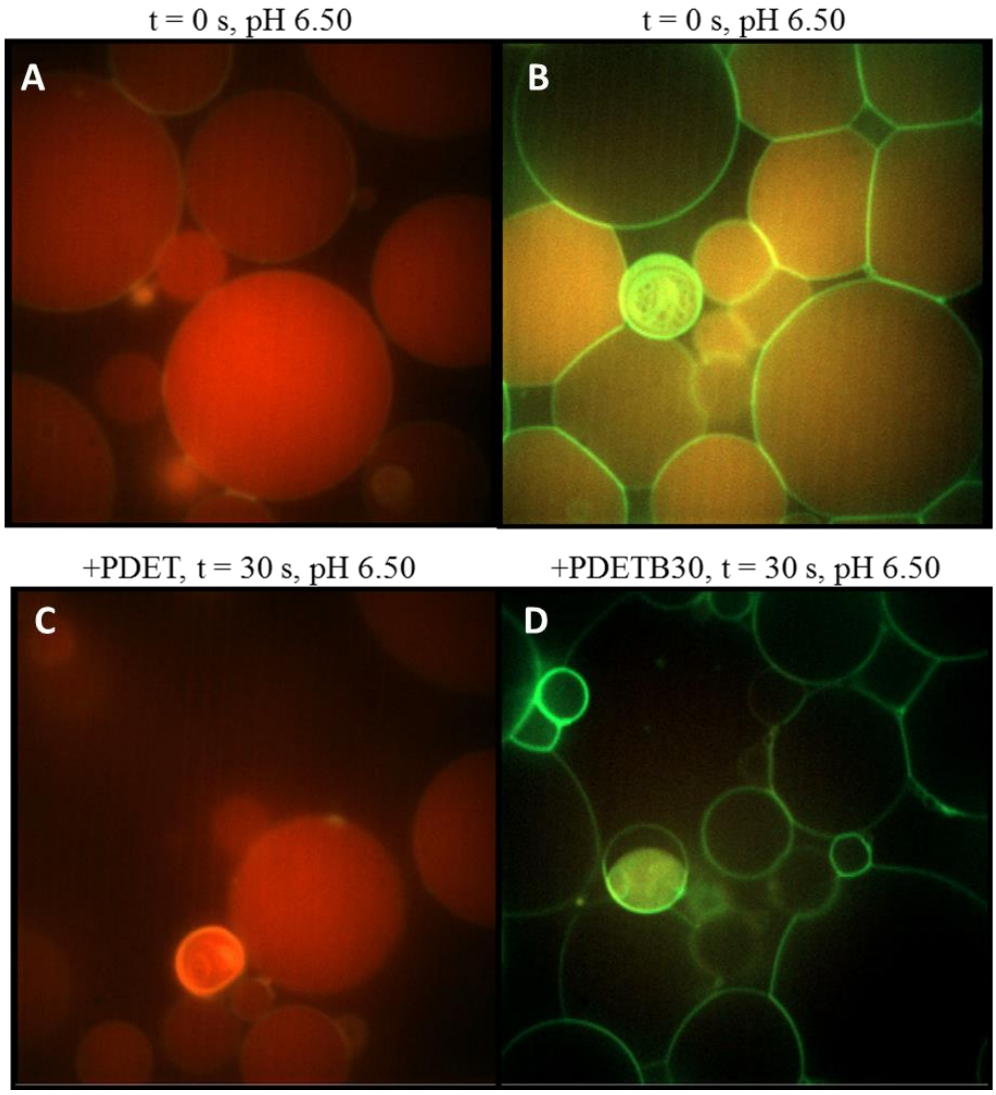

Figure 5.11 - Destabilization of GUV membranes. Intravesicle red fluorescence indicates sucrose-Texas Red. Green fluorescence indicates membrane lipid DHPE-Bodipy FL. GUVs were suspended in 100 mM phosphate buffer at pH 6.5. PDET (A) or PDETB30 (B) in isosmotic phosphate buffer was added at achieve a final concentration of 50 µg ml^{-1}. GUVs after 30 seconds incubation (C and D). Images captured using Zeiss spinning disc confocal microscope at 100×.

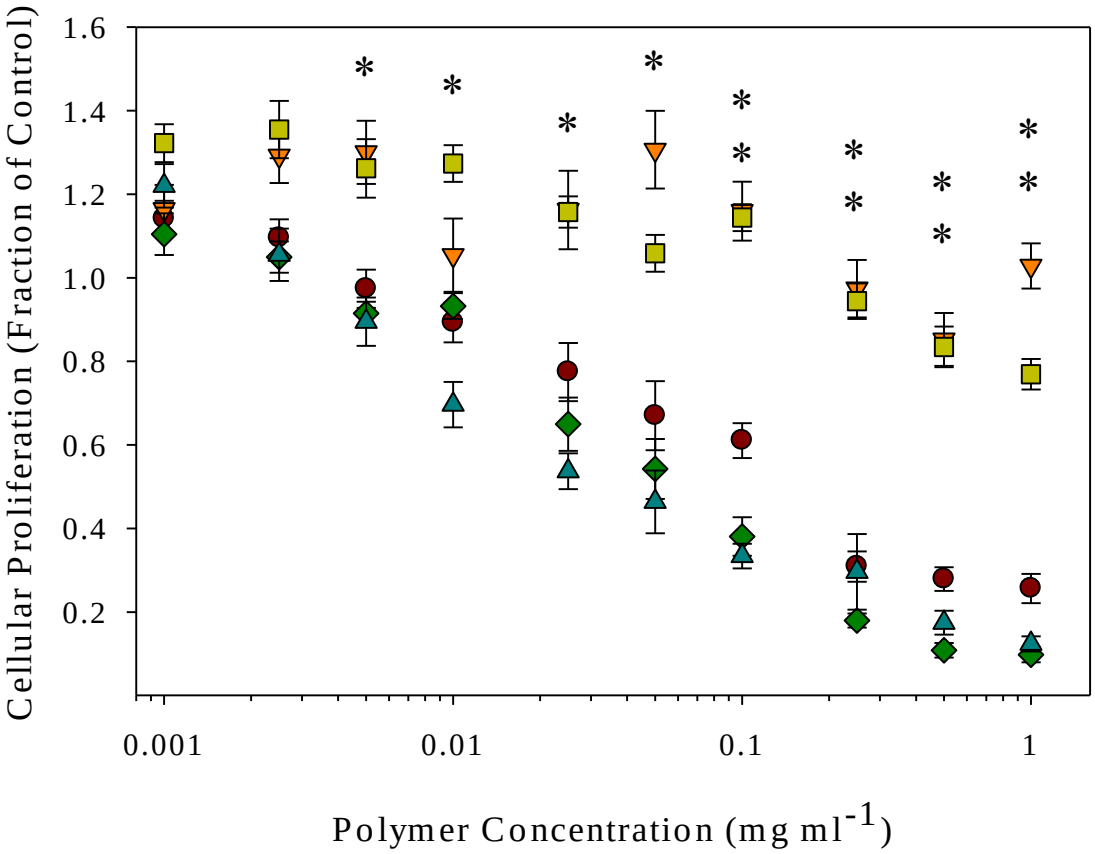

Figure 5.12 - Cytocompatibility of polycationic nanogels as a function of polymer concentration. Symbols represent PDET (●), PDETB20 (▼), PDETB30 (■), PDETBA20 (◊), or PDETBA30 (▲). The relative viability of Caco-2 cells was determined by MTS assay following 90 min nanogel exposure and is expressed as a fraction of the control (untreated) cells. Data are expressed as means ± SEM, n = 8. Lines are to guide the eye. Statistical significance determined via pairwise t-test between cells exposed to PDETB20 and PDET or PDETB30 and PDET (* $p < 0.005$).

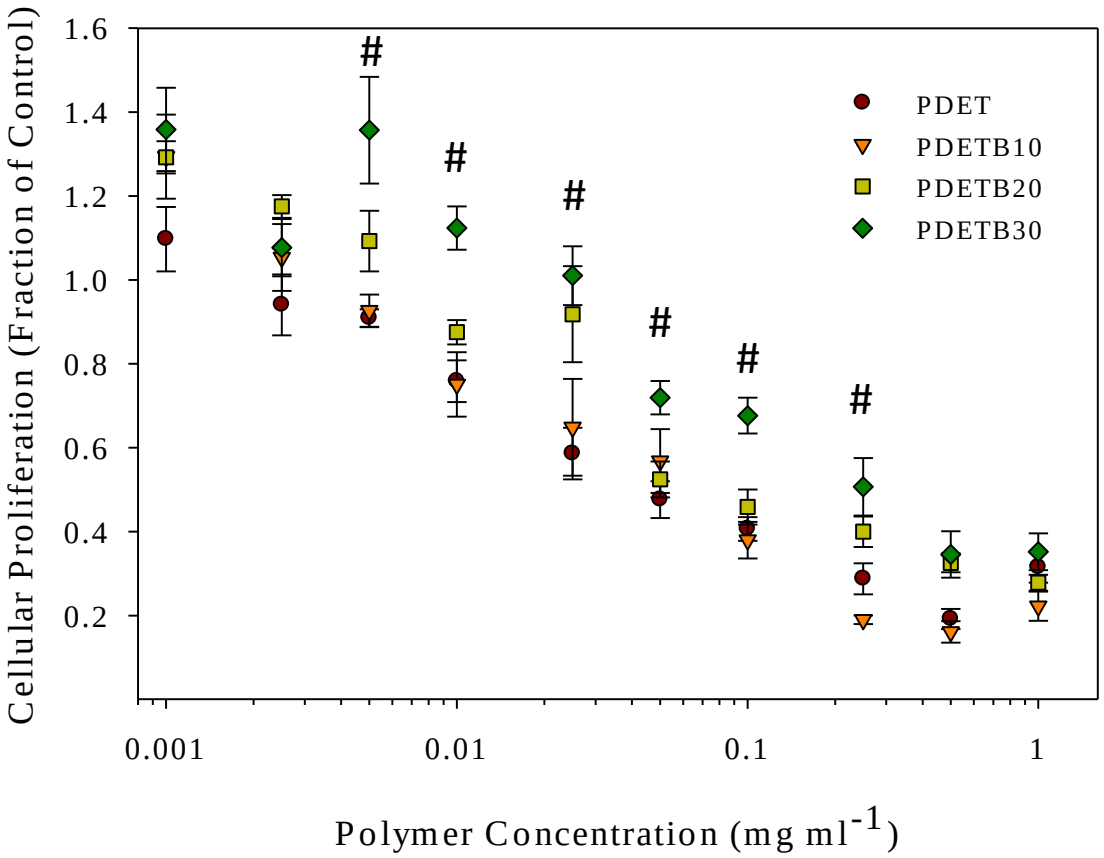

Figure 5.13 - Cytocompatibility of P(DEAEMA-g-PEGMA) and P(DEAEMA-co-TBMA-g-PEGMA) nanogels as a function of polymer concentration. The relative proliferation of RAW 264.7 cells was determined by MTS assay following 3 h nanogel exposure and is expressed as a fraction of the control (untreated) cells. Data are expressed as means ± SEM, n = 4. Statistical significance determined via pairwise t-test between cells exposed to PDETB30 or PDET (# $p < 0.05$).

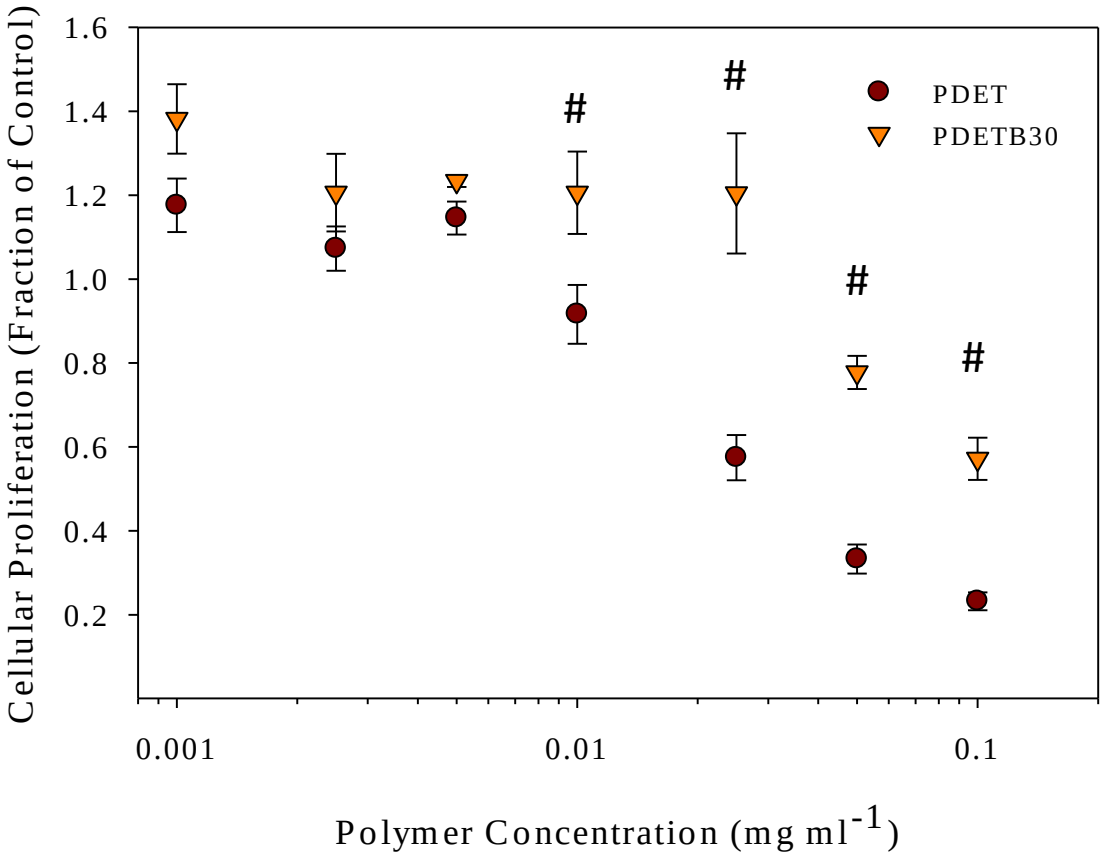

Figure 5.14 - Cytocompatibility of PDET and PDETB30 nanogels as a function of polymer concentration following 24 h exposure. The relative proliferation of RAW 264.7 cells was determined by MTS assay and is expressed as a fraction of the control (untreated) cells. Data are expressed as means ± SEM, n = 4. Statistical significance determined via pairwise t-test between cells exposed to PDET or PDETB30 (# $p < 0.05$).

REFERENCES

1. Dufresne MH, Elsabahy M, and Leroux JC. Pharmaceutical Research 2008;25(9):2083-2093.

2. Fischer D, Li YX, Ahlemeyer B, Krieglstein J, and Kissel T. Biomaterials 2003;24(7):1121-1131.

3. Gao XL, Yao L, Song QX, Zhu L, Xia Z, Xia HM, Jiang XG, Chen J, and Chen HZ. Biomaterials 2011;32(33):8613-8625.

4. Liu ZH, Zhang ZY, Zhou CR, and Jiao YP. Progress in Polymer Science 2010;35(9):1144-1162.

5. Thomas M and Klibanov AM. Proceedings of the National Academy of Sciences of the United States of America 2002;99(23):14640-14645.

6. Zhou JB, Liu J, Cheng CJ, Patel TR, Weller CE, Piepmeier JM, Jiang ZZ, and Saltzman WM. Nature Materials 2012;11(1):82-90.

7. Fisher O, Kim T, Dietz S, and Peppas N. Pharmaceutical Research 2009;26(1):51-60.

8. Fisher OZ and Peppas NA. Macromolecules 2009;42(9):3391-3398.

9. Liechty WB, Scheuerle RL, and Peppas NA. Polymer 2013;under review.

10. Convertine AJ, Benoit DSW, Duvall CL, Hoffman AS, and Stayton PS. Journal of Controlled Release 2009;133(3):221-229.

11. Kurisawa M, Yokoyama M, and Okano T. Journal of Controlled Release 2000;68(1):1-8.

12. Stachowiak JC, Hayden CC, and Sasaki DY. Proceedings of the National Academy of Sciences of the United States of America 2010;107(17):7781-7786.

13. Angelova MI and Dimitrov DS. Faraday Discussions 1986;81:303-+.

14. Chen RJ, Eccleston ME, Yue ZL, and Slater NKH. Journal of Materials Chemistry 2009;19(24):4217-4224.

15. Liechty WB, Chen R, Farzaneh F, Tavassoli M, and Slater NKH. Advanced Materials 2009;21(38-39):3910-3914.

16. Murthy N, Robichaud JR, Tirrell DA, Stayton PS, and Hoffman AS. Journal of Controlled Release 1999;61(1-2):137-143.

17. Cheung CY, Murthy N, Stayton PS, and Hoffman AS. Bioconjugate Chemistry 2001;12(6):906-910.

18. Yessine M-A and Leroux J-C. Advanced Drug Delivery Reviews 2004;56(7):999-1021.

19. Chen RJ, Yue ZL, Eccleston ME, and Slater NKH. Biomaterials 2008;29(32):4333-4340.

20. Kusonwiriyawong C, van de Wetering P, Hubbell JA, Merkle HP, and Walter E. European Journal of Pharmaceutics and Biopharmaceutics 2003;56(2):237-246.

21. Palermo EF, Lee D-K, Ramamoorthy A, and Kuroda K. The Journal of Physical Chemistry B 2010;115(2):366-375.

22. Li S and Malmstadt N. Soft Matter 2013.

23. Hong S, Leroueil PR, Janus EK, Peters JL, Kober M-M, Islam MT, Orr BG, Baker JR, and Banaszak Holl MM. Bioconjugate Chemistry 2006;17(3):728-734.

24. Takigawa DY and Tirrell DA. Abstracts of Papers of the American Chemical Society 1983;185(Mar):81-Poly.

25. Mecke A, Majoros IJ, Patri AK, Baker JR, Holl MMB, and Orr BG. Langmuir 2005;21(23):10348-10354.

26. Kim SK. American Journal of Roentgenology Radium Therapy and Nuclear Medicine 1968;104(3):522-&.

Chapter 6: Internalization pathways of membrane-disruptive, pH-responsive nanogels

6.1. INTRODUCTION

Cellular internalization of polymer nanoparticles is a complex phenomenon that depends on size [1, 2], shape [3, 4], polymer chemistry [5], and surface characteristics of drug delivery vehicles. Understanding the mechanism of internalization is critical because the internalization pathway influences subcellular trafficking, sorting, and exposure to variable enzymatic and pH conditions. In mammalian cells, the principal pathways of internalization are clathrin-mediated endocytosis, caveloae-mediated endocytosis, macropinocytosis, or other energy-independent pathways [6]. Phagocytic cells, such as macrophages and dendritic cells can ingest material through phagocytosis.

Clathrin-mediated endocytosis is a ubiquitous internalization pathway that serves as the primary mode of internalization for macromolecules. Endocytic vesicles evolving from clathrin-coated pits will deliver their contents to early endosomes and will subsequently experience vesicular acidification. Caveloae-mediated endocytosis occurs in membrane invaginations lined with the protein caveloae and cholesterol. Vesicles generated from caveloae-mediated endocytosis do not undergo acidification. Macropinocytosis, similar to phagocytosis, occurs via actin-dependent membrane protrusions. This pathway is common to many cell types and results in the formation of large macropinosomes approximately 1 – 5 μm in diameter [6]. In macrophages, macropinosomes typically become acidified, shrink, and subsequently fuse with lysosomes [7]. The fate of macropinosomes is less clear in other cell types. Studies of macropinosome-endosome mixing in A431 cells revel little fluid or membrane exchange with that of conventional endosomes[8].

Historically, the constitutive endocytic activity of the clathrin-mediated pathway has been the most attractive mechanism for internalization. Caveloae-mediated internalization is comparatively slow [9] and the small vesicle size (50 – 60 nm) precludes the entry of many nanoparticle delivery systems. As this pathway generally avoids non-productive lysosomal accumulation, it holds promise as target for drug delivery of biomacromolecules. Some recent evidence [10] suggests caveloae-mediated internalization plays a critical role in transfection efficiency of cationic polymer-DNA complexes for gene delivery gene delivery.

Many mechanistic studies of nanoparticle uptake rely on the parallel analysis of flow cytometry and confocal microscopy to evaluate internalization and subcellular fate. While powerful when used in combination, both flow cytometry and confocal microscopy are subject to individual limitations. Uncertainty in the internalization (vs. surface adsorption) of fluorescent probes is a limitation of conventional flow cytometry whereas the statistical analysis of confocal micrographs can be laborious due to limited sample throughput. This chapter describes the use of imaging flow cytometry as a robust technique to simultaneously gather statistical cytometry data and high-resolution images of thousands of cells. This technique is used to study the uptake and intracellular localization of fluorescent PDET30 nanogels to elucidate the principal mechanisms of internalization in the model cell lines, Caco-2 and RAW 264.7.

6.2. Materials and Methods

6.2.1. Fluorescent Polymer Synthesis

PDETB30 was synthesized and purified as described in Section 4.2.1 and 4.2.2. To enable the covalent conjugation of a fluorescent probe, 2-aminoethyl methacrylate

hydrochloride (AEMA) was included in the pre-polymer feed mixture at 5 mol% of DEAEMA. The resulting copolymer was named PDETB30f to signify the amine functionality. The primary amine of AEMA was verified with a fluorescamine assay after synthesis and purification.

Oregon Green 488 carboxylic acid, succinimdyl ester (OG488) was purchased from Molecular Probes (Eugene, OR). The solid dye was dissolved in DMSO to yield a 10 mg ml^{-1} solution. To form the fluorescent polymer conjugate, PDETB30f was suspended at 10 mg ml^{-1} in 150 mM sodium bicarbonate buffer, pH 8.30. OG488 was added to the PDETB30f suspension to give a 1:1 mol ratio between AEMA and OG488. The reaction was stirred gently in the dark for 6 h. Following reaction completion, unreacted dye was separated from labeled PDETB30f through dialysis against DI water. Dialysis proceeded for 3 days in 12,000 – 14,000 MWCO dialysis tubing (Spectrum Labs, Rancho Dominguez, CA) for 3 days. Labeled nanogels, PDETB30-OG488, were lyophilized in the dark for 3 days.

6.2.2. Cell Culture

General cell culture reagents and cell maintenance/passaging procedures are found in Section 5.2.3.

6.2.3. Mechanism of Nanogel Uptake

Chlorpromazine hydrochloride (98%), Nystatin, and Wortmannin (98%) were purchased from Sigma-Aldrich (St. Louis, MO). 5-N,N-dimethyl amiloride was purchased from Enzo Life Sciences (Farmingdale, NY). Filipin III was purchased from Cayman Chemical (Ann Arbor, MI). Inhibitor toxicity to Caco-2 cells and RAW 264.7 cells was evaluated using MTS assays as descried in Section 5.2.4.

RAW 264.7 cells or Caco-2 cells were seeded at 1×10^5 cells/well in 6-well plates and allowed to grow to 80% confluence before exposure. Immediately prior to exposure to inhibitors, cells were washed 1× with 2 mL DPBS and media was replaced with 1.8 mL serum-free DMEM. Concentrated suspensions (20×) of inhibitors were added to wells in 100 µL increments and allowed to incubate with cells for 30 min in a 37°C, 5% CO_2 atmosphere. Cells inhibited by refrigeration were placed at 4°C for 30 min prior to nanogel exposure.

Following the 30 min equilibration period, 100 µL of PDETB30-OG488 at 500 µg ml^{-1} in PBS was added to test well to yield a final concentration of 25 µg ml^{-1}. Control wells received 100 µL PBS. Nanogel exposure occurred for 60 min at 37°C or 4°C. Following the exposure period, cells were rinsed 3× DPBS (with calcium and magnesium) and the media was replaced with 2 mL serum-free DMEM. Hoechst 33342 was added to each well for nuclear staining at a final concentration of 2.5 µg ml^{-1}. The nuclear staining process was completed for 30 min for RAW 264.7 cells and 45 min for Caco-2 cells at 37°C, 5% CO_2. Following Hoechst incubation, cells were rinsed 3× with DPBS (w/out calcium and magnesium).

RAW 264.7 cells were isolated by replacing the final DPBS wash with 1 mL flow cytometry buffer and gently scraping the cells. Cell suspensions from each well were transferred to microfuge tubes and centrifuged for 5 min at 500×g. The supernatant was discarded and cell pellet re-suspended in 100 µL flow cytometry buffer. Flow cytometry buffer was prepared by combining FBS, DPBS, and N_3Na to form 1% FBS and 0.1% N_3Na in DPBS.

Caco-2 cells were isolated by replacing the final DPBS wash with 500 µL 0.25% trypsin-EDTA and incubating at 37°C, 5% CO2 for 8 min. Trypsin was neutralized by adding 3 mL DMEM with 10% FBS and without phenol red. Cell suspensions were centrifuged for 5 min at 500×g. The supernatant was discarded and cell pellet re-suspended in 100 µL flow cytometry buffer.

All cell suspensions were kept on ice until analysis with Image Stream Cytometry. Propidium iodide (PI) was used as a live/dead discriminator and was added to cell suspensions immediately before analysis at a final concentration of 1 µg mL^{-1}.

6.2.4. Image Stream Cytometry

Analysis of uptake mechanisms and siRNA delivery was conducted using an Amnis ImageStream (Seattle, WA) imaging flow cytometer equipped with lasers at 405 nm, 488 nm, 658 nm, and 785 nm. For uptake studies, fluorescent data were collected using Channel 1 (430 – 505 nm, Hoechst), Channel 2 (505 – 595 nm, OG488), Channel 4 (595 – 660 nm, PI), and Channel 6 (745 – 800 nm, side scatter). Brightfield images were collected in Channel 5. Cells were imaged with a 60× objective. Fluid velocity was set to a nominal value of 40 mm/sec. Fluorescent compensation matrices were constructed using Amnis IDEAS® software and verified manually for proper fit. At least 5,000 cells were collected for analysis. Dead cells (PI positive) were excluded from analysis. Out-of-focus cells were also excluded from further analysis by gating the Gradient RMS feature in IDEAS® software. This feature detects image sharpness by calculating large changes in pixel values across the brightfield image. Typically, cells with Gradient RMS value <40 were considered out of focus.

6.2.5. Statistical Analysis

Statistical comparisons between experimental and control groups were made with two-tailed, unpaired, Student's t-test. Differences were accepted as statistically significant with $p < 0.05$.

6.3. Results and Discussion

6.3.1. Fluorescent Polymer Synthesis

To enable visualization of nanogel subcellular localization in siRNA delivery experiments, a fluorescent version of the PDETB30 nanogel was necessary. A primary amine-containing analogue of PDETB30, termed PDETB30f, was successfully synthesized through the inclusion of AEMA in the nanogel core. Following previous work [11], solid AEMA was added to the pre-polymer mixture immediately before sonication. While this monomer is stable in its hydrochloride salt form, it readily undergoes a cyclic rearrangement to 2-hydroxyethyl methacrylamide upon neutralization [12]. Moreover, AEMA can undergo a Michael addition to the polymer chain. Thus, the use of AEMA inevitably results in a mixture of reaction products. While AEMA served as a suitable functionalization site for a fluorescent conjugate, future generations of fluorescent nanogels will utilize a more stable and predictable reactant.

Oregon Green 488 (OG488), an amine reactive dye, was conjugated to primary amines in the nanogel core. Prior to the conjugation reaction, the primary amine content of PDETB30f was determined to be$47.5 \pm 0.6 \mu mol\ g^{-1}$, which represents a 32% incorporation efficiency. OG488 was subsequently added to PDETB30f at 1:3 mol ratio of dye to amine. This ratio was used to maintain consistency in the fluorescent loading (mol dye:g polymer) with a previous synthesis. Following dialysis and lyophilization, the

Oregon Green 488 functionalization was tested with fluorescence spectroscopy and the percent functionalization calculated with UV absorbance and comparison to an Oregon Green 488 standard curve.

The fluorescence emission (λ_{ex} = 465 nm) spectra of the labeled nanogel (PDETB30-OG488) is shown in Figure 6.1. The fluorescent labeling was estimated at 19.1 ± 0.4 μmol g^{-1} using a standard curve of OG488 in PBS and at 17.1μmol g^{-1} using the absorbance at 496 nm and the OG-488 extinction coefficient (ε) of 70,000 L mol^{-1} cm^{-1}.

6.3.2. Mechanism of Cellular Internalization

6.3.2.1. Toxicity of Endocytosis Inhibitors

Prior to testing the uptake inhibition of PDETB30-OG488, the specific pharmacological inhibitors were tested for toxicity against the two model cell lines, RAW 264.7 and Caco-2. Cytotoxicity was determined using an MTS assay as described in Section 5.2.4. Toxicity data for specific inhibitors is seen in Figure 6.2. To ensure inhibitory activity, the concentration used in inhibition experiments was selected as the maximum possible concentration before the onset of cytotoxicity.

6.3.2.2. Nanogel Uptake

In this study, several uptake inhibitors (Table 6.1) were applied to Caco-2 and RAW 264.7 cells to elucidate the primary uptake pathways into enterocytes and phagocytes, respectively. As demonstrated in the previous chapter, the membrane-disruptive activity of PDETB30 is highly dependent on environmental conditions (e.g. pH). Therefore, to exert their membrane-disruptive effect and enable cytoplasmic

delivery of encapsulate cargoes, these polybasic nanogels must be exposed to a slightly acidic environment. Some internalization pathways, such as caveloae-mediated endocytosis and lipid raft endocytosis, do not result in vesicular acidification. Thus, these trafficking pathways are both undesirable and unproductive, as PDETB30 is far less membrane disruptive at pH values of the extracellular milieu. In contrast, pathways such as clathrin-mediated endocytosis or macropinocytosis are preferred because of their progressive vesicular acidification; a process that will enable PDETB30 to undergo a volume phase transition and destabilize the surrounding vesicular membrane.

In the mechanistic studies of nanogel internalization, it was particularly important to verify that the Oregen Green 488 (OG488)-labeled nanogels were located inside the cell rather than on the periphery. In order to accomplish this, two image masks were created in the cell brightfield channel. The total cell mask (Figure 6.3) encompasses the entire cell contents. The cell interior mask (Figure 6.3) is slightly smaller than the total cell mask and encompasses cell contents *inside* the cell membrane.

The internalization coefficient is a ratio of the OG488 floursence *inside the cell* and OG488 fluoresence *inside and around the cell*, where the cell boundaries are determined by masks shown in Figure C.5. Two representative images illustrate the difference between extracellular or membrane-bound fluoresncence (Internalization Coefficeint < 0) and intracellular fluoresence (Internalization Coefficient < 0). The population formed by live, focused, single cells with internalized OG488 was used as the basis for all studes of internalization mechanism.

6.3.2.3. Nanogel uptake Caco-2 cells

Figure 6.4 shows the intracellular fluorescence of PDETB30-OG488 (relative to uninhibited control) in Caco-2 cells. Corresponding fluorescent and brightfield micrographs are seen in Figure 6.5. Incubation with chlorpromazine did not have a significant effect on the uptake of PDETB30-OG488, indicating that clathrin-mediated endocytosis is not a dominant uptake pathway for these nanogels in Caco-2 cells. Inhibitors of caveloae-mediated endocytosis, Filipin III and Nystatin, resulted in a 14% and 12%, respectively, reduction in intracellular fluorescence of PDETB30-OG488. Inhibitors of macropinocytosis, wortmannin and amiloride, resulted in the greatest decrease in intracellular fluorescence. Wortmannin caused a 39% reduction in intracellular fluorescence and amiloride caused a 31% reduction.

Inhibition of energy-dependent processes by incubation at 4°C caused a 63% reduction in the intracellular fluorescence. Notably, an appreciable portion of PDETB30-OG488 uptake in Caco-2 cells occurs through an energy-independent process. Other reports have noted energy-independent transport of nanoparticles, specifically with respect to cationic lipids and breast cancer cells [13] and PLGA nanoparticles and Caco-2 cells[14]. This process is thought to be due to particle fusion with the cell membrane and has been reported in several types of cationic delivery vectors, including lipoplexes [15], dendrimers [16], and crosslinked poly(ethyleneimine) nanogels [17]. PDETB30 is mildly membrane-disruptive under physiological conditions and may permit the cellular influx of nanogel particles through the transient membrane perturbation and nanopore formation as outlined in Chapter 5.

6.3.2.4. Nanogel uptake RAW 264.7 cells

Figure 6.6 shows the intracellular fluorescence of PDETB30-OG488 (relative to uninhibited control) in RAW 264.7 cells and corresponding fluorescent and brightfield micrographs are seen in Figure 6.7. These data suggest that a multiple internalization pathways are responsible for PDETG30-OG488 uptake in RAW macrophages.

The dominant uptake pathways are clathrin-mediated endocytosis and macropinocytosis. The inhibition of clathrin-mediated endocytosis with chlorpromazine decreased the uptake of PDETB30-OG488 by 45% and the inhibition of macropinocytosis with amiloride reduced uptake by 68%. The caveloae-mediated endocytic pathway is active, albeit less than clathrin-mediated endocytosis or macropinocytosis, as inhibition of caveloae-mediated endocytosis with nystatin caused a slight decrease in the nanogel uptake (~18%). Notably, uptake was not significantly inhibited by cholesterol-sequestering agent Filipin III. This suggests that caveloae-mediated endocytosis plays a minor role in the internalization of PDETB30-OG488 by macrophages. The energy-independent internalization of PDETB30-OG488 was appreciable in RAW 264.7 cells, though this pathway was less prominent than in Caco-2 cells.

Although macrophages are capable of phagocytosis, the inhibition of PI3K, required for actin polymerization and phagosome and macropinosome formation [18], with wortmannin resulted in a ~25% decrease in PDETB30-OG488 internalization. The lack of phagocytic uptake from RAW 264.7 macrophages may be ascribed to their ~100 nm size. The generally accepted lower size limit for phagocytosis is approximately 500 nm [19]. Another explanation comes from the lack of fetal bovine serum in the cell

culture media. Macrophages rely on the adsorption of opsonin proteins to cell surface receptors such as Fc receptors and complement receptors to initiate phagocytosis. The lack of serum proteins in the cell culture media may limit initiation of phagocytic internalization.

The presence of multiple internalization mechanisms is consistent with other reports of hydrophobically modified particles [20]. Banquy et al. [21] observed a difference in uptake of hydrogel nanoparticles depending on nanoparticle modulus. RAW 264.7 macrophages internalized soft particles preferentially through macropinocytosis and stiff particles through clathrin-dependent endocytosis.

6.3.2.5. Intracellular staining

Intracellular punctate staining of PDETB30-OGG488 was analyzed in a semi-quantitative fashion using Amnis IDEAS® software. The intracellular spot mask was created by identifying staining patterns with spot pixel values at least 10 times greater than the surrounding cell background. A software algorithm was used to count the number of spots per cell. A demonstrative example of 0 spots, 3 spots (low spot count), and 9 spots (high spot count) is shown in Figure 6.8.

Figure 6.9 and Figure 6.10 show the spot count distributions for Caco-2 cells and RAW 264.7 cells, respectively. Unfortunately, this analysis reveals limited insight into the subcellular fate of PDETB30-OG488 as a function of uptake mechanism. The number of counted spots is primarily a function of population fluorescent intensity. For example, when macropinocytosis of PDETB30-OG488 is inhibited by amiloride in RAW 264.7 cells (Figure 6.10, Panel F) the number of counted spots decreased relative to

uninhibited uptake (Figure 6.10, Panel A). Similar observations were noted for Caco-2 cells.

6.4. CONCLUSIONS

The mechanisms of cellular internalization of fluorescent nanogels were studied using ImageStream cytometry in Caco-2 cells and RAW 264.7 cells. Despite the lack of any targeting moieties, these nanogels are internalized readily by both Caco-2 cells and RAW 264.7 macrophages. After 60 min exposure, the intracellular PDETB30-OG488 fluorescence increased over 25× in Caco-2 cells and over 80× in RAW cells. Macropinocytosis is the dominant mechanism of nanogel internalization in Caco-2 cells while clathrin-mediated endocytosis and macropinocytosis are the dominant mechanism of internalization in RAW 264.7 cells. Membrane vesicles arising from clathrin-mediated endocytosis and macropinocytosis both undergo acidification. As PDETB30 requires a slightly acidic pH to exert its membrane-destabilizing effects, these internalization pathways are desirable for uptake and subsequent endosomal escape of PDETB30 and encapsulated therapeutics. Further efforts will analyze the ability of PDETB30 (and fluorescent analogue PDETB30-OG488) to enable cytoplasmic delivery of functional small interfering RNA.

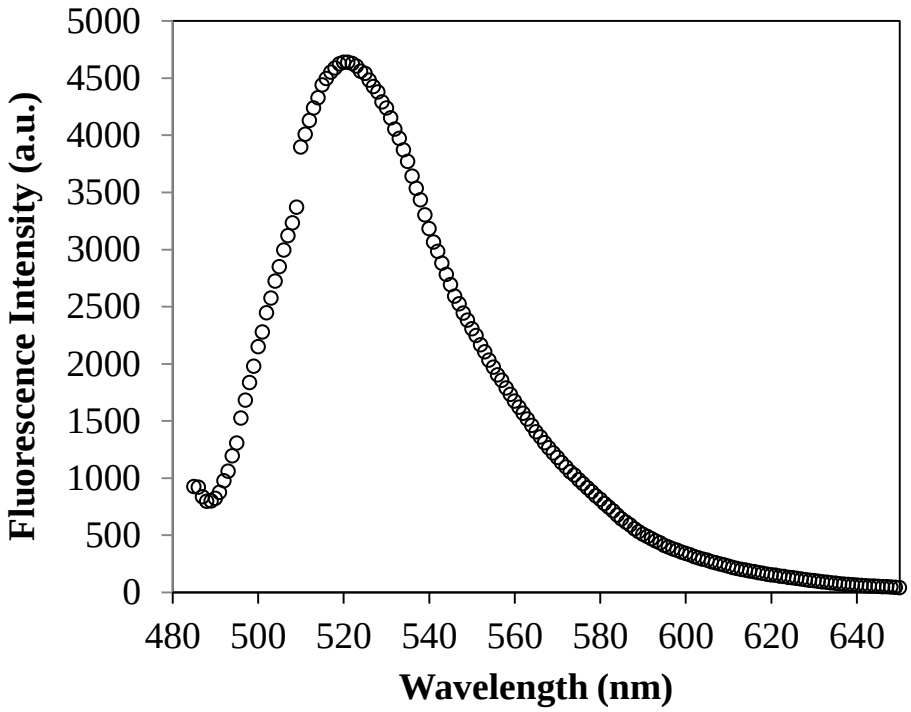

Figure 6.1 – Fluorescent emission spectra of PDETB30-OG488 at 0.125 mg ml^{-1} in PBS. λ_{ex} = 465 nm.

Table 6.1 – Uptake Inhibitors and their inhibitory effects

Molecule	Inhibitory Effect	Concentration Used	Concentrations Tested
Chlorpromazine	Clathrin-mediated endocytosis by dissociating clathrin lattice	10 μM	1 – 100 μM
Filipin III	Caveloae via cholesterol binding	1.5 μM	0.05 – 50 μM
Nystatin	Caveloae/Lipid Raft Endocytosis	50 μg/mL	1 – 1000 μg/mL
Wortmannin	Macropinocytosis/phagocytosis by inhibiting PI3K	100 nM	0.5 – 500 nM
Amiloride	Macropinocytosis via preventing Na+/H+ exchange	250 μM	1 – 1000 μM

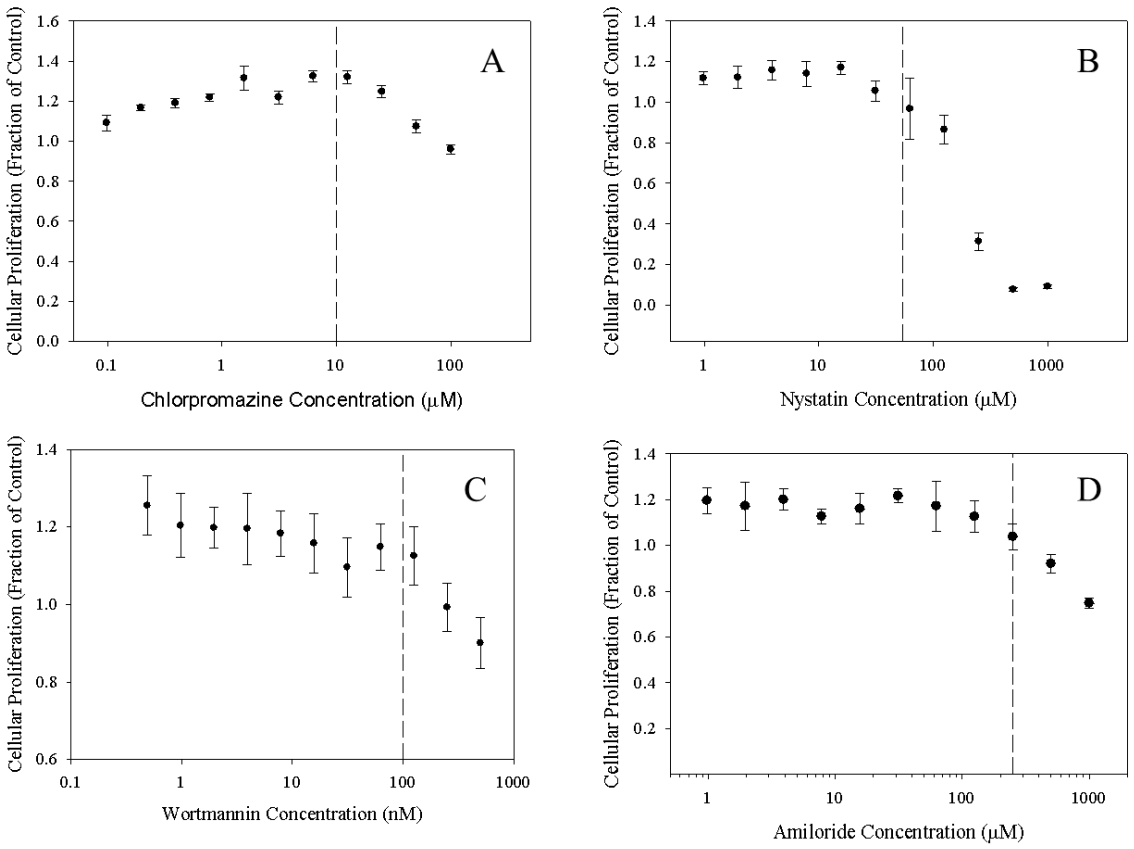

Figure 6.2 – Cytotoxicity of inhibitors on Caco-2 cells following 90 min exposure. Cellular proliferation relative to untreated control was determined via MTS assay. Data represent the mean of quadruplicate samples ±s.e.m. Dashed vertical line designates the concentration used in inhibition studies.

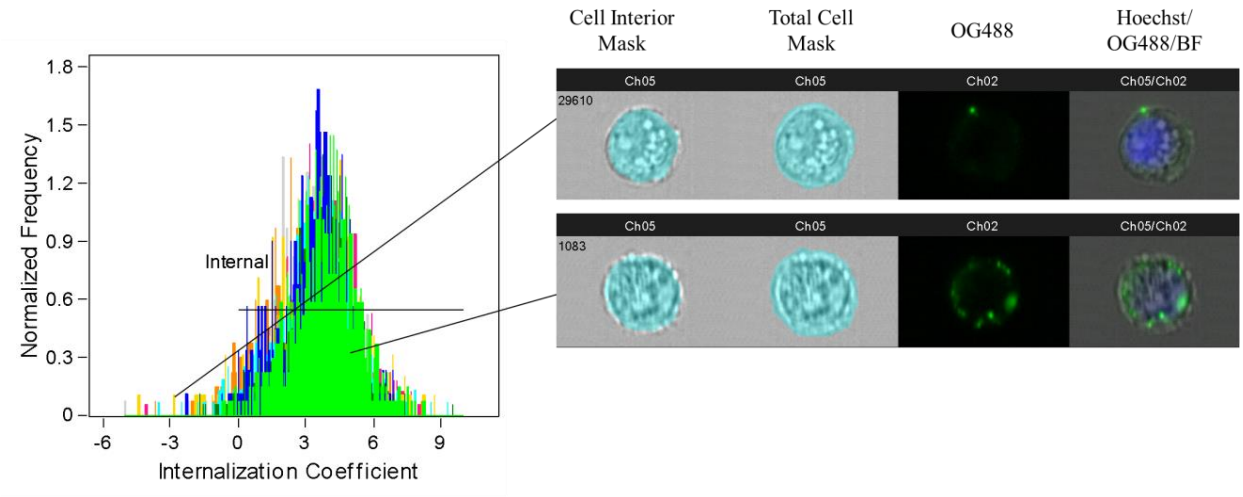

Figure 6.3. – Internalization coefficient of fluorescent nanogels. Fluorescent intensity of PDETB30-OG488 in uptake inhibition studies was calculated from cells with internalization coefficient > 0.

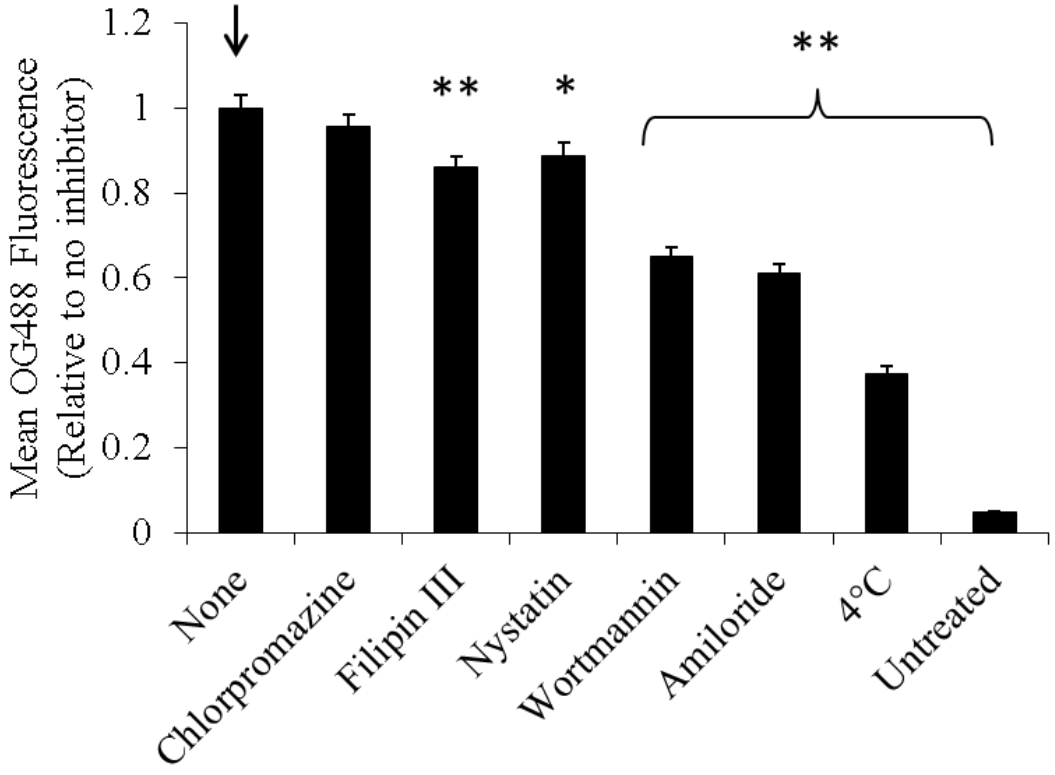

Figure 6.4 – Uptake inhibition in Caco-2 cells. Intracellular PDETB30-OG488 fluorescence relative to non-inhibited control. Caco-2 cells pre-incubated with inhibitors for 30 min prior to 60 min exposure to 25 μg ml^{-1} PDETB30-OG488. Bars represent the mean of 2 pooled experiments ±s.e.m. *$p < 0.05$, **$p < 0.01$. Arrow designates control group.

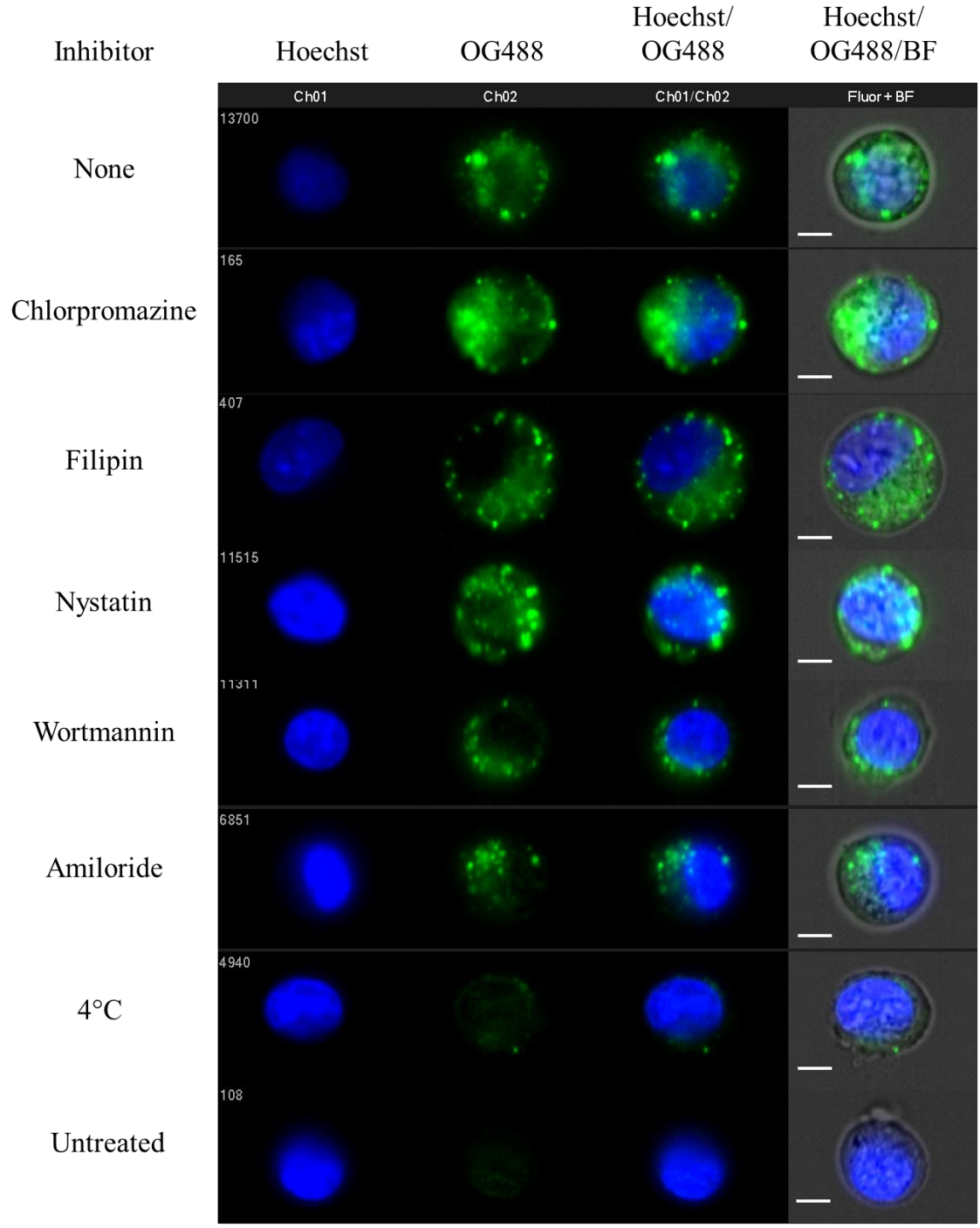

Figure 6.5 – Representative fluorescent micrographs of Caco-2 cells exposed to endocytosis inhibitors and PDETB30-OG488.Images sampled from median intensity region of OG488 fluorescent histogram. Scale bar represents 7 μm.

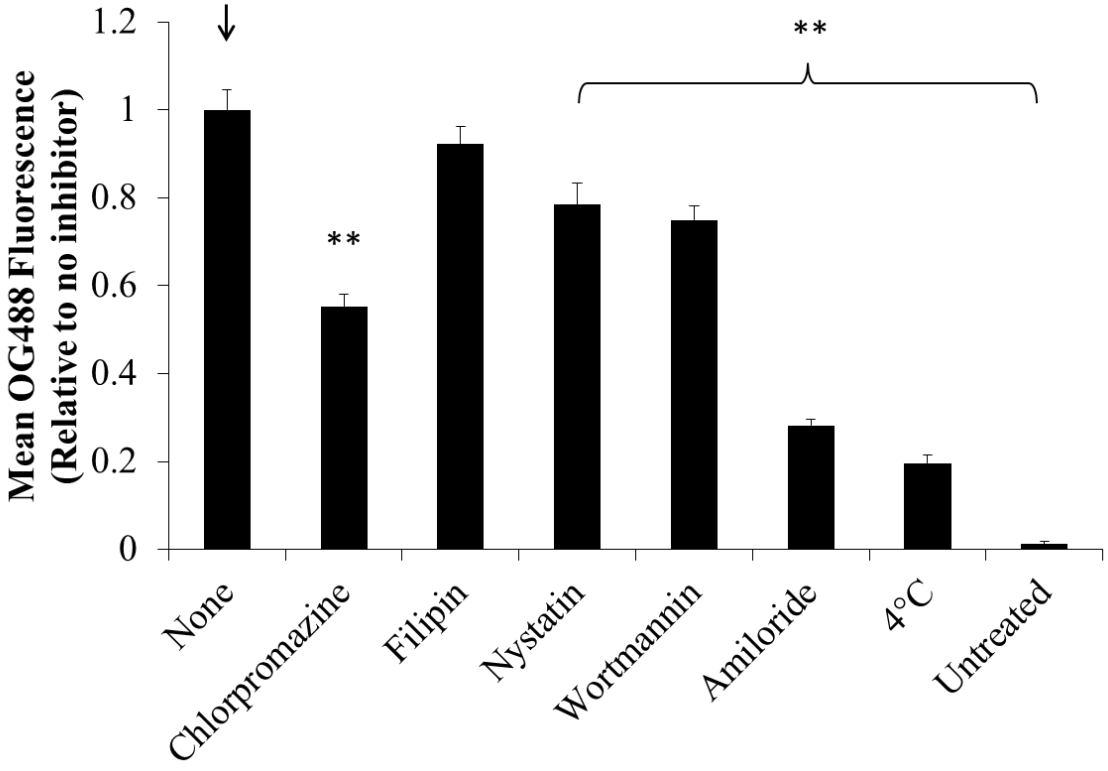

Figure 6.6 – Uptake inhibition in RAW 264.7 cells. Intracellular PDETB30-OG488 fluorescence relative to non-inhibited control. RAW 264.7 cells pre-incubated with inhibitors for 30 min prior to 60 min exposure to 25 μg ml^{-1} PDETB30-OG488. Bars represent the mean of 2 pooled experiments ±s.e.m. *$p < 0.05$, **$p < 0.01$. Arrow designates control group.

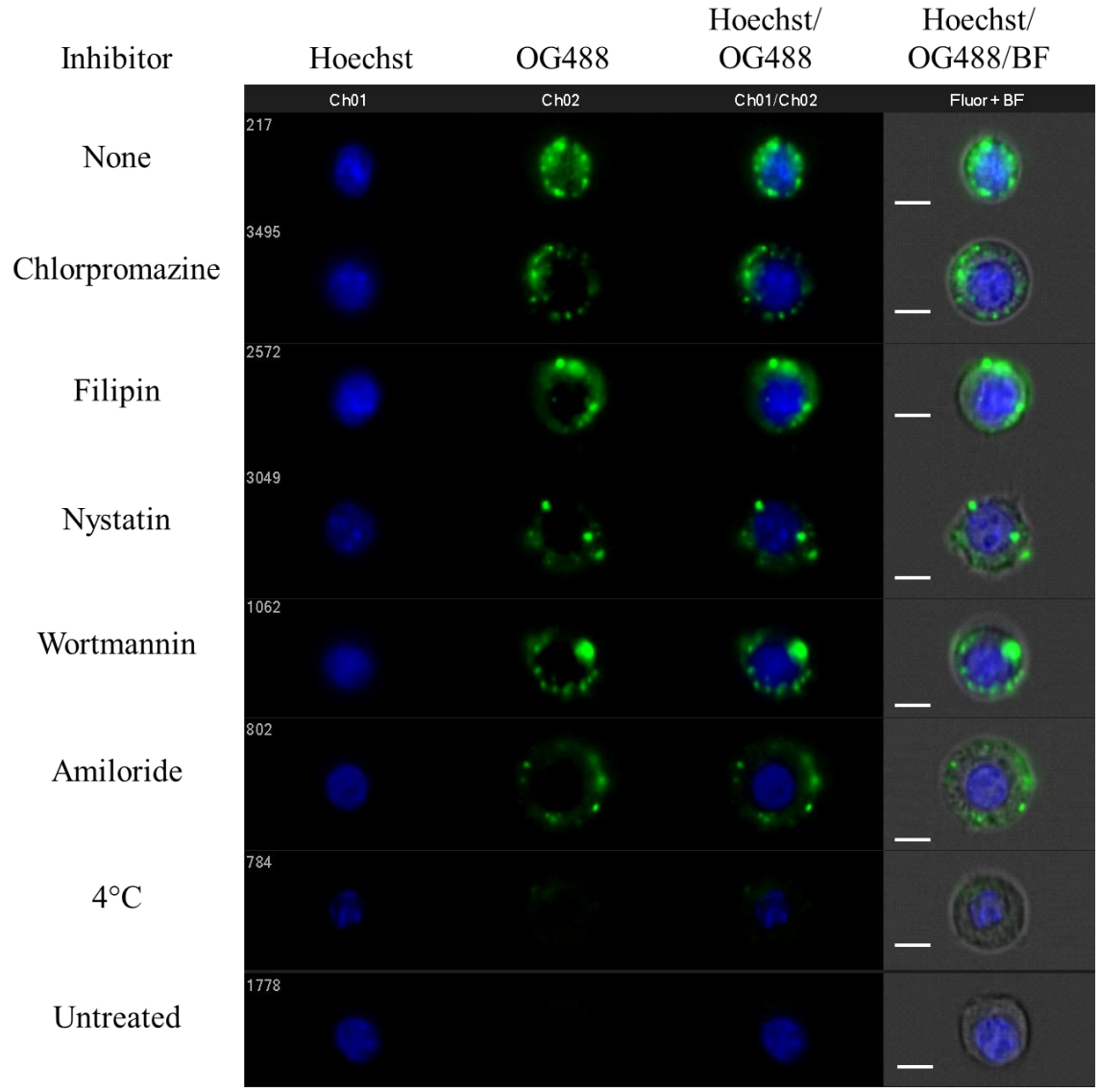

Figure 6.7 – Representative fluorescent micrographs of RAW 264.7 cells exposed to endocytosis inhibitors and PDETB30-OG488. Images sampled from median intensity region of OG488 fluorescent histogram. Scale bar represents 7 μm.

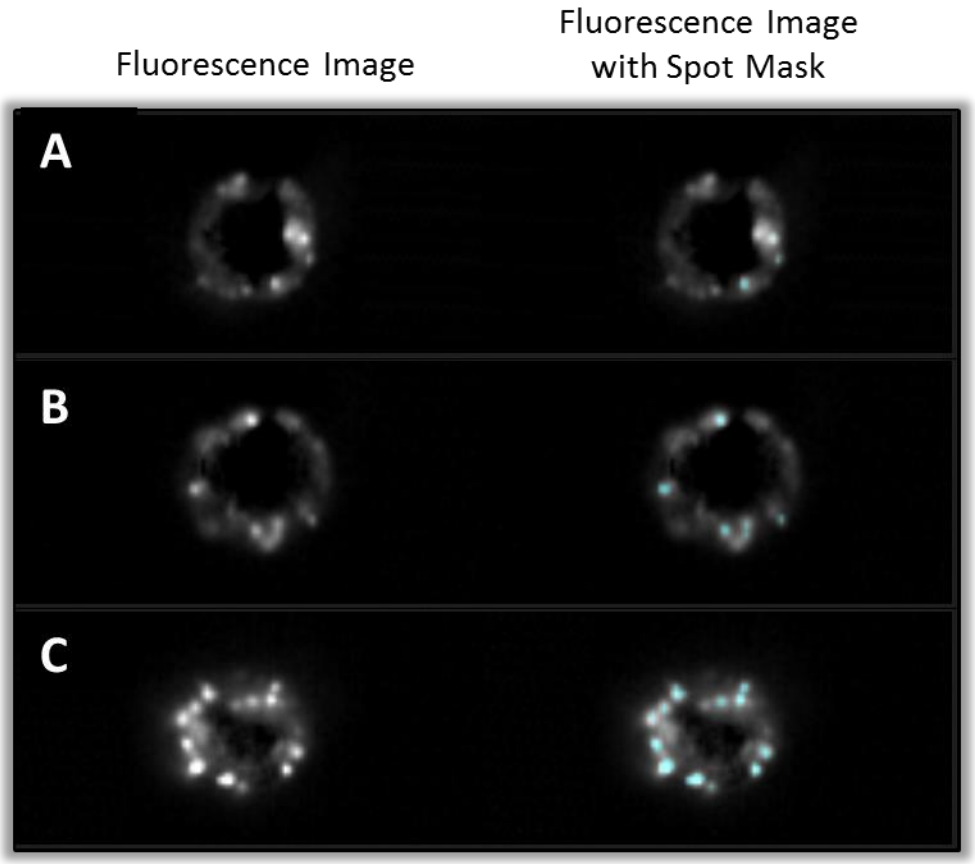

Figure 6.8. – Spot counting of intracellular nanogels. Left images show fluorescent intensity (white) of fluorescently-labeled PDESSB30-OG488. Three representative images of low (1 spot) count (A), intermediate (5 spots) count (B), and high (9 spots) count. Spot masks are shown in turquoise overlaid against high-intensity areas in the fluorescent image.

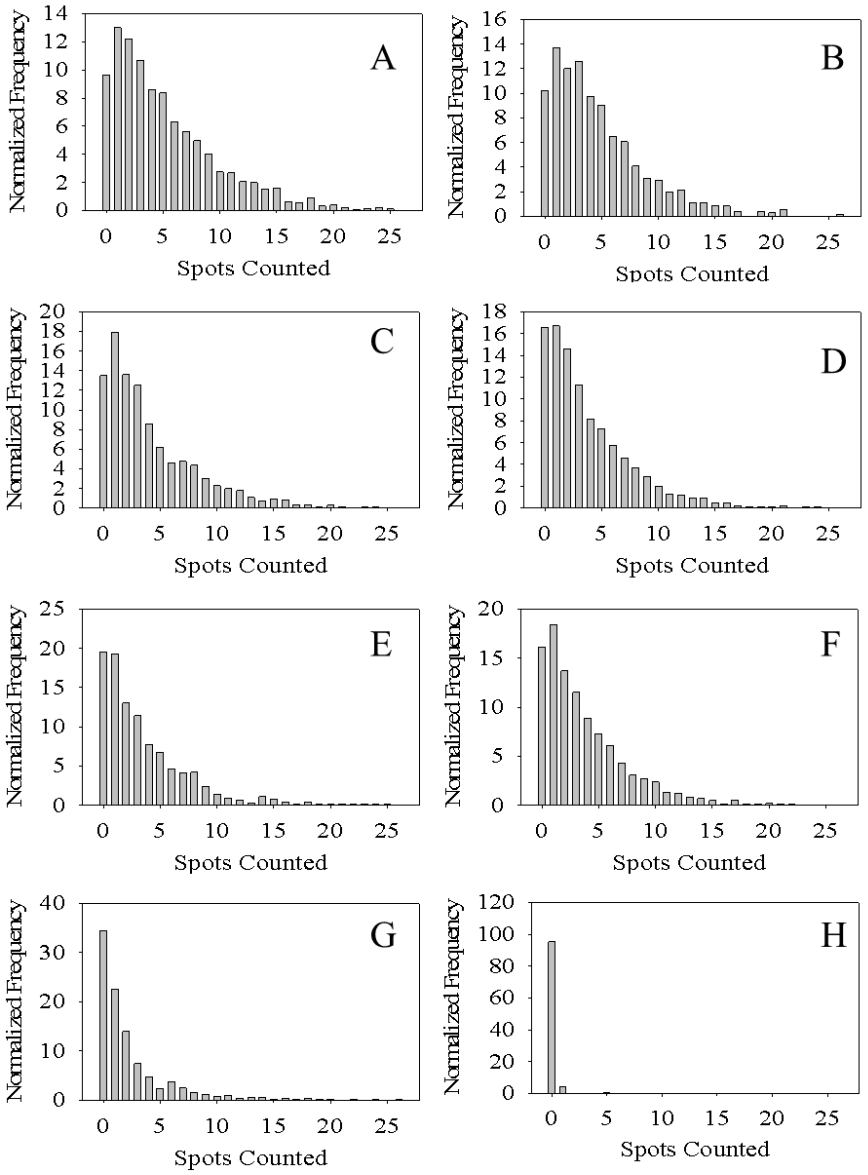

Figure 6.9 – Frequency distributions of intracellular staining of PDETB30-OG488 in Caco-2 cells. Cellular internalization examined in the presence of no inhibitor (A), chlorpromazine (B), filipin III (C), nystatin (D), wortmannin (E), amiloride (F), or 4°C (G). Untreated (no PDETB30-OG488) is shown in panel H. Caco-2 cells were pre-incubated with inhibitors for 30 min, exposed to 25 µg ml^{-1} PDETB30-OG488 for 60 min, and imaged via ImageStream cytometry after 60 min further incubation. Histograms generated from image analysis of at least 500 cells.

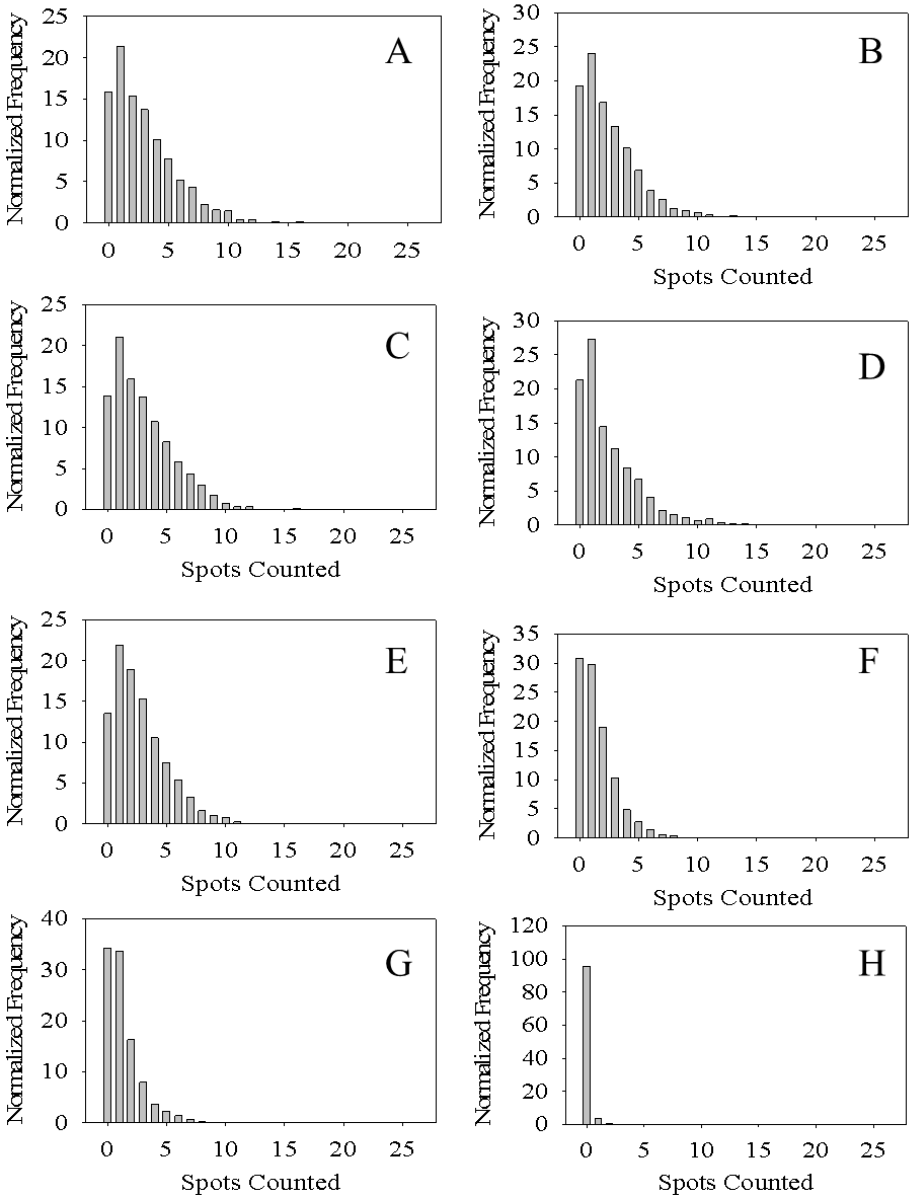

Figure 6.10 – Frequency distributions of intracellular staining of PDETB30-OG488 in RAW 264.7 cells. Cellular internalization examined in the presence of no inhibitor (A), chlorpromazine (B), filipin III (C), nystatin (D), wortmannin (E), amiloride (F), or 4°C (G). Untreated (no PDETB30-OG488) is shown in panel H. RAW 264.7 cells were pre-incubated with inhibitors for 30 min, exposed to 25 µg ml^{-1} PDETB30-OG488 for 60 min, and imaged via ImageStream cytometry after 60 min further incubation. Histograms generated from image analysis of at least 500 cells.

REFERENCES

1. Desai MP, Labhasetwar V, Walter E, Levy RJ, and Amidon GL. Pharmaceutical Research 1997;14(11):1568-1573.

2. Rejman J, Oberle V, Zuhorn IS, and Hoekstra D. Biochemical Journal 2004;377:159-169.

3. Chithrani BD, Ghazani AA, and Chan WCW. Nano Letters 2006;6(4):662-668.

4. Caldorera-Moore M, Guimard N, Shi L, and Roy K. Expert Opinion on Drug Delivery 2010;7(4):479-495.

5. Ulery BD, Phanse Y, Sinha A, Wannemuehler MJ, Narasimhan B, and Bellaire BH. Pharmaceutical Research 2009;26(3):683-690.

6. Hillaireau H and Couvreur P. Cellular and Molecular Life Sciences 2009;66(17):2873-2896.

7. Khalil IA, Kogure K, Akita H, and Harashima H. Pharmacological Reviews 2006;58(1):32-45.

8. Hewlett LJ, Prescott AR, and Watts C. Journal of Cell Biology 1994;124(5):689-703.

9. Conner SD and Schmid SL. Nature 2003;422(6927):37-44.

10. van der Aa MAEM, Huth US, Hafele SY, Schubert R, Oosting RS, Mastrobattista E, Hennink WE, Peschka-Suss R, Koning GA, and Crommelin DJA. Pharmaceutical Research 2007;24(8):1590-1598.

11. Fisher OZ. Novel pH-Responsive Microgels and Nanogels as Intelligent Polymer Therapeutics vol. Ph.D. Austin, TX: University of Texas at Austin, 2008. pp. 246.

12. Read ES, Thompson KL, and Armes SP. Polymer Chemistry 2010;1(2):221-230.

13. Kapoor M and Burgess DJ. Pharmaceutical Research 2013;30(4):1161-1175.

14. Weissenboeck A, Bogner E, Wirth M, and Gabor F. Pharmaceutical Research 2004;21(10):1917-1923.

15. Lu JJ, Langer R, and Chen JZ. Molecular Pharmaceutics 2009;6(3):763-771.

16. Zhang ZY and Smith BD. Bioconjugate Chemistry 2000;11(6):805-814.

17. Vinogradov SV, Kohli E, and Zeman AD. Molecular Pharmaceutics 2005;2(6):449-461.

18. Bohdanowicz M, Cosio G, Backer JM, and Grinstein S. Journal of Cell Biology 2010;191(5):999-1012.

19. Groves E, Dart AE, Covarelli V, and Caron E. Cellular and Molecular Life Sciences 2008;65(13):1957-1976.

20. Nam HY, Kwon SM, Chung H, Lee SY, Kwon SH, Jeon H, Kim Y, Park JH, Kim J, Her S, Oh YK, Kwon IC, Kim K, and Jeong SY. Journal of Controlled Release 2009;135(3):259-267.

21. Banquy X, Suarez F, Argaw A, Rabanel JM, Grutter P, Bouchard JF, Hildgen P, and Giasson S. Soft Matter 2009;5(20):3984-3991.

Chapter 7: Cytoplasmic delivery of functional siRNA using pH-responsive nanoscale hydrogels

7.1. INTRODUCTION

The landmark discovery of RNA interference (RNAi) in 1998 has sparked a massive research effort in all fields of biological science and redefined our understanding of gene regulation mechanisms [1]. Theoretically, RNAi mediated by siRNA could be used as a powerful and versatile treatment modality to treat nearly any disease resulting from aberrant gene expression. Owing to its remarkable potency and reversible therapeutic effect, siRNA holds extraordinary promise as a new biological therapeutic. As with many biotherapeutics, efficient delivery has been implicated as the major hurdle to its widespread clinical application [2].

Several materials-based strategies exist to circumvent the delivery challenges associated with cytoplasmic delivery of small interfering RNA. The most common classes of materials are lipids and lipidoids, polycationic polymers, and siRNA conjugates [2]. Lipids are perhaps the most widely studied class of materials for siRNA delivery and lipid-based formulations for RNAi have progressed to the clinic in greater number than other delivery systems [3]. The first evidence of RNAi in humans was demonstrated using a polycationic cyclodextrin nanoparticles [4]. Recently, alternative strategies have emerged to enable siRNA delivery to target cells and tissues. Khormaee, et al. [5] recently reported the use of a membrane-disruptive anionic pseudo-peptide to deliver siRNA in vivo. Polysaccharides from yeast cell walls have been used to deliver inflammation-suppressing siRNA via oral administration [6]

Amine-containing methacrylates, such as 2-(diethylaminoethyl) methacrylate (DEAMA) [7] and 2-(dimethylaminoethyl) methacrylate (DMAEMA) [8], are attractive

foundations for polymeric nucleic acid-delivery systems because of their ability to form cooperative electrostatic interactions with polyanionic siRNA. Chapters 4 – 6 have explored the aqueous solution properties, membrane-disruptive properties, and internalization mechanisms of pH-responsive nanoscale hydrogels (nanogels).

The nanogel with the most promising attributes for siRNA delivery consists of a (1) ionizable core of 2-(diethylaminoethyl methacrylate) (DEAEMA), (2) hydrophobic comonomer of *tert*-butyl methacrylate (TBMA), and (3) grafted corona of poly(ethylene glycol). This nanogel (PDETB30) undergoes a volume phase transition from collapsed hydrophobe to swollen hydrophile at approximately pH 6.5 and is highly disruptive to model membrane systems in this transition region. Additionally, PDETB30 displays excellent biocompatibility to Caco-2 cell and RAW 264.7 cells in in vitro toxicity assays.

However, a critical aspect of intracellular delivery systems is a mechanism for elimination or degradation. Disulfide linkers can be cleaved by the reductive tripeptide glutathione (GSH); present at intracellular concentrations of 1 - 11 mM [9]. By incorporating these linkers into polycationic nanogels, we can impart degradability to the network while retaining their mechanical integrity and pH-responsive behavior (Figure 7.1).

This chapter describes the synthesis and characterization of nanogels with reducible disulfide crosslinks and compares their suitability as siRNA carriers with non-degradable PDETB30 nanogels.

7.2. MATERIALS AND METHODS

7.2.1. Synthesis of disulfide crosslinker

Dichloromethane (>99.5%) was purchased from Fisher Scientific (Plainfield, NJ). Methacryloyl chloride (97%) and anhydrous pyridine (99.8%) were purchased from Sigma-Aldrich (St. Louis, MO). 2-Hydroxyethyldisulfide (90%) was purchased from Acros (Geel, Belgium).

The homobifunctional disulfide crosslinker, bis(2-methacryloyloxyethyl) disulfide (SSXL), was synthesized according to the method reported by Gao, et al. [10]. Briefly, organic solvents were dried over $MgSO_4$ before use. Dichloromethane was purged with N_2 for 15 min and placed in a dry nitrogen atmosphere (O_2 < 0.1 ppm, H_2O < 0.1 ppm). Pyridine (15.8 mL, 0.195 mol) and bis(2-hydroxyethyl) disulfide (10.00 g, 0.065 mol) were added to cold (4°C) dichloromethane and agitated briefly. Methacryloyl chloride was added dropwise to the stirring organic mixture over the course over 20 min. The flask was then sealed and removed from the ice bath and the reaction was allowed to proceed for 12 h in a nitrogen atmosphere.

The crude reaction product, in dichloromethane, was successively washed with 1 N HCl, 1 N NaOH, and DI water. The organic phase was retained and dried to a viscous yellow liquid via rotary evaporation. The product was then dissolved in diethyl ether and passed through a column of sodium carbonate and basic alumina. Diethyl ether was removed through rotary evaporation, again yielding a viscous yellow liquid.

Additional flash chromatography purification was performed using a Teledyne-Isco Companion Automated Flash Chromatography Instrument (Lincoln, NE) equipped with a 100 g silica column. The solvent gradient was established as follows: Solvent A –

hexanes, Solvent B- ethyl acetate. The gradient was adjusted from 0 – 15% B over 40 minutes and then from 15 – 100% B over 10 minutes. Fractions of interest were determined by monitoring absorbance at 258 nm. Product fractions were pooled and solvent was removed by rotary evaporation to yield a viscous, yellow liquid.

7.2.2. Characterization of disulfide crosslinker

The composition of raw materials, purification fractions, and final product of the SSXL synthesis were investigated using a Varian (Palo Alto, CA) DirectDrive 400 MHz nuclear magnetic resonance spectrometer equipped with automatic sampler. Chloroform-d ($CDCl_3$, 99.8%) was obtained from Acros Organics (Fairlawn, NJ). All glassware, including NMR Tubes (Wilmad Lab Glass, Vineland, NJ), 2 mL sample vials, and Pasteur pipettes were dried overnight in a vacuum oven. SSXL was dissolved at 1% (vol/vol) in CDC_{l3} for 1H-NMR analysis. All NMR Spectra were analyzed using SpinWorks 3^{TM} software.

Mass spectrometry was performed courtesy of the Mass Spectrometry Facility in the Department of Chemistry and Biochemistry, University of Texas at Austin.

7.2.3. Polymer Synthesis

7.2.3.1. Synthesis of degradable nanogel

To impart a mechanism for biodegradation to the responsive nanogel PDETB30[2], SSXL was used as a replacement for tetra(ethylene glycol) dimethacrylate (TEGDMA) in the photoemulsion polymerization. SSXL was added to pre-polymer mixture at 2.5

[2] See Appendix A – Nanogel nomenclature for copolymer naming convention

mol% of total monomer and photoemulsion polymerization and nanogel purification proceeded as described in Section 4.2.1 and Section 4.2.2. The resulting nanogel, termed PDESSB30, was stored in a desiccator at -20°C until further use.

7.2.3.2. Fluorescent Polymer Synthesis

A fluorescent version of PDESSB30 was synthesized and purified as in identical fashion to the description in Section 6.2.1. Like the synthesis of PDETB30-OG488, the covalent conjugation of Oregon Green 488 (OG488) was enabled by the incorporation of primary amines in the PDESSB30 core. Again, 2-aminoethyl methacrylate hydrochloride (AEMA) was included in the pre-polymer feed mixture at 5 mol% of DEAEMA. The resulting copolymer was named PDESSB30f to signify the amine functionality. The primary amine of AEMA was verified with a fluorescamine assay after synthesis and purification.

Oregon Green 488 carboxylic acid, succinimdyl ester (OG488, Molecular Probes, Eugene, OR) was dissolved in DMSO to yield a 10 mg ml^{-1} solution. To form the fluorescent polymer conjugate, PDESSB30f was suspended at 10 mg ml^{-1} in 150 mM sodium bicarbonate buffer, pH 8.30. OG488 was added to the PDESSB30f suspension to give a 1:1 mol ratio between AEMA and OG488. The reaction was stirred gently in the dark for 6 h. Following reaction completion, unreacted dye was separated from labeled PDESSB30-OG488 through dialysis against DI water. Dialysis proceeded for 3 days in 12,000 – 14,000 MWCO dialysis tubing (Spectrum Labs, Rancho Dominguez, CA) for 3 days. Labeled nanogels, PDESSB30-OG488, were lyophilized in the dark for 3 days.

7.2.4. Degradable Nanogel Characterization

Several characterization techniques were employed to study the physicochemical properties of the PDESSB30 nanogels in comparison to the TMBA analogue, PDETB30. Dynamic light scattering was used to determine the hydrodynamic diameter of PDESSB30 as a function on environmental pH and was performed as described in Section 4.2.4. Measurements of the ζ-potential were performed to evaluate the effective surface charge as function of environmental pH and were performed as described in Section 4.2.6. Transmission electron microscopy (TEM) was used to determine the diameter of the dry nanogels and was conducted as described in Section 4.2.5. Evaluations of RAW 264.7 metabolic activity upon exposure to PDESSB30 and PDETB30 were conducted using a commercially-available MTS assay kits as described in Section 5.2.4.

7.2.5. RNA Binding

RNA complexation buffer was prepared by dissolving 3.15 g sodium phosphate dibasic heptahydrate, 0.02 g potassium phosphate monobasic monohydrate, 0.20 g potassium chloride, and 8.01 g sodium chloride in Milli-Q purified water. Following salt dissolution, the solution pH was adjusted to pH 5.50 using 1 N HCl and ultrapure water was added to bring the final solution volume to 100 mL. To remove nucleases, diethylpyrocarbonate (DEPC) was added at 0.1% and incubated at room temperature overnight. The buffer solution was then autoclaved to remove DEPC. Polymer-siRNA complexes were formed by combining aqueous solutions of nanogels, siRNA, 10x RNAse-free PBS, and RNAse-free water to obtain desired concentrations.

Silencer® GAPDH siRNA, Quant-iT™ Ribogreen® RNA Assay Kit, and RNAse Free H_2O were purchased from Life Technologies (Carlsbad, CA). Free siRNA in solution was measured using the Ribogreen® assay according to manufacturer's instructions. Nanogel suspensions were diluted in RNAse free complexation buffer (pH 5.50). Concentrated siRNA was added to yield 500 ng ml^{-1} RNA in a nanogel suspension at designated concentrations. Measurements of the free siRNA were taken after 60, 120, and 180 minute complexation periods.

7.2.6. Cell Culture

General cell culture reagents and cell maintenance/passaging procedures are found in Section 5.2.3. In all cytometry studies, Caco-2 cells or RAW 264.7 cells were seeded to 6-well plates and allowed to grow to 80% confluency before use.

7.2.7. siRNA delivery

DyLight 647-labeled small interfering RNA (Sense: DY647-UAAGGCUAUGAAGAGAUACUU) was purchased from Thermo Scientific (Lafayette, CO). Cy3-labeled Silencer® Negative Control No. 1 siRNA was purchased from Life Technologies (Carlsbad, CA). Fluorescent nanogels, PDETB30-OG488 and PDESSB30-OG488 were synthesized and purified as described in Section 6.2.1 and Section 7.2.3.2, respectively.

Concentrated suspensions (20×) of fluorescent nanogels (PDETB30-OG488 or PDESSB30-OG488), fluorescent siRNA (DY647-siRNA or Cy3-siRNA), or fluorescent nanogels and fluorescent siRNA were prepared to contain 0.5 mg mL^{-1} nanogel, 26.5 μg mL^{-1} (~2000 nM) siRNA, 1× complexation buffer, and RNAse free H_2O. Control

samples (nanogel or siRNA) were prepared in a similar fashion, replacing the volume of the absent component(s) with RNAse free H_2O.

To separate nanogel/siRNA complexes from complexation buffer, 4 vol equivalents of acetone was added to the suspension following the designated complexation period. The acetone serves to induce a polyelectrolyte-ionomer transition [11]. Suspensions were centrifuged at 15,000 rpm for 5 min and supernatant was discarded. Residual solvent evaporated after 15 min in a laminar flow hood. Polymer/siRNA complexes were resuspended in the original complexation volume of RNAse free PBS at pH 7.40.

Following resuspension, 100 μL of nanogel/siRNA complexes at 500 μg ml^{-1} in PBS were added to each test well to yield a final concentration of 25 μg ml^{-1}. Control wells received 100 μL PBS or100 μL of the corresponding nanogel-only or siRNA-only solution. Nanogel exposure occurred for designated time points at 37°C or 4°C. Following the exposure period, cells were rinsed 3× DPBS (with calcium and magnesium) and the media was replaced with 2 mL serum-free DMEM.

For Image Stream cytometry, Hoechst 33342 was added to each well for nuclear staining at a final concentration of 2.5 μg ml^{-1}. The nuclear staining process was completed for 30 min for RAW 264.7 cells and 45 min for Caco-2 cells at 37°C, 5% CO_2. Following Hoechst incubation, cells were rinsed 3× with DPBS (w/out calcium and magnesium). No nuclear stain was used in conventional flow cytometry experiments.

RAW 264.7 cells were isolated by replacing the final DPBS wash with 1 mL flow cytometry buffer and gently scraping the cells. Cell suspensions from each well were transferred to microfuge tubes and centrifuged for 5 min at 500×g. The supernatant was

discarded and cell pellet re-suspended in flow cytometry buffer. Flow cytometry buffer was prepared by combining FBS, DPBS, and N_3Na to form 1% FBS and 0.1% N_3Na in DPBS.

Caco-2 cells were isolated by replacing the final DPBS wash with 500 µL 0.25% trypsin-EDTA and incubating at 37°C, 5% CO2 for 8 min. Trypsin was neutralized by adding 3 mL DMEM with 10% FBS and without phenol red. Cell suspensions were centrifuged for 5 min at 500×g. The supernatant was discarded and cell pellet re-suspended in flow cytometry buffer.

All cell suspensions were kept on ice until analysis with Image Stream Cytometry. Propidium iodide (PI) was used as a live/dead discriminator and was added to cell suspensions immediately before analysis at a final concentration of 1 µg mL^{-1}.

7.2.7.1. Flow cytometry

Efficiency of PDETB30- and PDESSB30-mediated Cy3-siRNA delivery was compared using a BD FACSCalibur (San Jose, CA) flow cytometer equipped with lasers at 488 nm and 635 nm. Fluorescent data were collected using FL-2 (570 – 600 nm, Cy3) and FL-3 (653 - 669 nm, PI). Dead or dying cells were identified with propidium iodide. Typically, 40,000 cells were collected per sample.

7.2.7.2. Image Stream Cytometry

Analysis of uptake mechanisms and siRNA delivery was conducted using an Amnis Image Stream (Seattle, WA) imaging flow cytometer equipped with lasers at 405 nm, 488 nm, 658 nm, and 785 nm. Fluorescent data were collected using Channel 1 (430 – 505 nm, Hoechst), Channel 2 (505 – 595 nm, OG488), Channel 4 (595 – 660 nm, PI),

Channel 5 (660 – 745 nm, DY647), and Channel 6 (745 – 800 nm, side scatter). Brightfield images were collected in Channel 3.

Cells were imaged with a 60× objective. Fluid velocity was set to a nominal value of 40 mm/sec. Fluorescent compensation matrices were constructed using Amnis IDEAS® software and verified manually for proper fit. At least 5,000 cells were collected for analysis. Dead cells (PI positive) were excluded from analysis. Out-of-focus cells were also excluded from further analysis by gating the Gradient RMS feature in IDEAS® software. This feature detects image sharpness by calculating large changes in pixel values across the brightfield image. Typically, cells with Gradient RMS value <40 were considered out of focus[3].

7.2.8. siRNA-Mediated Gene Silencing

GAPDH Positive Control siRNA, KD Alert Assay Kits, and 10× Phosphate Buffered Saline (RNAse free) were purchased from Life Technologies (Carlsbad, CA). Caco-2 cells were seeded to tissue-culture treated 96-well plates at 2,500 cells/well and allowed equilibrate 24 hours before use. GAPDH siRNA was loaded into PDETB30 or PDESSB30 nanogels as outlined in Section 7.2.5. Following 60 min incubation in complexation buffer, nanogel/siRNA complexes were precipitated through the addition of acetone and centrifuged at 15,000 rpm for 5 min. Supernatant was discarded and complexes were resuspended in RNAse free PBS. Prior to use, Caco-2 cells were washed 1× with PBS and media replaced with serum free DMEM. Concentrated (20×) nanogel/siRNA complexes or control suspensions were added to test wells and incubated at 37°C, 5% CO_2 for 60 min. Following the 60 min exposure period, cells were washed

[3] See Appendix C – Gating strategy for ImageStream cytometry for information on gating and analysis

3× with pre-warmed PBS and media replaced with complete DMEM. Cells were incubated at 37°C, 5% CO_2 prior to conducting the KD Alert gene silencing assay according the manufacturer's instructions. Care was taken to adjust the microplate reader sensitivity to remain within the GAPDH enzyme calibration curve established according to the manufacturer's instructions.

7.2.9. Statistical Analysis

Statistical comparisons between experimental and control groups were made with two-tailed, unpaired, Student's t-test. Differences were accepted as statistically significant with $p < 0.05$.

7.3. Results and Discussion

7.3.1. Synthesis of disulfide crosslinker

A homobifunctional crosslinker 2-bis-(2-methacryloyloxyethyl disulfide) was synthesized (Figure 7.2) to endow responsive DEAEMA-based nanogels with a mechanism for biodegradation, namely reductive cleavage of the disulfide bonds. At the time of this study, this bifunctional linker was not commercially available. However, this crosslinker is now available commercially (with hydroquinone inhibitor) from Sigma-Aldrich (CAS No. 36837-97-5).

The synthesis and purification of 2-bis-(2-methacryloyloxyethyl disulfide) (SSXL) was successful; the reaction resulted in a molar yield of approximately 50%. The structure of SSXL was verified with ^{1}H-NMR. The spectra, shown in Figure 7.3, show peaks at δ = 1.95 ppm (1H, H_2C=C-), 2.96 ppm (1H, H_2C=C-), 4.45 (2H, CH_2-C$\boldsymbol{H}_2$-S-),

5.60 ppm (2H, -O-C***H***$_2$-CH_2-), and 6.14 ppm (3H, CH_3-C=). Analysis of the mass spectra (Figure 7.4) reveals a product of the expected molecular weight, 290 Da.

7.3.2. Degradable Nanogel Synthesis and Characterization

Disulfide-crosslinked nanogels containing an ionizable core of DEAEMA-co-TBMA and PEG corona were successfully synthesized via photoemulsion polymerization. This synthesis was conducted in identical fashion to our previous reports [11-13] and resulted in a similar yield (~1.2 g of nanogel) to previous syntheses. Replacing the non-degradable linker TEGDMA (as used in PDET, PDETB30, etc.) with SSXL had no identifiable change on physicochemical properties like pH-dependent swelling (Figure 7.5.), ζ-potential (Figure 7.6), and cytotoxicity to RAW 264.7 cells (Figure 7.7).

As shown in Figure 7.5, the critical swelling pH for PDESSB30 is 6.55. These nanogels have a z-average diameter of 96 nm at pH 8.5 and 126 nm at pH 6.0. The breadth of the volume phase transition is similar to PDETB30, occurring over 1.45 pH units. The value reported for PDETB30 in Chapter 4 is 1.56 pH units. PDESBB30 nanogels exhibit a PdI of 0.12 – 0.15 throughout the volume phase transition.

The nanoscale dimensions of PDESSB30 were verified by TEM and the dry particle size was determined to be 50 ± 17 nm. As shown in Figure 7.8 and tabulated in Table 4.5., this is quite similar to previous nanogel syntheses.

After confirming that size, swelling, and surface charge of the nanoscale hydrogels were unaffected by the change in crosslinker, studies were conducted to quantify the kinetics and extent of degradation in response to glutathione, a reductive

tripeptide. Previous experiments[4] served to establish a linear relationship between observed count rate (counts per second) and particle concentration (mg mL^{-1}) in dynamic light scattering experiments. This relationship was used to conduct a semi-quantitative, real-time measurement of degradation of SSXL-crosslinked nanoscale hydrogels in reductive aqueous suspension. The experiments were conducted using a Malvern ZetaSizer Nano ZS with the sample cell set to 37°C and measurements collected approximately every 3 minutes. After a brief equilibration period, sample cuvettes were injected with PBS or aqueous glutathione to bring the final concentration to 1 mM or 10 mM glutathione in PBS.

The degradation profiles, as seen in Figure 7.9, offer insight on the apparent glutathione sensitivity and kinetics of polymer degradation. A reduction in observed count rate is taken as a reduction in particle concentration and is an indicator of glutathione-induced degradation. Interestingly, the concentration of glutathione required to induce significant polymer degradation lies between the average minimum (1 mM) and maximum (11 mM) concentrations of intracellular glutathione. This attribute is compelling because it gives SSXL-crosslinked nanoscale hydrogels the ability to remain intact in the extracellular milieu and degrade in the intracellular environment. These data indicate the time-scale for degradation is fairly rapid, on the order of minutes.

Upon exposure to 10 mM glutathione, nearly 50% of the PDESSB30 degradation exposed to 10 mM GSH occurs within 15 min. Nearly all degradation is completed by 60 minutes. Similar results for count rate degradation were observed for dithiothreitol

[4] See Appendix X – Practical considerations in dynamic light scattering

(DTT), but are not shown here. For comparison, the observed count rate for PDESSB30 in PBS remained constant over the time-course of the experiment.

These observations were confirmed using Nanosight (Amesbury, UK) nanoparticle tracking analysis. At an identical glutathione:PDESSB30 to that employed in light scattering studies, exposure to 10 mM glutathione for 15 min at 37°C caused a 52% reduction in the particle concentration from 33.2×10^8 particles ml^{-1} to 17.5×10^8 particles ml^{-1} (data not shown).

After 2 hours exposure to GSH, samples were inspected visually via TEM for evidence of degradation. As seen in Figure 7.10, discrete particles were not detected at any region on the TEM grid, indicating near complete degradation of polymer networks.

This application of light scattering to monitor PDESSB30 degradation kinetics worked well for this initial application, though other methods may provide complementary insight into the degradation kinetics and extent of disulfide degradation. Analysis of degradation fragments using gel permeation chromatography (GPC) was problematic due to the high polydispersity of the linear polymer chains and incomplete nanogel degradation at intermediate time points. Colorimetric methods, such as Ellman's assay [14], were not sufficiently sensitive to detect free sulfhydryl groups in degraded PDESSB30. The theoretical maximum (assuming 100% conversion) for sulfhydryl groups at 1 mg mL^{-1} PDESSB30 in aqueous suspension is approximately 150 nM. Increasing the nanogel concentration beyond this concentration resulted in significant absorption due to solution turbidity.

7.3.3. Fluorescent Nanogel Synthesis

To enable visualization of nanogel subcellular localization in siRNA delivery experiments, a fluorescent version of the PDESSB30 nanogel was necessary. A primary amine-containing analogue of PDESSB30, termed PDESSB30f, was successfully synthesized and purified using the methods outlined in Sections 6.2.1.

Oregon Green 488 (OG488), an amine reactive dye, was conjugated to primary amines in the nanogel core. Prior to the conjugation reaction, the primary amine content of PDESSB30f was determined to be 17.0 ± 0.4 μmol g^{-1}, which represents a 11.5% incorporation efficiency. OG488 was subsequently added to PDESSB30f at 1:1 mol ratio of dye to amine. Following dialysis and lyophilization, the Oregon Green 488 functionalization was tested with fluorescence spectroscopy and the percent functionalization calculated with UV absorbance and comparison to an Oregon Green 488 standard curve.

The fluorescence emission (λ_{ex} = 465 nm) spectra of the labeled nanogel (PDESSB30-OG488) is shown in Figure 7.13. The fluorescent labeling was estimated at 16.9 ± 0.3 μmol g^{-1} using a standard curve of OG488 in PBS and at 19.5 μmol g^{-1} using the absorbance at 496 nm and the OG-488 extinction coefficient (ε) of 70,000 L mol^{-1} cm^{-1}, suggesting near 100% conjugation efficiency.

7.3.4. siRNA Loading Efficiency of pH-responsive nanogels

The ability of nanogels to encapsulate siRNA is an important determinant in their ability to deliver therapeutically relevant dosages of RNA to disease sites and initiate gene silencing. PDETB30 clearly displays the most desirable attributes for an endosomolytic drug delivery vehicle, but also contains fewer ionizable DEAEMA groups

than PDET or PDETBA30. Previous work [15] demonstrated that cationic polymer were able to bind DNA more efficiently with increasing cationic density. Thus, the RNA binding capacity was evaluated in a high-throughput fashion analogous to that described by Siegwart et al. [16]. RNA binding was evaluated as a function of nanogel composition, RNA:nanogel mass ratio, and complexation time to determine the loading efficiency of each nanogel.

The fraction of free RNA (F_f) was calculated by taking the ratio of fluorescent intensity of sample solutions to fluorescent intensity of a polymer-free control RNA solution. Both measurements were corrected for background fluorescence and the fraction of bound RNA, $F_b = 1 - F_f$. These data for a 60 min complexation period are in Figure 7.11. These results indicate that all formulations can efficiently bind free siRNA until a 1:1 mass ratio of polymer and siRNA and this binding is relatively independent of polymer composition. Nearly identical results were obtained for complexation periods of 120 and 180 min.

One limitation of this experimental technique is that it cannot distinguish the difference between RNA bound through surface adsorption or electrostatic encapsulation. Of these two, the latter is the more desirable as encapsulation and entrapment will afford better protection of RNA cargoes. As discussed previously, all polymer networks exhibit a positive surface charge at pH 5.50, so it is highly probable that anionic RNA can be adsorbed onto the particle surface through electrostatic interactions. Thus, this initial experiment likely overestimates the true RNA loading capacity of the nanogels.

To separate the effects of surface adsorption and electrostatic encapsulation, nanogels polymer and siRNA were allowed to complex in the acidic complexation buffer

(PBS, pH 5.50) for 60 minutes and were subsequently transferred to 3× volume of serum free DMEM. By immersing the polymer/siRNA complexes in a more basic solution, the effective surface charge can be reduced from approximately 30 mV to nearly neutral (0 ± 5 mV). This step change in surface charge serves to electrostatic interactions between nanogel surface and siRNA, permitting desorption of RNA from the surface.

According to the light scattering data presented in Chapter 4, this pH will completely or partially (depending on nanogel composition) collapse the network structure, serving to entrap RNA in the network core and limit diffusion out of the network. As seen in Figure 7.12 for a 10:1 mass ratio of polymer to siRNA, approximately 70% of the RNA is retained in the bound state following immersion in DMEM. Sample loading efficiencies for each nanogel formulation are tabulated for 100:1 and 1:1 nanogel:siRNA ratios (g/g) in Table 7.1.

Qualitative evidence of nanogel/siRNA binding can be seen in Figure 7.14. Complexes of PDETB30-OG488 and DY647-siRNA (prepared as described in Section 7.2.7.) were visualized using Image Stream cytometry. As expected, the siRNA-loaded nanogels are too small to visualize with brightfield microscopy, but the fluorescent signal from PDETB30-OG488 and DY647-siRNA was visible. As seen in the DY647 vs. OG488 intensity plot in Figure 7.14, nearly all PDETB30-OG488 nanogels contain DY647-siRNA. Analogous observations were made for complexes of PDESSB30-OG488 and DY647-siRNA.

7.3.5. Nanogel-mediated delivery of siRNA

7.3.5.1. Flow cytometry

The ability of PDETB30, and its degradable analogue PDESSB30, to deliver fluorescent siRNA to Caco-2 cells was evaluated using flow cytometry. Figure 7.15 shows the influence of exposure time on uptake of Cy3-siRNA. As expected, the naked siRNA is not able to efficiently enter Caco-2 cells. However, by complexation with PDETB30 or PDESSB30, the median fluorescence is increased by a factor of 5× after 5 min of exposure. Notably, siRNA delivery via PDETB30 and PDESSB30 result in a rapid increase in siRNA fluorescence from 0 – 5 min, followed by an approximately linear increase in median fluorescence from 5 min – 60 min.

As discussed in Chapter 6, the mechanism of internalization in Caco-2 cells is primarily macropinocytosis. This is an energy dependent internalization pathway and uptake of nanogel/Cy-3siRNA complexes is predictably inhibited by uptake at 4°C (Figure 7.16). Moreover, these data corroborate the observations of Chapter 6 (Figure 6.4 and Figure 6.6), whereby PDETB30 can be internalized through an energy-independent pathway. Following 60 min uptake at 4°C, cells exposed to PDETB30/Cy3-siRNA and PDESSB30/Cy3-siRNA exhibit greater median fluorescence than cells exposed to Cy3-siRNA alone.

These data suggest that PDETB30 and PDESSB30 are capable of delivery siRNA to Caco-2 cells. This work served as the basis for further study of the intracellular distribution of fluorescent nanogel/siRNA complexes and evaluation of the gene silencing activity of encapsulated siRNA.

7.3.5.2. Image Stream Cytometry

As described in Chapter 6, Image Stream cytometry was used to simultaneously acquire statistical flow cytometry data and high-resolution fluorescent micrographs. Additionally, the imagine analysis capabilities of Image Stream cytometry permit the sorting and gating of events with particular image features, such as cellular internalization (vs. surface adsorption) or probe colocalizaition.

As shown in Figure 7.17A, PDETB30-OG488 is an efficient delivery vehicle for DY647-siRNA in RAW macrophages. Both PDETB30-OG488 and PDESSB30-OG488[5] enhance the cytoplasmic fluorescence of DY647-siRNA relative to the siRNA only (blue histogram) and untreated control (gray histogram) cells. Figure 7.17B shows the OG488 fluorescent intensity histogram in untreated (gray), PDETB30-OG488 (green), and PDETB30-OG488/DY647-siRNA (red) treated samples. Notably, the fluorescent signal in the cells treated with nanogels only is greater than that of cells treated with nanogels/siRNA. This suggests that the internalization of nanogel/siRNA complexes is less efficient than nanogels alone.

Figure 7.18 shows representative fluorescent micrographs of RAW 264.7 cells. Cell nuclei are shown in blue (Hoechst), PDETB30-OG488 in green, and siRNA in red (DY647). Areas of nanogel/siRNA colocalizaition appear yellow on the fluorescent overlay.

Panels A - C show representative images of cells exposed only to 100 nM DY647-siRNA for 60 min, panels D - F show representative images of cells exposed only to 25 μg mL^{-1} PDETB30-OG488 for 60 min, and panels G – I show representative

[5] For clarity, only results generated from PDETB30-OG488 treated samples are shown, PDESSB30 samples demonstrated nearly identical intensity histograms and fluorescent micrographs.

images of cells exposed 25 μg mL^{-1} PDETB30-OG488 and 100 nM DY647-siRNA for 60 minutes. As expected due to its high MW (~13 kDa) and negative charge, little to no internalization was observed by the naked siRNA. In panels G – I (PDETB30-OG488/DY647-siRNA), the siRNA staining pattern appears mostly diffuse and distributed near the cell membrane. Several bright, colocalized spots appear in panels H and I, suggesting some vesicular entrapment of polymer/siRNA complexes. Vesicular entrapment, and/or lysosomal accumulation, is expected in a portion of the nanogel/siRNA complexes due to the heterogeneous internalization pathways presented by RAW 264.7 cells.

Similar observations were made for Caco-2 cells exposed to PDETB30/DY647-siRNA or DY647-siRNA under identical conditions. The fluorescent intensity histograms for DY64 and OG488 are shown in Figure 7.19A and Figure 7.19B, respectively. Comparing the median fluorescent values from Figure 7.17 (RAW 264.7 cells) and Figure 7.19 (Caco-2 cells) suggests a comparable level of nanogel and siRNA internalization in to these two cell types. The notable exception to this observation is the decreased PDETB30-OG488 intensity in RAW cells exposed to PDETB30-OG488/DY647-siRNA. This effect is not present in Caco-2 cells, which rely primarily on macropinocytosis to internalize PDETB30-OG488. As shown in Figure 6.6, RAW 264.7 cells uptake PDETB30-OG488 through a combination of clathrin-mediated endocytosis and macropinocytosis. This suggests that the clathrin-dependent uptake of nanogels is hampered by the presence of siRNA in the nanogel.

7.3.6. siRNA-Mediated Gene Silencing

Delivery efficacy of functional siRNA to model cells lines is an important parameter in the assessment of polymeric delivery systems. In these studies, GAPDH was chosen as the target gene for siRNA knockdown. GAPDH is a well-known housekeeping gene, ubiquitously expressed in nearly all cell types, and is involved in the reduction of NAD^+ to NADH in the glycolysis pathway. Knockdown was assessed using a KDAlert™ GAPDH Assay Kit and monitoring the increase in fluorescence (em:520/ex:590) over a 4 minute period. This gene target was originally selected to facilitate a broad comparison of gene knockdown and transfection conditions for the cell types (Caco-2 and RAW 264.7) chosen for these studies.

GAPDH knockdown, shown in Figure 7.20, reveal that GAPDH siRNA delivered via PDETB30 induces a robust gene silencing effect, reducing GAPDH expression by 60 – 85%. This knockdown effect occurred at multiple polymer:siRNA ratios ranging from 8:1 – 1000:1.

Figure 7.21 compares the siRNA-mediated gene silencing in Caco-2 cells treated with PDETB30/siRNA or PDESSB30/siRNA at a 200:1 nanogel:siRNA ratio. Both nanogel formulations are capable of delivering functional siRNA. Knockdown efficiency was 53% for cells treated with PDESSB30/siRNA and 83% for cells treated with PDETB30/siRNA. Based on flow cytometry data in Figure 7.15, Caco-2 cells treated with PDETB30/siRNA exhibited characteristically higher siRNA fluorescence than did cells treated with PDESSB30/siRNA. Therefore, the superior knockdown efficiency of PDETB30/siRNA relative to PDESSB30/siRNA is likely due to increased siRNA delivery efficiency by the former combination.

While GAPDH siRNA and KD Alert assays were suitable for initial studies of gene silencing in Caco-2 cells, this assay did not transfer well to RAW 264.7 macrophages. The linear range for detecting GAPDH enzyme activity can typically accommodate approximately 2,000 – 10,000 cells/well. In Caco-2 cells (doubling time ~ 60 h), the cell density at the time of assay (~48 h after transfection) is expected to be 1 - 2× the seeding density. In contrast, RAW 264.7 cells grow much more rapidly, with a doubling time ~15 h. Therefore, RAW 264.7 cells will undergo 3 – 4 doubling cycles between transfection and assay. Thus, RAW 264.7 cells were typically seeded at a low density (1,000 cells/well in 96-well plates) for these studies. Any variations in the cell seeding density were then amplified by successive rounds of RAW division. This becomes problematic because the KD Alert relies on comparison of experimental wells to external control wells. In practice, high variability in the RAW cell density at assay time limited the utility of the KD Alert assay kit in evaluating any PDETB30/siRNA-mediated gene silencing in RAW cells. Analysis methods that provide an internal control, such as qPCR, are better suited for evaluation of gene silencing.

7.4. CONCLUSIONS

A disulfide crosslinker was synthesized to allow degradation of pH-responsive nanogels in reductive environments. This crosslinker was incorporated into responsive nanogels, termed PDESSB30, with little to no changes on physicochemical properties including critical swelling pH, nanogel size, or in vitro biocompatibility. These nanogels degrade within minutes upon exposure to physiological levels of glutathione as determined by light scattering and electron microscopy. Analysis of cellular internalization demonstrated efficient uptake of siRNA delivered via degradable

(PDESSB30) and non-degradable (PDETB30) nanogels. Moreover, both PDESSB30 and PDETB30 are capable of delivering functional siRNA to Caco-2 cells, achieving gene silencing of 47% and 83%, respectively. The combination of attractive physicochemical properties and siRNA delivery efficiency make PDETB30 and PDESSB30 attractive candidates for further development as therapeutic siRNA delivery systems.

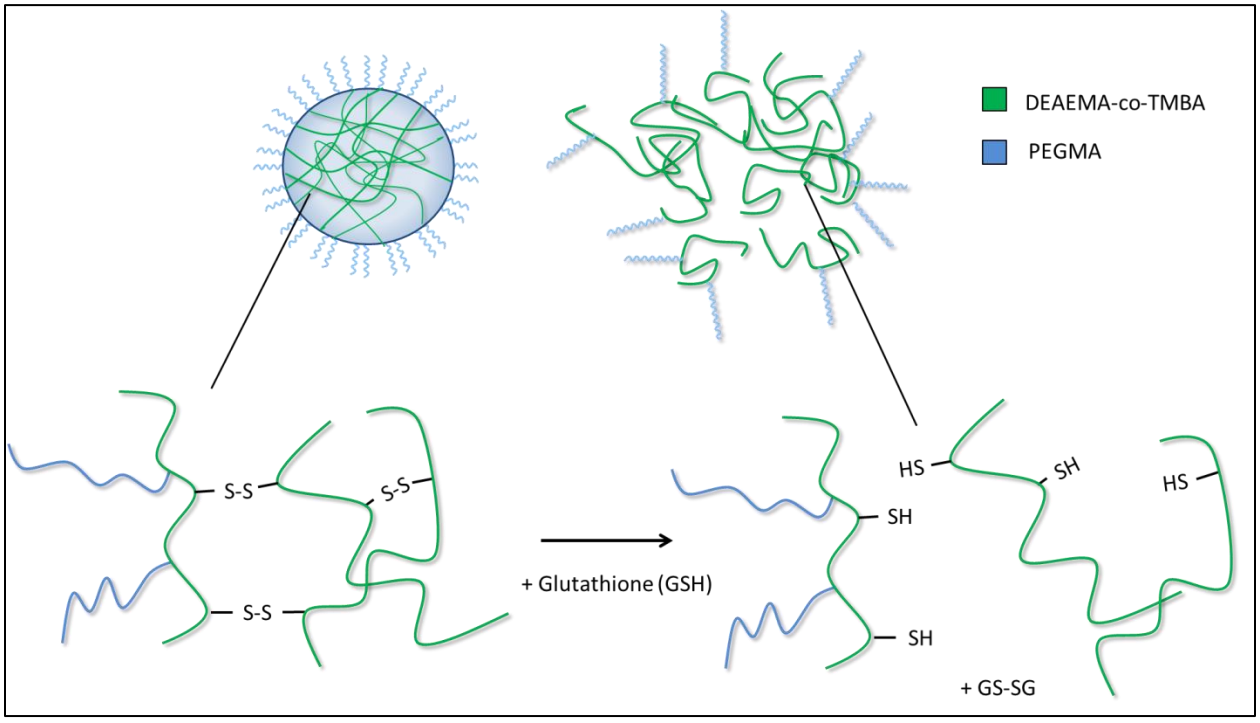

Figure 7.1–Degradable nanogel in response to glutathione. Disulfide crosslinks are sensitive to reductive conditions.

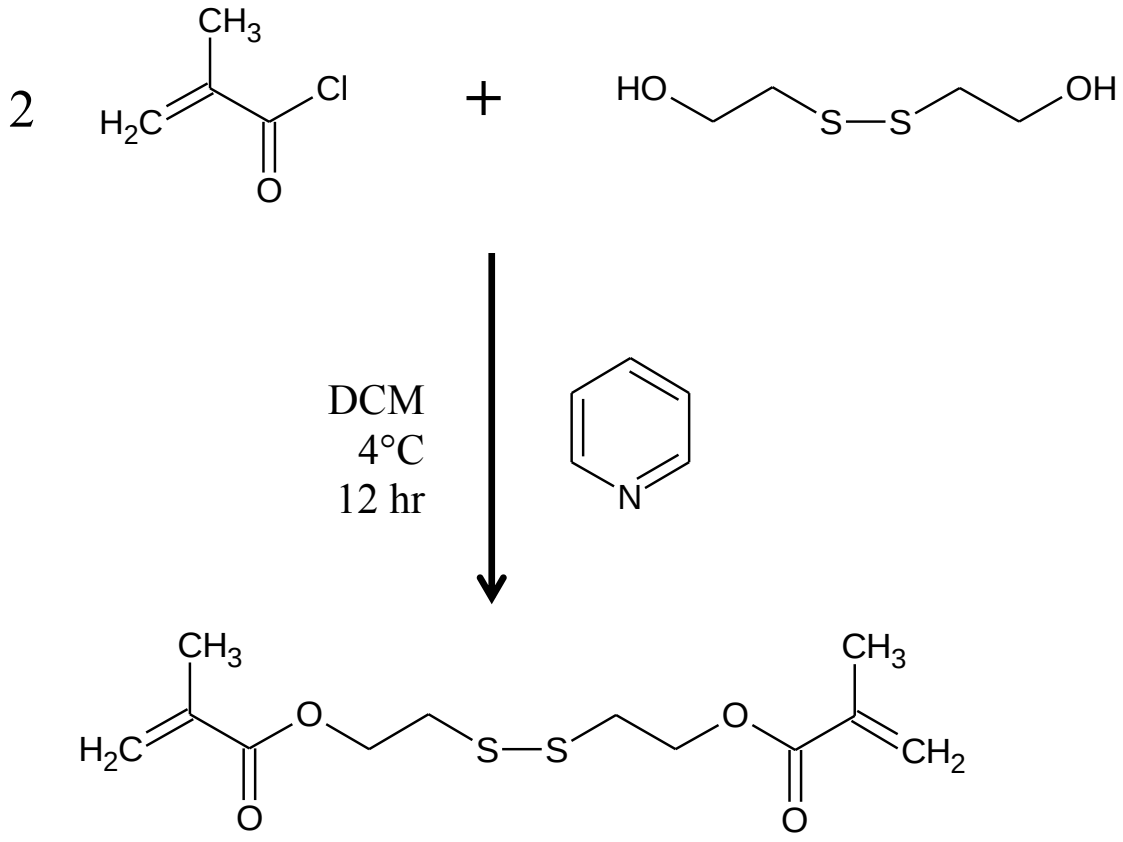

Figure 7.2 - Reaction scheme for bis(2-methacryloyloxyethyl) disulfide.

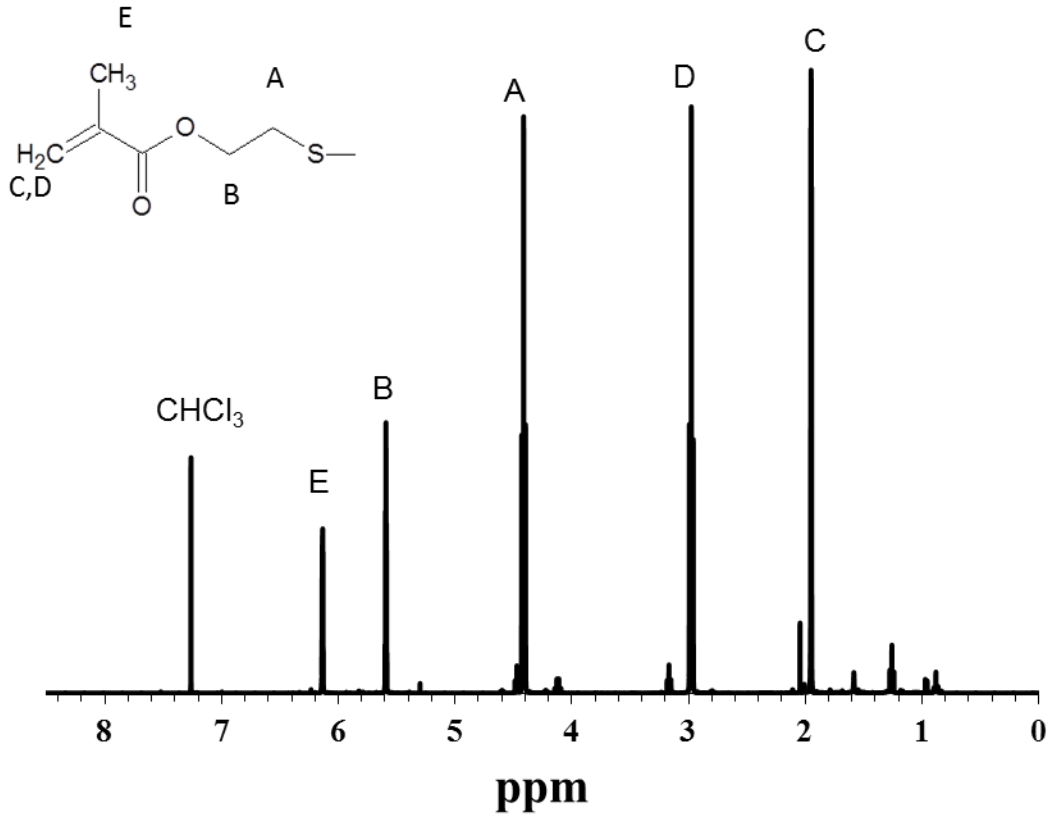

Figure 7.3 - ^{1}H-NMR spectrum of bis(2-methacryloyloxyethyl) disulfide (SSXL) in $CDCl_3$

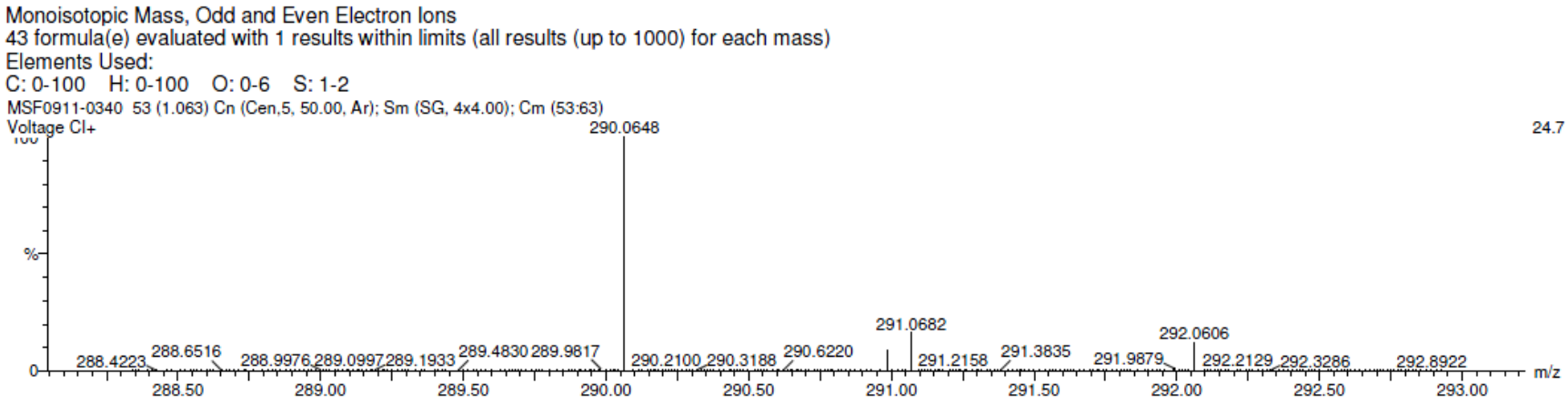

Figure 7.4 - Mass spectrum of purified bis(2-methacryloyloxyethyl) disulfide. Anticipated molecular weight of the bis(2-methacryloyloxyethyl) disulfide = 290.4 g/mol.

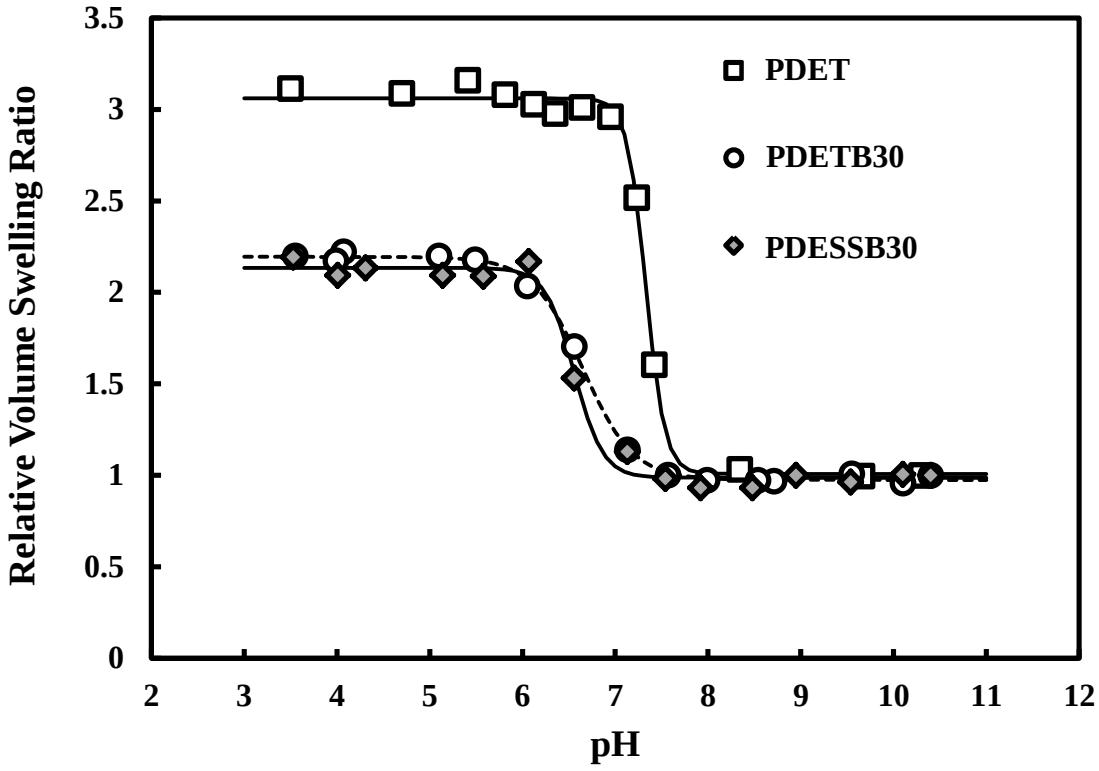

Figure 7.5 - pH-responsive behavior of nanogels in suspended in PBS. PDET (□), PDETB30 (○), and PDESSB30 (♦).

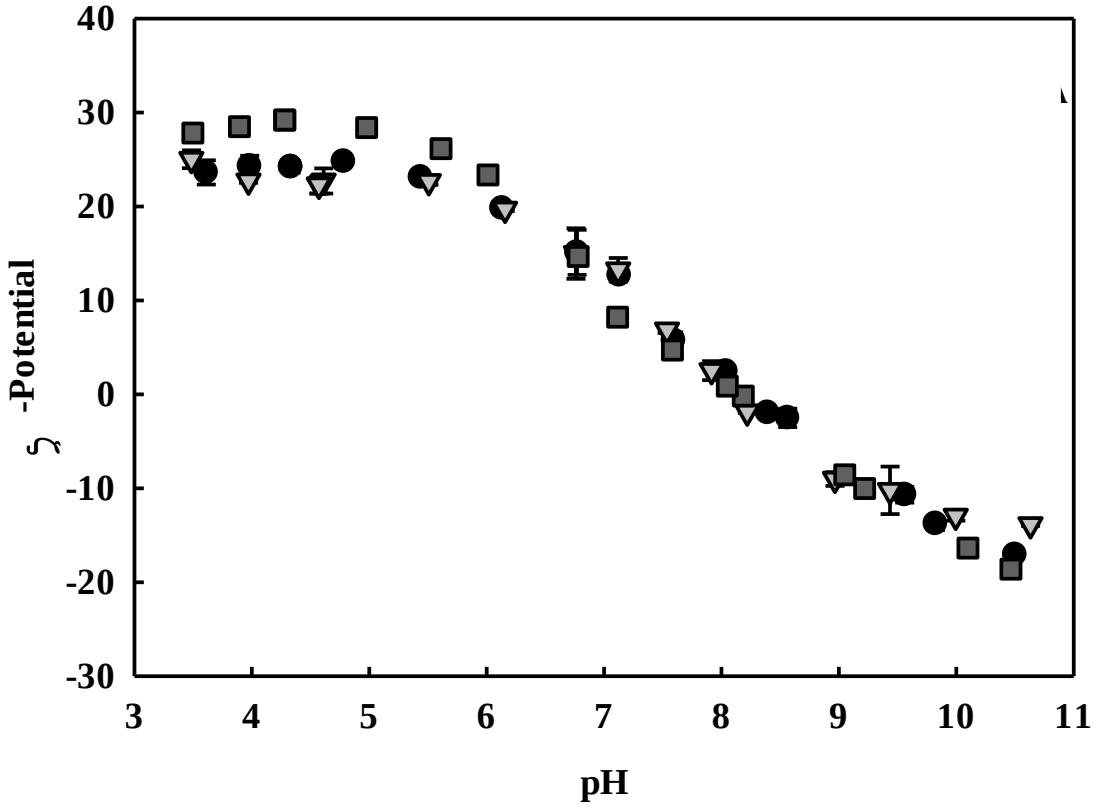

Figure 7.6 - Effective surface ζ-potential of various polymer formulations PDET (●), PDETB30 (▼), and PDESSB30 (□). Data points represent the mean of 3 measurements ± SD. Reproduced with permission from [17].

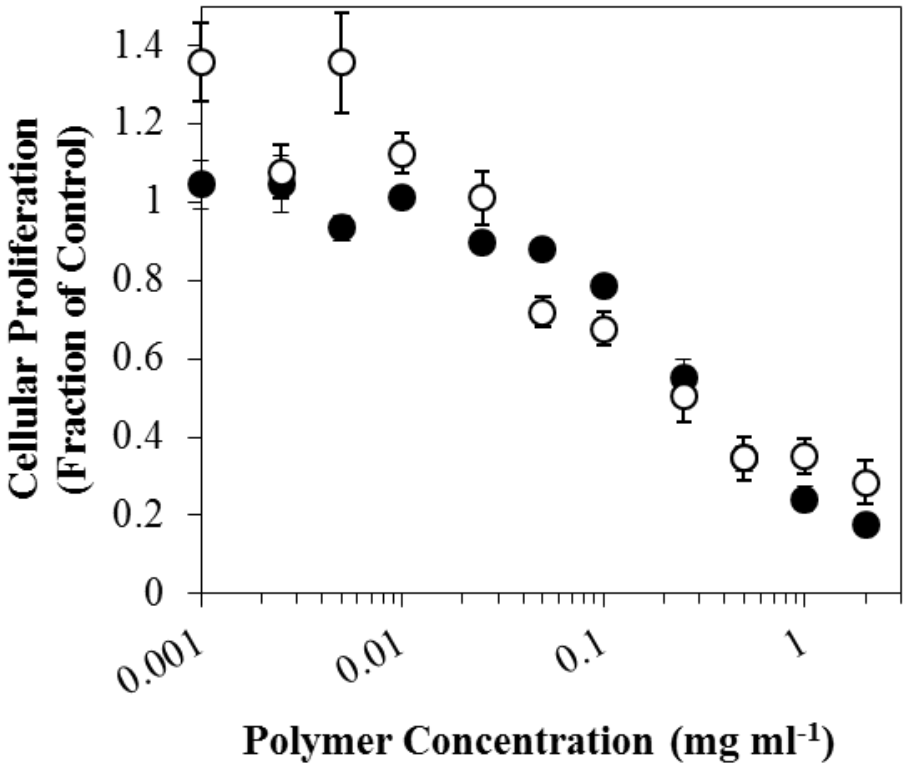

Figure 7.7. - Relative proliferation of RAW 264.7 cells upon exposure to PDESSB30 (●) or PDETB30 (○) for 360 min. The relative proliferation of RAW cells was determined by MTS assay and is expressed as a fraction of the control (untreated) cells. Data are expressed as mean ± SEM, n = 4.

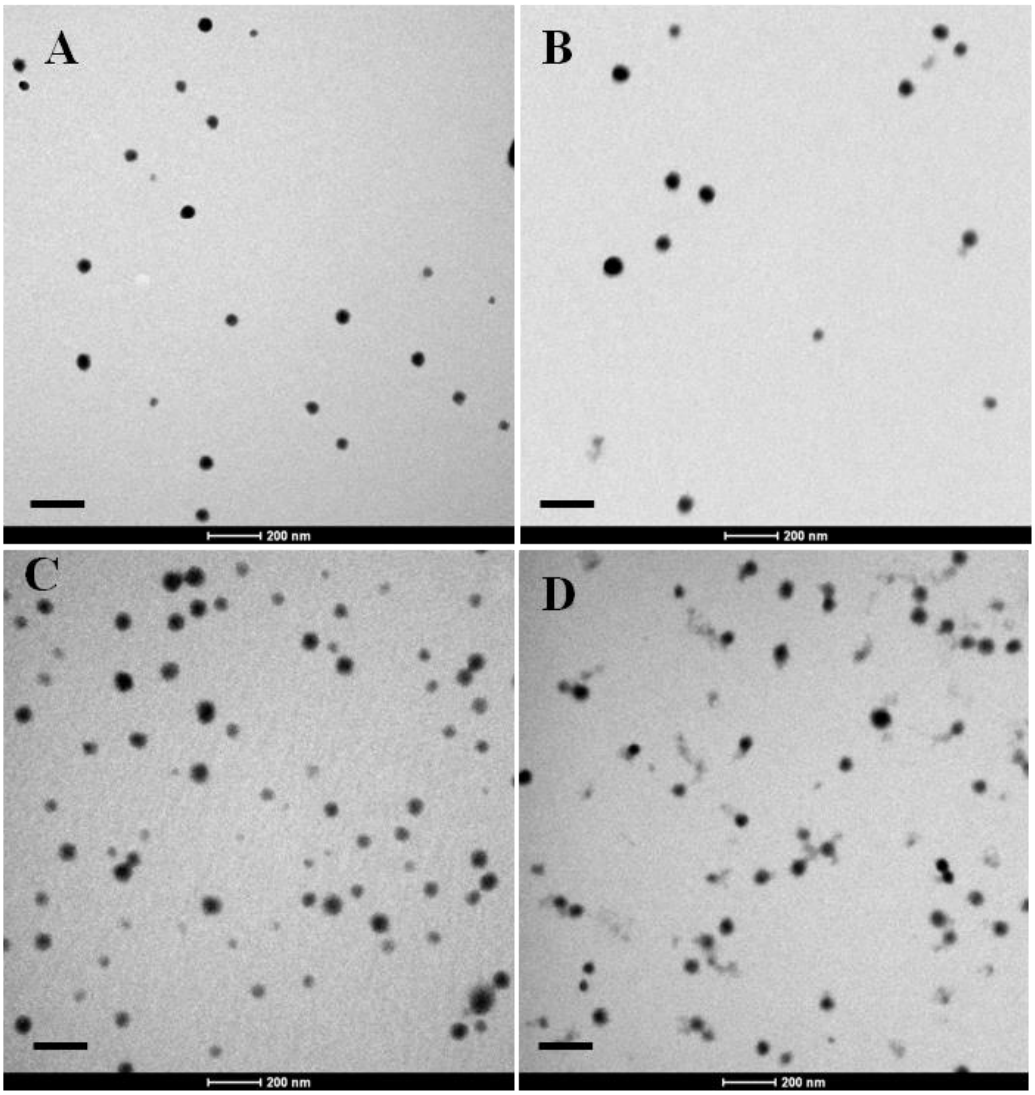

Figure 7.8 - Representative transmission electron microscopy images of PDET, PDETBA30 (B), PDETB30 (C), and PDESSB30 (D). Particles stained with uranyl acetate and images collected at 43,000×. Scale bar represents 200 nm. Reproduced with permission from [17].

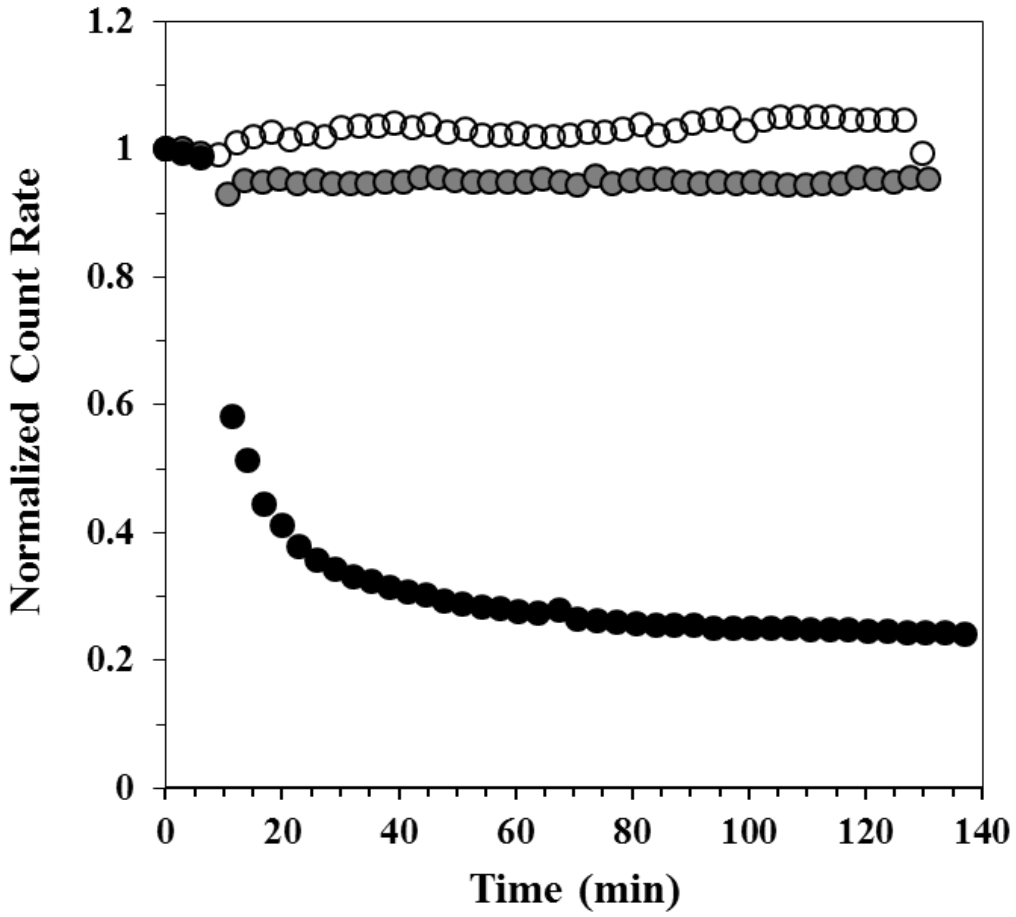

Figure 7.9 - Light scattering analysis of glutathione-induced degradation. Nanogels dissolved in PBS and exposed to 1 mM (gray) and 10 mM (black) concentrations of glutathione (GSH) and incubated at 37°C.

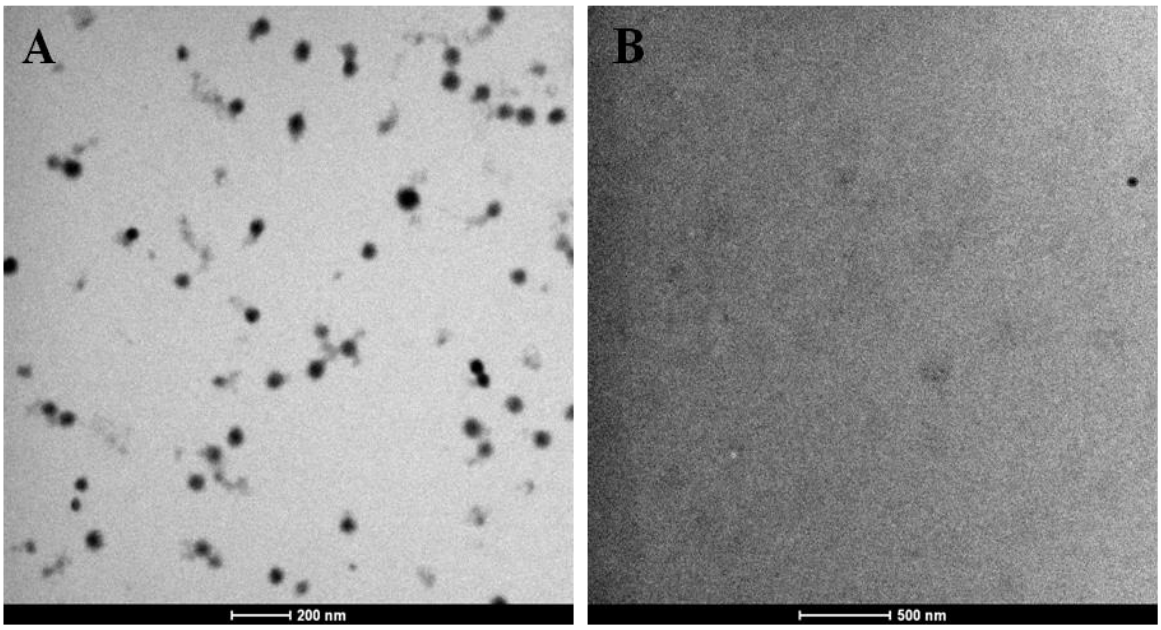

Figure 7.10 - Representative transmission electron microscopy images of PDESSB30 incubated for 2 hours in (A) DI water and (B) 10 mM glutathione solution (left). Particles stained with uranyl acetate and images collected at 26,500× (left) and 20,500× (right).

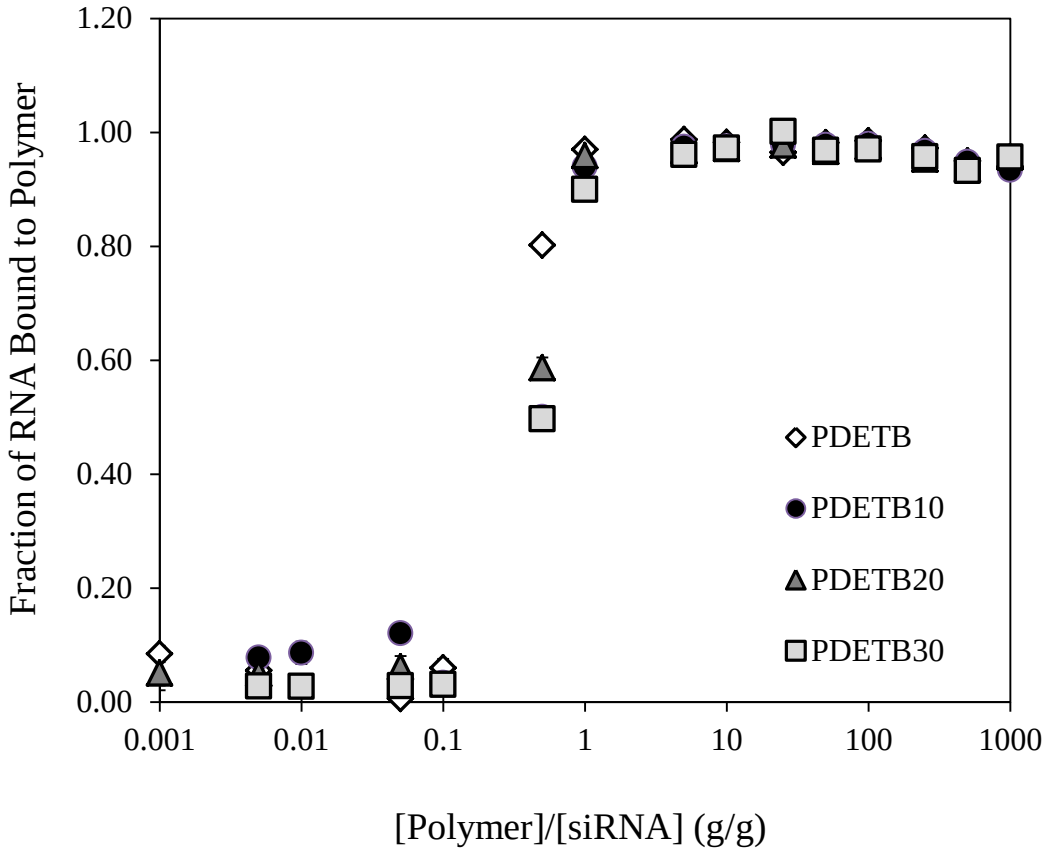

Figure 7.11. - RNA Loading capacity of poly(DEAEMA-g-PEGMA) (PDET), and poly(DEAEMA-co-BMA-g-PEGMA) (PDETB10), (PDETB20), and (PDETB30) in PBS, pH 5.50. Data represent mean ± s.d. (n = 3).

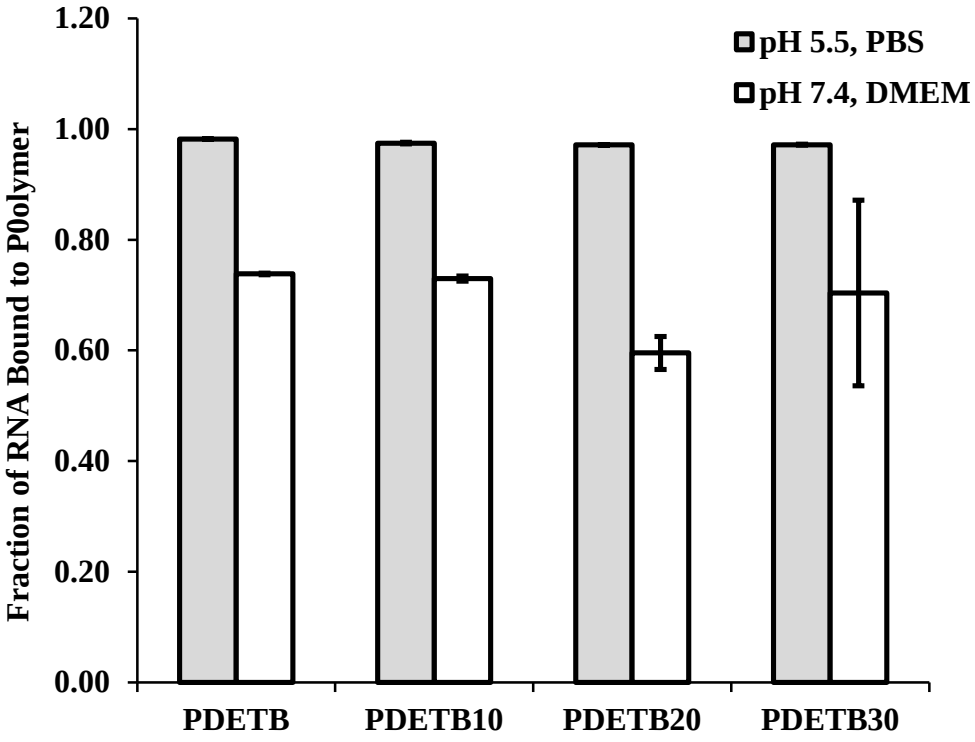

Figure 7.12 - RNA loading of poly(DEAEMA-g-PEGMA) (PDET), and poly(DEAEMA-co-BMA-g-PEGMA) (PDETB10), (PDETB20), and (PDETB30) in PBS, pH 5.50 (gray) and in serum-free DMEM, pH 7.40 (white). Polymer and siRNA were combined at a ratio of 10:1 [polymer]:[siRNA]. Fraction of bound RNA determined by Ribogreen assay following 180 min incubation in PBS and 30 min incubation in DMEM. Bars represent the mean ± s.d. (n = 3).

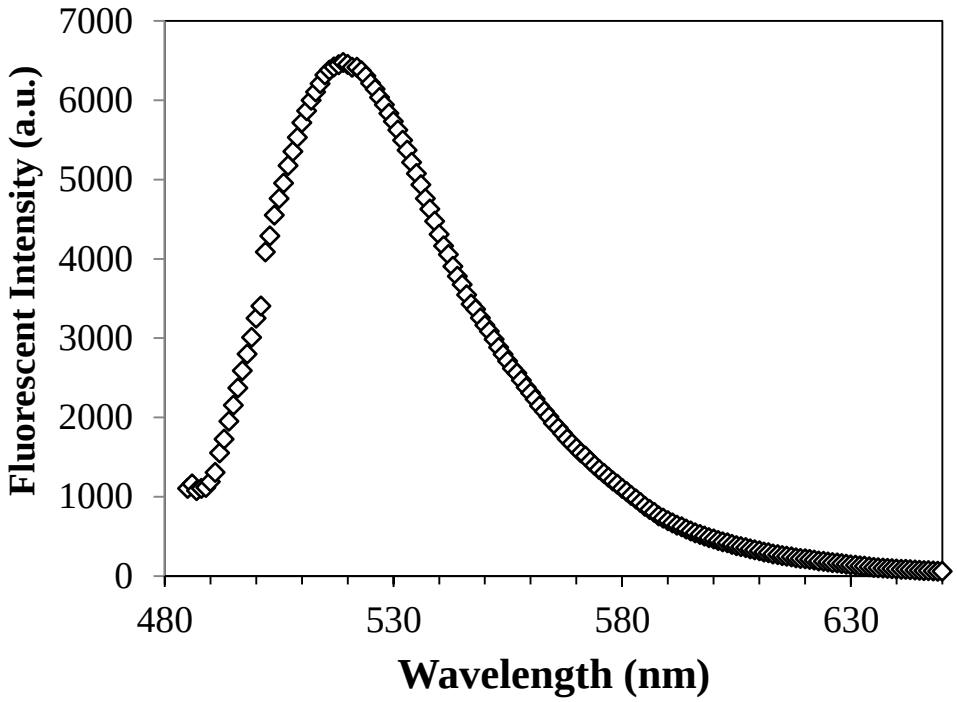

Figure 7.13 – Fluorescent emission spectra of PDESSB30-OG488.

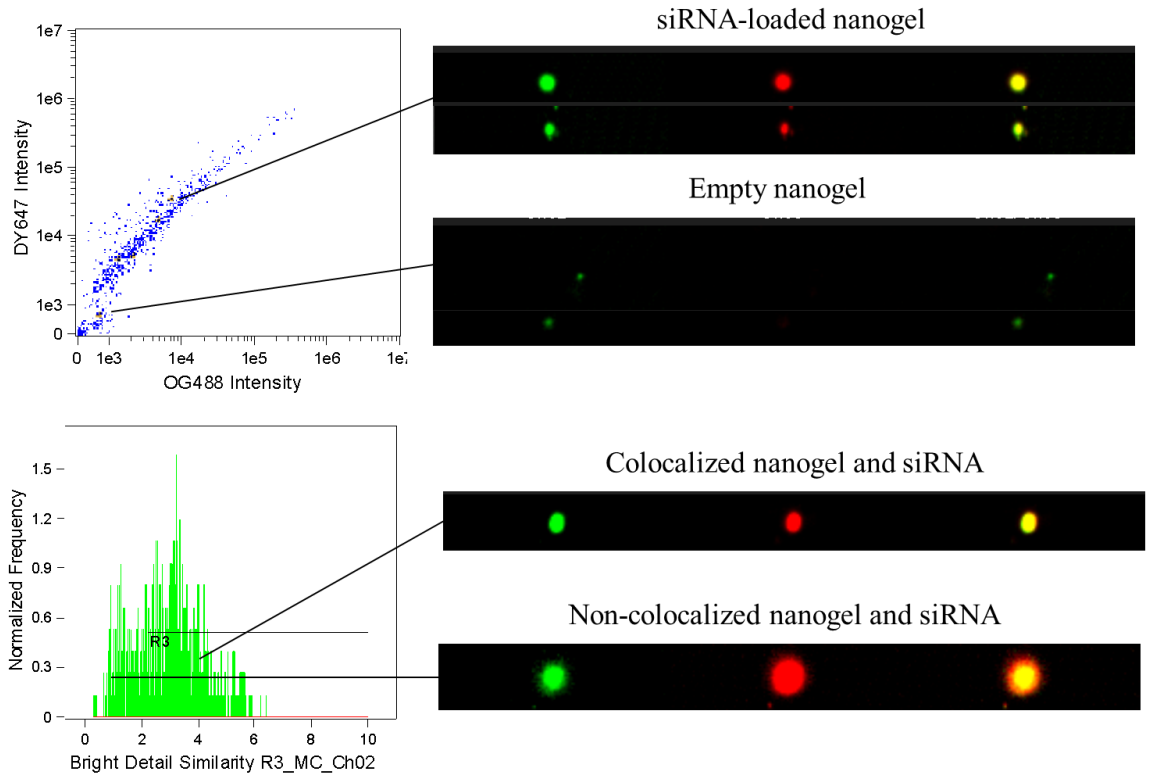

Figure 7.14 - Fluorescent micrographs of PDETB30-OG488 and DY647-siRNA

Table 7.1 –Loading efficiencies for nanogels and siRNA. Fraction of bound RNA determined by Ribogreen assay following 60 min complexation with nanogels. Data represent mean of triplicate samples ± s.d.

		Loading Efficiency	
Nanogel	**Nanogel:siRNA (g/g)**	**pH 5.50**	**pH 7.40**
PDET	100	0.99 ± 0.003	0.72 ± 0.02
PDETB10	100	0.98 ± 0.002	0.71 ± 0.01
PDETB20	100	0.97 ± .0003	0.63 ± 0.01
PDETB30	100	0.97 ± 0.001	0.67 ± 0.05
PDET	1	0.97 ± 0.001	0.58 ± 0.06
PDETB10	1	0.94 ± 0.001	0.51 ± 0.09
PDETB20	1	0.96 ± 0.002	0.50 ± 0.12
PDETB30	1	0.90 ± 0.006	0.48 ± 0.06

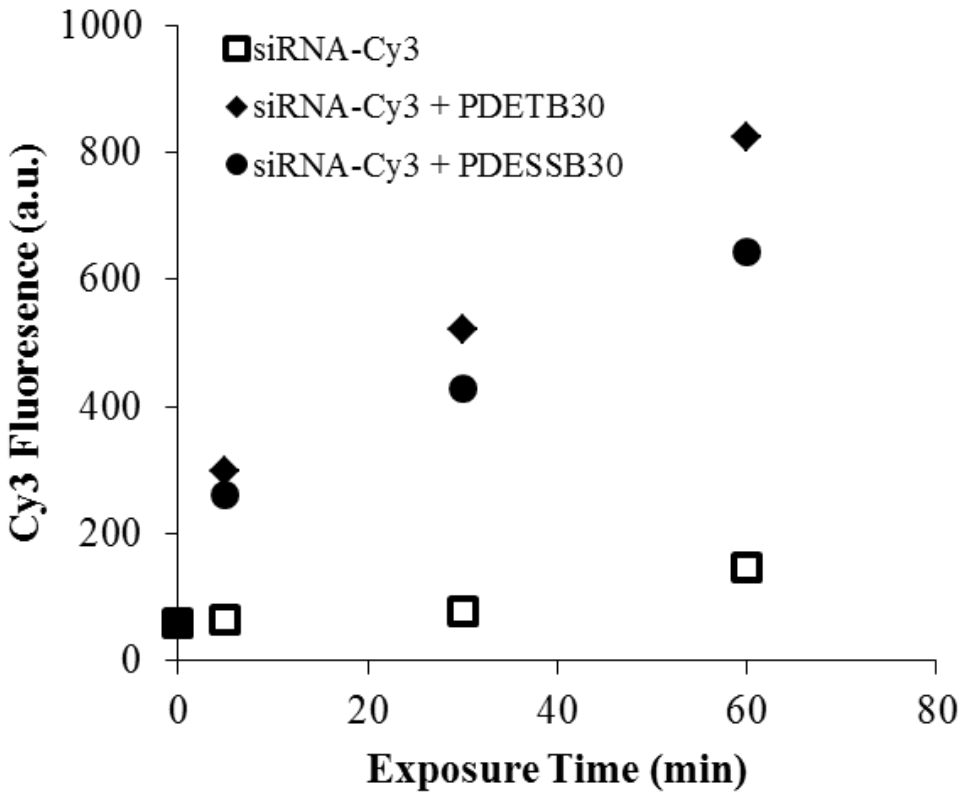

Figure 7.15 – siRNA delivery to Caco-2 cells as a function of incubation time. Nanogel/Cy3-siRNA complexes were prepared at a 20:1 nanogel/siRNA ratio (g/g) and incubated with cells for designated time points. Data points represent the median fluorescence of live cells as determined by flow cytometry. Dead cells excluded via propidium iodide.

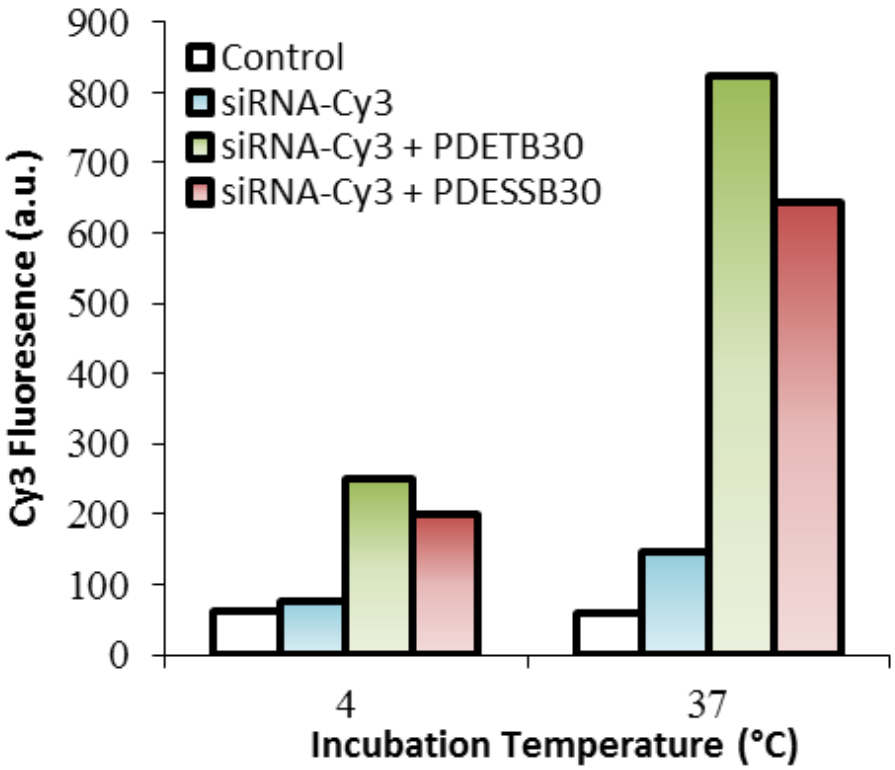

Figure 7.16 – siRNA delivery to Caco-2 cells as a function of nanogel composition and incubation temperature. Nanogel/Cy3-siRNA complexes were prepared at a 20:1 nanogel/siRNA ratio (g/g) and incubated with Caco-2 cells for 60 min. Data points represent the median fluorescence of live cells as determined by flow cytometry. Dead cells excluded via propidium iodide.

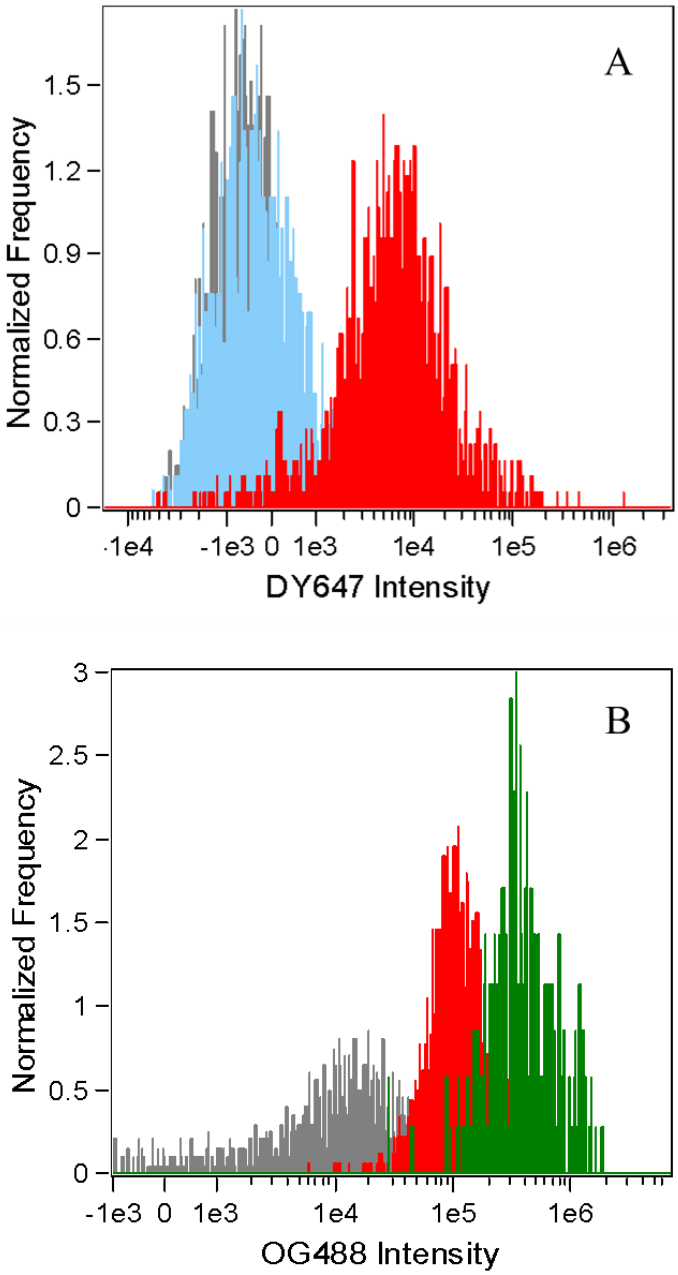

Figure 7.17 - Fluorescence intensity of RAW 264.7 cells in siRNA delivery experiments. Fluorescence intensity histograms of DY647-siRNA (A) and PDETB30-OG488 (B). Fluorescence histograms generated from live, focused, single cells exposed to PBS (untreated, gray), DY647-siRNA alone (blue), PDETB30-OG488 alone (green), or PDETB30-OG488/DY647-siRNA (red). Data represent the results of two pooled experiments.

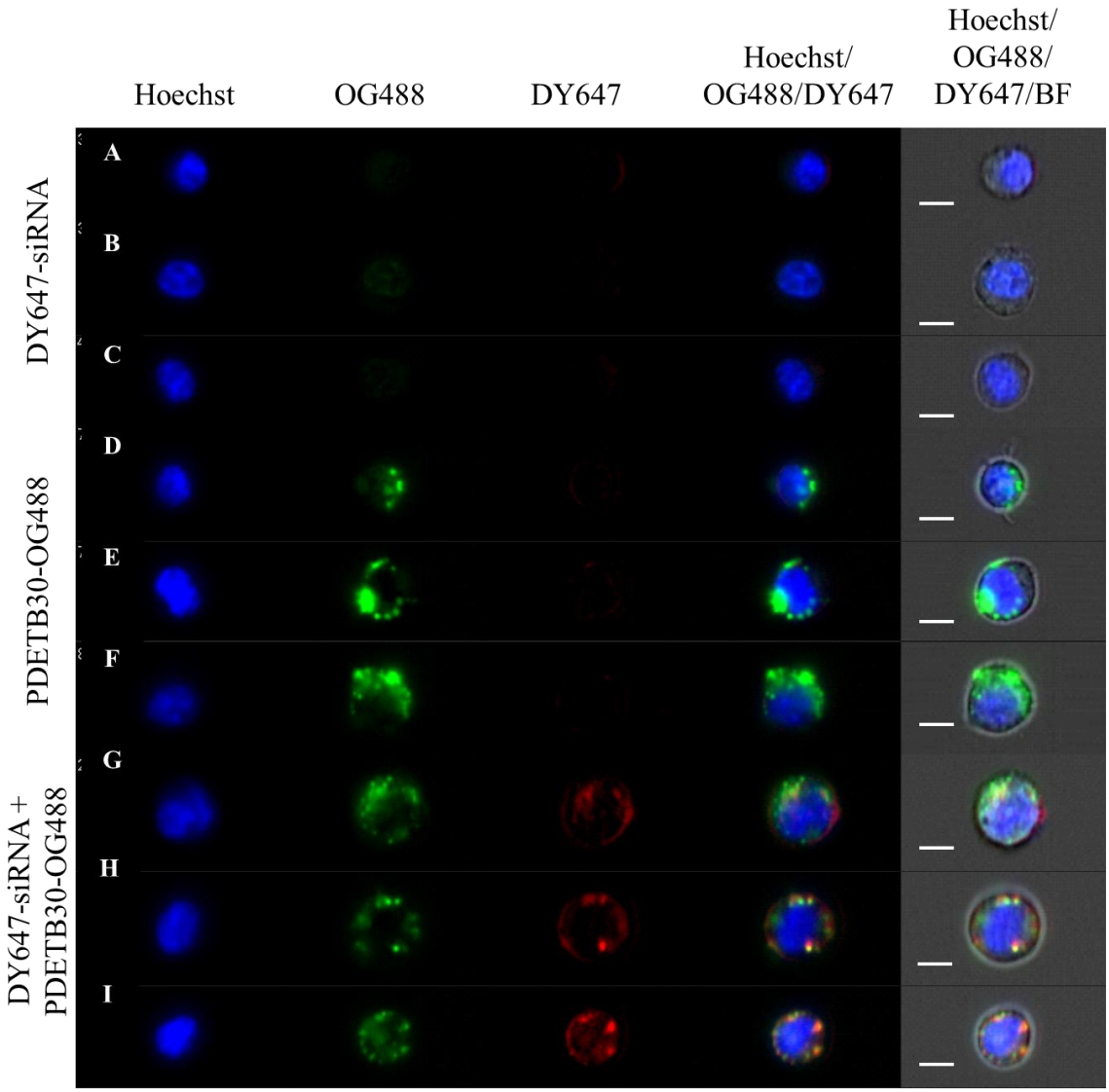

Figure 7.18 - DY647-siRNA delivery to RAW 264.7 cells. Nuclear stain (Hoechst 33342) shown in blue, PDETB30-OG488 (Oregon Green 488) shown in green, and DY647-siRNA (DyLight 647) shown in red. Three representative examples of RAW 264.7 cells exposed to DY647-siRNA alone (A-C), PDETB30-OG488 along (D – F), or PDETB30-OG488/DY647-siRNA (G – I) are shown. Images sampled from median region of DY647 histogram. Scale bar represents 7 μm.

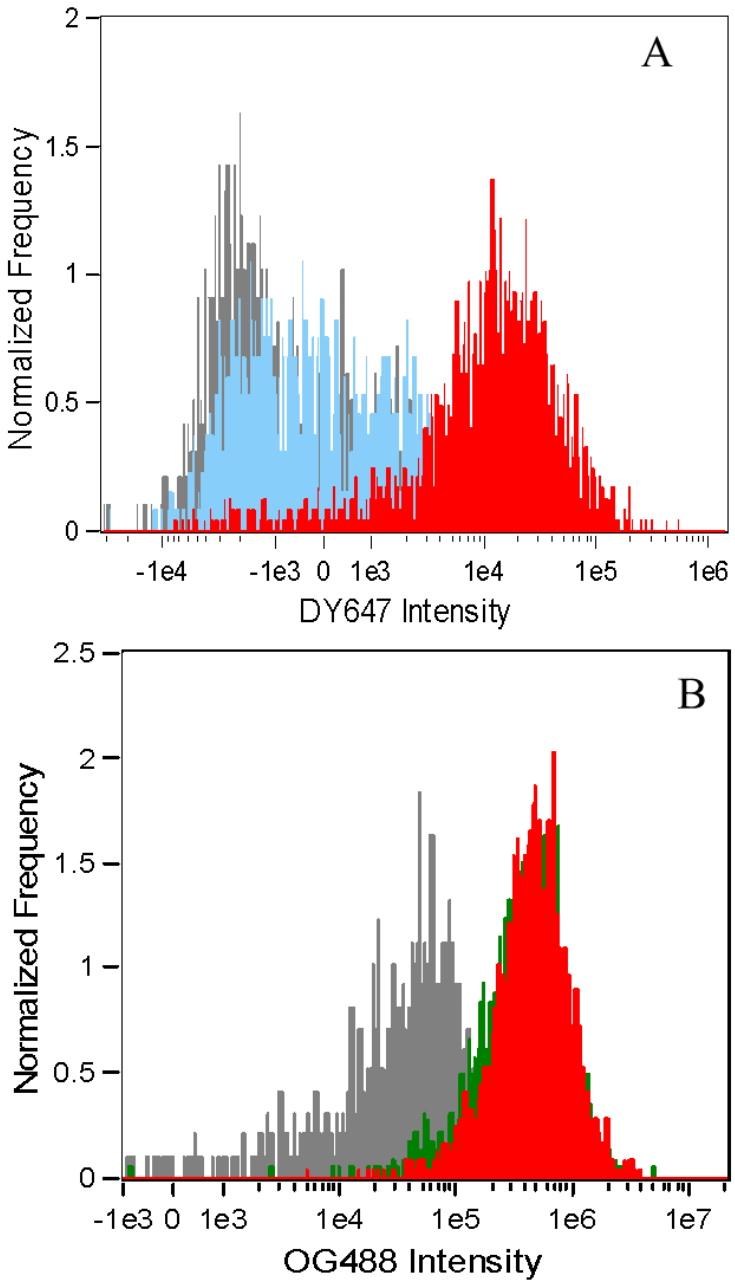

Figure 7.19 - Fluorescence intensity of Caco-2 cells in siRNA delivery experiments. Fluorescence intensity histograms of DY647-siRNA (A) and PDETB30-OG488 (B). Fluorescence histograms generated from live, focused, single cells exposed to PBS (untreated, gray), DY647-siRNA alone (blue), PDETB30-OG488 alone (green), or PDETB30-OG488/DY647-siRNA (red). Data represent the results of two pooled experiments.

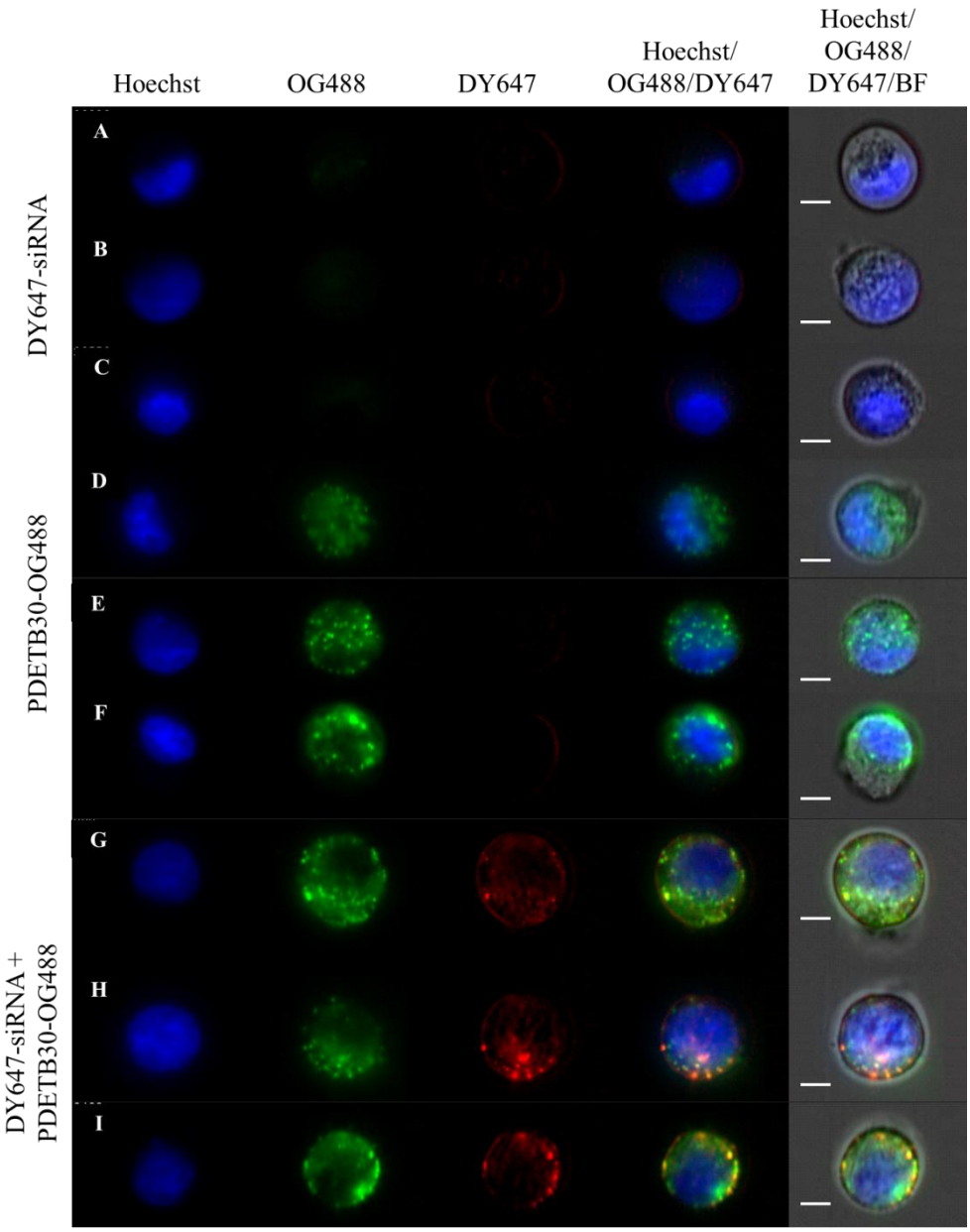

Figure 7.20 - DY647-siRNA delivery to RAW 264.7 cells. Nuclear stain (Hoechst 33342, blue), PDETB30-OG488 (Oregon Green 488, green), and DY647-siRNA (DyLight 647, red) are shown. Three representative examples of RAW 264.7 cells exposed to DY647-siRNA alone (A-C), PDETB30-OG488 alone (D – F), or PDETB30-OG488/DY647-siRNA (G – I) are shown. Images sampled from median region of DY647 histogram. Scale bar represents 7 µm.

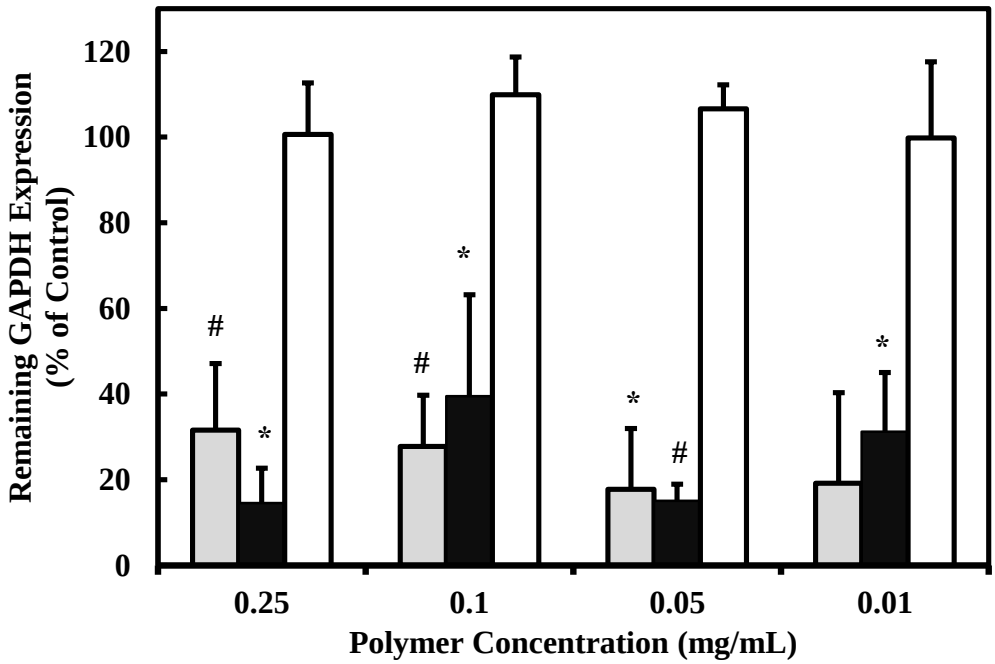

Figure 7.21 – GAPDH knockdown in Caco-2 cells following exposure to PDETB30/siRNA. Cells exposed to siRNA-loaded nanogels at designated concentrations of PDETB30 and 250 ng mL^{-1} (~20 nM, gray) or 1250 ng mL^{-1} (~100 nM, black) GAPDH siRNA. Expression levels measured 48 hrs after transfection. Bars represent the mean of % remaining expression GAPDH expression ± s.d. (n = 3). * $p < 0.05$, # $p < 0.01$

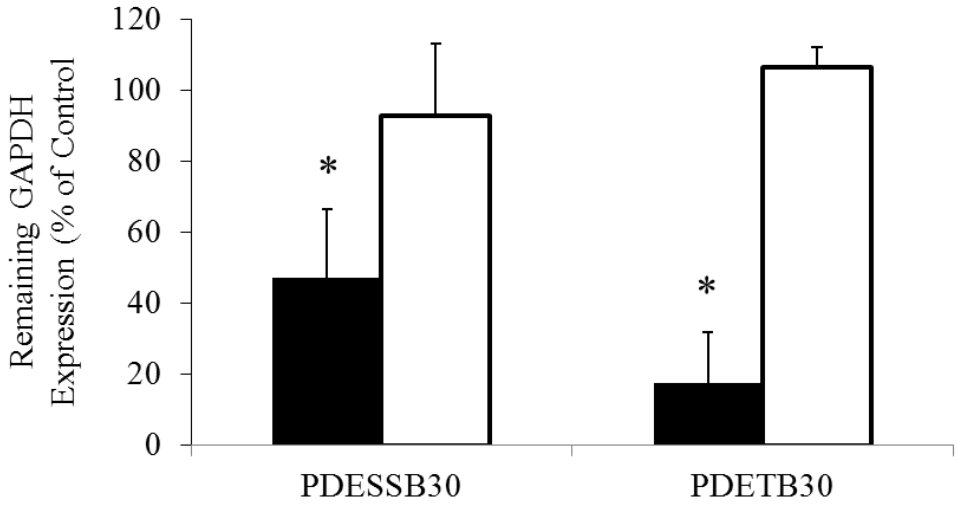

Figure 7.22 – GAPDH knockdown in Caco-2 cells following exposure to PDETB30/siRNA or PDESSB30/siRNA. Cells exposed to siRNA-loaded nanogels at 200:1 nanogel:siRNA ratio (g/g, 50 μg mL^{-1} nanogel and 0.25 μg ml^{-1} siRNA). Expression levels measured 48 hrs after transfection. Bars represent the mean of % remaining expression GAPDH expression ± s.d. (n = 3). * $p < 0.05$

REFERENCES

1. Fire A, Xu S, Montgomery MK, Kostas SA, Driver SE, and Mello CC. Nature 1998;391(6669):806.

2. Whitehead KA, Langer R, and Anderson DG. Nature Reviews Drug Discovery 2009;8(2):129-138.

3. Zhou J, Shum K-T, Burnett J, and Rossi J. Pharmaceuticals 2013;6(1):85-107.

4. Davis ME, Zuckerman JE, Choi CHJ, Seligson D, Tolcher A, Alabi CA, Yen Y, Heidel JD, and Ribas A. Nature 2010;464(7291):1067-1070.

5. Khormaee S, Choi Y, Shen MJ, Xu BY, Wu HT, Griffiths GL, Chen RJ, Slater NKH, and Park JK. Advanced Functional Materials 2013;23(5):565-574.

6. Aouadi M, Tesz GJ, Nicoloro SM, Wang M, Chouinard M, Soto E, Ostroff GR, and Czech MP. Nature 2009;458(7242):1180-1184.

7. Tamura A, Oishi M, and Nagasaki Y. Biomacromolecules 2009;10(7):1818-1827.

8. Convertine AJ, Benoit DSW, Duvall CL, Hoffman AS, and Stayton PS. Journal of Controlled Release 2009;133(3):221-229.

9. Winter PM, Cai KJ, Chen J, Adair CR, Kiefer GE, Athey PS, Gaffney PJ, Buff CE, Robertson JD, Caruthers SD, Wickline SA, and Lanza GM. Magnetic Resonance in Medicine 2006;56(6):1384-1388.

10. Gao H, Tsarevsky NV, and Matyjaszewski K. Macromolecules 2005;38(14):5995-6004.

11. Liechty WB, Scheuerle RL, and Peppas NA. Polymer 2013;under review.

12. Fisher OZ and Peppas NA. Macromolecules 2009;42(9):3391-3398.

13. Fisher O, Kim T, Dietz S, and Peppas N. Pharmaceutical Research 2009;26(1):51-60.

14. Boyne AF and Ellman GL. Analytical Biochemistry 1972;46(2):639-&.

15. Dufresne MH, Elsabahy M, and Leroux JC. Pharmaceutical Research 2008;25(9):2083-2093.

16. Siegwart DJ, Whitehead KA, Nuhn L, Sahay G, Cheng H, Jiang S, Ma ML, Lytton-Jean A, Vegas A, Fenton P, Levins CG, Love KT, Lee H, Cortez C, Collins SP, Li YF, Jang J, Querbes W, Zurenko C, Novobrantseva T, Langer R, and Anderson DG. Proceedings of the National Academy of Sciences of the United States of America 2011;108(32):12996-13001.

17. Liechty WB, Caldorera-Moore M, Phillips MA, Schoener C, and Peppas NA. Journal of Controlled Release 2011;155(2):119-127.

Chapter 8: Nanogels with bio-inspired pseudo-peptides to impart network hydrophobicity and enable intracellular delivery of small interfering RNA

8.1. INTRODUCTION

Synthetic polymers with reduced charge density, high molecular weight, and hydrophobic comonomers have received recent attention as high-efficiency, low-toxicity drug delivery vehicles [1]. Zhou et al. [2], recently described a series of lactone-based terpolymers of varying hydrophobicity and cationic charge density. Other previous reports [3-5] have explored the incorporation of hydrophobic amino acid grafts to pH-responsive linear polymers and their utility in therapeutic protein delivery [6]. These studies found that phenylalanine grafts were particularly effective at enhancing the membrane-disruptive capabilities of the polymer while remaining relatively biocompatible.

To investigate whether a phenylalanine moiety can impart similar hydrophobicity to P(DEAEMA-g-PEGMA) nanoscale hydrogels while enhancing relative biocompatibility, a methacrylamide-derivatized phenylalanine was synthesized. This functional monomer, N-methacryloyl L-phenylalanine methyl ester (MAPA), has been used previously in to increase the hydrophobicity of poly(hydroxyethyl methacrylate) P(HEMA) microparticles in hydrophobic interaction chromatography applications [7]. In a related study, Türkmen, et al. [8] synthesized circa 150 nm P(HEMA-co-MAPA) nanospheres and explored their utility in adsorption of the model antibody immunoglobulin G.

This chapter investigates the use of MAPA as a hydrophobic comonomer in pH-responsive nanoscale hydrogels for intracellular delivery of siRNA. The aqueous solution properties, membrane-disruptive properties, cytocompatibility, and siRNA delivery efficiency are evaluated. Where relevant, the in vitro and physicochemical properties are compared to the unmodified P(DEAEMA-g-PEGMA), PDET, or the best-performing P(DEAEMA-co-TBMA-g-PEGMA) analogue, PDETB30.

8.2. Materials and Methods

8.2.1. Materials

L-phenylalanine methyl ester hydrochloride, anhydrous triethylamine, methacryloyl chloride, hexanes, 2-(diethylamino) ethyl methacrylate (DEAEMA), Tetra(ethylene glycol) dimethacrylate (TEGDMA), Poly(ethylene glycol) methyl ether methacrylate (PEGMA), Mn ~ 2080 – 50 wt% solution in H2O, myristyltrimethyl ammonium bromide (MyTAB) and diethylpyrocarbonate (DEPC) were purchased from Sigma-Aldrich (St. Louis, MO). Irgacure 2959 was donated by Ceiba Geigy (Tarrytown, NY).

Sodium hydroxide solution (NaOH, 1N), hydrochloric acid solution (HCl, 1N), methylene chloride, basic alumina – 300 mesh, sodium chloride (NaCl), disodium phosphate heptahydrate (Na2HPO4 • 7H2O) sodium phosphate monohydrate (NaH2PO4 • H2O), sodium azide (N_3Na), and Thermo Scientific HyClone USDA Tested Fetal Bovine Serum (FBS) were purchased from Fisher Chemical (South Plainfield, NJ). Brij-30 was purchased from Acros Organics (Fair Lawn, NJ).

Dulbecco's Modified Eagles Medium (DMEM) with 4500 mg L^{-1} glucose and sodium bicarbonate, without L-glutamine and sodium pyruvate, were obtained from Sigma-Aldrich (St. Louis, MO). Phosphate buffered saline (PBS) without calcium and magnesium and 200 mM L-glutamine solution were purchased from MediaTech (Manassas, VA). CellTiter 96® AQueous Non-Radioactive Cell Proliferation Assay (MTS) was purchased from Promega (Madison, WI). Cell scrapers for RAW264.7 cells were purchased from BD Falcon (Franklin Lakes, NJ). Propidium Iodide (PI), 1 mg mL^{-1} solution in water and RNAse Free water were purchased from Life Technologies (Grand Island, NY).

Unless otherwise specified, the water used in these experiments was purified by a Millipore Milli-Q Plus to a volume resistivity of 18.2 MΩ•cm.

8.2.2. MAPA synthesis and purification

The synthesis scheme was adapted from previous reports [9, 10] and the reaction was conducted as follows: The reactive free base of L-phenylalanine methyl ester hydrochloride was extracted by dissolving the solid L-phenylalanine methyl ester hydrochloride in 1 N NaOH and extracting with methylene chloride. The resulting solution was chilled to 0°C and 2 molar equivalents anhydrous triethylamine were added. Methacryloyl chloride was added dropwise to the mixing solution under nitrogen. The purge continued with stirring for 4 hours, after which the reaction mixture was sealed and allowed to react overnight at room temperature. The reaction mixture was purified by successive equivolume washes of 1 N HCl, saturated $NaHCO_3$, and saturated NaCl. The organic phase was concentrated using rotary evaporation and purified using a Companion

Automated Flash Chromatography Instrument (Teledyne-Isco, Lincoln, NE) equipped with a 100 g silica column. Column was equilibrated with 500 ml hexanes, purification run length was set to 50 min with a solvent flow rate of 35 ml min-1. The solvent gradient was established as follows: Solvent A – hexanes, Solvent B - ethyl acetate. The gradient was adjusted from 0 – 40% B over 25 minutes and held for 10 minutes, then 40% - 100% B over 10 minutes. Fractions of interest were determined by monitoring absorbance at 258 nm. The fractions were pooled and concentrated by rotary evaporation to yield a viscous, clear liquid. Subsequent drying in a vacuum oven produced a crystalline, white powder of N-methacryloyl L-phenylalanine methyl ester (MAPA). The chemical structure and molecular weight were verified using ^{1}H-NMR and Mass Spectrometry, respectively.

8.2.3. Polymer synthesis

Hydrogel particles of nanoscale dimensions were synthesized via UV-initiated free radical photoemulsion polymerization/crosslinking according to previous reports from our laboratory [11-13]. Briefly, DEAEMA and TEGDMA were passed through a column of basic alumina powder to remove inhibitor prior to use. MAPA was synthesized as described. Poly(ethylene glycol) methyl ether methacrylate (PEGMA), Mn ~ 2080 was used as received. DEAMA, TEGDMA, and MAPA were added to an aqueous solution containing 5 wt% PEGMA, Irgacure 2959 at 0.5 wt% of total monomer, 4 mg mL^{-1} Brij-30 and ionic surfactant MyTAB. The mixture was emulsified using a Misonix Ultrasonicator (Misonix, Inc., Newtown, CT). The emulsion was purged with nitrogen gas and exposed to a UV source for 2.5 hr with constant stirring.

8.2.4. Polymer purification

During the initial stages of purification, we attempted the previously described polyelectrolyte-ionomer purification method [11, 13]. However, the initial polymer-ionomer collapse and centrifugation of the reaction mixture resulted in a highly turbid, acetone-rich supernatant. After decanting the supernatant, the amount of remaining flocculated ionomer was uncharacteristically low and did not resuspend well in 0.5 N HCl. Thus, further purification efforts focused on the turbid supernatants from purification cycles 1 and 2. These fractions were pooled and cooled to -80°C in 50 ml centrifuge tubes. Following 24 h at -80°C, the supernatant stratified into a clear acetone-rich phase and semi-solid, turbid aqueous phase. The organic phase was carefully decanted and the remaining aqueous layer was again frozen at -80°C for 24 h. Following additional decanting of the organic phase, the aqueous layer was transferred to 12 – 14 kDa MWCO Regenerated Cellulose Dialysis tubing (Spectrum Labs, Rancho Dominguez, CA). Polymer particles were dialyzed against ultrapure water for 7 days with the water changed twice daily. Following dialysis, polymers were flash frozen in liquid N_2 and lyophilized for 5 days.

8.2.5. ^{1}H-NMR spectroscopy

The composition of crosslinked PDETM30 was investigated using a Varian (Palo Alto, CA) DirectDrive 400 MHz nuclear magnetic resonance spectrometer equipped with automatic sampler. Deuterium oxide (D2O, 99.9%) was obtained from Cambridge Isotope Laboratories (Andover, MA). Deuterium chloride (DCl, 100.0%) was obtained from Acros Organics (Fairlawn, NJ). All glassware, including NMR Tubes (Wilmad Lab

Glass, Vineland, NJ), 2 mL sample vials, and Pasteur pipettes were dried overnight in a vacuum oven. Polymer samples of approximately 40 mg were weighed directly in sample vials and D_2O was added to bring the final polymer concentration to 20 mg mL^{-1}. Samples were briefly sonicated in a sonic bath and transferred to NMR tubes for subsequent analysis. All NMR Spectra were analyzed using SpinWorks 3™ software.

8.2.6. Dynamic light scattering analysis

Measurements of the z-average particle size were collected at 25°C using a Malvern Zetasizer NanoZS (Malvern Instruments Corp., Malvern, UK) operating with a 633 nm laser source equipped with MPT-2 Autotitrator. DLS measurements of particle size and pH-responsive behavior were conducted by resuspending lyophilized particles in PBS at 0.5 mg mL^{-1}. The suspension pH was adjusted to 10.5 using 1 N NaOH and gradually lowered to pH 3.5 using 1 N HCl. Measurements of the z-average particle size were collected at 25°C and pH intervals of 0.5.

8.2.7. Transmission electron microscopy

Transmission electron micrographs were collected using a FEI Tecnai (Hillsboro, OR) Transmission Electron Microscope (80 kV) at magnifications from 16,500× to 160,000×. Lyophilized particles were diluted in ddH_2O and stained with 2% uranyl acetate immediately prior to imaging. Typically, 5 μL of 0.02 w/v% of particle suspension was dropped onto a 400-mesh Formvar-coated copper TEM grid (Electron Microscopy Sciences, Hatfield, PA) and excess liquid wicked off using filter paper. An equivalent volume of 2 w/v% uranyl acetate was then added to the grid and allowed to

stain for 60 seconds before excess liquid was wicked away with filter paper. Particle volume in the dry state was taken as the cube of mean diameter from TEM images. Particle diameters were calculated from the particle area as determined by an ImageJ particle sizing algorithm. Reported values represent the mean ± standard deviation ($n > 50$).

8.2.8. Electrophoretic light scattering

Measurements of the effective surface charge were collected 25°C using a Malvern Zetasizer NanoZS (Malvern Instruments Corp., Malvern, UK) operating with a 633 nm laser source equipped with MPT-2 Autotitrator. Measurements of ζ-potential as a function of pH were conducted by resuspending lyophilized particles in 5 mM phosphate buffer at 0.5 mg mL^{-1}. The suspension pH was adjusted to 10.5 using 1 N NaOH and gradually lowered to pH 3.5 using 1 N HCl. Electrophoretic light scattering measurements of the surface ζ-potential were collected at 25°C with nanogels suspended in 5 mM sodium phosphate.

8.2.9. Hemolysis assays

Sheep blood in sodium citrate was obtained from Hemostat Laboratories (Dixon , CA) and used for up to two weeks after receipt. Phosphate buffers (0.15 M) from pH 5.0 – 8.0 were prepared by dissolving predetermined amounts of monosodium phosphate and disodium phosphate in ultrapure DI water. The buffer pH was adjusted as needed using 1 N HCl or 1 N NaOH. Dry nanoscale hydrogels were suspended in 150 mM phosphate buffer at the desired pH at a concentration of 2.5 mg ml^{-1} and allowed to equilibrate

overnight. Erythrocytes were isolated from whole sheep blood by 3 successive washes with freshly prepared 150 mM NaCl. Red blood cells (RBCs) were separated by centrifugation from 10 minutes at 2,000×g. The supernatant and remaining buffy coat were carefully aspirated and discarded. After removing the supernatant following the final wash, RBCs were suspended in a volume of 150 mM phosphate buffer identical to that of the original blood aliquot at the pH matching that of the suspended polymers. This solution was diluted 10-fold in 150 mM phosphate buffer to yield an RBC suspension of approximately 5×10^8 cells/mL. In a typical experiment, 1×10^8 RBCs were exposed to polymer concentrations from 1 μg mL^{-1} – 2 mg mL^{-1} while shaking in a bead bath (LabArmor, Cornelius, OR) pre-equilibrated at 37°C. Following a 60 min incubation period, samples were centrifuged at 14,500 RPM for 5 min to separate cells and membrane fragments. An aliquot of each sample was transferred to a clear 96-well plate and hemoglobin absorbance was measured at 541 nm. Negative controls (0% lysis) consisted of 150 mM phosphate buffer at experimental pH and positive controls (100% lysis) consisted of RBCs incubated in ultrapure DI water.

8.2.10. Cell Culture

Human colorectal adenocarcinoma cells (Caco-2) and murine macrophages (RAW 264.7) were maintained in Dulbecco's Modified Eagles Medium (DMEM) supplemented with 100 U mL^{-1} penicillin, 100 μg mL^{-1} streptomycin, and 10% fetal bovine serum (FBS) (Complete DMEM). Caco-2 cells were used between passage 34 and 62. RAW 264.7 cells were used between passage 9 and 17. Caco-2 cells were passaged by washing with pre-warmed Dulbecco's phosphate buffered saline (DPBS) and

subsequent incubation with 0.25% Trypsin-EDTA at 37°C. Trypsin was neutralized by addition of fresh, prewarmed DMEM and cells were separated by centrifugation. The resulting pellet was suspended in 10 mL DMEM and cell count was determined using a Scepter Automated Cell Counter (Millipore, Billerica, MA) with 60 μm tips. The cell suspension was diluted as necessary and added to tissue-culture treated flasks or multi-well plates. Caco-2 cells were typically passaged at 1:5 ratio with media replenished every 2-3 days. RAW 264.7 cells were passaged by washing with prewarmed DPBS and replacing the original culture volume with fresh DMEM. Cells were removed from the flask surface by gentle scraping with a 25 cm cell scraper. The number of suspended cells was counted using a Scepter Automated Cell Counter and diluted as necessary for addition to tissue culture flasks or multi-well plates. RAW 264.7 cells were typically passaged every 2 days.

8.2.11. Cytocompatibility Studies

In vitro cytocompatibility was determined for polycationic nanoscale hydrogel networks using commercially available cytotoxicity assays. MTS assays were performed using the CellTiter 96 AQueous One Solution Cell Proliferation Assay kit in which the soluble tetrazolium salt [3-[4,5-dimethylthiazol-2-yl]-5-(3-carboxymethoxyphenyl)-2-(4-sulfophenyl)-2H-tetrazolium] (MTS) is reduced to a purple formazan product. The absorbance of the formazan product is proportional to the number of viable cells. Stock solutions of polymer were suspended in PBS and allowed to equilibrate overnight. Caco-2 cells were seeded in 96-well plates at 10,000 cells/well and incubated for 36 hours prior in 200 μL DMEM. RAW 264.7 cells were seeded in 96-well plates at 10,000 cells/well

and incubated for 36 hours prior to assay in 200 μL DMEM. Media was aspirated and cells were washed 1× with DPBS and incubated in 160 μL serum-free DMEM for 30 minutes. Following this incubation period, polymer stock solutions at 5× were added to cells for designated exposure times.

Following the exposure period (90 min or 360 min), media and polymer were aspirated and replaced with a DMEM/MTS solution. Absorbance at 490 nm was recorded after 4 hours or 90 min incubation in the DMEM/MTS solution for Caco-2 and RAW, respectively.

8.2.12. siRNA Complexation

RNA complexation buffer was prepared by dissolving 3.15 g sodium phosphate dibasic heptahydrate, 0.02 g potassium phosphate monobasic monohydrate, 0.20 g potassium chloride , and 8.01 g sodium chloride in Milli-Q purified water. Following salt dissolution, the solution pH was adjusted to pH 5.50 using 1 N HCl and ultrapure water was added to bring the final solution volume to 100 mL. To remove nucleases, diethylpyrocarbonate (DEPC) was added at 0.1% and incubated at room temperature overnight. The buffer solution was then autoclaved to remove DEPC. Polymer-siRNA complexes were formed by combining aqueous solutions of PDETM30, siRNA, 10x RNAse-free PBS, and RNAse-free water to obtain desired concentrations. Typically, complexation was allowed to commence for 60 min and polymer-siRNA were complexed at a 10:1 – 20:1 ratio (g polymer/g siRNA).

8.2.13. siRNA Internalization

DyLight 647-labeled small interfering RNA (Sense: DY647-UAAGGCUAUGAAGAGAUACUU) was purchased from Thermo Scientific (Lafayette, CO). (P(DEAEMA-co-MAPA-g-PEGMA) (PDETM30) was synthesized and purified as described in Section 8.2.4. Flow cytometry buffer was prepared by combining FBS, DPBS, and N_3Na to form 1% FBS and 0.1% N_3Na in DPBS.

Concentrated suspensions (20×) of PDETM30, PDETM30/DY647-siRNA, or DY647-siRNAwere prepared to contain 0.5 mg mL^{-1} PDETM30, 26.5 μg mL^{-1} (~2000 nM) DY647-siRNA, 1× complexation buffer, and RNAse free H_2O. Control samples (PDETM30 only, DY647-siRNA only) were prepared in a similar fashion, replacing the volume of the absent component(s) with RNAse free H_2O.

RAW 264.7 cells or Caco-2 cells were seeded at 1× 10^5 cells/well and allowed to grow to 80% confluence before exposure. Immediately prior to exposure to PDETM30/DY647-siRNA, cells were washed 1× with 2 mL DPBS and media was replaced with 1.9 mL serum-free DMEM. Concentrated suspensions of PDETM30, PDETM30/DY647-siRNA, or DY647-siRNA were added to wells in 100 μL increments and allowed to incubate with cells for 60 min in a 37°C, 5% CO_2 atmosphere. Following this incubation period, cells were rinsed 3× DPBS (with calcium and magnesium) and the media was replaced with 2 mL serum-free DMEM. Hoechst 33342 was added to each well for nuclear staining at a final concentration of 2.5 μg ml^{-1}. The nuclear staining process was completed for 30 min for RAW 264.7 cells and 45 min for Caco-2 cells at

37°C, 5% CO_2. Following Hoechst incubation, cells were rinsed 3× with DPBS (w/out calcium and magnesium).

RAW 264.7 cells were isolated by replacing the final DPBS wash with 1 mL flow cytometry buffer and gently scraping the cells. Cell suspensions from each well were transferred to microfuge tubes and centrifuged for 5 min at 500×g. The supernatant was discarded and cell pellet re-suspended in 100 µL flow cytometry buffer.

Caco-2 cells were isolated by replacing the final DPBS wash with 500 µL 0.25% trypsin-EDTA and incubating at 37°C, 5% CO_2 for 8 min. Trypsin was neutralized by adding 3 mL DMEM with 10% FBS and without phenol red. Cell suspensions were centrifuged for 5 min at 500×g. The supernatant was discarded and cell pellet re-suspended in 100 µL flow cytometry buffer. All cell suspensions were kept on ice until use. Propidium iodide (PI) was used as a live/dead discriminator and was added to cell suspensions immediately before analysis at a final concentration of 1 µg mL^{-1}.

Analysis of cellular internalization was conducted using an Amnis ImageStream (Seattle, WA) imaging flow cytometer equipped with lasers at 405 nm, 488 nm, 658 nm, and 785 nm. Fluorescent data were collected using Channel 1 (430 – 505 nm, Hoechst), Channel 4 (595 – 660 nm, PI), Channel 5 (660 – 745 nm, DY647), and Channel 6 (745 – 800 nm, side scatter). Cells were imaged with a 60× objective. Fluid velocity was set to a nominal value of 40 mm/sec. Fluorescent compensation matrices were constructed using Amnis IDEAS® software and verified manually for proper fit. At least 5,000 cells were collected for analysis. Dead cells (PI positive) were excluded from analysis. Out-of-focus cells were also excluded from further analysis by gating the Gradient RMS feature in IDEAS® software. This feature detects image sharpness by calculating large

changes in pixel values across the brightfield image. Typically, cells with Gradient RMS value <40 were considered out of focus.

8.3. RESULTS AND DISCUSSION

8.3.1. MAPA synthesis and purification

The acrylation of L-phenylalanine methyl ester (L-PhME) was performed according the to the reaction scheme in Figure 8.1. The methyl ester analogue of L-phenylalanine was chosen to avoid side reactions with unprotected carboxylate group of L-phenylalanine. Initially, the hydrochloride salt of L-PhME was added to cold (4°C) dichloromethane (DCM). However, after a short period of stirring, the entire mixture turned to a cloudy solid, likely due to chemical incompatibility between the DCM solvent and the salt form of L-PhME. To isolate the free base of L-PhME, approximately 200 mL of 1N NaOH was added to the solid organic mixture and agitated briefly. The entire mixture was transferred to a separatory funnel and inverted several times. After settling, the DCM phase was collected and saved (Extract fraction 1). The remaining basic aqueous fraction was washed twice more with approximately 65 mL of DCM (Extract fractions 2 and 3). A final organic wash with 65 mL DCM was accompanied by the addition of 9 g of NaCl to the basic aqueous phase (Extract fraction 4). Subsequent ^{1}H-NMR and thin layer chromatography (TLC) analysis revealed the vast majority of L-PhME partitioned into the organic phase during the first DCM wash (Extract fraction 1). The remaining extract fractions contained quantities of L-PhME barely perceptible by

^{1}H-NMR. Therefore, Extract fraction 1 was concentrated via rotary evaporation and used as described in Section 8.2.2. and Figure 8.1.

Following preliminary purification (described in Section 8.2.2 and concentration via partial rotary evaporation, the reaction product mixture consisted of a viscous liquid. Exhaustive rotary evaporation led to a crystallization of white solid on the flask walls. Thus, sufficient DCM was left in the flask to maintain the reaction product in solution. Column chromatography proceeded in 3 successive runs with approximately 1 mL of viscous reaction product added to the column per run. A sample chromatogram from the flash chromatography is shown in Figure 8.2.

The ^{1}H-NMR spectrum of the purified MAPA product is shown in Figure 8.3 and peak assignments and relative areas in Table 8.1. The peak areas match the expected proton ratios and the spectrum corresponds well with published reports [9, 10]. The high-resolution mass spectrum (Figure 8.4) also confirms successful synthesis and isolation of the intended product. The mass spectrum shows the presence of one peak at 248 Da, corresponding to the MZ+ fragment. The expected molecular weight of MAPA is 247 Da. The MAPA monomer exhibits long-term stability when stored dry at 4°C. Additional mass spectroscopy studies revealed no loss of structural fidelity following 18 months of storage under these conditions (data not shown).

8.3.2. Polymer synthesis and purification

The nanogel purification process employed in this study is distinctly different than our previous reports. In contrast to all other previous formulations, the P(DEAEMA-co-MAPA-g-PEGMA) (PDETM30) nanogels did not flocculate or sediment

following the acetone-induced polyelectrolyte-polymer transition[6] (described in Chapter 4). Rather, the supernatant from purification cycle 1 was a milky, slightly translucent solution. The centrifuged pellet, normally a white mass, was much smaller and less densely packed than typically observed. The supernatants from all tubes were then pooled and placed in a -80°C freezer to undergo fractional freezing purification. After 24 hours, the supernatants had phase-separated into a clear, acetone-rich organic phase, a hazy interface layer, and a white, quasi-solid, water-rich aqueous phase. The organic layer, and any dissolved unreacted monomers or surfactant unimers, was carefully decanted and discarded. The remaining quasi-solid thawed to a turbid, white liquid solution within minutes, suggesting a low freezing temperature and considerable acetone content. This solution was subjected to another round of fractional freezing with similar phase separation observed after 24 h at -80°C. Following removal of the clear, acetone-rich phase, the turbid aqueous fraction dialyzed extensively to remove acetone, unreacted monomers, and surfactants.

8.3.3. ^{1}H-NMR spectroscopy

The proton NMR spectrum (Figure 8.6) corresponds well with the ^{1}H-NMR spectra of crosslinked P(DEAEMA-co-BMA-g-PEGMA) in D_2O as seen in Chapter 4, Figure 4.7. The oxyethylene protons (-O-C$\boldsymbol{H_2}$-C$\boldsymbol{H_2}$-) from grafted PEGMA are evident in a strong peak at δ = 3.6 ppm and the terminal methoxy protons (-O-C$\boldsymbol{H}_3$) from grafted PEGMA are visible at δ = 3.3 ppm. The inset spectra also confirm the presence of MAPA and DEAEMA functional groups in the polymer. The left inset shows the

[6] Described in Chapter 4, Section 4.3.2.

aromatic protons from MAPA at δ = 7.2 – 7.4 ppm. The right inset shows the ethylamino (-CH_2-C***H***$_3$)$_2$ protons from DEAEMA at approximately δ = 1.25 ppm.

Identification of residual surfactant is somewhat problematic in the spectra of this crosslinked polymer nanogel. The primary surfactant used during synthesis, Brij-30, displays prominent peaks in chemical shift regions near or overlapping with the PEGMA (δ ~ 3.6 ppm) or DEAEMA (δ ~ 1.2 ppm) peaks. Other minor peaks exist in the ^{1}H-NMR spectra of Brij-30, such as that of the etheric protons bridging the tetraethylene glycol portion and dodecane portion of Brij-30 (-O-C***H***$_2$-C***H***$_2$-$C_{10}H_{21}$). These protons are visible at δ = 3.445 ppm and δ = 1.58 ppm in $CDCl_3$. No distinct peaks are observed near these chemical shifts in Figure 8.6. Also, the terminal hydroxyl group of Brij-30 demonstrates a chemical shift of δ ~ 2.8 ppm in organic solvents like $CDCl_3$. However, this peak is not expected to appear in D_2O due to the rapid exchange rate with surrounding hydrogen or deuterium. In practice, the ^{1}H-NMR spectra of neat solutions of Brij-30 result in sharp, well-defined peaks at the expected chemical shift. The spectrum in Figure 8.6 does not contain any such peaks and those present near δ = 3.6 ppm and δ = 1.2 ppm are characteristically broad, in accordance with the previous work (Chapter 4, Section 4.3.3) of polymer NMR. From these observations, it appears the fractional freezing and dialysis purification was sufficient to remove Brij-30 from PDETM30.

A conclusive determination about the presence or absence of MyTAB was also problematic. In part, the polyelectrolyte-ionomer flocculation and sedimentation was designed to expel the cationic surfactant MyTAB through electrostatic repulsion. As this formulation did not undergo the polyelectrolyte-ionomer purification, the presence of residual MyTAB may be expected. A small, sharp peak around δ = 3.1 ppm may

correspond to the methyl protons on the quarternized amino group of MyTAB. ^{1}H-NMR analysis of neat MyTAB in DMSO-d_6 reveals strong peaks near δ = 3.08 ppm (9 protons) and δ = 1.28 ppm (24 protons).

Compared to the area of the PEGMA methoxy protons (Peak *c*, Figure 8.6), the peak at δ = 3.1 ppm has relative molar ratio between these two groups can be estimated by:

$$\frac{n_{MyTAB}}{n_{PEGMA}} = \frac{A_{MyTAB,3.1}/9}{A_{PEGMA,3.3}/3} \quad \textbf{(8.1)}$$

where $A_{MyTAB,3.1}$ is the integrated area of the putative methyl protons adjacent to the quarternized amine of MyTAB, 9 is the number of equivalent protons associated with this peak, $A_{PEGMA3.3}$ is the integrated area of the terminal methoxy group of PEGMA, and 3 is the number of equivalent protons. Thus, the estimated molar ratio of MyTAB to PEGMA is 0.061. Considering the nanogels are approximately 0.5 mol% PEGMA (according to Table 4.4), the approximate molar ratio of MyTAB to PDETM30 is ~3 × 10^{-4}. This suggests that MyTAB, if present, is present only in a very small proportion.

8.3.4. Dynamic light scattering analysis

Dynamic light scattering was used to study the physicochemical properties of the PDETM30 nanogels, including size, swelling ratio, and critical swelling pH. The hydrodynamic diameter and polydispersity index reported represent those determined by Cumulants analysis as outlined in ISO 13321 [14]. Figure 8.7 depicts representative intensity-weighted sized distributions of PDETM30 in the collapsed (pH 9) and swollen

(pH 6) state. The existence of a single population suggests that the Cumulants method is appropriate for this analysis.

The z-average diameter and polydispersity are plotted as a function of pH in Figure 8.8. The PDETM30 nanogels are significantly larger in aqueous suspension than analogous preparations with t-butyl methacrylate (TBMA)[7]. PDETM30 exhibits a collapsed diameter of approximately 150 nm. In contrast, PDETB30 exhibits a collapsed diameter of approximately 92 nm [13]. Upon exposure to increasingly acidic conditions, PDTEM30 undergoes a phase conformation from collapsed hydrophobe to swollen hydrophile. This phase conformation results in a distinct change in volumetric swelling, the magnitude of which is driven by a balance between the free energy of polymer-solvent interactions, osmotic pressure generated by mobile counterions inside the gel, and elastic contractile response to gel deformation [15].

The critical swelling pH was calculated according to Equations 4.2 and 4.3 and determined to be $pH_c = 7.00$. By comparison, the pH_c of PDET and PDETB30 were measured at 7.37 and 6.65, respectively. Prior studies have demonstrated that increased network hydrophobicity leads to a decrease in the pH_c [13, 16]. Therefore, the network hydrophobicity imparted by the MAPA comonomer is intermediate relative the PDET (no comonomer) and PDETB30 (TBMA comonomer). The breadth of the phase transition, simply the pH difference between swollen and collapsed states, is approximately 0.9 pH units. The breadth of the phase transitions for PDET and PDETB30 are approximately 0.65 and 1.56, respectively.

[7] The aqueous solution properties of P(DEAEMA-co-TBMA-g-PEGMA) nanogels are discussed in Chapter 4.

The polydispersity index (PdI), is given by a ratio of the second (μ_2) and first moment (Γ) of the Cumulants analysis (μ_2/Γ^2)[8] and describes the apparent width of the size distribution [14]. Typically, with PdI in this manner, a PdI of <0.05 is considered monodisperse and a PdI of >0.7 is considered polydisperse. The PDETM30 nanogels have a narrow size distribution in aqueous suspension; the PdI was estimated at 0.10 – 0.12 throughout the measurement. In contrast, nearly all other syntheses resulted in nanogels with PdI ~ 0.18 – 0.22.

8.3.5. Transmission electron microscopy

The dry diameter of PDETM30 nanogels was determined to be 47.9 ± 19.6 nm by transmission electron microscopy (TEM). The diameter was calculated by determining the particle area in ImageJ® and calculating the corresponding circular diameter. Images acquired at 26,500× and 43,000× were used to construct a number-average particle size distribution. Representative TEM micrographs are shown in Figure 8.9 and the calculated number-average particle size distribution in Figure 8.10. The TEM micrographs reveal circular particles, which corresponds to a roughly spherical morphology. Moreover, the dry particle mean size and size distribution correspond well with those determined for TBMA and TBAEMA nanogels in Chapter 4[9].

[8] See Appendix B: Practical Considerations in Light Scattering for a more detailed treatment of the Cumulants analysis.
[9] See Figure 4.9 for a representative number-average dry particle size distribution of PDETB30.

8.3.6. Electrophoretic light scattering

Measurements of the ζ-potential were performed to evaluate the colloidal stability and effective surface charge in response to dynamic pH. The ζ-potential of PDETM30 is compared to the TMBA analogue, PDETB30, in Figure 8.11. Similar to the other copolymer nanogels described in Chapter 4, Figure 4.13, PDETM30 possess a reversible surface charge and isoelectric point (IEP) ~ 7.67. The surface charge is slightly positive at physiological pH, ζ-potential ~ 1.22 mV. The maximum ζ-potential at pH 3.5 is approximately 16 mV. In contrast, the maximum ζ-potential for PDETB30 at pH 3.5 is approximately 28 mV. A potential reason for this disparity may be an increase in the PEG graft density on PDETM30 and therefore an increase in charge shielding by the PEG corona. Evidence from the ^{1}H-NMR spectra of crosslinked nanogels in DCl in Figure 4.7 and Figure 8.6 support this assertion. Comparing the relative areas between PEGMA protons and DEAEMA protons in a given copolymer gives a semi-quantitative estimate of the relative prevalence of PEGMA on the surface of the nanogel. This estimate, for the ratio of PDETM30 to PDETB30, yields a value of 4.45, suggesting that PDETM30 has a higher proportion of PEGMA to DEAEMA than does PDETB30. This method of estimation is only semi-quantitative, however, in that significant signal attenuation occurs in the ^{1}H-NMR analysis of crosslinked polymer networks. The nanogel interior, even in the swollen state, is a likely a highly viscous network of polymer chains. Therefore, this comparative method likely underestimates the DEAEMA content and overestimates the PEGMA content. There is also a possibility that PDETM30 contains identical PEGMA content to PDETB30 and simply a lower molar

proportion of DEAEMA. This result is not likely, given the nature and extent of the pH-responsive transition observed by DLS in Figure 8.8. Further investigations to quantify the ionizable amine content via acid titration are currently underway to more conclusively address this question.

8.3.7. Hemolysis assays

The membrane-disruptive properties of PDETM30 were investigated using the hemolysis assay described in Chapter 5. These studies serve to provide insight on the combinations of pH values and concentrations at which the nanogels are most able to destabilize lipid bilayers. These studies are shown to be a rapid screen to approximate endosomolytic ability of synthetic polymer for intracellular drug delivery [17, 18].

The pH values tested in this analysis range from pH 5.0 – pH 8.0; experiments performed at pH 5.00, 5.50, 6.00, 6.50, 7.00, 7.20, 7.40, 7.60, 7.80, and 8.00. The concentrations tested range from 1 – 100 μg ml^{-1}; with experiments performed with 100, 50, 25, 10, 5, 2.5, and 1 μg ml^{-1} PDET, PDETM30 or PDETB30 suspended in 150 mM phosphate buffer at the specified pH.

The pH- and concentration-dependent hemolysis was determined according to Equation 8.2:

$$\%\,\boldsymbol{Hemolyis} = \frac{A_{sample} - A_{blank}}{A_{max} - A_{blank}} \tag{8.2}$$

Where A_{sample} represents RBCs exposed to polymer at a given pH and concentration, A_{blank} is the absorbance of the supernatant after RBC exposure to phosphate buffer at a given pH, and A_{max} represents maximum lysis following RBC exposure to DI water.

The hemolytic ranges of PDET, PDETM30, and PDETB30 are shown on the contour plots in Figure 8.12 and arranged in order of membrane-disruptive ability. There is a clear dependence of polymer composition on the ability to destabilize erythrocyte membranes. The trends for membrane destabilization mirror those observed in DLS analysis. In Section 8.3.4., the pH_c values for these three copolymer formulations are 7.37 for PDET, 7.00 for PDETM30., and 6.65 for PDETB30. Moreover, the values for transition breadth ($pH_{swollen} - pH_{collapsed}$) are 0.65 for PDET, 0.9 for PDETM30, and 1.45 for PDETB30.

Notably, the pH range for maximum hemolysis follows a similar trend. PDET displays maximum hemolysis around pH 7.4 – 7.6; conditions that correspond to its determined pH_c. Similarly, PDETM displays maximum hemolysis around pH 6.5 – 7.2 and PDETB30 displays maximum hemolysis around pH 6.0 – pH 7.0. These data suggest that the phase transition is critically important to modulate membrane-disruptive behavior. At pH values above the phase-transition, the collapsed nanogel may be well protected by PEG grafts and may not have sufficient exposed surface area to interact with, and destabilize, lipid bilayers. At pH values well below the phase transition, the swollen nanogel may be sufficiently ionized to mitigate any hydrophobic interactions between the exposed nanogel surface and the lipid bilayer of erythrocyte membranes. In the transition region, the partially-swollen nanogel may contain a heterogeneous mixture of ionized and hydrophobic segments. The partial ionization will permit osmotic swelling and the surface area of each nanogel will increase by a factor proportional to $d^2_{swollen}/d^2_{collapsed}$. This leads to a concomitant decrease in the surface PEG graft density and may permit increased hydrophobic association between the nanogel surface and lipid

bilayers. The analysis of pyrene emission in Chapter 5 provides additional support for relationship between nanogel hydrophobicity and membrane-disruptive activity.

A comparative hemolysis profile for PDETB30 and PDETM30 is shown in Figure 8.13. These data show the pH-dependent hemolysis at a single nanogel concentration (50 μg ml^{-1}). In practice, nanogels concentrations of 5 – 50 μg ml^{-1} were used in transfection experiments. As seen in this comparison, PDETM30 is substantially less effective at erythrocyte disruption in the pH range (pH 5.50 – 6.50) expected in early endosomes. While PDETB30 demonstrates nearly 100% hemolysis at pH 6.50 and pH 6.00, PDETM30 demonstrates 32% and 20%, respectively. However, PDETM30 is relatively non-disruptive (~8% hemolysis) at physiological pH where PDETB30 demonstrates ~60% hemolysis at pH 7.4. This suggests that while PDETM30 is not as potent as the TMBA analogue PDETB30, it may have some utility in intracellular delivery applications, particularly as a mild membrane-destabilizing agent.

8.3.8. Cytocompatibility

The influence of polymer composition on cytotoxicity was examined in Chapter 5. In this work, the polymer toxicity was inversely related to the ionizable amine content (i.e. nanogels containing less DEAEMA were less cytotoxic under tested conditions). The LD_{50}, or polymer dose that results 50% reduction in cellular metabolic activity, was estimated by fitting cytotoxicity data with a four parameter Hill model of the form:

$$y = y_0 + \frac{a \cdot x^b}{c^b + x^b} \tag{8.2}$$

Where y is the measured cellular proliferation (relative to untreated cells), y_0 is the background signal or lower asymptote, $a - y_0$ is the range for the fit, b is the slope of the response curve, and x is the polymer concentration (mg mL^{-1}) to which the cells were exposed for designated time points. This model is a typical dose-response curve commonly employed to model ligand-receptor binding and drug concentration-effects [19].

Based on the data presented in Chapter 5 and the aqueous solution properties of PDETM30 discussed heretofore in this Chapter, it is expected that PDETM30 will exhibit cytotoxicity at intermediate levels relative to P(DEAEMA-g-PEGMA) (PDET) and P(DEAEMA-co-TMBA-g-PEGMA) (PDETB30).

8.3.8.1. Caco-2 Cells

PDETM30 demonstrates both time- and concentration-dependent toxicity, as shown in Figure 8.14. Exposure times of 90 minutes and 360 minutes were chosen to as liberal and conservative approximations for the mean intestinal transport time, estimated to be approximately 3 – 4 h in humans [20]. According to the MTS assay, PDETM30 caused no decrease in cellular proliferation (relative to untreated control) in Caco-2 cells at concentrations up to 0.25 μg mL^{-1} for 90 min exposure or 0.10 mg mL^{-1} for 360 min exposure. The calculated LD_{50} values for PDETM30 and Caco-2 cells are 1.18 mg mL^{-1} for 90 min exposure and 0.43 mg mL^{-1} for 360 min exposure.

PDETM30 displays comparable toxicity to PDETB30 and improved toxicity relative to PDET (Figure 8.15). The similarity in toxicity profile of PDETM30 and PDETB30 can be seen in Figure 8.15 for 90 min exposure and Figure 8.16 for 360 min

exposure. This result is expected based on the previous relationships between polymer composition, aqueous solution properties, and cytotoxicity developed in Chapter 5. Below concentrations of 0.25 mg mL^{-1}, both PDETM30 and PDETB30 display negligible toxicity. In fact, these nanogels appear to exert a stimulatory effect on the metabolic activity of Caco-2 cells under the test conditions. As expected from the ionizable amine density, PDET is considerably more toxic than the hydrophobically-modified nanogels PDETB30 and PDETM30.

8.3.8.2. RAW 264.7 Cells

Similar the observations in Chapter 5, RAW 264.7 cells were categorically more sensitive to the presence of nanogels than were Caco-2 cells. The LD_{50} for PDETM30 was estimated to be 0.27 mg mL^{-1} for 90 min exposure and 0.14 mg mL^{-1} for 360 min exposure (Figure 8.17). The nature of this increase in toxicity can be ascribed to the phagocytic activity of the RAW macrophages. Whereas nanogels will be internalized through nonspecific uptake pathways in Caco-2 cells, there will be additional uptake from phagocytosis in RAW 264.7 cells. In all further studies examining cellular internalization of DY647-siRNA/PDETM30 complexes, PDETM30 was used at a concentration (0.025 mg mL^{-1}) well below the toxic thresholds for Caco-2 and RAW 264.7 cells.

8.3.9. siRNA Internalization

Imaging flow cytometry was used to assess the ability of PDETM30 to facilitate the delivery of siRNA to model cell lines. This technique offers a powerful combination

of qualitative visual evidence and quantitative statistical counting. In this analysis of siRNA internalization, imaging flow cytometry was used to investigate the proportion of siRNA positive cells and the relative quantity of siRNA uptake by comparing fluorescent intensity between DY647-siRNA/PDETM30-treated and untreated samples. Moreover, detailed image analysis comparing thousands of combined fluorescent and brightfield images permitted the assessment of cellular internalization (vs. surface adsorption) and intracellular texture.

As seen in the micrographs in Figure 8.18, PDETM30 enables the cytoplasmic delivery of DY647-siRNA to RAW 264.7 cells. Cell nuclei are shown in blue (Hoechst) and siRNA in red (DY647). Panels A - C show representative images of cells exposed 25 $\mu g\ mL^{-1}$ PDETM30 and 100 nM DY647-siRNA for 60 minutes. Panels D - F show representative images of cells exposed only to 100 nM DY647-siRNA for 60 min. As expected due to its high MW (~13 kDa) and negative charge, little to no internalization was observed by the naked siRNA. Following complexation with PDEM30, the siRNA internalization increased substantially. Similar observations were made for Caco-2 cells exposed to PDETM30/DY647-siRNA or DY647-siRNA under identical conditions (Figure 8.19).

Figure 8.20 shows the total number (and proportion) of siRNA positive cells relative to untreated control. Cells were deemed siRNA positive by gating the entire Channel 5 (Em: 660 – 745 nm, DY647) fluorescent intensity histogram of an untreated control sample. Cells in this range of fluorescent intensity were considered siRNA negative. Cells with fluorescent intensity greater than this gated region were considered siRNA positive. As seen in Figure 8.20, PDETM30 enables siRNA internalization in

nearly 100% of RAW 264.7 cells (Panel A) and approximately 93% of Caco-2 cells (Panel B). As previously mentioned in Section 8.2.13., only live cells with suitable brightfield focus were analyzed. This rapid and ubiquitous internalization is encouraging, particularly in the absence of any dedicated targeting ligands to promote internalization.

The fluorescent intensity histograms in Figure 8.21 reveal that PDETM30 drastically increases the fluorescent signal of DY647-siRNA. These histograms compare populations exposed to DY647-siRNA alone (blue) or PDETM30/DY647-siRNA (red). In accordance with Figure 8.20, these observations are consistent in both RAW 264.7 cells (Figure 8.21, Panel A) and Caco-2 cells (Figure 8.21, Panel B). The similarity in median fluorescence intensity between RAW 264.7 cells (~33,000) and Caco-2 cells (~30,000) suggests that phagocytosis, a mechanism of internalization in the RAW macrophages, does not account for a significant fraction of the internalized siRNA.

A major advantage of imaging flow cytometry is the ability to distinguish between intracellular and surface localization of fluorescent probes. Extensive rinsing of cells with PBS is typically employed prior to conventional flow cytometry; generally this is sufficient for the putative removal of surface-adsorbed ligands. In this analysis, the brightfield cell image and fluorescent siRNA image were compared to determine the extent of internalization, or internalization coefficient. This parameter is defined by the ratio of intensity inside the cell to the intensity of the entire cell, where inside the cell and entire cell are defined by masks created in the brightfield channel. Positive values for the internalization coefficient signify intracellular localization, while negative values signify membrane localization. Values near zero signify a mix of these two staining patterns.

As seen in Figure 8.22, the median internalization coefficient is positive for both RAW 264.7 cells (Panel A) and Caco-2 cells (Panel B), indicating that PDETM30 facilitates intracellular delivery of DY647-siRNA to these two cell types. A similar analysis examined the colocalization of DY647-siRNA and cell nuclei stained with Hoechst 33342. As expected, there was no evidence for nuclear localization of DY647-siRNA.

Figure 8.23 illustrates the distribution in intracellular spots of siRNA in RAW 264.7 cells and Caco-2 cells. Punctate staining patterns are typically associated with vesicular entrapment of fluorescently labeled molecules. A spot counting algorithm in IDEAS® software was used to determine the number of punctate spots in each live, focused cell. The spot mask was established to identify bright spots 3 – 2000 pixels in area. With a 60× objective, each pixel corresponds to 0.3 μm × 0.3 μm. Therefore, the mask was able to identify punctate spots of approximately 0.58 μm – 4.78 μm in diameter. Mature late endosomes have a diameter of 0.25 – 1 μm [21] and lysosomal compartments can range from 0.5 nm – 1.5 μnm [22]. Thus, this method will not accurately account for all endolysosomal entrapment but can theoretically detect vesicular entrapment in some late endosomes and most lysosomes.

The spot count distributions in Figure 8.23 suggest a diffuse staining pattern (few spots) of DY647-siRNA fluorescence rather than a punctate staining pattern (many spots). These distributions are in good agreement with the micrographs from Figure 8.18 and Figure 8.19, which show few distinct spots in the intracellular siRNA fluorescence. Given that over 90% of RAW 264.7 cells and Caco-2 cells contain detectable DY647-siRNA fluorescence, the lack of spots cannot be simply ascribed to a lack of

internalization. These data suggest that PDETM30 is an efficient vehicle for enabling internalization and endosomal escape of siRNA.

8.4. CONCLUSIONS

A reactive phenylalanine derivative, N-methacryloyl L-phenylalanine methyl ester (MAPA) was successfully synthesized in order to modulate hydrophobicity and physicochemical properties of pH-responsive nanogels. The structure and molecular weight of the intended MAPA product were verified via ^{1}H-NMR and mass spectroscopy, respectively. The MAPA monomer was used in a photoemulsion polymerization to create P(DEAEMA-co-MAPA-g-PEGMA) nanogels. These responsive polymer networks have a roughly spherical morphology and dry diameter of approximately 47 nm, as determined by TEM. These nanogels exhibit a volume phase transition from collapsed hydrophobe to swollen hydrophile around pH 7.0, as determined by DLS. DLS measurements also indicate a relatively narrow distribution of particle sizes with a z-average diameter of approximately 150 nm.

In many of the in vitro assays, PDETM30 displayed intermediate performance relative to unmodified nanogel PDET and the best performing TBMA-modified nanogel PDETB30. For comparison, relevant physical and in vitro properties of PDETM30 and PDETB30 are summarized in Table 8.2 and Table 8.3. In studies of membrane destabilization using sheep erythrocytes, PDETM30 was most disruptive at pH values proximal to its critical pH for phase transition. Relative to the PDET nanogels, PDETM30 was a more potent agent for membrane destabilization but was less effective than PDETB30. Similarly, PDETM30 demonstrates improved cytocompatibility relative

to PDET and comparable cytocompatibility to PDETB30. Moreover, PDETM30 displays no overt toxicity to Caco-2 cells or RAW 264.7 cells at conventional transfection concentrations (< 50 μg ml^{-1}) for up to 6 h exposure.

Analysis of cellular internalization demonstrated rapid and ubiquitous uptake of the DY647-siRNA; over 90% of live cells contained siRNA after only 60 min of exposure. Image analysis of the RAW 264.7 cells and Caco-2 cells indicates a predominately diffuse staining pattern in the cells, suggesting endosomal escape by the siRNA cargo.

From these data, it is clear that inclusion of the MAPA comonomer improves in vitro performance characteristics (lower pH_c, greater hemolysis, improved cytocompatibility) relative to the unmodified PDET. Despite decreased performance characteristics relative to PDETB30 (higher pHc, lower hemolysis, comparable cytocompatibility), PDETM30 facilitates efficient intracellular delivery of siRNA. Ongoing studies are evaluating the knockdown efficiency of siRNA delivered via PDETM30.

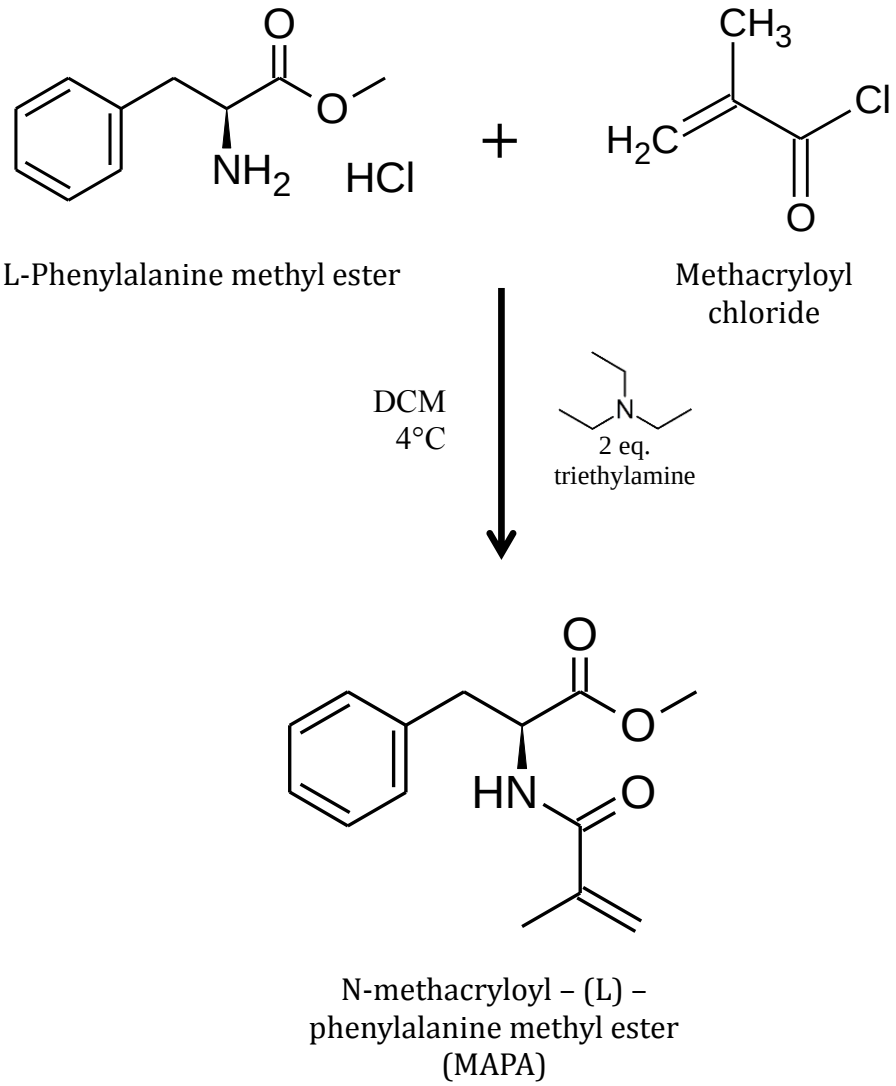

Figure 8.1 - Reaction scheme for N-methacryloyl L-phenylalanine methyl ester (MAPA) monomer

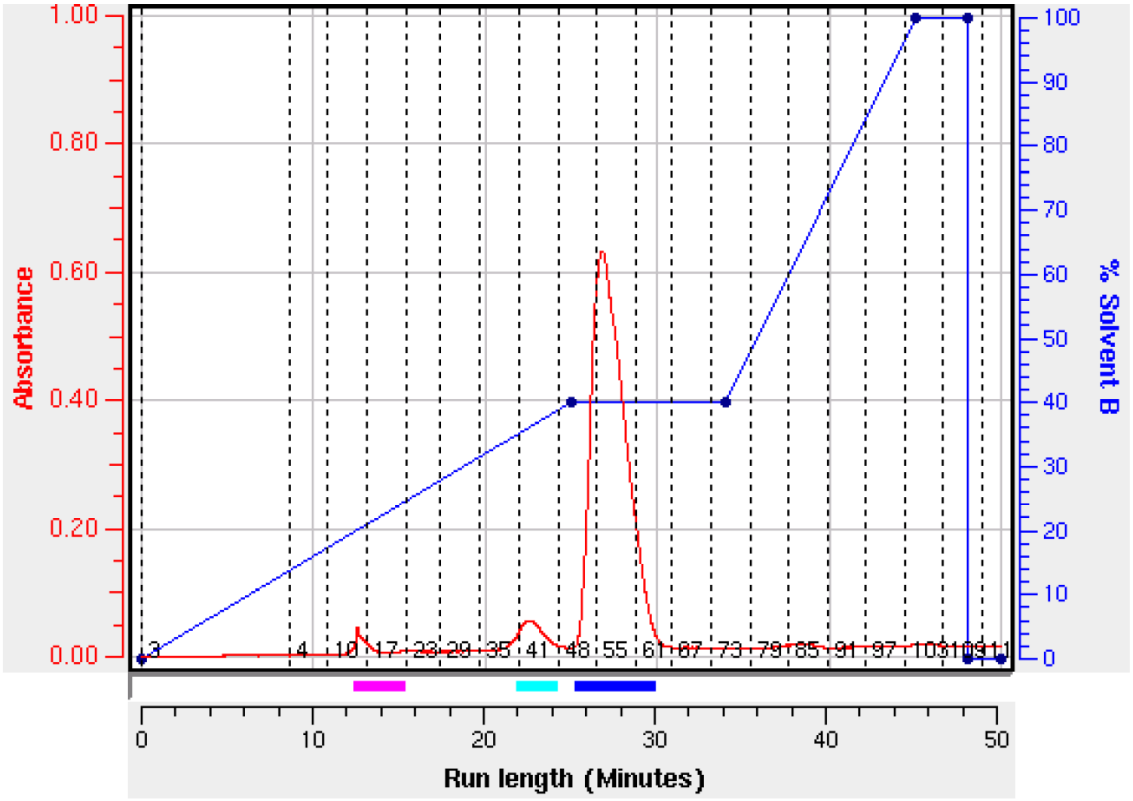

Figure 8.2- Purification of MAPA reaction products using flash chromatography. Eluent absorbance at 258 nm is shown in red (left axis) and solvent (Solvent A – hexanes; Solvent B – ethyl acetate) gradient is shown in blue (right axis).

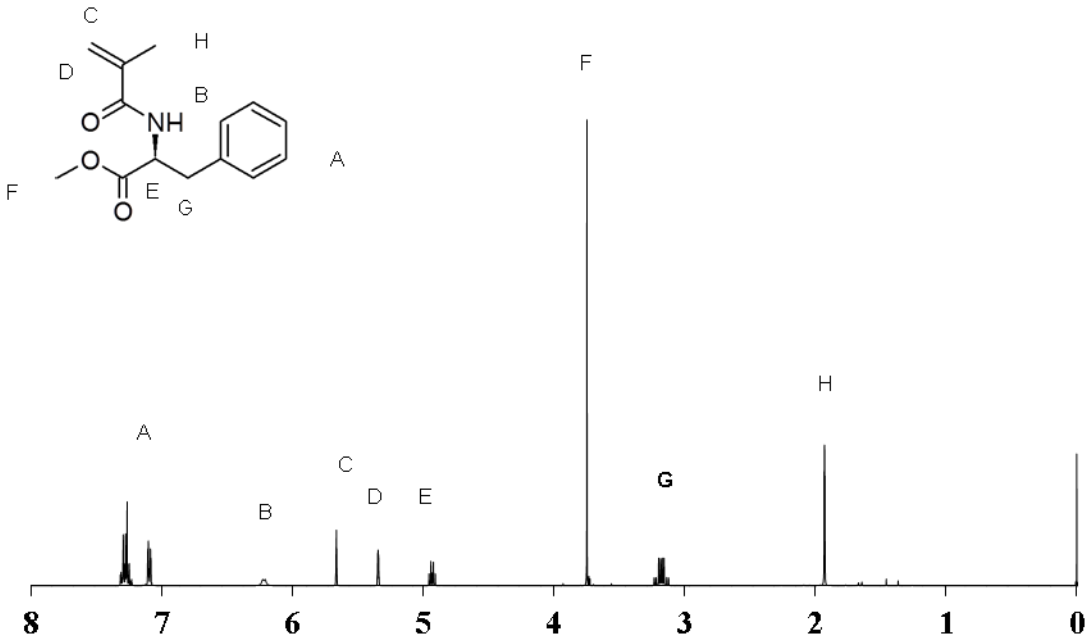

Figure 8.3 - ^{1}H-NMR Spectrum of purified N-methacryloyl L-phenylalanine methyl ester (MAPA) monomer in $CDCl_3$.

Table 8.1 – Peak assignments and relative integration values of the ^{1}H-NMR spectrum of purified N-methacryloyl L-phenylalanine methyl ester (MAPA) monomer

Peak Assignment	δ (ppm)	Protons	Integration Value
A	7.05 – 7.30	5, R-$C_6\boldsymbol{H}_5$	5.416
B	6.10 – 6.28	1, R-N***H***-R	1.082
C	5.60 – 5.70	1, R-C=C$\boldsymbol{H}_2$	1.046
D	5.30 – 5.40	1, R-C=C$\boldsymbol{H}_2$	1.049
E	4.85 – 5.00	1, R_2-C***H***-NH-R	1.105
F	3.65 – 3.85	3, -O-C$\boldsymbol{H}_3$	3.000
G	3.12 – 3.28	2, Ph-C$\boldsymbol{H}_2$-R	2.101
H	1.85 – 2.03	3, R-C$\boldsymbol{H}_3$	3.010

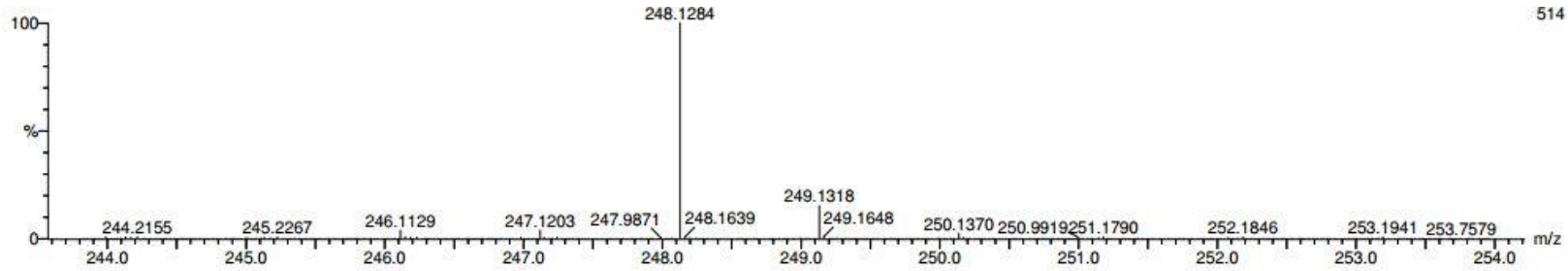

Figure 8.4 - Mass spectrum of purified N-methacryloyl L-phenylalanine methyl ester. Anticipated molecular weight of the MAPA product = 247 g/mol.

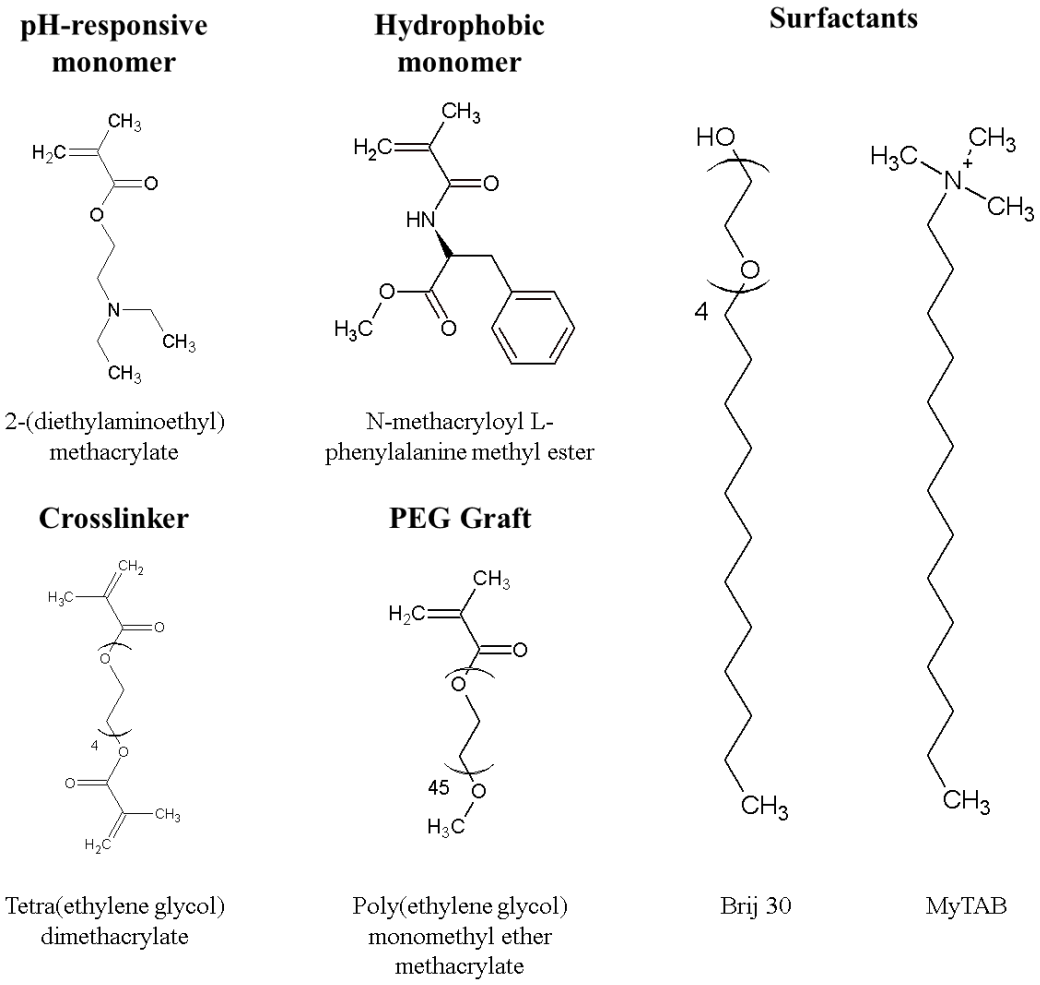

Figure 8.5 – Monomers and surfactants used in the synthesis of P(DEAEMA-co-MAPA-g-PEGMA) (PDETM30).

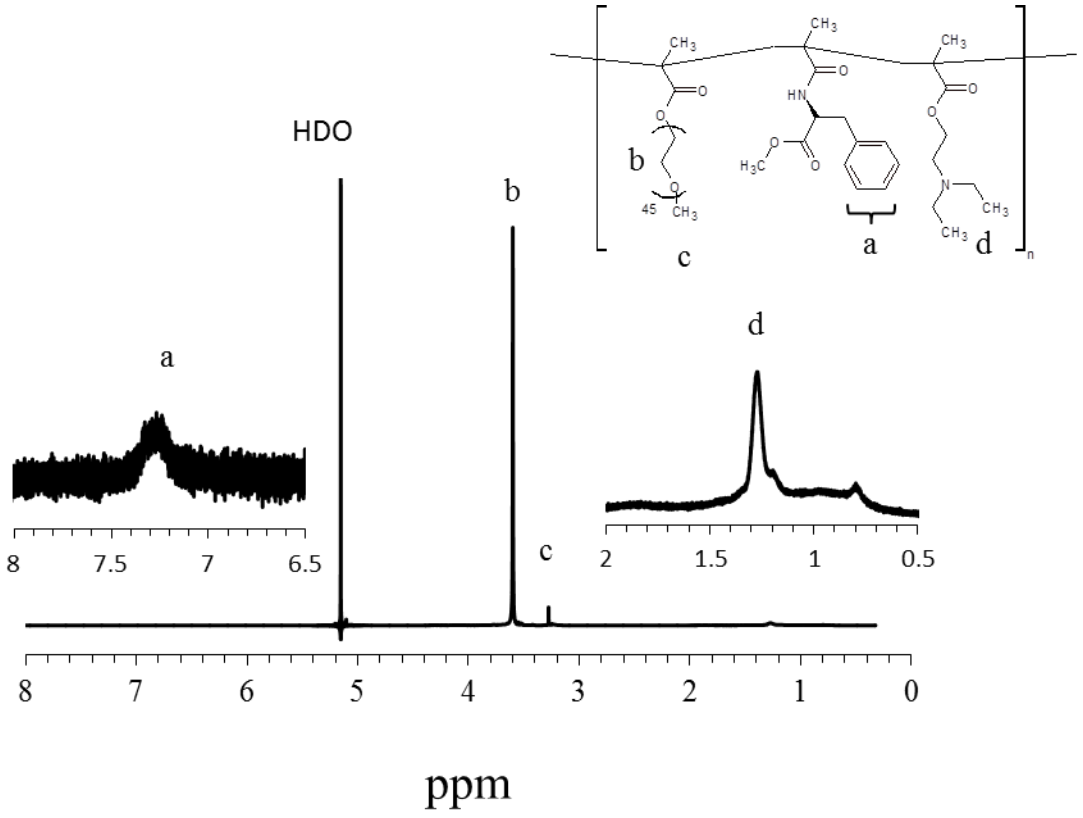

Figure 8.6 - ^{1}H-NMR spectra of crosslinked P(DEAEMA-co-MAPA-g-PEGMA) (PDETM30) in 0.1 N DCl/D_2O.

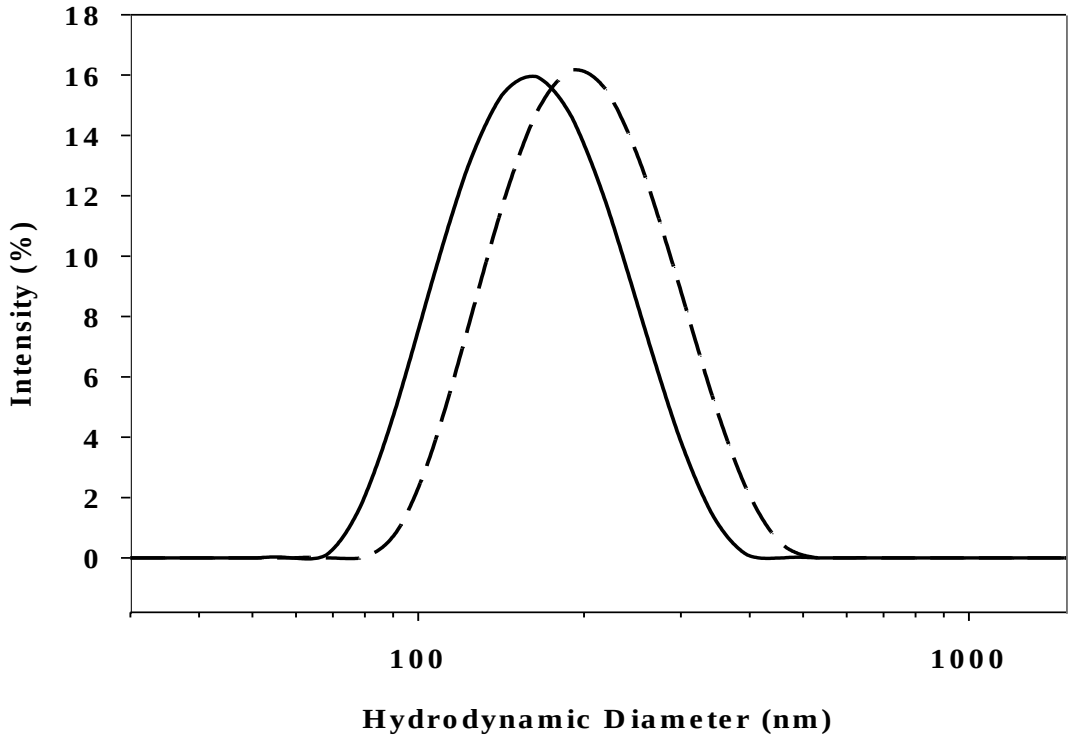

Figure 8.7 - Representative intensity-weighted particle size distribution for PDETM30 in the collapsed (solid) and swollen (dashed) state. Distribution in the collapsed state is from a measurement at pH 9.0 and distribution in the swollen state is from a measurement at pH 6.0.

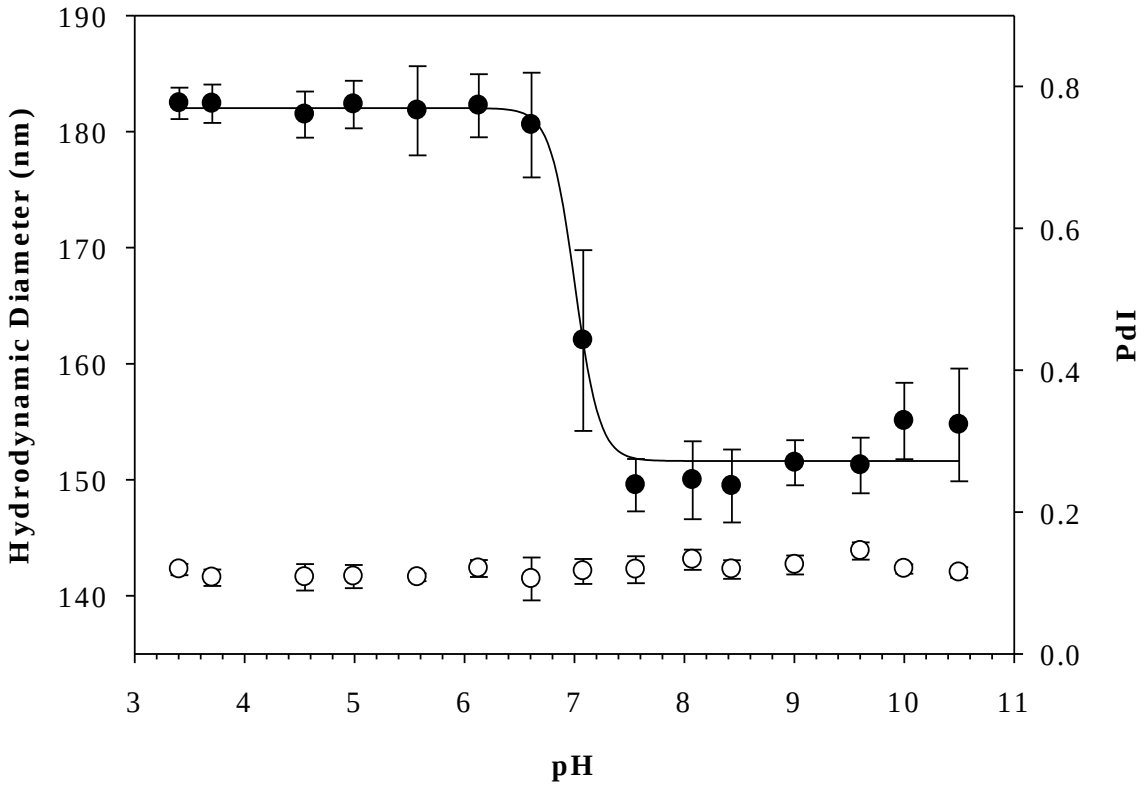

Figure 8.8 – Z-average diameter (●, left axis) and polydispersity (○, right axis) of P(DEAEMA-co-MAPA-g-PEGMA) networks crosslinked with 2.5 mol% TEGDMA in response to dynamic pH. Data points represent the mean of 3 sequential runs of 12 measurements each and error bars represent the standard deviation. The line represents a hyperbolic tangent best fit.

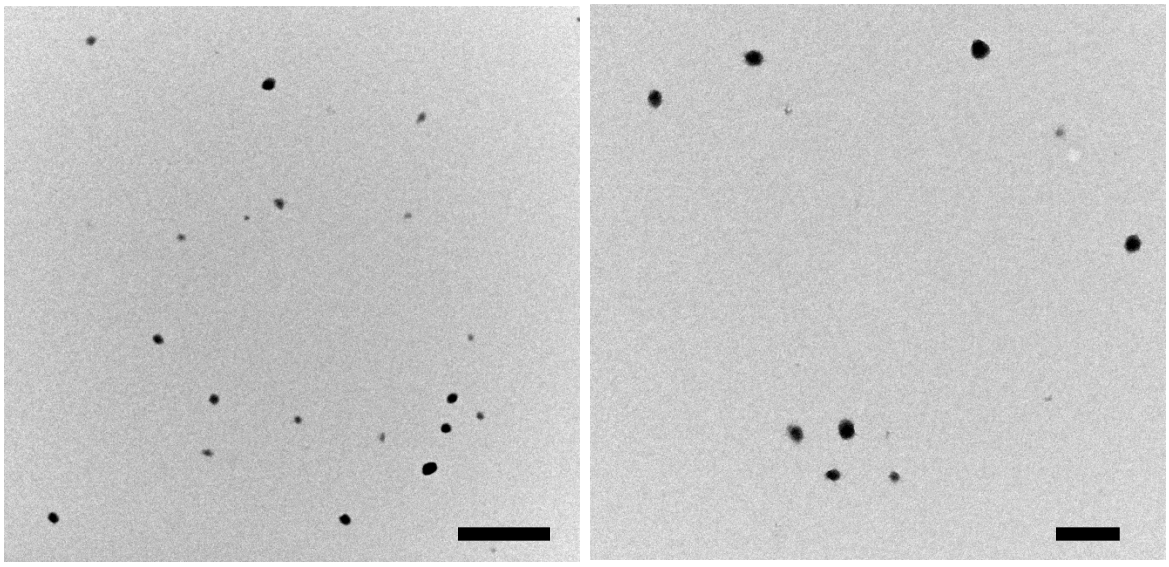

Figure 8.9 - Representative transmission electron microscopy image of TEGDMA-crosslinked P(DEAEMA-*co*-MAPA-*g*-PEGMA). Particles stained with uranyl acetate and images collected at 26,500× (A) and 43,000× (B). Scale bar represents 500 nm (A) or 200 nm (B).

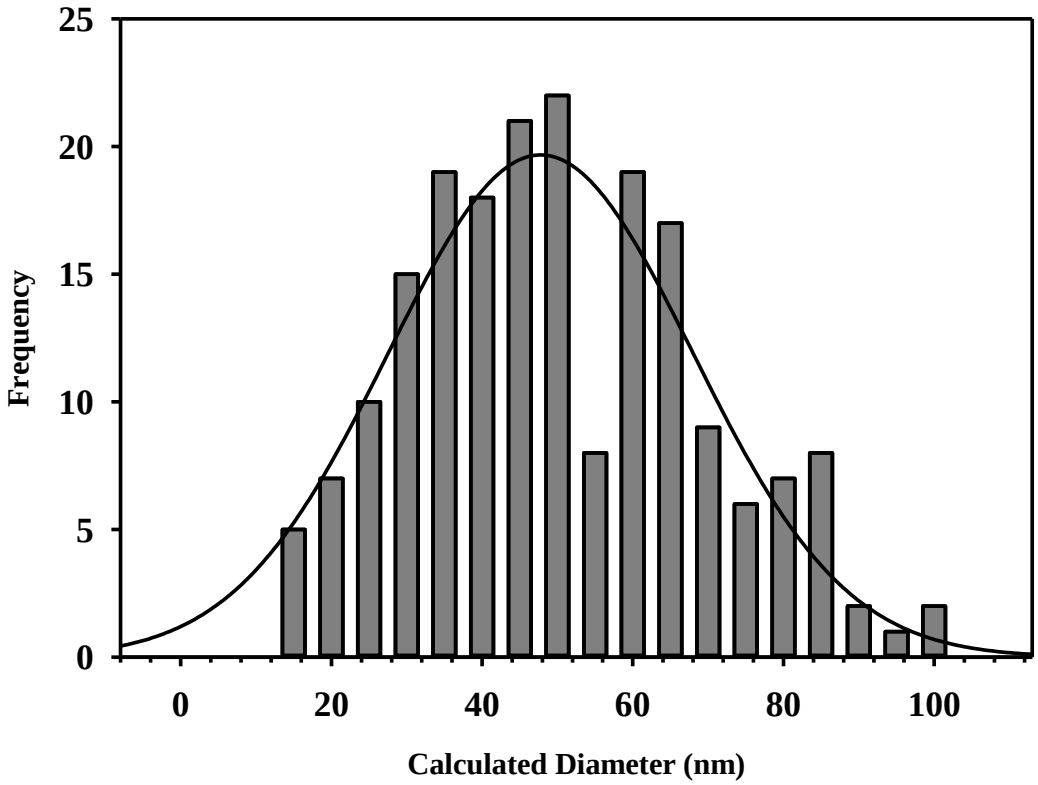

Figure 8.10 - Number-average particle size distribution of P(DEAEMA-co-MAPA-g-PEGMA) (PDETM30) generated by quantitative particle sizing from TEM micrographs. Distribution mean = 47.9, std. dev. = 19.6, n = 197. Bars represent calculated data and line represents best fit Gaussian distribution ($R^2 = 0.839$).

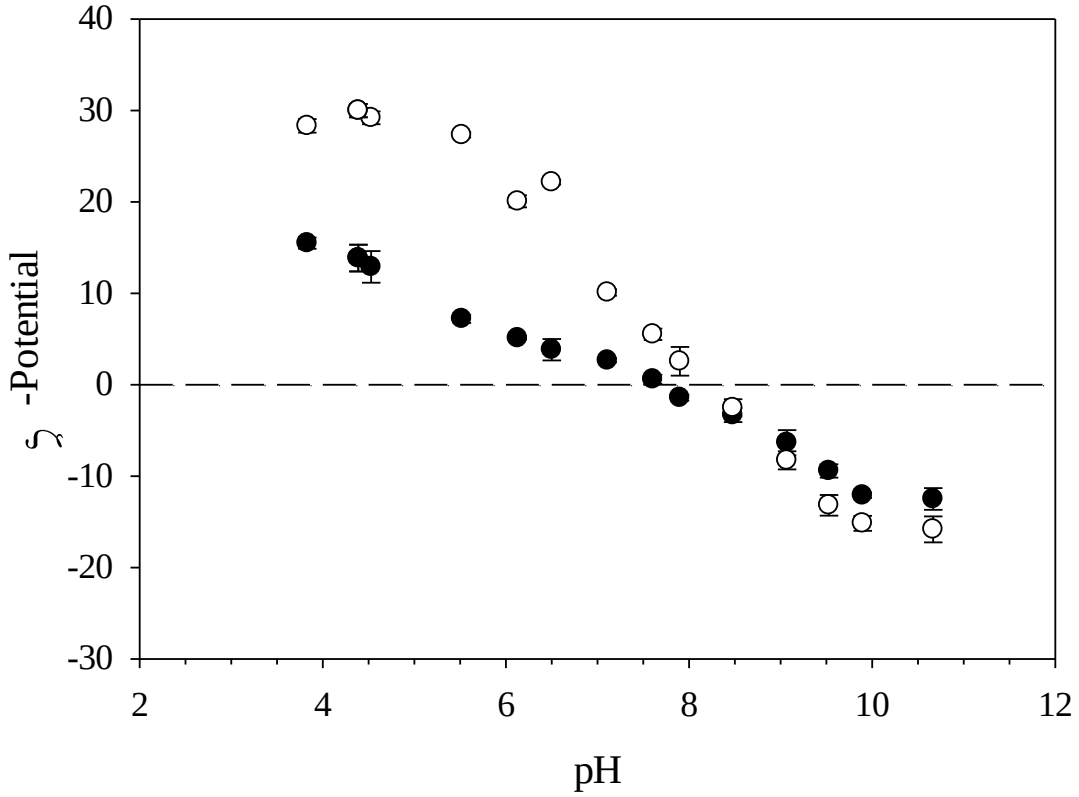

Figure 8.11 - Effective zeta-potential of P(DEAEMA-co-MAPA-g-PEG) PDETM30 (●) compared to P(DEAEMA-co-BMA-g-PEG) PDETB30 (○). Data points represent the mean of 3 sequential measurements ± s.d.

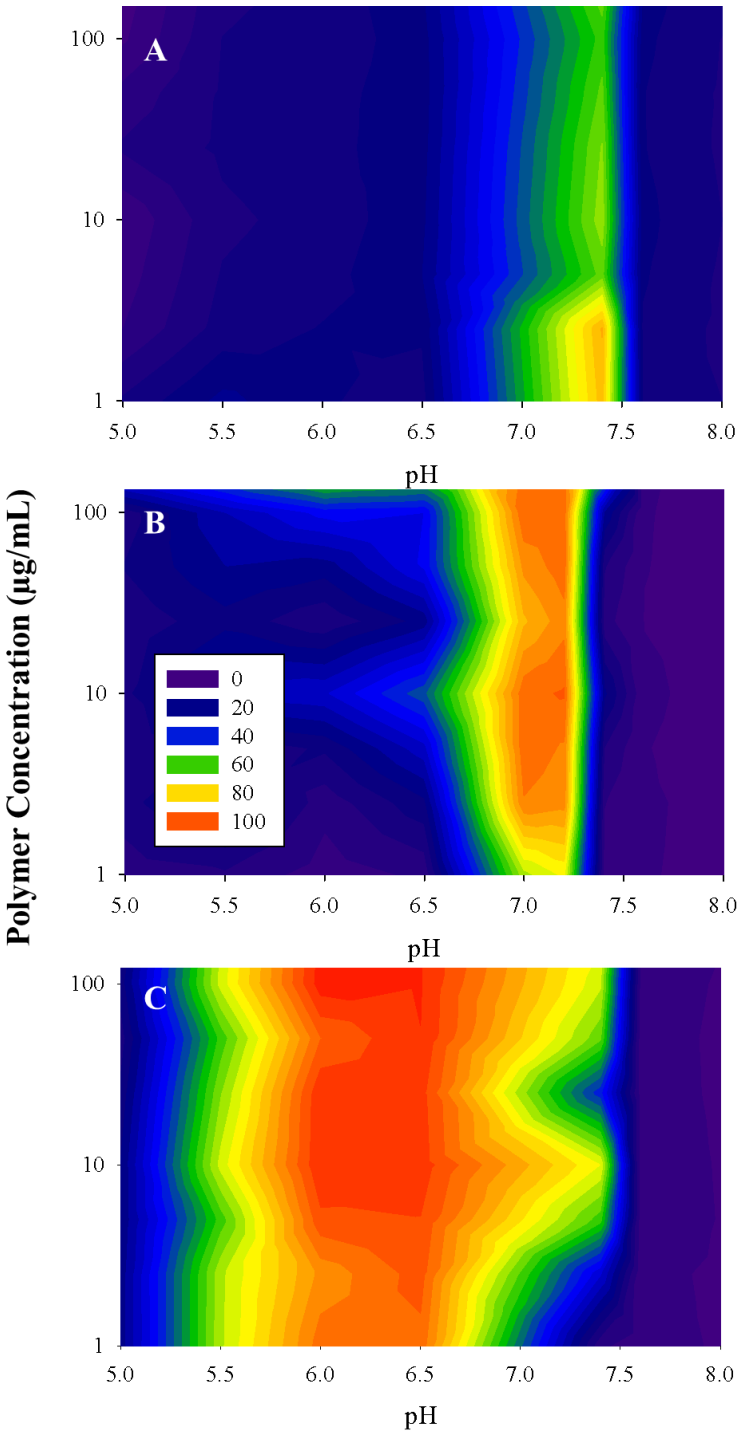

Figure 8.12 – Membrane-disruptive activity of pH-responsive nanogels PDET (A), PDETM30 (B), and PDETB30 (C). Sheep erythrocytes used as model membrane and hemoglobin release measured at $\lambda = 490$ nm.

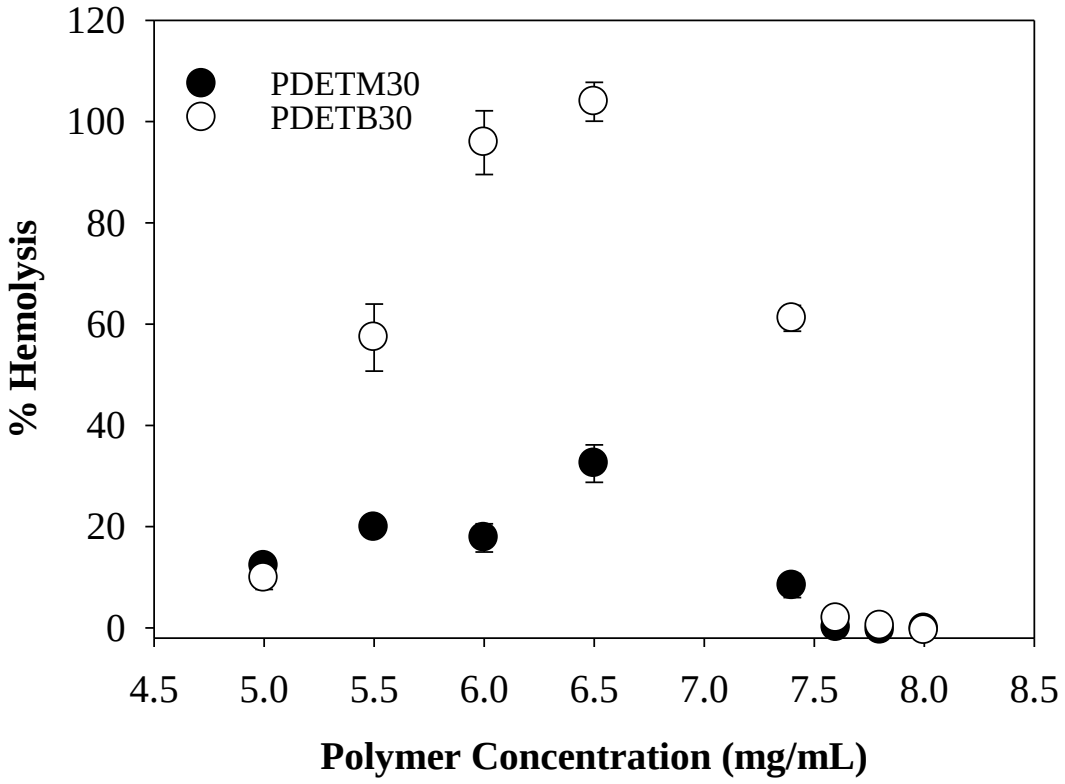

Figure 8.13 – Comparative hemolysis profile for PDETM30 (●) and PDETB30 (○) at 0.05 mg mL^{-1}. Data points represent the mean of a single experiment conducted in triplicate ± standard deviation.

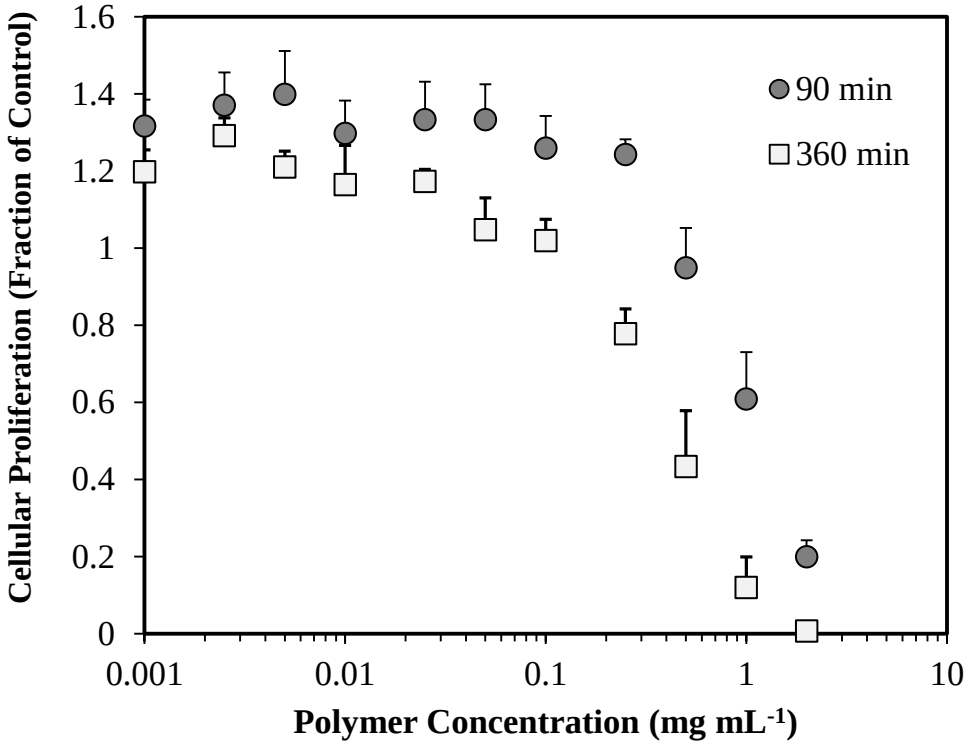

Figure 8.14 - Relative proliferation of Caco-2 cells upon exposure to P(DEAEMA-co-MAPA-g-PEG) (PDETM30) for 90 minutes (●) or 6 hours (■). The relative proliferation of Caco-2 cells was determined by MTS assay and is expressed as a fraction of the control (untreated) cells. Data are expressed as mean ± SEM, n = 4.

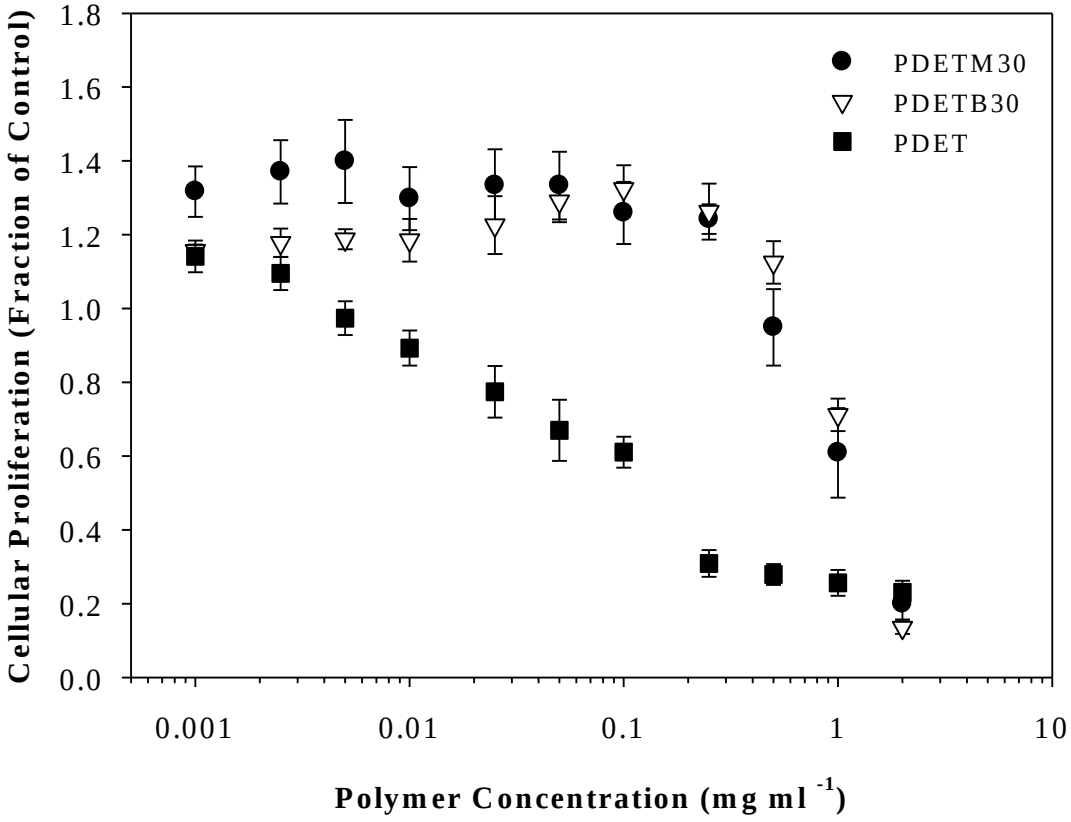

Figure 8.15 – Relative proliferation of Caco-2 cells upon exposure to PDETM30 (■), PDETB30 (◊), or PDET (■) for 90 min. The relative proliferation of RAW cells was determined by MTS assay and is expressed as a fraction of the control (untreated) cells. Data are expressed as mean ± SEM, n = 4.

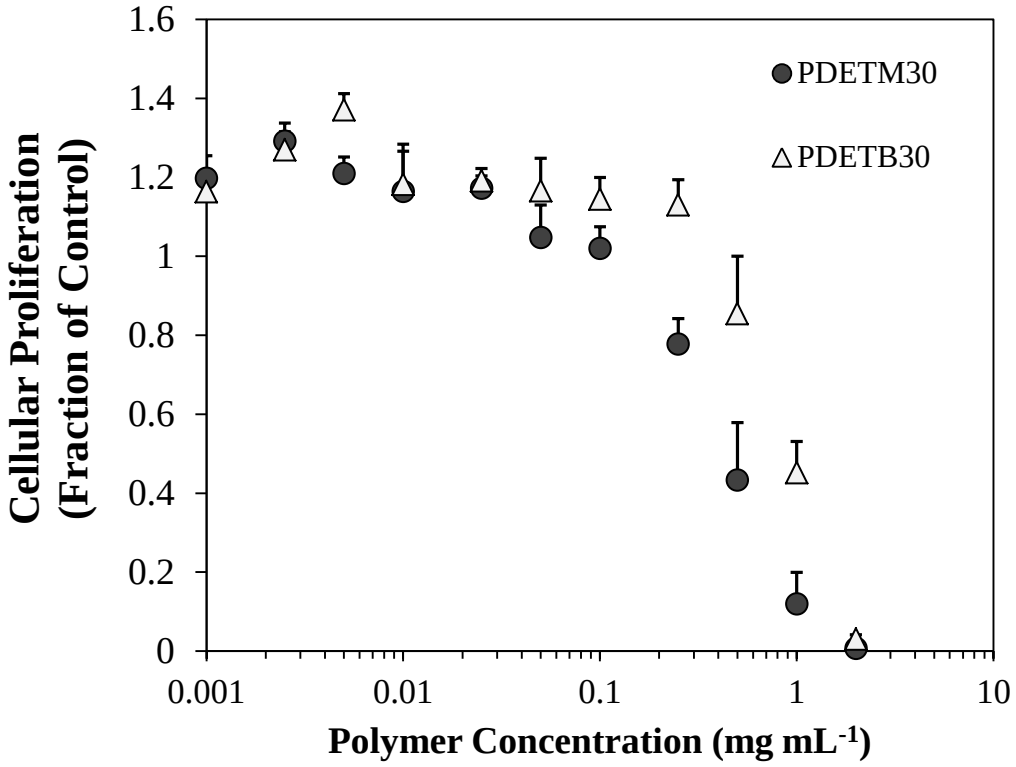

Figure 8.16 - Relative proliferation of Caco-2 cells upon exposure to PDETM30 (■) or PDETB30 (Δ) for 360 min. The relative proliferation of Caco-2 cells was determined by MTS assay and is expressed as a fraction of the control (untreated) cells. Data are expressed as mean ± SEM, n = 4.

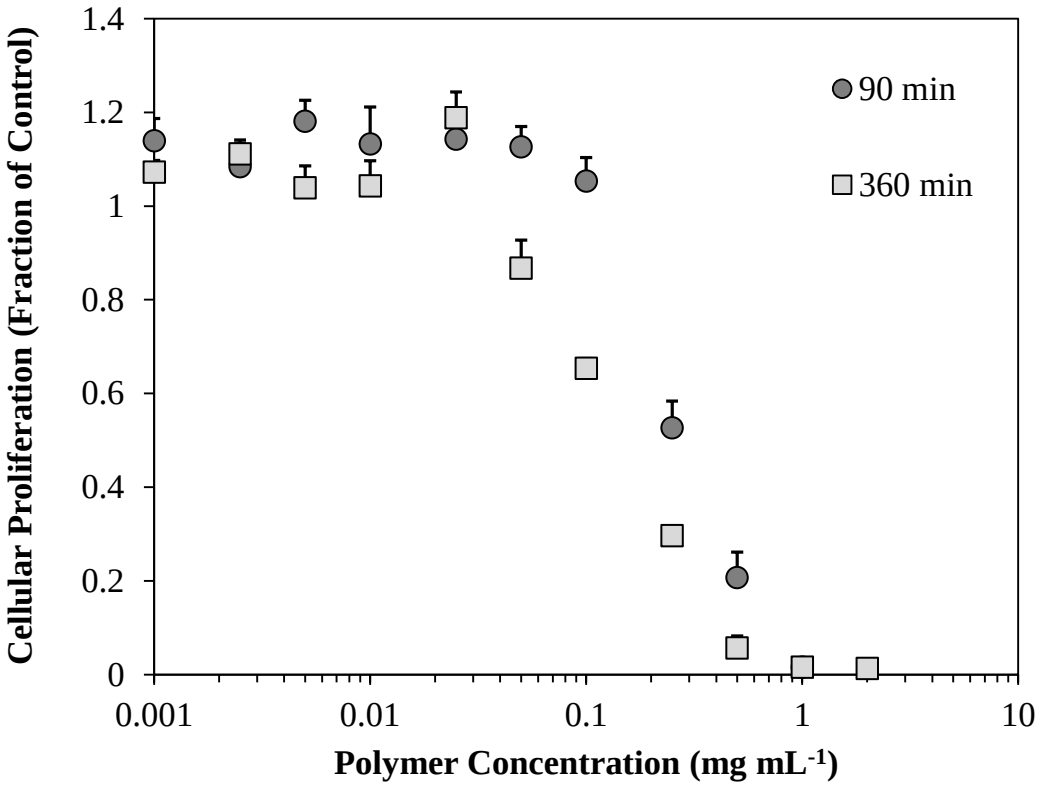

Figure 8.17 - Relative proliferation of RAW 264.7 cells upon exposure to P(DEAEMA-co-MAPA-g-PEG) (PDETM30) for 90 minutes (●) or 6 hours (■). The relative proliferation of RAW cells was determined by MTS assay and is expressed as a fraction of the control (untreated) cells. Data are expressed as means ± SEM, n = 4.

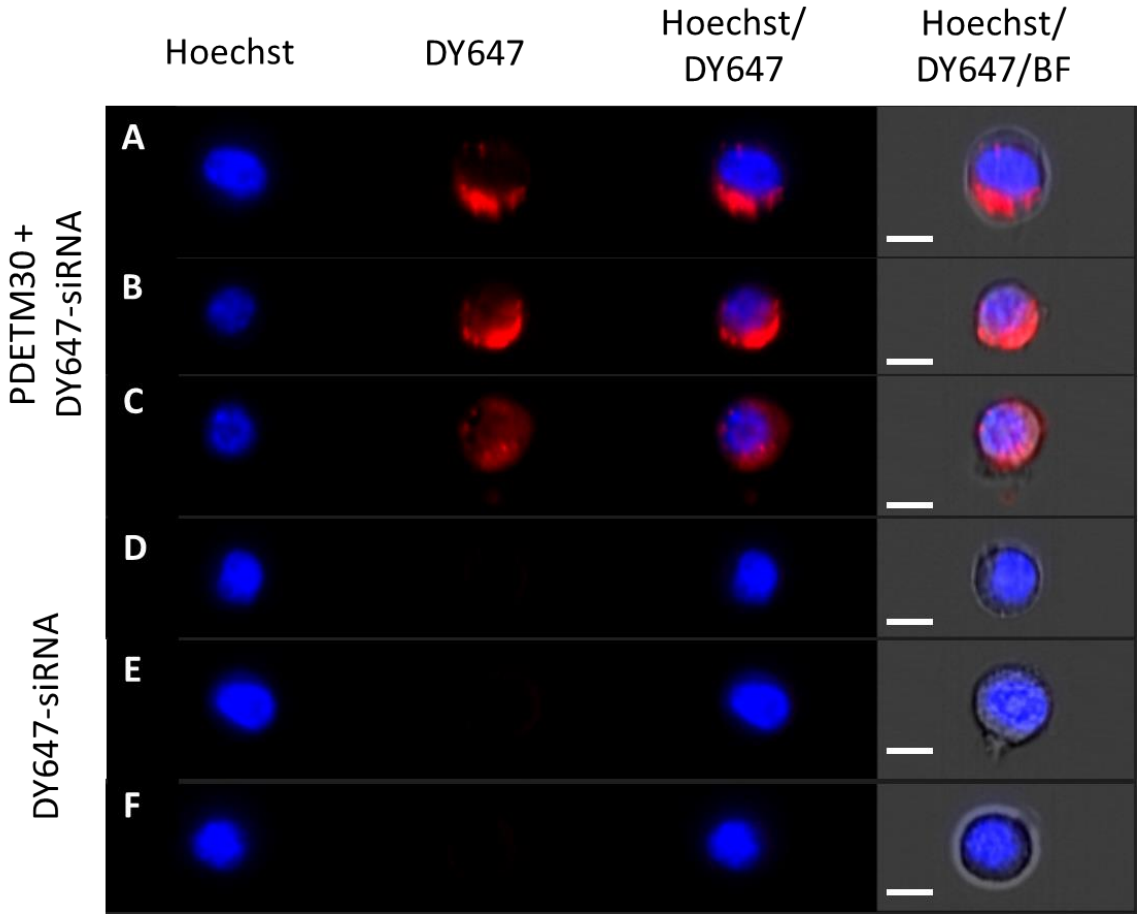

Figure 8.18 – DY647-siRNA delivery to RAW 264.7 cells. Nuclear stain (Hoechst 33342) shown in blue and DY647-siRNA (DyLight 647) shown in red. Two representative examples of RAW 264.7 cells exposed to PDETM30/DY647-siRNA (A-C) or DY647-siRNA alone (D-F) are shown. Scale bar represents 7 μm.

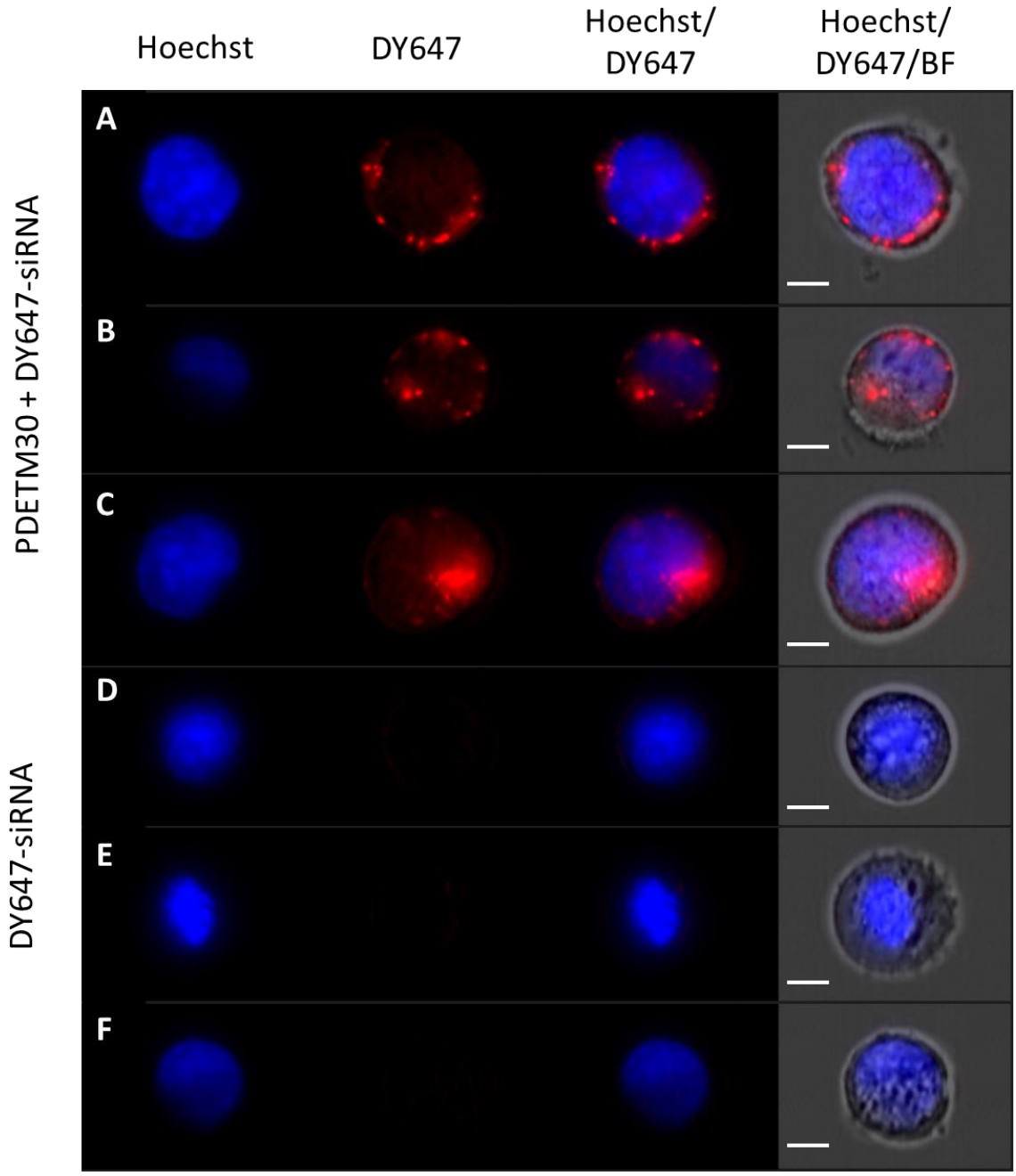

Figure 8.19 - DY647-siRNA delivery to Caco-2 cells. Nuclear stain (Hoechst 33342) shown in blue and DY647-siRNA (DyLight 647) shown in red. Three representative examples of Caco-2 cells exposed to PDETM30/DY647-siRNA (A-C) or DY647-siRNA alone (D-F) are shown. Scale bar represents 7 μm.

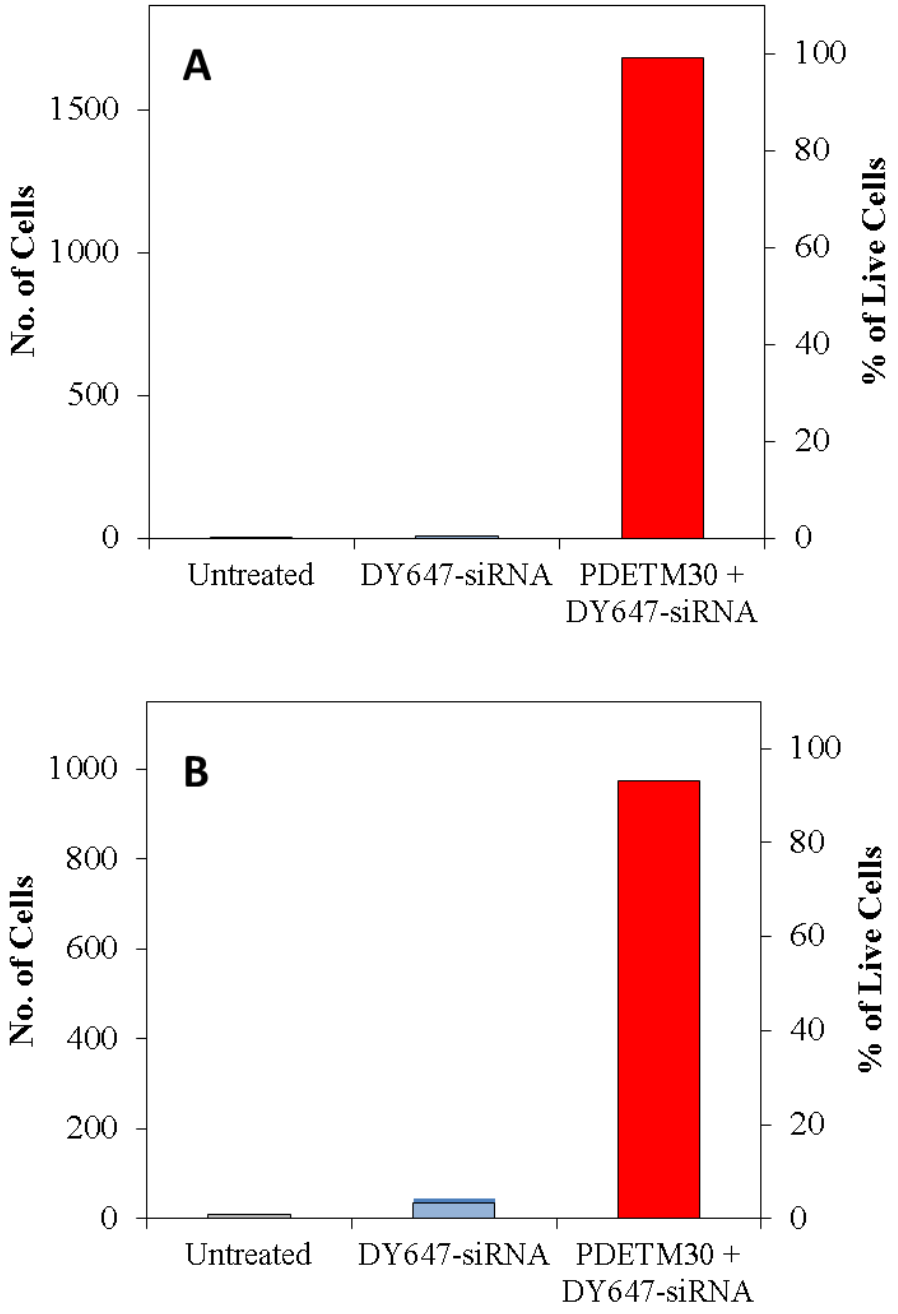

Figure 8.20 – Number (left axis) and proportion (right axis) of live cells with internalized DY647-siRNA. Untreated cells (gray), cells exposed to 100 nM DY647-siRNA alone (blue) or 100 nM DY647-siRNA + 25 μg ml^{-1} PDETM30 (red) in RAW 264.7 cells (A) and Caco-2 cells (B). Data represent pooled fractions from two independent experiments.

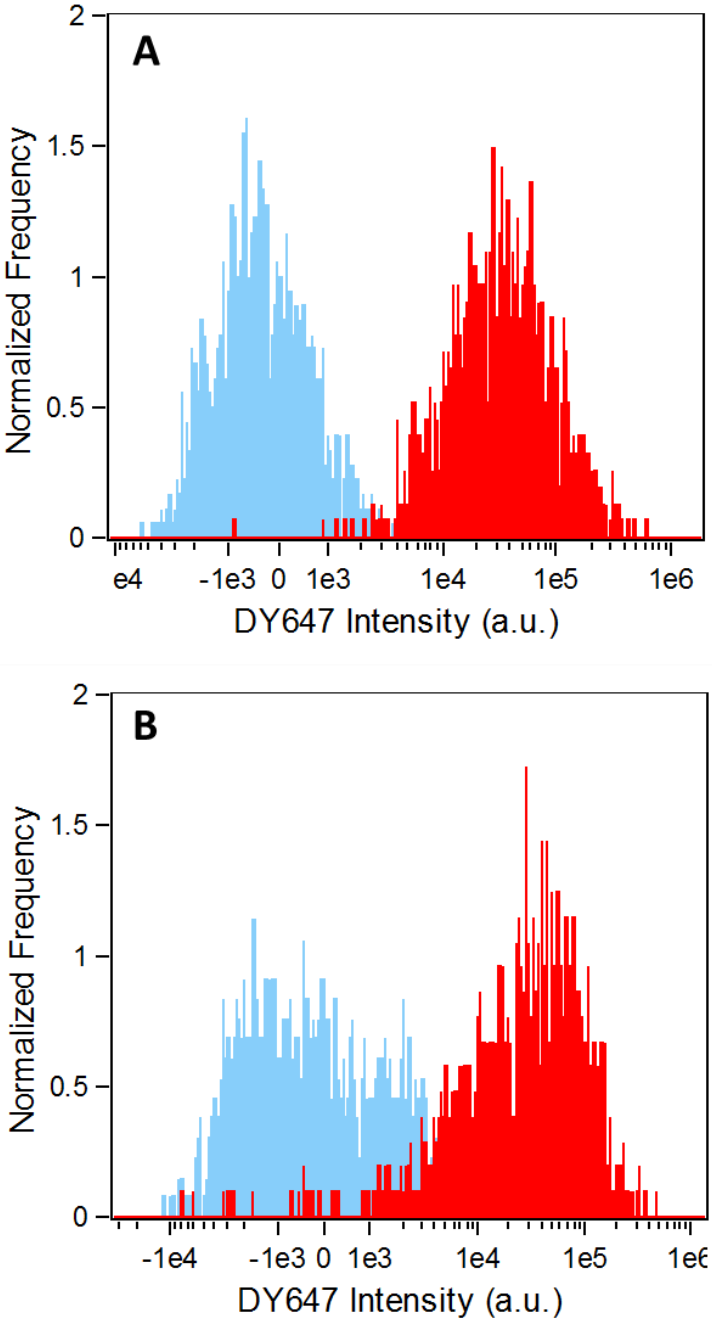

Figure 8.21 - Fluorescence intensity of DY647-siRNA in RAW 264.7 cells (A) and Caco-2 cells (B). Fluorescence histograms generated from cells exposed to DY647-siRNA alone (blue) or PDETM30/ DY647-siRNA (red). Data represent pooled fractions from two independent experiments.

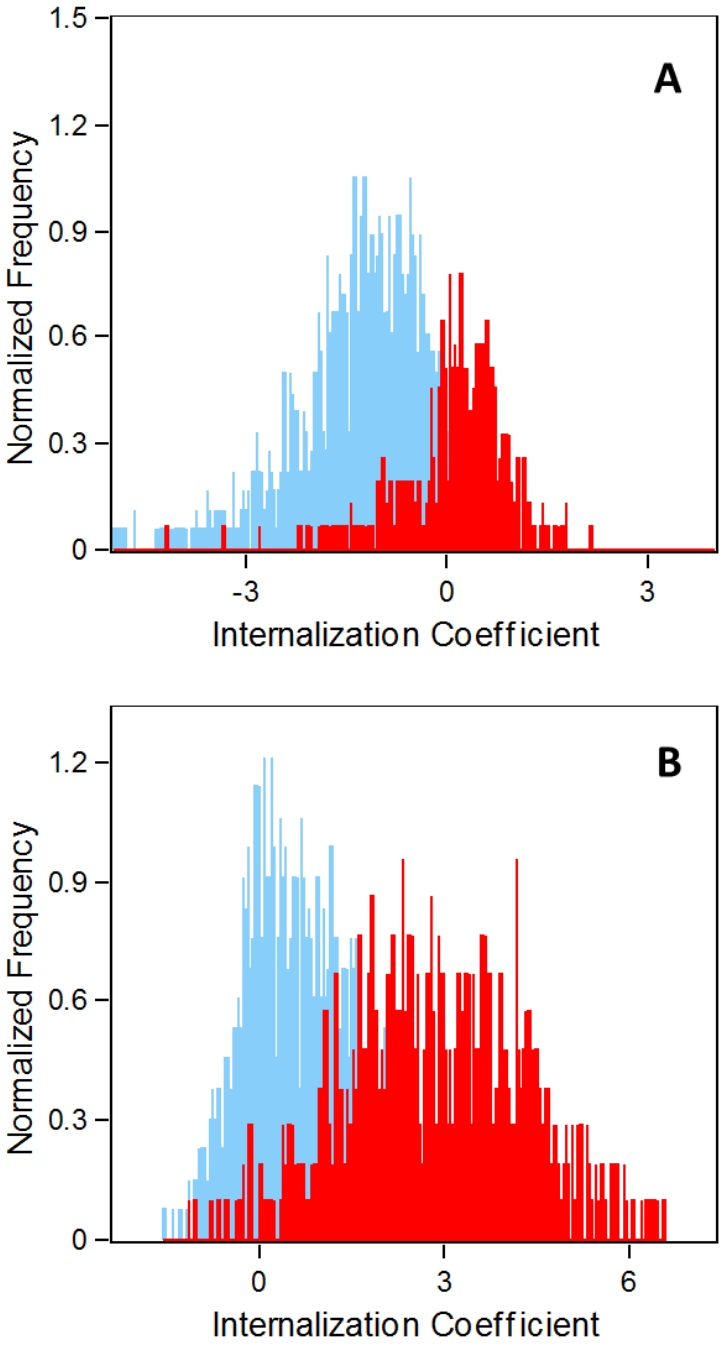

Figure 8.22 - Internalization coefficient of DY647-siRNA in RAW 264.7 cells (A) and Caco-2 cells (B). Histograms generated from image analysis of cells exposed to DY647-siRNA alone (blue) or PDETM30/ DY647-siRNA (red). Data represent pooled fractions from two independent experiments.

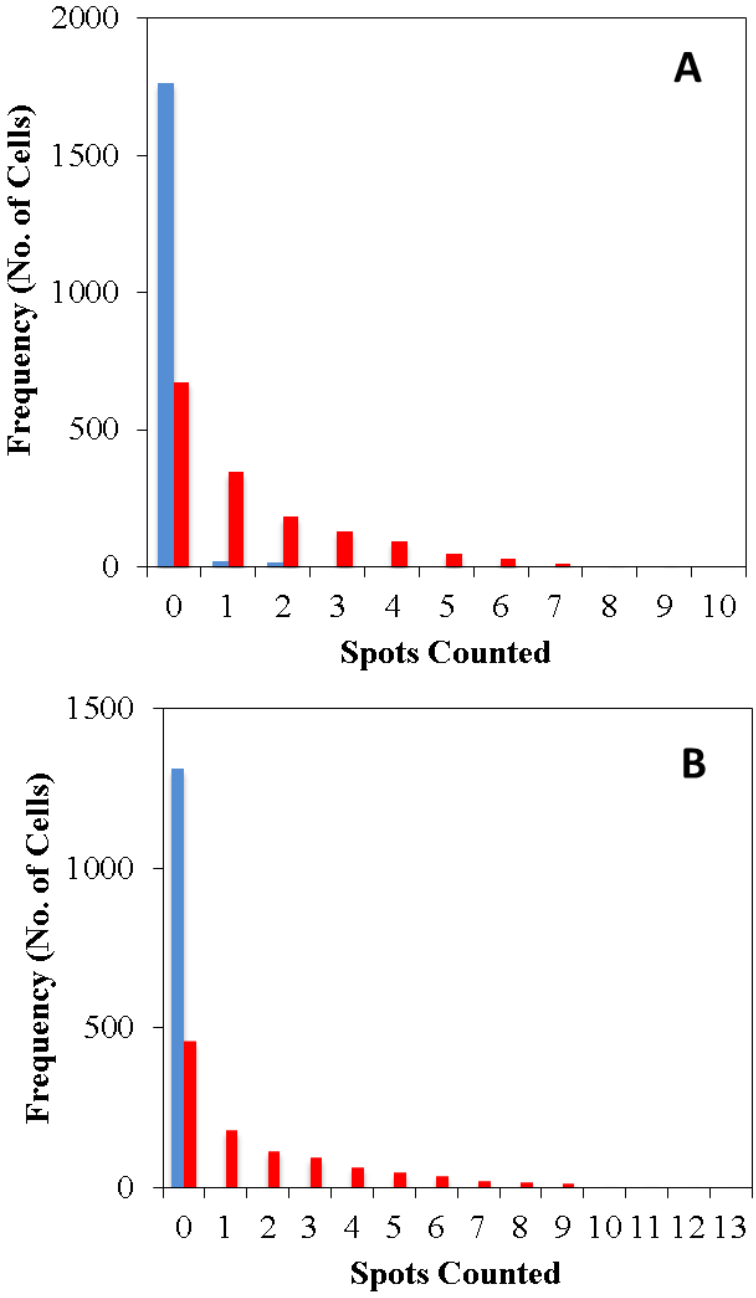

Figure 8.23 – Intracellular texture, or spot counting, of DY647-siRNA in RAW 264.7 cells (A) and Caco-2 cells (B). Histograms generated from image analysis of cells exposed to DY647-siRNA alone (blue) or PDETM30/ DY647-siRNA (red). Data represent pooled fractions from two independent experiments.

Table 8.2- Physical properties of PDETM30 nanogels compared to PDETB30

	Hydrophobic Monomer	D_H at pH 8.0 (nm)	D_H at pH 6.0 (nm)	ζ-Potential at pH 8.0 (mV)	ζ-Potential at pH 6.0 (mV)	Dry Diameter (nm)
PDETB30	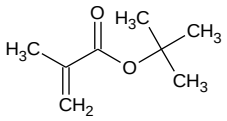	93.4	121	2.6 ± 1.6	21.6 ± 0.7	50 ± 17
PDETM30	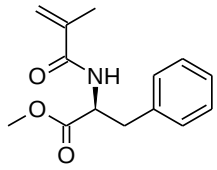	151.4	184.1	-1.4 ± 0.3	5.12 ± 0.2	47.9 ± 19

Table 8.3 - In vitro properties of PDETM30 compared to PDETB30

	Hydrophobic Monomer	Hemolysis at pH 7.4[1](%)	Hemolysis at pH 6.5[1] (%)	LD_{50} in RAW Cells[2] (mg ml^{-1})	LD_{50} in Caco-2 Cells[2] (mg ml^{-1})	DY647-siRNA delivery[3]
PDETB30	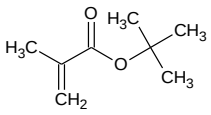	61.1 ± 2.5	103.9 ± 3.8	N/A	1.23	1.2×10^4
PDETM30	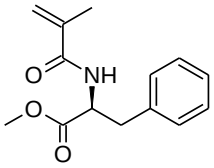	8.0 ± 0.2	32.4 ± 3.7	0.27	1.18	3.3×10^4

[1] Hemolysis using a polymer concentration of 0.05 mg ml^{-1}
[2] Toxicity determined using MTS assay following 90 min polymer exposure
[3] Median fluorescence of DY647-siRNA in single, focused, live RAW 264.7 cells as determined by ImageStream analysis

REFERENCES

1. Mastrobattista E and Hennink WE. Nature Materials 2012;11(1):10-12.

2. Zhou JB, Liu J, Cheng CJ, Patel TR, Weller CE, Piepmeier JM, Jiang ZZ, and Saltzman WM. Nature Materials 2012;11(1):82-90.

3. Chen RJ, Eccleston ME, Yue ZL, and Slater NKH. Journal of Materials Chemistry 2009;19(24):4217-4224.

4. Chen R, Khormaee S, Eccleston ME, and Slater NKH. Biomaterials 2009;30(10):1954-1961.

5. Chen RJ, Yue ZL, Eccleston ME, and Slater NKH. Biomaterials 2008;29(32):4333-4340.

6. Liechty WB, Chen R, Farzaneh F, Tavassoli M, and Slater NKH. Advanced Materials 2009;21(38-39):3910-3914.

7. Oncel S, Uzun L, Garipcan B, and Denizli A. Industrial & Engineering Chemistry Research 2005;44(18):7049-7056.

8. Turkmen D, Denizli A, Ozturk N, Akgol S, and Elkak A. Biotechnology Progress 2008;24(6):1297-1303.

9. Sanda F, Abe T, and Endo T. Journal of Polymer Science Part a-Polymer Chemistry 1997;35(13):2619-2629.

10. Schwarz-Barac S, Ritter H, and Schollmeyer D. Macromolecular Rapid Communications 2003;24(4):325-330.

11. Fisher OZ and Peppas NA. Macromolecules 2009;42(9):3391-3398.

12. Fisher O, Kim T, Dietz S, and Peppas N. Pharmaceutical Research 2009;26(1):51-60.

13. Liechty WB, Scheuerle RL, and Peppas NA. Polymer 2013;under review.

14. Standardization IOf. ISO 13321: Particle Size Analysis - Photon Correlation Spectroscopy. 1996.

15. Brannon-Peppas L and Peppas NA. Chemical Engineering Science 1991;46(3):715-722.

16. Siegel RA and Firestone BA. Macromolecules 1988;21(11):3254-3259.

17. Manganiello MJ, Cheng C, Convertine AJ, Bryers JD, and Stayton PS. Biomaterials 2012;33(7):2301-2309.

18. Plank C, Oberhauser B, Mechtler K, Koch C, and Wagner E. Journal of Biological Chemistry 1994;269(17):12918-12924.

19. Khinkis LA, Levasseur L, Faessel H, and Greco WR. Nonlinearity in biology, toxicology, medicine 2003;1(3):363-377.

20. Yuen KH. International Journal of Pharmaceutics 2010;395(1-2):9-16.

21. Huotari J and Helenius A. EMBO Journal 2011;30(17):3481-3500.

22. Glunde K, Guggino SE, Solaiyappan M, Pathak AP, Ichikawa Y, and Bhujwalla ZM. Neoplasia 2003;5(6):533-545.

Chapter 9: Conclusions and Future Recommendations

The work described in this thesis outlines the development and evaluation of nanoscale delivery systems for small interfering RNA. These delivery systems were examined with a hierarchical screening process for physical and biological characterization and evaluated according to several design criteria. These design criteria were dictated by the physiological demands of an effective endosomolytic nanocarrier and include requirements for size, surface charge, pH response, cytotoxicity, siRNA binding, and siRNA delivery.

As a first order screen, nanogel size and critical swelling pH were the most important design parameters. For effective intracellular drug delivery, a cationic nanogel carrier should avoid a conformational transition at or near physiological pH. A preferred transition pH is that of the endosomes (pH 5.5 – pH 6.5) to ensure that encapsulated siRNA cargo may remain protected at physiological pH. Many amine-based monomers, including the principal monomer used in this work (2-diethylaminoethyl methacrylate) have a pKa near pH 7 – 8. Therefore, the polymer composition was modulated to shift the pH for onset of critical phenomena toward the endosomal pH region and away from the physiological pH region. Initial studies examined the competing influence of two *tert*-butyl containing methacrylate monomers, *tert*-butyl methacrylate (TMBA) and *tert*-butylamino methacrylate (TBAEMA), on the aqueous solution properties of pH-responsive nanogels.

In P(DEAEMA-co-TBMA-g-PEGMA) copolymers, increasing TBMA serves to decrease the onset of pH-dependent swelling, reaching ~ pH 7.2 with maximum volume swelling ~ pH 5.50 in PDETB30. Moreover, TBMA broadens the transition from

collapsed hydrophobe and swollen hydrophile in light scattering and pyrene fluorescence spectroscopy studies. In P(DEAEMA-co-TBAEMA-g-PEGMA) copolymers, the compositional dependence is less obvious. Pyrene fluorescence spectroscopy reveals an increase in the critical pH for hydrophobic-hydrophilic phase transition but dynamic light scattering reveals no compositional trend in the volume swelling transition.

Second order screens evaluated the membrane-disruptive activity. As siRNA is unable to cross cell membranes, a suitable delivery system should facilitate its passage through cell membrane barriers to permit cytoplasmic localization. Three model membrane systems were used to assess the membrane-disruptive ability of responsive nanogels as a function of environmental pH and concentration.

Red blood cells were used as model lipid membranes to investigate the influence of pH on membrane destabilization. These studies served to approximate the endosomolytic ability of nanogels as a function of pH, particularly that of endosomal pH (5.5 – 6.5), by quantifying the release of hemoglobin from damaged erythrocyte membranes. In all nanogel formulations, the pH range of maximum hemolysis was in excellent agreement with the pH range for the phase transition as determined by pyrene fluorescence spectroscopy.

Lactate dehydrogenase (LDH) leakage assays in Caco-2 cells were used to evaluate the untoward membrane disruption at physiological pH. These studies served to investigate the influence of polymer composition and exposure time on membrane damage to live cells. These studies corroborate the importance of the pH-dependent phase transition on membrane-disruptive behavior. Nanogels with a phase transition at

lower pH values (e.g. PDETB30) were less disruptive to Caco-2 cell membranes than were nanogels with higher pH values (e.g. PDET, PDETBA30).

Confocal micrscopy analysis of synthetic lipid vesicles in pH 6.50 buffer revealed the putative mechanism of membrane destabilization to be transient pore formation. In these investigations, PDETB30 permitted the rapid efflux of an encapsulated fluorescent dye while leaving the lipid membrane intact. PDET, which demonstrates a phase transition at approximately pH 7.3 and minimal hemolysis at pH 6.50, was not disruptive to the lipid vesicles under the experimental conditions. The conclusion of these studies yielded one nanogel formulation (PDETB30) with a critical transition near endosomal pH and an excellent combination of pH-dependent membrane disruption and biocompatibility.

Third order screens evaluated the siRNA loading capacity and siRNA delivery to target cell types. These investigations revealed that PDETB30 enables the internalization (primarily through macropinocytosis), vesicular escape, and functional gene silencing activity of siRNA cargoes. Internalization of nanoparticles is a highly complex and regulated cellular process which has tremendous bearing on the intracellular fate of internalized nanoparticles. Understanding the mechanism of uptake is critical to enabling (or increasing) productive intracellular delivery of any biotherapeutic.

In this thesis, the use of TBMA to modulate physicochemical properties and create responsive nanogels with desirable drug delivery characteristics was quite effective. However, the lack of a nanogel degradation mechanism will undoubtedly limit the in vivo utility of these nanogel carriers. To impart a mechanism for nanogel degradability, a custom homobifunctional disulfide crosslinker was synthesized and used

to permit nanogel degradation in the reductive intracellular environment. Additional modifications to enhance biocompatibility, such as the replacement of TBMA with a reactive phenylalanine derivative (MAPA) were also investigated. Though replacement of TBMA did not increase biocompatibility, the resulting nanogels are efficient delivery vehicles for siRNA and merit further investigation.

There are many facets of this work that are ripe for further investigation. More detailed information regarding the degradation kinetics of disulfide-crosslinked nanogels and chemical nature of corresponding degradation products will be important in future in vivo or perhaps clinical applications. Comprehensive evaluation of gene silencing in is also an area for future study. GAPDH was suitable in this initial work for comparison across several cell lines, further development should investigate more therapeutically relevant disease targets and cell lines. Macrophage cells have traditionally been difficult to transfect with siRNA delivery systems. However, mounting evidence suggests the culture conditions (2D vs. 3D, substrate stiffness, etc.) play an important role their susceptibility to transfection. Further efforts in this direction should seek to more accurately recapitulate the native target cell environment. Moreover, i*n vitro* models for predicting *in vivo* and clinical efficacy are notoriously poor. For a true assessment of the utility and performance of these nanogels in siRNA delivery applications, progression to *in vivo* disease models is a critical step.

Appendices

APPENDIX A: POLYMER NOMENCLATURE

The naming convention of the copolymer nanoscale hydrogels described in this thesis was established to reflect the copolymer composition.

Table A.1: Naming convention for copolymer formulations

Name	Copolymer	Primary Monomer	Comonomer	Comonomer Ratio[1]	Crosslinker	Chapter
PDET	P(DEAEMA-g-PEGMA)	DEAEMA		0	TEGDMA	4,5
PDETB10	P(DEAEMA-co-TMBA-g-PEGMA)	DEAEMA	TBMA	10	TEGDMA	4,5
PDETB20	P(DEAEMA-co-TBMA-g-PEGMA)	DEAEMA	TBMA	20	TEGDMA	4,5
PDETB20	P(DEAEMA-co-TBMA-g-PEGMA)	DEAEMA	TBMA	20	TEGDMA	4,5
PDETB30	P(DEAEMA-co-TBMA-g-PEGMA)	DEAEMA	TBMA	30	TEGDMA	4 – 8
PDETBA10	P(DEAEMA-co-TBAEMA-g-PEGMA)	DEAEMA	TBAEMA	10	TEGDMA	4,5
PDETBA20	P(DEAEMA-co-TBAEMA-g-PEGMA)	DEAEMA	TBAEMA	20	TEGDMA	4,5
PDETBA30	P(DEAEMA-co-TBAEMA-g-PEGMA)	DEAEMA	TBAEMA	30	TEGDMA	4,5
PDESSB30	P(DEAEMA-co-TBMA-g-PEGMA)	DEAEMA	TBAEMA	30	SSXL	7
PDETM30	P(DEAEMA-co-MAPA-g-PEGMA)	DEAEMA	TBAEMA	30	TEGDMA	8

[1]Per 100 mol of primary monomer

Abbreviations: DEAEMA: 2-(diethylaminoethyl methacrylate), TBMA: *tert*-butyl methacrylate, TBAEMA: *tert*-butylaminoethyl methacrylate, MAPA: N-methacryloyl L-phenylalanine methyl ester, TEGDMA: tetra(ethylene glycol) dimethacrylate, SSXL: bis(2-methacryloyloxyethyl) disulfide, PEGMA: poly(ethylene glycol) monomethyl ether methacrylate (M_n – 2,080)

APPENDIX B: PRACTICAL CONSIDERATIONS IN DYNAMIC LIGHT SCATTERING

Dynamic light scattering (DLS), also termed photon correlation spectroscopy and quasi-elastic light scattering, is a powerful technique to calculate the hydrodynamic diameter of particles undergoing Brownian motion in solution. In general, a typical light scattering experiment is conducted by passing a monochromatic incident beam through a solution of volume, V, and detector at a fixed angle, Θ. The scattering volume V is formed by the intersection of incident beam and detector. The time-dependent fluctuations in scattered light intensity due to random diffusion can be resolved into a time-correlation function via an autocorrelator, where the intensity correlation approaches 1 at small times ($\tau \rightarrow 0$) and approaches 0 at long times ($\tau \rightarrow \infty$). A graphical illustration of this behavior is shown in Figure B.1.

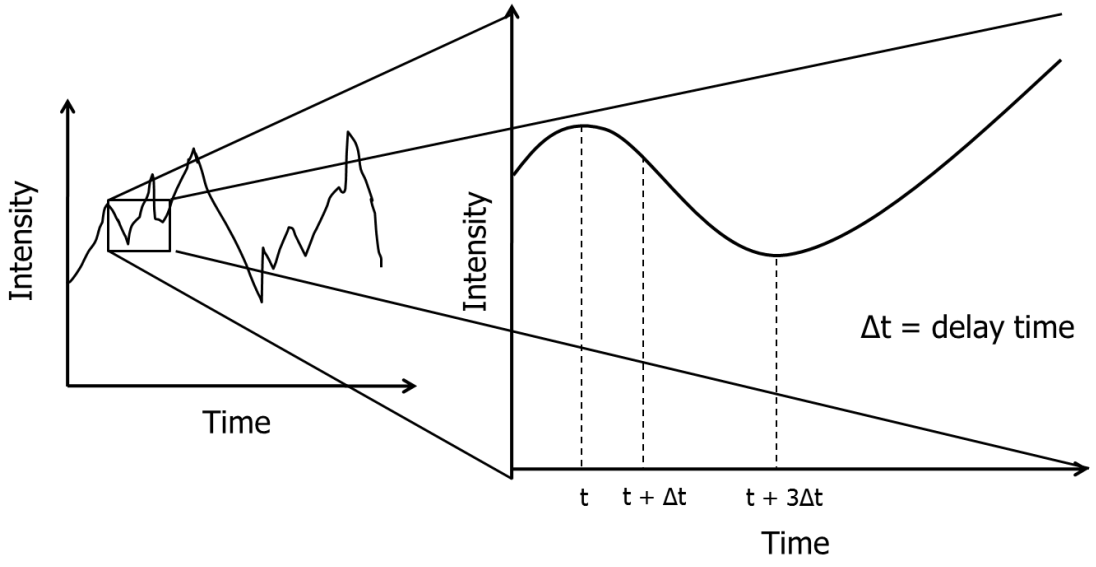

Figure B.1 - Time-dependent intensity fluctuations in dynamic light scattering

These fluctuations can be averaged over time to form a correlation function, which describes the characteristic decay in similarity of scattered light intensity as a

function of time. One should note that in light scattering of macromolecular samples, relatively small macromolecules will give rise to a correlation function that is valid for very short times, as a small macromolecule diffuses more quickly and its spatial position at time t + Δt is less likely to be related to its spatial position at time t. Conversely, relatively large marcomolecules will give rise to a correlation function that persists for much longer times, because the macromolecule is diffusing more slowly. Common methods of interpreting the autocorrelation function include fitting a single exponential to the correlation function, as done in the cumulant analysis (defined in ISO13321 Part 8), or to fit a multiple exponential to the correlation function, as done in CONTIN or NNLS algorithms. Of these, the Cumulants analysis is the most common and valid for a single population of spherical particles. In this analysis, the correlation function is fit to the exponential described by:

$$C(\tau) = \int G(\Gamma) \cdot e^{-\Gamma \tau} d\Gamma \tag{B.1}$$

Where Γ is the characteristic decay rate, τ is time, and G(Γ) is proportional to the relative scattering from each species within the given population. Thus, the correlation function can be considered the sum of all exponential decay functions from all species. For convenience, this exponential function is expanded in a Taylor series, where the coefficients of τ are termed Cumulants. Typically, the first and second moments of this Taylor series expansion are considered the most important. The first moment, Γ, can be given by:

$$\Gamma = D \cdot q^2 \tag{B.2}$$

Where D is the translational diffusion coefficient and q is the scattering vector, given by:

$$q = \frac{2\pi n}{\lambda_0} 2 \cdot \sin\left(\frac{\theta}{2}\right) \tag{B.3}$$

Where n is the index of refraction (1.5174 for PDEAEMA (Brandup and Immergut 1989), λ_0 is the incident light source wavelength (633 nm), and Θ is the scattering angle (173°). The second moment, μ2, is given by:

$$\mu_2 = \left(D^2 - D^{*2}\right) \cdot q^4 \tag{B.4}$$

Where D* is the population-average translational diffusion coefficient. Once the translational diffusion coefficient is known, it can be used to calculate the particle hydrodynamic diameter using the familiar Stokes-Einstein equation:

$$D_H = \frac{kT}{3\pi\eta D} \tag{B.5}$$

Where k is the Boltzmann constant, T is the absolute temperature, and η is the dynamic viscosity at zero shear. It is worth noting that the calculated hydrodynamic diameter is inversely proportional to viscosity. Therefore, errors in viscosity estimation are manifested directly by proportional errors in the calculated hydrodynamic diameter.

Furthermore, this equation assumes that particles undergoing Brownian motion are non-interacting spheres, so careful attention must be paid to determine a concentration regime to ameliorate the influence of particle interactions and multiple scattering events. Measuring the z-average particle size as a function of concentration (Figure) revealed that the calculated diameter remained relatively constant (±5 nm) from 0.01 – 1.0 mg mL^{-1}. Furthermore, this concentration range agrees with the linear region

identified in Figure B.3, where the instrument count rate (kcps) is directly related to the concentration. Following this analysis, 0.5 mg mL^{-1} polymer solutions were used for subsequent light scattering studies.

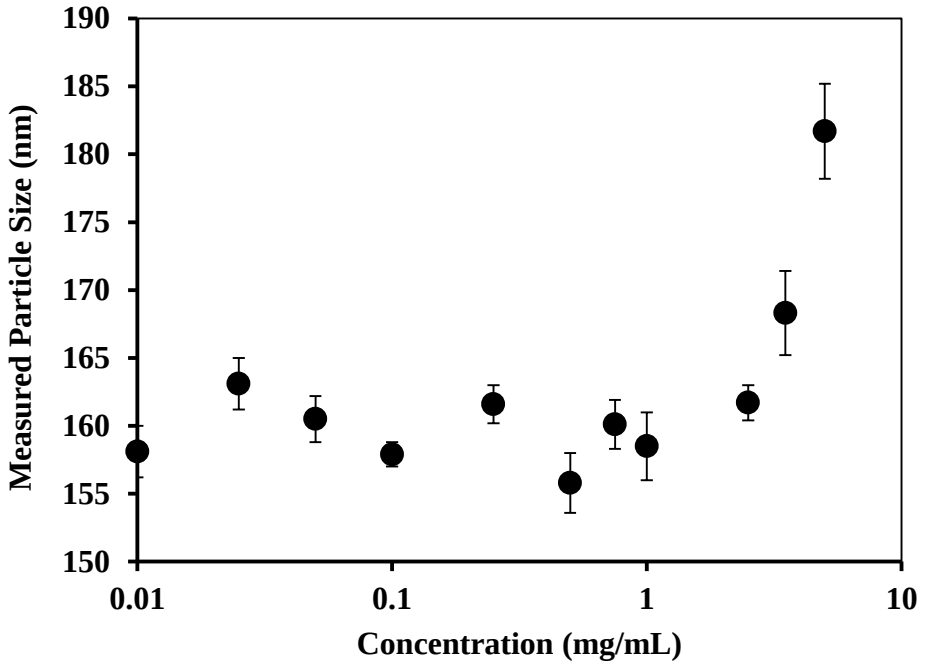

Figure B.2 - Z-average diameter of representative nanoscale hydrogels in PBS at variable concentration.

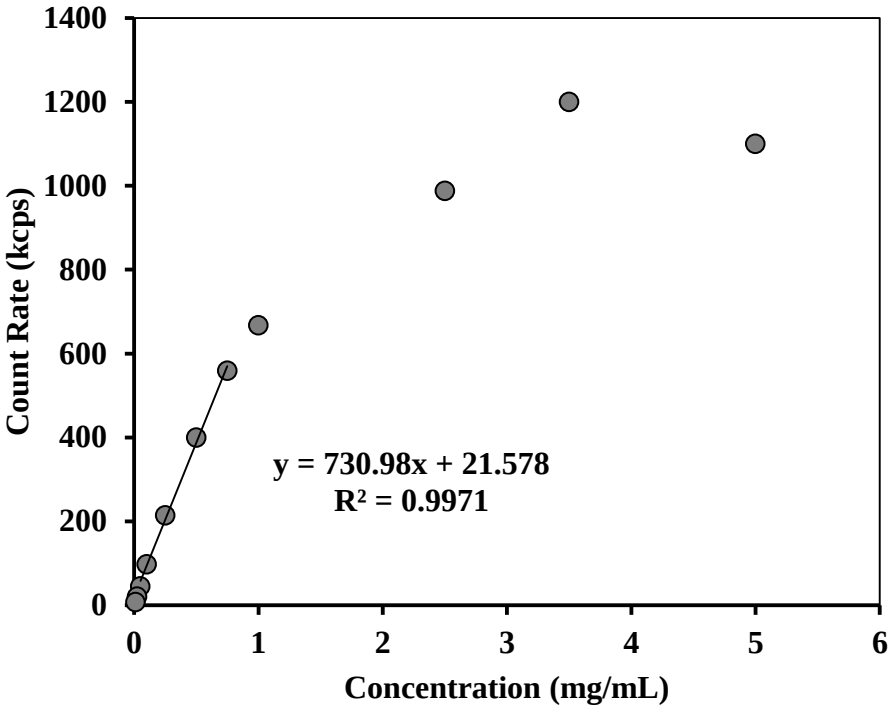

Figure B.3 - Count rate (kcps) as a function of particle concentration. In the concentration range where z-average size is independent of concentration, count rate exhibits a linear dependence.

References

Brandup, J. and E. H. Immergut, Eds. (1989). Polymer Handbook

New York, John Wiley and Sons.

APPENDIX C: GATING STRATEGY FOR IMAGING FLOW CYTOMETRY

This appendix describes the sequential gating strategy employed to analyze images in the mechanistic study of cellular internalization (Chapter 6) and later in the RNA internalization studies (Chapters 6 – 8). In the subsequent sections, named populations selected by gating are denoted in quotations (e.g. "Cells", "Single Cells", etc.)

Cell and Debris Discrimination

"Cells" were separated from debris by gating according to side scatter (a measure of cell complexity or granularity) vs. brightfield area, as shown in Figure C.1.

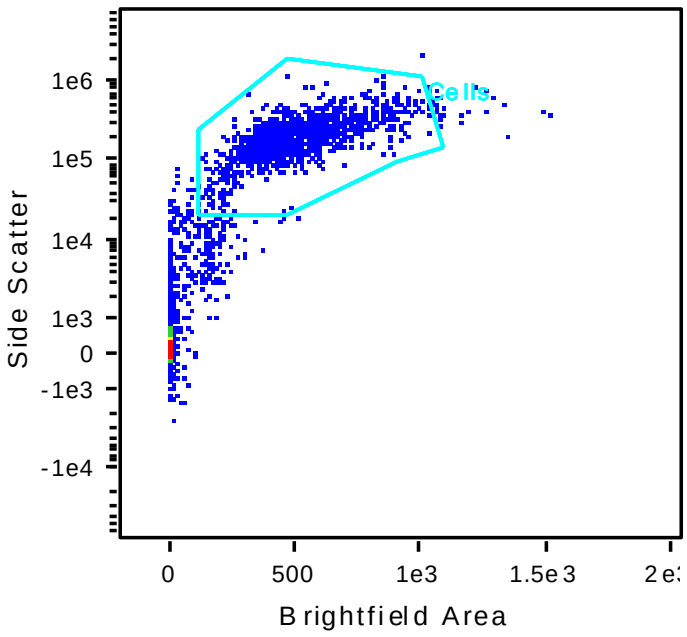

Figure C.1. – Side scatter vs. Brightfield area of Caco-2 cells in Imaging flow cytometry.

Single Cell and Multi-Cell Discrimination

From the "Cells" population, "Single Cells" were selected by examining the brightfield aspect ratio vs. brightfield area. Typically, single cells have a high aspect ratio (0.8 – 1.0) and moderate area (300 – 700 μm^2) for Caco-2 cells or 200 – 500 μm^2 for RAW cells.

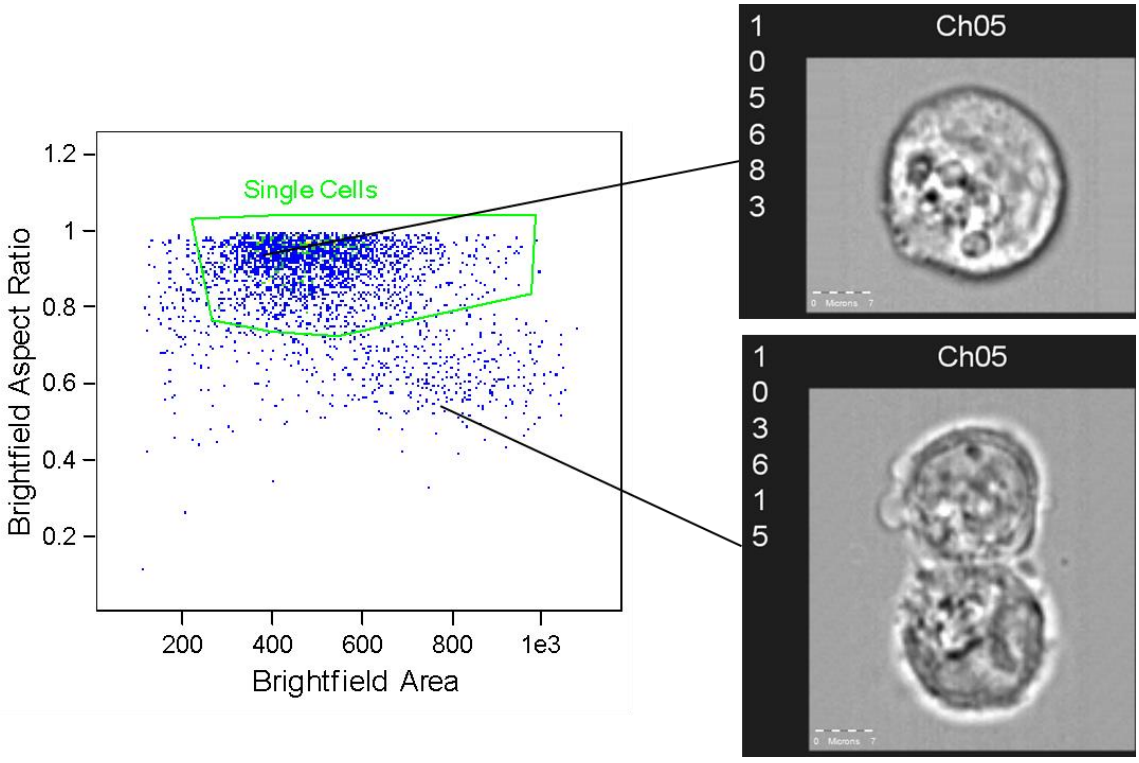

Figure C.2. – Aspect Ratio vs. Area for separating single cells from aggregates or clumps.

Focused Cell Discrimination

To discriminate between focused and unfocused "Single Cells", the Gradient RMS feature in IDEAS® software was used. This feature measures image sharpness by examining large changes in pixel values of a given image. Sharp, or in-focus, images will have characteristically higher Gradient RMS values. Typically, the lower limit for Gradient RMS was set to 40. Images with Gradient RMS of 40 and greater form the population "Focused Cells". At camera magnification used for these studies (60×), the depth of field is 2.5 µm. Thus, if the outer circumfrence of a given cell is in focus, the focal plane represents a 2.5 µm slice through the center section of the cell.

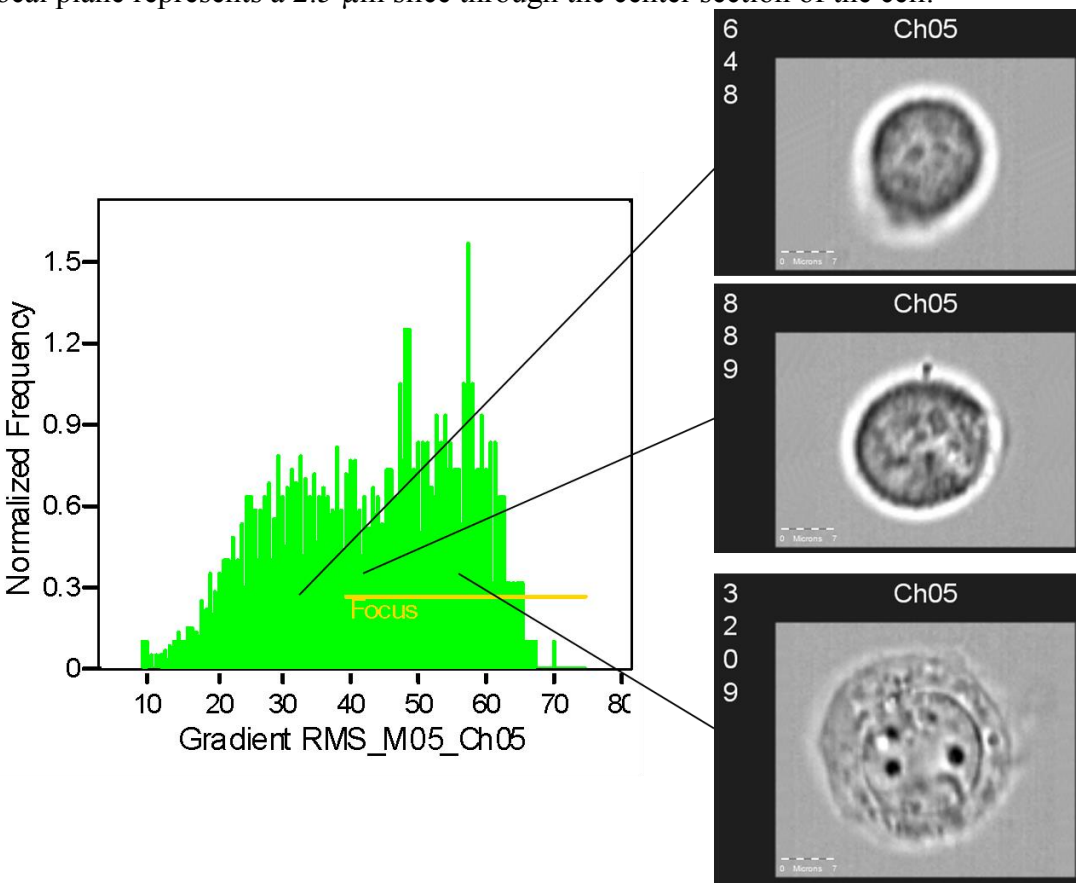

Figure C.3. – Discrimination between focused and unfocused cells according to their brightfield Gradient RMS feature.

LIVE/DEAD DISCRIMINATION

To separate live cells from dead or dying cells, propidium iodide was added to the cell suspensions as a live/dead discriminator. Propidium iodide is impermeable to live cell membranes and thus will present only in dead or dying cells with compromised membrane integrity. In a typical flow cytometry run, "Live Cells" formed approximately 90% of the single, focused cell population.

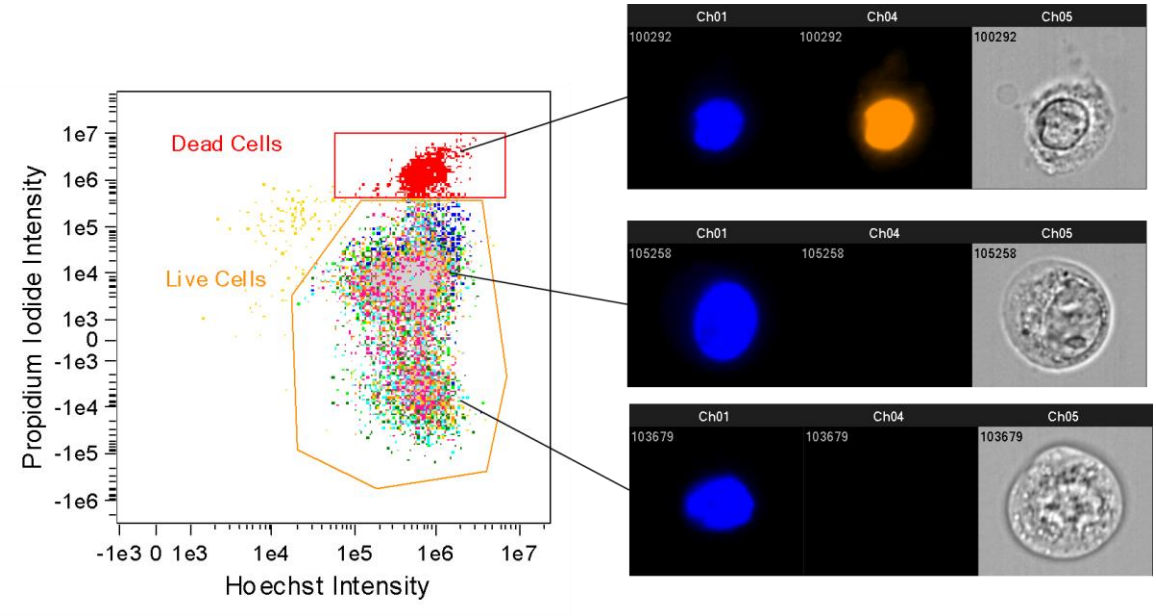

Figure C.4. – Live/dead discrimination of Caco-2 cells using propidium iodide fluorescence.

APPENDIX D: CONTROLLED DRUG DELIVERY FROM ALGINATE SPHERES IN A DESIGN-BASED LEARNING COURSE

AC 2012-5008: CONTROLLED DRUG DELIVERY FROM ALGINATE SPHERES IN DESIGN-BASED LEARNING COURSE

Dr. Steve R Marek, University of Texas, Austin

Steve R. Marek is a lecturer in the Department of Biomedical Engineering at the University of Texas, Austin. He received a B.S. in chemical and biomolecular engineering with a minor in biomedical engineering at the Georgia Institute of Technology in 2005. He earned a Ph.D. in chemical engineering at the University of Texas, Austin, in 2009 and transitioned to the College of Pharmacy, Division of Pharmaceutics, for his postdoctoral research in pulmonary drug delivery. He began his career as a teaching faculty member at the University of Texas, Austin, in 2011. Marek's primary teaching responsibilities comprises the biomedical engineering laboratory courses. His previous research interests included small-molecule organic synthesis, intelligent hydrogels for controlled drug delivery, pulmonary drug delivery, and materials characterization.

Mr. William Liechty, University of Texas, Austin

William B. Liechty is a NSF Graduate Research Fellow in the Department of Chemical Engineering at the University of Texas, Austin, conducting research under the direction of Prof. Nicholas Peppas. He received a B.S.E. in chemical engineering from the University of Iowa in 2007 and studied at the University of Cambridge as a Gates Scholar until 2008. His research interests include responsive materials, RNA interference, and intracellular delivery of biological therapeutics.

Dr. James W. Tunnell, University of Texas, Austin

James W. Tunnell is an Associate Professor in the Department of Biomedical Engineering at the University of Texas, Austin. He earned a B.S. in electrical engineering from the University of Texas, Austin, in 1998, and a Ph.D. in bioengineering from Rice University in 2003. He was awarded a National Research Service Award from the NIH to fund his postdoctoral fellowship in the Spectroscopy Laboratory at the Massachusetts Institute of Technology from 2003-2005. He joined the faculty of the University of Texas in the fall of 2005. Tunnell's research focuses in the broad field of biomedical optics with a specific focus on using optical spectroscopy and imaging for disease diagnosis and treatment, particularly that of cancer. Tunnell has received the following awards/honors: Outstand BME Graduate Alumnus from Rice University (2010), Coulter Fellow (2010), Ralph E. Powe Junior Faculty Enhancement Award from the Oak Ridge Associated Universities (2007), Early Career Award from the Wallace H. Coulter Foundation (2008, 2006), National Research Service Award from the NIH (2004), and Best Basic Science Paper from the American Society for Laser Medicine and Surgery (2000). He has published 30 refereed journal articles, presented at more than 70 international and national conferences, and edited one book. He is an Associate Editor for the Annals of Biomedical Engineering. He has served on the program committees for CLEO, OSA, and IEEE-LEOS, and he is the General Chair of 2012 CLEO annual meeting. He is a member of OSA, ASLMS, IEEE-EMBS, and BMES.

Controlled Drug Delivery from Alginate Spheres in Design-Based Learning Course

Abstract

Engineering design is a central concept driving our engineering curriculum and an integral component of the practice of engineering. Frequently, design concepts are not introduced in Biomedical Engineering at the university level until the last year of the undergraduate curriculum, generally in the form of a Senior Design course. Though students have been widely exposed to the scientific method, many reach their senior year in college surprised to find out that a design method also exists. Design is characterized by an iterative sequence of steps that involve identifying a need, defining the problem, developing solutions, evaluating solutions, and communicating results and recommendations. Seniors consistently requested, through exit surveys, introduction to design earlier in their academic experience. Furthermore, earlier introduction to design has also recently been recognized as a retention tool of engineering students[1] because they are able to understand the dynamic and creative nature of engineering, a topic often lost in the first two years of engineering.

In order to provide early and consistent exposure to the engineering design process, we have implemented a design-based laboratory course featuring experiments in biomaterials design and drug delivery. Controlled drug delivery is an important application of biomedical engineering incorporating key aspects of mass transport, physiology, and biomaterials. This lab segment, which spanned five laboratory sections and four 1 hour lectures, led the students through the design, synthesis, and characterization of a particle-based matrix drug delivery device using ionically-crosslinked alginate spheres and several model drugs, fluorescein, tartrazine, erythrosin B, and bovine serum albumin. The experimental portion of the module included the synthesis of crosslinked alginate spheres of differing sizes, automated sizing of the spheres using microscopy and ImageJ, loading of a model drug into the spheres using equilibrium sorption or dispersed encapsulation, and the quantification of the dye release using absorbance on a UV/Vis plate reader. Students were evaluated by review of their laboratory notebooks, including methods, observations, calculations, and relevant plots. Additionally, assigned background research, which consisted of sourcing information from scientific literature and online resources, was recorded in the notebook.

Ultimately, this course is an interesting approach to provide the first-year students an overview of what the biomedical engineering field encompasses by providing hands-on experience in several different areas of research and getting the students excited about their field of study. Analysis of course surveys revealed a significantly greater perceived course value relative to the previous seminar-based course.

Introduction

Engineering design is the central, overarching concept driving our engineering curriculum and the broader practice of engineering; however, design concepts previously were not introduced in Biomedical Engineering (BME) at the University of Texas at Austin until the senior year. While students have been exposed to the "scientific method" since grade school, many of these students reach their senior year in college surprised to find out that a "design method" also exists. Design is characterized by an iterative sequence of steps that involve identifying a need, defining the problem, developing solutions, evaluating solutions, and communicating results. Exiting seniors, via surveys, consistently request introduction to design earlier in their academic experience. Earlier introduction to design has also recently been recognized as a retention tool of engineering students[1] because they are able to understand the dynamic and creative nature of engineering, a topic often lost in the first two years of engineering curriculum that is heavy on basics such as mathematics and physics. Increasing enrollment and retention in engineering has been a major focus of the NSF in an effort to keep the US technologically competitive.

Course Description

BME 102L, Principles of Biomedical Engineering Design Lab, is a new freshman design course intended to introduce incoming students to the field of biomedical engineering while concurrently introducing them to engineering design at the forefront of their engineering education. The course, having just completed its second year of implementation, features a one-hour lecture and a three-hour laboratory period each week for 15 weeks. The students work in teams of 3-4, gaining valuable team-building skills; however, the primary objective of this course is to apply a systematic set of engineering design skills to bring a "real world" biomedical project to a working prototype.

This course has replaced the previous course, BME 102, Principles of Biomedical Engineering. The previous course was strictly a one-hour lecture, once a week, with no laboratory component. While the old course still provided an introduction to BME for freshmen, it neither provided hands-on nor design-based learning. Lectures were generally provided by guest speakers, which included active faculty in the department, and had the format of a seminar series. Common lecture topics included current research and general BME topics.

The primary learning objectives of this course are:

- Broad understanding of the BME discipline
- Familiarization with the engineering design paradigm
- Hands-on and problem-based learning
- Development of team-building skills
- Recognition of creativity in engineering design

The drug-delivery module is the first of three sections in this new course, which leads the freshmen students through several aspects of design in the biomedical engineering field, and exposes them to all three tracks in The University of Texas at Austin BME department. Since this module is the first in the series, it has the most rigorous (*i.e.* least open-ended) project guidelines. The students are introduced to the concept of engineering design, but in a directed manner. Unlike the later modules where each group has its own distinct solution to the problem

statement, this first module has only a handful of appropriate solutions. The second and third modules are prosthetics (using Lego NXT and LabVIEW) and cochlear implants (signal analysis and computation). In these later modules, the student teams are able to design novel solutions to provided problem statements.

The students are immediately introduced to the concept of the engineering design method. In the first lecture, they are asked to describe the difference between science and engineering, and examples of science discoveries vs engineering accomplishments. They are then led through the components of a typical design process (*e.g.* a home-use medical thermometer) with each step of the process explained and illustrated with examples. This newfound knowledge is then applied in the first laboratory session, where they are tasked with designing a controlled-release drug-delivery system. The next several lectures cover topics necessary to understand the laboratory experiments, such as absorption spectroscopy, Fick's Law, etc for the drug-delivery module. Throughout the semester, notebook maintenance is explained and emphasized, and the students are periodically provided feedback on the quality of their notebook recordings.

Drug-Delivery Module

The problem statement provided to the students requires them to develop a drug delivery system for the controlled release of a drug to treat a specific disease. Previous diseases used were type I diabetes and multiple sclerosis. The goal of a controlled drug-delivery device is to allow the drug concentration to be within the therapeutic window (Fig 1) for the maximum amount of time necessary for treatment of the disease. A typical dosing, whether it be via oral ingestion or IV, experiences a concentration profile similar to the burst release depicted below. The amount of time that the concentration of drug falls within the therapeutic window is relatively small. Thus, designing a controlled-release device that can provide delivery of the drug over a longer time period is typically desired. In this lab module, the students were asked to design a system that would follow the controlled release profile.

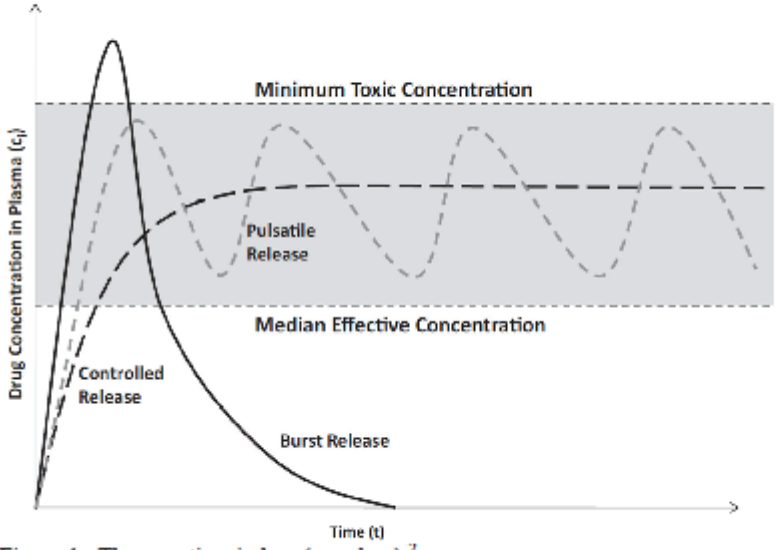

Figure 1. Therapeutic window (gray box).[2]

An outline of the laboratory part of the drug-delivery module from this class is below.

Lab 1: Planning

1. **Problem Definition.**
   - **a.** *Background research*. The students answered such questions as what are the symptoms and health effects of the disease? What are the causes and current treatments?
   - **b.** *Project Mission*. The students defined their specific design goals by a) concisely defining the product in one sentence, b) identifying the market opportunity for such a product, and c) identifying the customers and stakeholders.
   - **c.** *Product Specifications*. The students defined, quantitatively, what the product will do. They identified specific customer needs, product specifications (*e.g.* drug blood half-life, delivery method, etc.), and system constraints.
2. **Solution Development**
   - **a.** The students, as a team, developed three potential drug delivery solutions to meet the specifications identified in part 1. This section was a thought experiment, whereby the teams tried to identify the most realistic and effective drug delivery method.

Lab 2: Bead Synthesis

1. **Diffusion.** The students were asked to share their design solutions from the previous lab. The instructor provided feedback on why certain ideas may or may not work, and then led the students towards using spherical beads for controlled drug release. Diffusion and Fick's Law were introduced by the instructor.

2. **Bead Fabrication.** The students synthesized their alginate beads, as detailed below, including making the stock solutions of sodium alginate and calcium chloride, extruding the alginate solution, and filtering/collecting the neat beads. All materials and methods were recorded.
3. **Analysis.** The students were tasked with analyzing what they had just performed, in the context of controlled delivery via diffusion. They identified the physical parameters of Fick's Law and what might affect these values (*e.g.*, volume-to-surface-area, molecular weight, etc).

Lab 3: Sizing, Calibration, Drug Loading

1. **Bead Sizing.** The students were introduced to microscopy, image capture, and ImageJ image analysis.
2. **Calibration Curves.** The students were introduced to spectroscopy, Beer's Law, and serial dilutions for calibration curves.
3. **Drug Loading.** Since most students synthesized neat alginate beads, the drug was loaded via equilibrium sorption over the course of one week.

Lab 4: Drug Release

1. **Drug Release Profile.** The students collected samples of the release medium at specified time intervals to determine the release profile of their drug. After collecting all time points, the absorbance was measured on a spectrophotometer and the students converted the absorbances to drug concentrations from their calibration curve.
2. **Analysis.** The students had to objectively determine the success of their drug delivery device, based on their pre-determined product specifications. They were also tasked with repeating the design iteration (virtually), by identifying what changes could be made to the existing product in order to obtain the desired results.

Drug-Delivery Experimental Procedure

Initially, the students were tasked with creating an open-ended solution to the delivery of a drug to treat a certain disease. They were required to consult *reliable* internet sources to determine the design specifications necessary to provide a useful treatment for the disease. The students, as a team, had to incorporate all of these design specifications in to a possible drug delivery device. Some students proposed ideas similar to insulin pumps, others described skin patches, and yet others designed oral delivery agents. These ideas were shared with the class and discussed. However, the instructor directed the students towards using alginate beads as a simple method for building a controlled drug-delivery device. The positive and negative aspects of such a device were discussed (*e.g.*, the ease of administration vs. the limitations due to drug stability in the stomach).

Since the students had not taken previous drug delivery or transport courses, it was necessary to introduce these concepts in lecture and during lab. It was assumed that students had been introduced to neither diffusion nor Fick's Law, but that all students were familiar with derivatives (calculus is expected to be taken concurrently). A simple introduction to polymers and diffusion through polymers (matrix versus reservoir devices) was provided, and the students

were shown the Ritger-Peppas approximation[5] for diffusion out of a matrix device. The students were later encouraged to try to fit the Ritger-Peppas equation to their data.

The alginate beads were synthesized similar to previously published methods.[3] Sodium alginate was dissolved in distilled water (dH2O) at 2% (w/v). Slowly adding the alginate to a stirring beaker of water reduced the clumping of the alginate. This solution was then extruded through a needle via syringe into a 2% (w/v) calcium chloride solution. Different needle gauges (18, 20, 30) were used to provide beads of different sizes.

The beads were sized using a microscope and image analysis software (ImageJ[4]), and then loaded with "drug" via equilibrium partitioning over the course of a week. The chosen drugs were Erythrosin B, Tartrazine, Fluorescein, and bovine serum albumin (BSA).

The following week, the drug was released into a beaker and samples were taken at specified time intervals (1, 2, 3, 5, 7, 10, 15, 20, 25, 30, 45, 60, 75, 90, 120 min). A calibration curve of the drug was obtained from a serial dilution and the drug concentration was quantified by spectrophotometry (96-well plate reader). Curves showing the release profile were analyzed to determine if they met the required design specifications; if the profile did not meet the requirements, then adjustments were proposed to the bead delivery system.

Assessment

There were four main methods of assessment throughout the course, as shown in Table 1. Since most students taking the course are in their first college semester, good laboratory notebook habits were heavily stressed. The students were instructed to record everything in their notebooks including the description of the problem, materials and methods, data, and answers to analysis questions. By the end of the drug-delivery module, the students were expected to include graphs of their calibration curve as well as the release profile of their drug in their notebooks.

The other three grading criteria were participation, written summaries, and in-class assignments. The participation grade was included to ensure that the students arrived to the laboratory on time; even with a penalty in place, there were several instances of students arriving late to the 9:00 AM lab sessions. The written summaries included analysis of the performance of their designs. The in-class assignments included answers to questions posed to the students, such as at the beginning of each design project, where the students were required to identify the specifications and constraints of the system in question.

Table 1: Grading Criteria for BME 102L

Grading Criteria	**Percentage**
Design Notebook	20
Professional Participation	10
Written Summaries & Demos	30
In-Class Assignments	40

Results and Discussion

The "drug" compounds used were Erythrosin B, Tartrazine, Fluorescein, and BSA. It should be noted that the first three compounds are dyes approved by the FDA. All chemicals used during this experimental module are safe, presenting no safety issues to the students other than accidental clothing or skin staining. The safety of these compounds is very important, since very few of the students have had significant previous laboratory experience and therefore spillage of a toxic compound could be quite dangerous for them. Disposal of each component during this experiment was also easy due to the lack of toxicity.

Sodium alginate is the sodium salt of alginic acid, an anionic polysaccharide. Calcium, a divalent positive ion, has the ability to crosslink two carboxylic moieties of alginate molecules; upon contact with a calcium chloride solution, the alginate crosslinks and forms a hydrogel.

The students generally had very little trouble synthesizing the beads. However, if the students added the entire mass of sodium alginate to the beaker of water, the alginate would clump and it would take a very long time to fully dissolve. This problem was prevented by slowly adding the alginate over the course of about 20 min. Synthesis of beads using the 18g and 20g needles was fairly straightforward. The 30g needle, however, provided a substantial resistance; it was determined that shorter needles made this step much easier, and as such 0.5 in needle lengths were used.

Typical imaging and sizing of the beads yielded the values listed in Table 2. The largest difference in bead diameters was between the 18 g and 30 g needles (2.56 mm and 1.31 mm, respectively). Some students had difficulty with the "Particle Sizing" macro in ImageJ; this difficulty was typically due to poor image quality. The particles needed to not be touching each other. The particles also needed to be illuminated from below, to prevent shadows, and to provide a dark outline surrounding the bead. The images of beads shown in Figure 2 were suitable for standard image analysis on ImageJ. The only complications during construction of

the calibration curves were due to misunderstandings of how a pipette works or carelessness during the serial dilutions.

Table 2. Alginate Bead Sizing

Size	Small	Medium	Large
Needle Gauge	30	20	18
Effective Diameter (mm)*	1.31 ± 0.04	2.21 ± 0.02	2.56 ± 0.04

*Mean diameter represents effective spherical diameter calculated from ImageJ sizing algorithm ± standard error of the mean (sem).

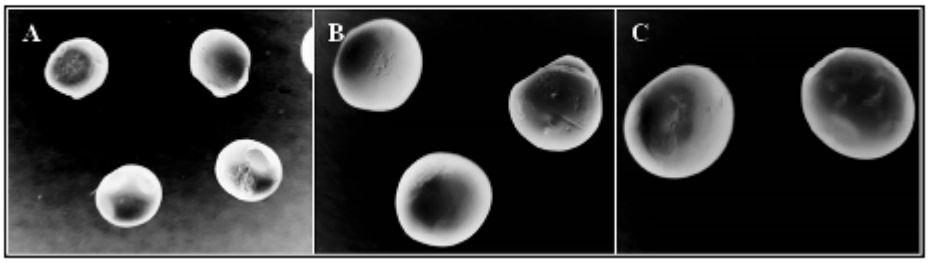

Figure 2. Optical micrographs of sodium alginate beads crosslinked with calcium chloride. (A) 30G, Small, (B) 20G, Medium, and (C)18G, Large needles.

After allowing the beads to absorb the drug for a week, the students then measured the release of the drug into a beaker of water. The time points were chosen to ensure that the beginning of the release profile, where there is a larger change in concentration, had sufficient data points to allow curve fitting. During the lecture portion of the course, the students were introduced to Fick's Law as well as some of the simplified solutions to Fick's Law for spherical matrix drug delivery devices. At early time points, the Ritger-Peppas equation[5] can be used ($\frac{M_t}{M_\infty} < 60\%$):

$$\frac{M_t}{M_\infty} = kt^n \qquad (1)$$

where M_t is the mass released at a given time t, M_∞ is the mass released at time infinity, k is a lumped parameter which includes the diffusion coefficient and other system-defining parameters, and n is the power parameter which accounts for the shape of the delivery device (0.5 for a slab, 0.46 for a cylinder, and 0.43 for a sphere). The value of n will only be 0.43 under ideal conditions, no swelling, and with a monodisperse particle size. This model is simple to employ, since Excel has a built-in power-law curve fitting utility; the students did not have to be extremely well-versed in Excel to accomplish this fitting.

An alternative model of drug release can be used instead; this model has an equation for both early time points[6] ($\frac{M_t}{M_\infty}$ < 60%) and late time points[7] ($\frac{M_t}{M_\infty}$ > 40%). For early time points,

$$\frac{M_t}{M_\infty} = 6\left(\frac{Dt}{\pi r^2}\right)^{1/2} - 3\left(\frac{Dt}{r^2}\right) \quad (2)$$

where D is the diffusion coefficient and r is the radius of the bead. For late time points,

$$\frac{M_t}{M_\infty} = 1 - \frac{6}{\pi^2} exp\left(-\frac{\pi^2 Dt}{r^2}\right). \quad (3)$$

Figure 3 shows the release profile of Erythrosin B from medium alginate beads (extruded through a 20g needle) which were subjected to one of three different drug-loading concentrations: 1.0 mg/mL, 0.3 mg/mL, or 0.1 mg/mL. Equations 2 and 3 were used to fit both the early and late time points of the release data, using Excel to do a manual curve fit. Because the volume of the release media was relatively constant throughout the entire experiment (ca. 100 mL), the conversion between mass and concentration was simply

$$C = \frac{M}{V}. \quad (4)$$

M_∞ was taken as the mass released once the value stopped changing for several time points in a row (ca. 2-3 hr), and the radius of the particles was measured via microscopy. This equation was then solved for *D* to obtain a diffusion coefficient of the model drug in alginate. It can be seen that the diffusion coefficient is a function of concentration. This exercise also illustrates the effect that loading concentration can have on a drug delivery device.

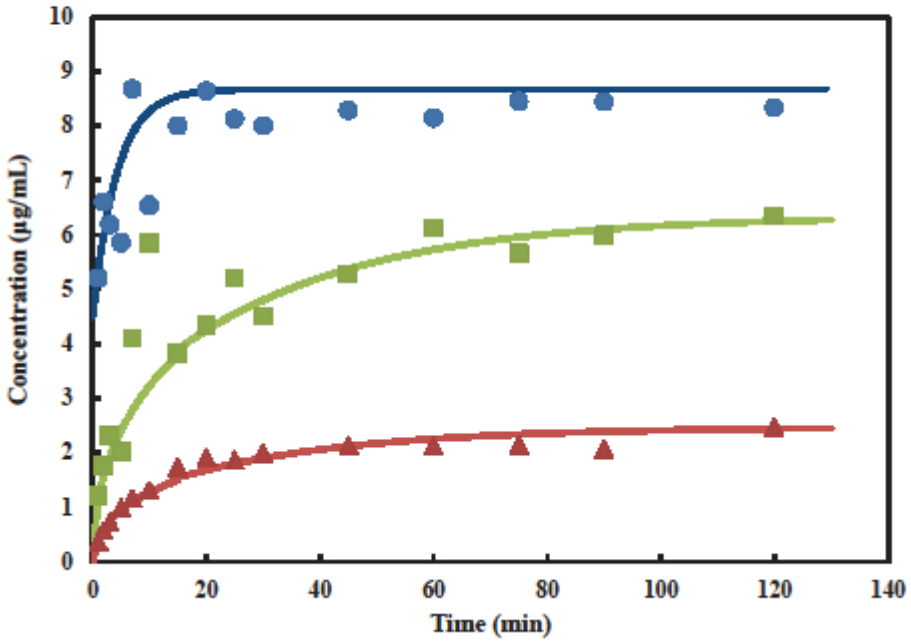

Figure 3. Release of Erythrosin B from alginate beads (size medium). The drug was loaded into the beads via equilibrium partitioning with concentrations of 1.0 mg/mL (●), 0.3 mg/mL (■), and 0.1 mg/mL (▲). Lines are curve fits from equations 2 and 3.

The course has just completed its second year (it is only offered in the Fall), and overall it has been well received by the students. Student comments were nearly exclusively positive, such as "awesome class." Other students provided more useful feedback such as "this design lab was the perfect introduction course to BME. It really helped me understand the details of each track, and each lab was extremely interesting."

The course instructor survey results also showed that the students enjoyed BME 102L. The students were presented with several questions at the end of the semester and asked to rank each on a scale of 1 to 5 where the meanings of 1 to 5 are described below. Many of the questions were related to the performance of the professor himself, but the response to three questions related to the course content are graphed below. These questions were

1. At this point in time, I feel that this course will be (or has already been) of value to me.
    i. Strongly disagree
    ii. Disagree
    iii. Neutral
    iv. Agree

v.Strongly agree

2. Overall, this course was …
   i.Very unsatisfactory
   ii.Unsatisfactory
   iii.Satisfactory
   iv.Very good
   v.Excellent
3. In my opinion, the workload in this course was …
   i.Excessive
   ii.High
   iii.Average
   iv.Light
   v.Insufficient

Based on the available options, for questions 1 and 2, higher numerical values indicate that more students felt the course was a useful or good course. For question 3, a value closer to 3 indicates that more students thought the course workload was fair. The survey results from five years of BME 102 (non-lab, non-design) were averaged and compared to the two years of BME 102L; these data are shown below in Figure 4. There was a statistical significance between the student opinions of BME 102 and 102L; overall, the students that took 102L thought the course was more valuable to them than those that took 102. Also, since 102 was merely a seminar course, the students felt that the workload was insufficient whereas those that took 102L felt that the course workload was more sufficient for a college-level class. There is currently no data indicating how well the students learned the design method; an exam will be implemented in the next iteration of the course to provide a more quantitative assessment. Also, since this course has only been taught since 2010, it is still unknown how it may affect retention.

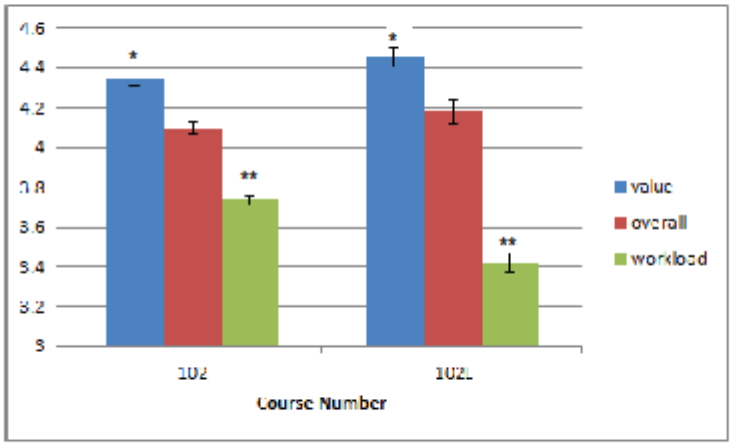

Figure 4. Course instructor survey results for BME 102 (seminar) and BME 102L (lab). The higher the numerical score for Value and Overall, the better the course. The closer the numerical score to 3 for Workload, the better the course. Error bars are ± SEM. * and ** indicate statistical significance with $p < 0.05$.

Given adequate resources in terms of stir plates, pipettes, beakers, etc. it is conceivable that each student could test an independent variable, such as bead size, chemical nature/MW of model drug, and crosslinking time. This level of flexibility and versatility allows the lab module to be uniquely tailored to institutional situation. Furthermore, the experimental degrees of freedom in this exercise provides a useful exercise in experimental design; to intelligently select the experimental conditions to uncover and support empirical trends.

Conclusions

A laboratory module consisting of the design and synthesis of a controlled drug delivery device was described. The assessment methods and student reception to the new module were also detailed. This module provides a safe means for students to learn about Fickian diffusion, spectroscopy, and polymers for use in a controlled drug-delivery device, while also learning about the engineering design process. We believe that this guided introduction to the engineering design method assisted the students in future class modules by providing them with both the framework necessary to approach an engineering design problem and an example solution to such a problem. Future iterations of the course, as well as surveys of previous students, will provide more insight into the students' grasp of design and retention in engineering.

References

1. Monroe, T.W., Mailander, M. & Lima, M. A Freshman Engineering Program in Biological & Agricultural Engineering. ***Int J Engng Ed*** **22**, 1129-1138 (2006).
2. Liechty, W.B., Kryscio, D.R., Slaughter, B.V. & Peppas, N.A. Polymers for Drug Delivery Systems. ***Annual Review of Chemical and Biomolecular Engineering*** **1**, 149-173 (2010).
3. Bayer, C.L., Herrero, É.P. & Peppas, N.A. Alginate Films as Macromolecular Imprinted Matrices. ***Journal of Biomaterials Science, Polymer Edition*** **22**, 1523-1534 (2011).
4. Abramoff, M.D., Magalhães, P.J. & Ram, S.J. Image processing with ImageJ. ***Biophotonics international*** **11**, 36-42 (2004).
5. Ritger, P.L. & Peppas, N.A. A simple equation for description of solute release II. Fickian and anomalous release from swellable devices. ***Journal of Controlled Release*** **5**, 37-42 (1987).
6. Crank, J. ***The mathematics of diffusion***. (Clarendon Press: 1979).
7. R. Baker, H. Lonsdale. ***Controlled release: mechanisms and rates***. A. Tanqueray, R. Lacey (Eds.), Controlled Release of Biologically Active Agents, Plenum, New York (1974)

References

Alarcon, C. D. H., S. Pennadam, and C. Alexander. 2005. "Stimuli responsive polymers for biomedical applications." *Chemical Society Reviews* no. 34 (3):276-285. doi: Doi 10.1039/B406727d.

Alexandridis, P., J. F. Holzwarth, and T. A. Hatton. 1994. "Micellization of poly(ethylene oxide)-poly(propylene oxide)-poly(ethylene oxide) triblock copolymers in aqueous solutions - thermodynamcis of copolymer association." *Macromolecules* no. 27 (9):2414-2425.

Alexis, F., E. Pridgen, L. K. Molnar, and O. C. Farokhzad. 2008. "Factors affecting the clearance and biodistribution of polymeric nanoparticles." *Molecular Pharmaceutics* no. 5 (4):505-515. doi: Doi 10.1021/Mp800051m.

Amalvy, J. I., E. J. Wanless, Y. Li, V. Michailidou, S. P. Armes, and Y. Duccini. 2004. "Synthesis and Characterization of Novel pH-Responsive Microgels Based on Tertiary Amine Methacrylates." *Langmuir* no. 20 (21):8992-8999. doi: 10.1021/la049156t.

Ameres, S. L., J. Martinez, and R. Schroeder. 2007. "Molecular basis for target RNA recognition and cleavage by human RISC." *Cell* no. 130 (1):101-112. doi: DOI 10.1016/j.cell.2007.04.037.

Angelova, M. I., and D. S. Dimitrov. 1986. "Liposome Electroformation." *Faraday Discussions* no. 81:303-+. doi: Doi 10.1039/Dc9868100303.

Aouadi, Myriam, Gregory J. Tesz, Sarah M. Nicoloro, Mengxi Wang, My Chouinard, Ernesto Soto, Gary R. Ostroff, and Michael P. Czech. 2009. "Orally delivered siRNA targeting macrophage Map4k4 suppresses systemic inflammation." *Nature* no. 458 (7242):1180-1184.

Avgoustakis, K., A. Beletsi, Z. Panagi, P. Klepetsanis, E. Livaniou, G. Evangelatos, and D. S. Ithakissios. 2003. "Effect of copolymer composition on the physicochemical characteristics, in vitro stability, and biodistribution of PLGA–mPEG nanoparticles." *International Journal of Pharmaceutics* no. 259 (1–2):115-127. doi: http://dx.doi.org/10.1016/S0378-5173(03)00224-2.

Bae, Y., S. Fukushima, A. Harada, and K. Kataoka. 2003. "Design of environment-sensitive supramolecular assemblies for intracellular drug delivery: Polymeric

micelles that are responsive to intracellular pH change." *Angewandte Chemie-International Edition* no. 42 (38):4640-4643. doi: DOI 10.1002/anie.200250653.

Bae, Y. H., T. Okano, R. Hsu, and S. W. Kim. 1987. "Thermosensitive Polymers as on-Off Switches for Drug Release." *Makromolekulare Chemie-Rapid Communications* no. 8 (10):481-485.

Bae, Y. H., T. Okano, and S. W. Kim. 1990. "Temperature-Dependence of Swelling of Cross-Linked Poly(N,N'-Alkyl Substituted Acrylamides) in Water." *Journal of Polymer Science Part B-Polymer Physics* no. 28 (6):923-936.

Banquy, X., F. Suarez, A. Argaw, J. M. Rabanel, P. Grutter, J. F. Bouchard, P. Hildgen, and S. Giasson. 2009. "Effect of mechanical properties of hydrogel nanoparticles on macrophage cell uptake." *Soft Matter* no. 5 (20):3984-3991. doi: Doi 10.1039/B821583a.

Bartlett, Derek W., and Mark E. Davis. 2006. "Insights into the kinetics of siRNA-mediated gene silencing from live-cell and live-animal bioluminescent imaging." *Nucl. Acids Res.* no. 34 (1):322-333. doi: 10.1093/nar/gkj439.

Beltran, Sagrario, John P. Baker, Herbert H. Hooper, Harvey W. Blanch, and John M. Prausnitz. 1991. "Swelling equilibria for weakly ionizable, temperature-sensitive hydrogels." *Macromolecules* no. 24 (2):549-551. doi: 10.1021/ma00002a032.

Bernstein, E., A. A. Caudy, S. M. Hammond, and G. J. Hannon. 2001. "Role for a bidentate ribonuclease in the initiation step of RNA interference." *Nature* no. 409 (6818):363-366.

Bhattarai, Narayan, Hassna R. Ramay, Jonathan Gunn, Frederick A. Matsen, and Miqin Zhang. 2005. "PEG-grafted chitosan as an injectable thermosensitive hydrogel for sustained protein release." *Journal of Controlled Release* no. 103 (3):609-624.

Bhavsar, Mayank D., Shenoy, Dinesh B., Amiji, Mansoor M. 2006. "Polymeric Nanoparticles for Delivery in the Gastro-Intestinal Tract." In *Nanoparticulates as Drug Carriers.* edited by V.P. Torchilin. London: Imperial College Press.

Blanchette, J., and N. A. Peppas. 2005. "Oral chemotherapeutic delivery: Design and cellular response." *Annals of Biomedical Engineering* no. 33 (2):142-149. doi: 10.1007/s10439-005-8973-8.

Bohdanowicz, M., G. Cosio, J. M. Backer, and S. Grinstein. 2010. "Class I and class III phosphoinositide 3-kinases are required for actin polymerization that propels phagosomes." *Journal of Cell Biology* no. 191 (5):999-1012. doi: DOI 10.1083/jcb.201004005.

Boussif, O., F. Lezoualch, M. A. Zanta, M. D. Mergny, D. Scherman, B. Demeneix, and J. P. Behr. 1995. "A versatile vector for gene and oligonucleotide transfer into cells in culture and in-vivo - polyethyleneimine." *Proceedings of the National Academy of Sciences of the United States of America* no. 92 (16):7297-7301.

Boyne, A. F., and G. L. Ellman. 1972. "Methodology for Analysis of Tissue Sulfhydryl Components." *Analytical Biochemistry* no. 46 (2):639-&.

Brandup, J, and E.H. Immergut. 1989. 3 ed, *Polymer Handbook*

New York: John Wiley and Sons.

Brannon-Peppas, L., and N. A. Peppas. 1991. "Equilibrium Swelling Behavior of pH-Sensitive Hydrogels." *Chemical Engineering Science* no. 46 (3):715-722.

Brannon-Peppas, Lisa, and James O. Blanchette. 2004. "Nanoparticle and targeted systems for cancer therapy." *Advanced Drug Delivery Reviews* no. 56 (11):1649-1659.

Bulmus, V., M. Woodward, L. Lin, N. Murthy, P. Stayton, and A. Hoffman. 2003. "A new pH-responsive and glutathione-reactive, endosomal membrane-disruptive polymeric carrier for intracellular delivery of biomolecular drugs." *Journal of Controlled Release* no. 93 (2):105-120. doi: DOI 10.1016/j.jconrel.2003.06.001.

Bütün, V., S. P. Armes, and N. C. Billingham. 2001. "Synthesis and aqueous solution properties of near-monodisperse tertiary amine methacrylate homopolymers and diblock copolymers." *Polymer* no. 42 (14):5993-6008. doi: http://dx.doi.org/10.1016/S0032-3861(01)00066-0.

Byrne, J. D., T. Betancourt, and L. Brannon-Peppas. 2008. "Active targeting schemes for nanoparticle systems in cancer therapeutics." *Advanced Drug Delivery Reviews* no. 60 (15):1615-1626. doi: DOI 10.1016/j.addr.2008.08.005.

Caldorera-Moore, M., N. Guimard, L. Shi, and K. Roy. 2010. "Designer nanoparticles: incorporating size, shape and triggered release into nanoscale drug carriers."

Expert Opinion on Drug Delivery no. 7 (4):479-495. doi: Doi 10.1517/17425240903579971.

Caldorera-Moore, Mary E., William B. Liechty, and Nicholas A. Peppas. 2011. "Responsive Theranostic Systems: Integration of Diagnostic Imaging Agents and Responsive Controlled Release Drug Delivery Carriers." *Accounts of Chemical Research* no. 44 (10):1061-1070. doi: 10.1021/ar2001777.

Cassidy, Jim, and Andreas G. Schätzlein. 2004. "Tumour-targeted drug and gene delivery: principles and concepts." *Expert Reviews in Molecular Medicine* no. 6 (19):1-17. doi: doi:10.1017/S1462399404008269.

Cerritelli, Simona, Diana Velluto, and Jeffrey A. Hubbell. 2007. "PEG-SS-PPS: Reduction-Sensitive Disulfide Block Copolymer Vesicles for Intracellular Drug Delivery." *Biomacromolecules* no. 8 (6):1966-1972. doi: 10.1021/bm070085x.

Chen, R. J., M. E. Eccleston, Z. L. Yue, and N. K. H. Slater. 2009. "Synthesis and pH-responsive properties of pseudo-peptides containing hydrophobic amino acid grafts." *Journal of Materials Chemistry* no. 19 (24):4217-4224. doi: Doi 10.1039/B902822f.

Chen, R. J., Z. L. Yue, M. E. Eccleston, and N. K. H. Slater. 2008. "Aqueous solution behaviour and membrane disruptive activity of pH-responsive PEGylated pseudo-peptides and their intracellular distribution." *Biomaterials* no. 29 (32):4333-4340. doi: DOI 10.1016/j.biomaterials.2008.07.040.

Chen, R., S. Khormaee, M. E. Eccleston, and N. K. H. Slater. 2009. "The role of hydrophobic amino acid grafts in the enhancement of membrane-disruptive activity of pH-responsive pseudo-peptides." *Biomaterials* no. 30 (10):1954-1961. doi: DOI 10.1016/j.biomaterials.2008.12.036.

Cheung, C. Y., N. Murthy, P. S. Stayton, and A. S. Hoffman. 2001. "A pH-sensitive polymer that enhances cationic lipid-mediated gene transfer." *Bioconjugate Chemistry* no. 12 (6):906-910.

Chithrani, B. D., A. A. Ghazani, and W. C. W. Chan. 2006. "Determining the size and shape dependence of gold nanoparticle uptake into mammalian cells." *Nano Letters* no. 6 (4):662-668. doi: Doi 10.1021/Nl052396o.

Cohen, S., T. Yoshioka, M. Lucarelli, L. H. Hwang, and R. Langer. 1991. "Controlled Delivery Systems for Proteins Based on Poly(Lactic Glycolic Acid)

Microspheres." *Pharmaceutical Research* no. 8 (6):713-720. doi: Doi 10.1023/A:1015841715384.

Conner, S. D., and S. L. Schmid. 2003. "Regulated portals of entry into the cell." *Nature* no. 422 (6927):37-44. doi: Doi 10.1038/Nature01451.

Convertine, Anthony J., Danielle S. W. Benoit, Craig L. Duvall, Allan S. Hoffman, and Patrick S. Stayton. 2009. "Development of a novel endosomolytic diblock copolymer for siRNA delivery." *Journal of Controlled Release* no. 133 (3):221-229.

Couvreur, P., I. Brigger, and C. Dubernet. 2002. "Nanoparticles in cancer therapy and diagnosis." *Advanced Drug Delivery Reviews* no. 54 (5):631-651.

Couvreur, P., C. Dubernet, and F. Puisieux. 1995. "Controlled Drug-Delivery with Nanoparticles - Current Possibilities and Future-Trends." *European Journal of Pharmaceutics and Biopharmaceutics* no. 41 (1):2-13.

Couvreur, P., B. Kante, M. Roland, P. Guiot, P. Bauduin, and P. Speiser. 1979. "Polycyanoacrylate Nanocapsules as Potential Lysosomotropic Carriers - Preparation, Morphological and Sorptive Properties." *Journal of Pharmacy and Pharmacology* no. 31 (5):331-332.

Couvreur, P., and F. Puisieux. 1993. "Nanoparticles and Microparticles for the Delivery of Polypeptides and Proteins." *Advanced Drug Delivery Reviews* no. 10 (2-3):141-162.

Cun, D., L. B. Jensen, H. M. Nielsen, M. Moghimi, and C. Foged. 2008. "Polymeric Nanocarriers for siRNA Delivery: Challenges and Future Prospects." *Journal of Biomedical Nanotechnology* no. 4 (3):258-275. doi: Doi 10.1166/Jbn.2008.328.

Davis, M. E., Z. Chen, and D. M. Shin. 2008. "Nanoparticle therapeutics: an emerging treatment modality for cancer." *Nature Reviews Drug Discovery* no. 7 (9):771-782. doi: Doi 10.1038/Nrd2614.

Davis, Mark E., Jonathan E. Zuckerman, Chung Hang J. Choi, David Seligson, Anthony Tolcher, Christopher A. Alabi, Yun Yen, Jeremy D. Heidel, and Antoni Ribas. 2010. "Evidence of RNAi in humans from systemically administered siRNA via targeted nanoparticles." *Nature* no. 464 (7291):1067-1070. doi: http://www.nature.com/nature/journal/v464/n7291/suppinfo/nature08956_S1.html .

de Fougerolles, Antonin R. 2008. "Delivery Vehicles for Small Interfering RNA In Vivo." *Human Gene Therapy* no. 19 (2):125-132. doi: doi:10.1089/hum.2008.928.

De, Priyadarsi, Sudershan R. Gondi, and Brent S. Sumerlin. 2008. "Folate-Conjugated Thermoresponsive Block Copolymers: Highly Efficient Conjugation and Solution Self-Assembly." *Biomacromolecules* no. 9 (3):1064-1070. doi: 10.1021/bm701255v.

Debord, J. D., and L. A. Lyon. 2003. "Synthesis and characterization of pH-responsive copolymer microgels with tunable volume phase transition temperatures." *Langmuir* no. 19 (18):7662-7664. doi: Doi 10.1021/La0342924.

des Rieux, A., V. Fievez, M. Garinot, Y. J. Schneider, and V. Preat. 2006. "Nanoparticles as potential oral delivery systems of proteins and vaccines: A mechanistic approach." *Journal of Controlled Release* no. 116 (1):1-27. doi: DOI 10.1016/j.jconrel.2006.08.013.

Desai, M. P., V. Labhasetwar, E. Walter, R. J. Levy, and G. L. Amidon. 1997. "The mechanism of uptake of biodegradable microparticles in Caco-2 cells is size dependent." *Pharmaceutical Research* no. 14 (11):1568-1573. doi: Doi 10.1023/A:1012126301290.

Devalapally, Harikrishna, Dinesh Shenoy, Steven Little, Robert Langer, and Mansoor Amiji. 2007. "Poly(ethylene oxide)-modified poly(beta-amino ester) nanoparticles as a pH-sensitive system for tumor-targeted delivery of hydrophobic drugs: part 3. Therapeutic efficacy and safety studies in ovarian cancer xenograft model." *Cancer Chemotherapy and Pharmacology* no. 59 (4):477-484.

Dincer, S., M. Turk, and E. Piskin. 2005. "Intelligent polymers as nonviral vectors." *Gene Therapy* no. 12:S139-S145. doi: DOI 10.1038/sj.gt.3302628.

Dong, L., A. K. Agarwal, D. J. Beebe, and H. R. Jiang. 2006. "Adaptive liquid microlenses activated by stimuli-responsive hydrogels." *Nature* no. 442 (7102):551-554. doi: Doi 10.1038/Nature05024.

Du, Yanan, Edward Lo, Shamsher Ali, and Ali Khademhosseini. 2008. "Directed assembly of cell-laden microgels for fabrication of 3D tissue constructs." *Proceedings of the National Academy of Sciences* no. 105 (28):9522-9527. doi: 10.1073/pnas.0801866105.

Dufresne, M. H., M. Elsabahy, and J. C. Leroux. 2008. "Characterization of Polyion Complex Micelles Designed to Address the Challenges of Oligonucleotide Delivery." *Pharmaceutical Research* no. 25 (9):2083-2093. doi: DOI 10.1007/s11095-008-9591-6.

Dufresne, M. H., and J. C. Leroux. 2004. "Study of the micellization behavior of different order amino block copolymers with heparin." *Pharmaceutical Research* no. 21 (1):160-169.

Duncan, R. 2003. "The dawning era of polymer therapeutics." *Nature Reviews Drug Discovery* no. 2 (5):347-360. doi: Doi 10.1038/Nrd1088.

Duncan, R., M. J. Vicent, F. Greco, and R. I. Nicholson. 2005. "Polymer-drug conjugates: towards a novel approach for the treatment of endrocine-related cancer." *Endocrine-Related Cancer* no. 12:S189-S199. doi: Doi 10.1677/Erc.1.01045.

Duncan, Ruth. 2006. "Polymer conjugates as anticancer nanomedicines." *Nature Reviews Cancer* no. 6:688-701.

Duscaronek, K., and D. Patterson. 1968. "Transition in swollen polymer networks induced by intramolecular condensation." *Journal of Polymer Science Part A-2: Polymer Physics* no. 6 (7):1209-1216.

Ekenseair, Adam K., Kristel W. M. Boere, Stephanie N. Tzouanas, Tiffany N. Vo, F. Kurtis Kasper, and Antonios G. Mikos. 2012. "Structure–Property Evaluation of Thermally and Chemically Gelling Injectable Hydrogels for Tissue Engineering." *Biomacromolecules* no. 13 (9):2821-2830. doi: 10.1021/bm300797m.

Elbashir, S. M., J. Harborth, W. Lendeckel, A. Yalcin, K. Weber, and T. Tuschl. 2001. "Duplexes of 21-nucleotide RNAs mediate RNA interference in cultured mammalian cells." *Nature* no. 411 (6836):494-498.

Emileh, A., E. Vasheghani-Farahani, and M. Imani. 2007. "Swelling behavior, mechanical properties and network parameters of pH- and temperature-sensitive hydrogels of poly((2-dimethyl amino) ethyl methacrylate-co-butyl methacrylate)." *European Polymer Journal* no. 43 (5):1986-1995. doi: DOI 10.1016/j.eurpolymj.2007.02.002.

Etrych, Tomás, Markéta Jelínková, Blanka Říhová, and Karel Ulbrich. 2001. "New HPMA copolymers containing doxorubicin bound via pH-sensitive linkage:

synthesis and preliminary in vitro and in vivo biological properties." *Journal of Controlled Release* no. 73 (1):89-102.

Fang, Chao, Bin Shi, Yuan-Ying Pei, Ming-Huang Hong, Jiang Wu, and Hong-Zhuan Chen. 2006. "In vivo tumor targeting of tumor necrosis factor-α-loaded stealth nanoparticles: Effect of MePEG molecular weight and particle size." *European Journal of Pharmaceutical Sciences* no. 27 (1):27-36.

Farmer, Terry G., Thomas F. Edgar, and Nicholas A. Peppas. 2008. "In Vivo Simulations of the Intravenous Dynamics of Submicrometer Particles of pH-Responsive Cationic Hydrogels in Diabetic Patients." *Industrial & Engineering Chemistry Research* no. 47 (24):10053-10063. doi: 10.1021/ie070957b.

Fire, Andrew, SiQun Xu, Mary K. Montgomery, Steven A. Kostas, Samuel E. Driver, and Craig C. Mello. 1998. "Potent and specific genetic interference by double-stranded RNA in Caenorhabditis elegans." *Nature* no. 391 (6669):806.

Fischer, D., Y. X. Li, B. Ahlemeyer, J. Krieglstein, and T. Kissel. 2003. "In vitro cytotoxicity testing of polycations: influence of polymer structure on cell viability and hemolysis." *Biomaterials* no. 24 (7):1121-1131. doi: Pii S0142-9612(02)00445-3.

Fisher, O., T. Kim, S. Dietz, and N. Peppas. 2009. "Enhanced Core Hydrophobicity, Functionalization and Cell Penetration of Polybasic Nanomatrices." *Pharmaceutical Research* no. 26 (1):51-60. doi: DOI 10.1007/s11095-008-9704-2.

Fisher, O. Z., and N. A. Peppas. 2009. "Polybasic Nanomatrices Prepared by UV-Initiated Photopolymerization." *Macromolecules* no. 42 (9):3391-3398. doi: Doi 10.1021/Ma801966r.

Fisher, Omar Z. 2008. *Novel pH-Responsive Microgels and Nanogels as Intelligent Polymer Therapeutics.* University of Texas at Austin, Austin, TX.

Frank-Kamenetsky, M., A. Grefhorst, N. N. Anderson, T. S. Racie, B. Bramlage, A. Akinc, D. Butler, K. Charisse, R. Dorkin, Y. Fan, C. Gamba-Vitalo, P. Hadwiger, M. Jayaraman, M. John, K. N. Jayaprakash, M. Maier, L. Nechev, K. G. Rajeev, T. Read, I. Rohl, J. Soutschek, P. Tan, J. Wong, G. Wang, T. Zimmermann, A. de Fougerolles, H. P. Vornlocher, R. Langer, D. G. Anderson, M. Manoharan, V. Koteliansky, J. D. Horton, and K. Fitzgerald. 2008. "Therapeutic RNAi targeting PCSK9 acutely lowers plasma cholesterol in rodents and LDL cholesterol in

nonhuman primates." *Proceedings of the National Academy of Sciences of the United States of America* no. 105 (33):11915-11920. doi: DOI 10.1073/pnas.0805434105.

Ganta, S., H. Devalapally, A. Shahiwala, and M. Amiji. 2008. "A review of stimuli-responsive nanocarriers for drug and gene delivery." *Journal of Controlled Release* no. 126 (3):187-204. doi: DOI 10.1016/j.jconrel.2007.12.017.

Gao, Haifeng, Nicolay V. Tsarevsky, and Krzysztof Matyjaszewski. 2005. "Synthesis of Degradable Miktoarm Star Copolymers via Atom Transfer Radical Polymerization." *Macromolecules* no. 38 (14):5995-6004. doi: 10.1021/ma0503099.

Gao, X. L., L. Yao, Q. X. Song, L. Zhu, Z. Xia, H. M. Xia, X. G. Jiang, J. Chen, and H. Z. Chen. 2011. "The association of autophagy with polyethylenimine-induced cytotoxity in nephritic and hepatic cell lines." *Biomaterials* no. 32 (33):8613-8625. doi: DOI 10.1016/j.biomaterials.2011.07.047.

Geng, Y., P. Dalhaimer, S. S. Cai, R. Tsai, M. Tewari, T. Minko, and D. E. Discher. 2007. "Shape effects of filaments versus spherical particles in flow and drug delivery." *Nature Nanotechnology* no. 2 (4):249-255. doi: 10.1038/nnano.2007.70.

Gil, E. S., and S. A. Hudson. 2004. "Stimuli-reponsive polymers and their bioconjugates." *Progress in Polymer Science* no. 29 (12):1173-1222. doi: DOI 10.1016/j.progpolymsci.2004.08.003.

Giladi, H., M. Ketzinel-Gilad, L. Rivkin, Y. Felig, O. Nussbaum, and E. Galun. 2003. "Small interfering RNA inhibits hepatitis B virus replication in mice." *Molecular Therapy* no. 8 (5):769-776. doi: Doi 10.1016/S1525-0016(03)00244-2.

Gillies, Elizabeth R., and Jean M. J. Frechet. 2005. "pH-Responsive Copolymer Assemblies for Controlled Release of Doxorubicin." *Bioconjugate Chemistry* no. 16 (2):361-368. doi: doi:10.1021/bc049851c.

Glunde, K., S. E. Guggino, M. Solaiyappan, A. P. Pathak, Y. Ichikawa, and Z. M. Bhujwalla. 2003. "Extracellular acidification alters lysosomal trafficking in human breast cancer cells." *Neoplasia* no. 5 (6):533-545.

Godbey, W. T., K. K. Wu, and A. G. Mikos. 1999. "Size matters: Molecular weight affects the efficiency of poly(ethylenimine) as a gene delivery vehicle." *Journal of Biomedical Materials Research* no. 45 (3):268-275.

Gosselin, M. A., W. J. Guo, and R. J. Lee. 2001. "Efficient gene transfer using reversibly cross-linked low molecular weight polyethylenimine." *Bioconjugate Chemistry* no. 12 (6):989-994.

Gref, R., A. Domb, P. Quellec, T. Blunk, R. H. Müller, J. M. Verbavatz, and R. Langer. 1995. "The controlled intravenous delivery of drugs using PEG-coated sterically stabilized nanospheres." *Advanced Drug Delivery Reviews* no. 16 (2–3):215-233. doi: 10.1016/0169-409x(95)00026-4.

Gref, R., M. Lück, P. Quellec, M. Marchand, E. Dellacherie, S. Harnisch, T. Blunk, and R. H. Müller. 2000. "'Stealth' corona-core nanoparticles surface modified by polyethylene glycol (PEG): influences of the corona (PEG chain length and surface density) and of the core composition on phagocytic uptake and plasma protein adsorption." *Colloids and Surfaces B: Biointerfaces* no. 18 (3–4):301-313. doi: http://dx.doi.org/10.1016/S0927-7765(99)00156-3.

Groves, E., A. E. Dart, V. Covarelli, and E. Caron. 2008. "Molecular mechanisms of phagocytic uptake in mammalian cells." *Cellular and Molecular Life Sciences* no. 65 (13):1957-1976. doi: DOI 10.1007/s00018-008-7578-4.

Guelen, Lars, Hugh Paterson, Joop Gaken, Michelle Meyers, Farzin Farzaneh, and Mahvash Tavassoli. 2003. "TAT-apoptin is efficiently delivered and induces apoptosis in cancer cells." *Oncogene* no. 23 (5):1153-1165.

Ham, George E. 1964. *Copolymerization*. Edited by H. Mark. 20 vols. Vol. 18, *High Polymers*. New York: Interscience Publishers.

Hammond, S. M., S. Boettcher, A. A. Caudy, R. Kobayashi, and G. J. Hannon. 2001. "Argonaute2, a link between genetic and biochemical analyses of RNAi." *Science* no. 293 (5532):1146-1150.

Hammond, Scott M., Emily Bernstein, David Beach, and Gregory J. Hannon. 2000. "An RNA-directed nuclease mediates post-transcriptional gene silencing in Drosophila cells." *Nature* no. 404 (6775):293-296.

Hayashi, H., M. Iijima, K. Kataoka, and Y. Nagasaki. 2004. "pH-sensitive nanogel possessing reactive PEG tethered chains on the surface." *Macromolecules* no. 37 (14):5389-5396. doi: Doi 10.1021/Ma049199g.

Heskins, M., and J. E. Guillet. 1968. "Solution Properties of Poly(N-isopropylacrylamide)." *Journal of Macromolecular Science, Part A: Pure and Applied Chemistry* no. 2 (8):1441 - 1455.

Heurtault, Béatrice, Patrick Saulnier, Brigitte Pech, Jacques-Emile Proust, and Jean-Pierre Benoit. 2003. "Physico-chemical stability of colloidal lipid particles." *Biomaterials* no. 24 (23):4283-4300. doi: 10.1016/s0142-9612(03)00331-4.

Hewlett, L. J., A. R. Prescott, and C. Watts. 1994. "The Coated Pit and Macropinocytic Pathways Serve Distinct Endosome Populations." *Journal of Cell Biology* no. 124 (5):689-703. doi: DOI 10.1083/jcb.124.5.689.

Hillaireau, H., and P. Couvreur. 2009. "Nanocarriers' entry into the cell: relevance to drug delivery." *Cellular and Molecular Life Sciences* no. 66 (17):2873-2896. doi: DOI 10.1007/s00018-009-0053-z.

Hoare, T. R., and D. S. Kohane. 2008. "Hydrogels in drug delivery: Progress and challenges." *Polymer* no. 49 (8):1993-2007. doi: DOI 10.1016/j.polymer.2008.01.027.

Hong, Seungpyo, Pascale R. Leroueil, Elizabeth K. Janus, Jennifer L. Peters, Mary-Margaret Kober, Mohammad T. Islam, Bradford G. Orr, James R. Baker, and Mark M. Banaszak Holl. 2006. "Interaction of Polycationic Polymers with Supported Lipid Bilayers and Cells: Nanoscale Hole Formation and Enhanced Membrane Permeability." *Bioconjugate Chemistry* no. 17 (3):728-734. doi: 10.1021/bc060077y.

Hu, Yuhua, Prabhani U. Atukorale, James J. Lu, James J. Moon, Soong Ho Um, Eun Chol Cho, Yana Wang, Jianzhu Chen, and Darrell J. Irvine. 2009. "Cytosolic Delivery Mediated via Electrostatic Surface Binding of Protein, Virus, or siRNA Cargos to pH-Responsive Core-Shell Gel Particles." *Biomacromolecules* no. 10 (4):756-765. doi: doi:10.1021/bm801199z.

Hu, Yuhua, Tamara Litwin, Arpun R. Nagaraja, Brandon Kwong, Joshua Katz, Nicki Watson, and Darrell J. Irvine. 2007. "Cytosolic Delivery of Membrane-Impermeable Molecules in Dendritic Cells Using pH-Responsive Core-Shell Nanoparticles." *Nano Letters* no. 7 (10):3056-3064. doi: 10.1021/nl071542i.

Huglin, M. B., Y. Liu, and J. L. Velada. 1997. "Thermoreversible swelling behaviour of hydrogels based on N-isopropylacrylamide with acidic comonomers." *Polymer* no. 38 (23):5785-5791. doi: 10.1016/s0032-3861(97)00135-3.

Huotari, J., and A. Helenius. 2011. "Endosome maturation." *EMBO Journal* no. 30 (17):3481-3500. doi: DOI 10.1038/emboj.2011.286.

Ignatova, M., S. Voccia, B. Gilbert, N. Markova, D. Cossement, R. Gouttebaron, R. Jerome, and C. Jerome. 2006. "Combination of electrografting and atom-transfer radical polymerization for making the stainless steel surface antibacterial and protein antiadhesive." *Langmuir* no. 22 (1):255-262. doi: Doi 10.1021/La051954b.

Inomata, H., S. Goto, and S. Saito. 1990. "Phase-Transition of N-Substituted Acrylamide Gels." *Macromolecules* no. 23 (22):4887-4888.

Judge, A. D., M. Robbins, I. Tavakoli, J. Levi, L. Hu, A. Fronda, E. Ambegia, K. McClintock, and I. MacLachlan. 2009. "Confirming the RNAi-mediated mechanism of action of siRNA-based cancer therapeutics in mice." *Journal of Clinical Investigation* no. 119 (3):661-673. doi: Doi 10.1172/Jci37515.

Kalyanasundaram, K., and J. K. Thomas. 1977. "Environmental effects on vibronic band intensities in pyrene monomer fluorescence and their application in studies of micellar systems." *Journal of the American Chemical Society* no. 99 (7):2039-2044. doi: 10.1021/ja00449a004.

Kamada, Haruhiko, Yasuo Tsutsumi, Yasuo Yoshioka, Yoko Yamamoto, Hiroshi Kodaira, Shin-ichi Tsunoda, Takayuki Okamoto, Yohei Mukai, Hiroko Shibata, Shinsaku Nakagawa, and Tadanori Mayumi. 2004. "Design of a pH-Sensitive Polymeric Carrier for Drug Release and Its Application in Cancer Therapy." *Clin Cancer Res* no. 10 (7):2545-2550. doi: 10.1158/1078-0432.ccr-03-0544.

Kamei, Noriyasu, Mariko Morishita, Hitomi Chiba, Nikhil J. Kavimandan, Nicholas A. Peppas, and Kozo Takayama. 2009. "Complexation hydrogels for intestinal delivery of interferon [beta] and calcitonin." *Journal of Controlled Release* no. 134 (2):98-102.

Kang, S. I., K. Na, and Y. H. Bae. 2003. "Physicochemical characteristics and doxorubicin-release behaviors of pH/temperature-sensitive polymeric nanoparticles." *Colloids and Surfaces a-Physicochemical and Engineering Aspects* no. 231 (1-3):103-112. doi: DOI 10.1016/j.colsurfa.2003.09.006.

Kapoor, M., and D. J. Burgess. 2013. "Cellular Uptake Mechanisms of Novel Anionic siRNA Lipoplexes." *Pharmaceutical Research* no. 30 (4):1161-1175. doi: DOI 10.1007/s11095-012-0952-9.

Katono, H., A. Maruyama, K. Sanui, N. Ogata, T. Okano, and Y. Sakurai. 1991. "Thermoresponsive swelling and drug release switching of interpenetrating polymer networks composed pf poly(acrylamide-co-butyl methacrylate) and poly(acrylic-acid)." *Journal of Controlled Release* no. 16 (1-2):215-227.

Khademhosseini, Ali, and Nicholas A. Peppas. 2013. "Micro- and Nanoengineering of Biomaterials for Healthcare Applications." *Advanced Healthcare Materials* no. 2 (1):10-12. doi: 10.1002/adhm.201200444.

Khalil, I. A., K. Kogure, H. Akita, and H. Harashima. 2006. "Uptake pathways and subsequent intracellular trafficking in nonviral gene delivery." *Pharmacological Reviews* no. 58 (1):32-45. doi: Doi 10.1124/Pr.58.1.8.

Khare, Atul R., and Nikolaos A. Peppas. 1995. "Swelling/deswelling of anionic copolymer gels." *Biomaterials* no. 16 (7):559-567.

Khinkis, L. A., L. Levasseur, H. Faessel, and W. R. Greco. 2003. "Optimal design for estimating parameters of the 4-parameter hill model." *Nonlinearity in biology, toxicology, medicine* no. 1 (3):363-77. doi: 10.1080/15401420390249925.

Khokhlov, A. R., and E. Y. Kramarenko. 1994. "Polyelectrolyte/Ionomer Behavior in Polymer Gel Collapse." *Macromolecular Theory and Simulations* no. 3 (1):45-59. doi: DOI 10.1002/mats.1994.040030104.

Khormaee, S., Y. Choi, M. J. Shen, B. Y. Xu, H. T. Wu, G. L. Griffiths, R. J. Chen, N. K. H. Slater, and J. K. Park. 2013. "Endosomolytic Anionic Polymer for the Cytoplasmic Delivery of siRNAs in Localized In Vivo Applications." *Advanced Functional Materials* no. 23 (5):565-574. doi: DOI 10.1002/adfm.201201945.

Klein, C., C. T. Bock, H. Wedemeyer, T. Wustefeld, S. Locarnini, H. P. Dienes, S. Kubicka, M. P. Manns, and C. Trautwein. 2003. "Inhibition of hepatitis B virus replication in vivo by nucleoside analogues and siRNA." *Gastroenterology* no. 125 (1):9-18. doi: Doi 10.1016/S0016-5085(03)00720-0.

Klouda, Leda, and Antonios G. Mikos. 2008. "Thermoresponsive hydrogels in biomedical applications." *European Journal of Pharmaceutics and Biopharmaceutics* no. 68 (1):34-45.

Kopecek, J. 2003. "Smart and genetically engineered biomaterials and drug delivery systems." *European Journal of Pharmaceutical Sciences* no. 20 (1):1-16. doi: Doi 10.1016/S0928-0987(03)00164-7.

Kost, J., and R. Langer. 2001. "Responsive polymeric delivery systems." *Advanced Drug Delivery Reviews* no. 46 (1-3):125-148.

Kriegel, C., and M. Amiji. 2011. "Oral TNF-alpha gene silencing using a polymeric microsphere-based delivery system for the treatment of inflammatory bowel disease." *Journal of Controlled Release* no. 150 (1):77-86. doi: DOI 10.1016/j.jconrel.2010.10.002.

Kurisawa, Motoichi, Masayuki Yokoyama, and Teruo Okano. 2000. "Transfection efficiency increases by incorporating hydrophobic monomer units into polymeric gene carriers." *Journal of Controlled Release* no. 68 (1):1-8. doi: 10.1016/s0168-3659(00)00246-7.

Kusonwiriyawong, C., P. van de Wetering, J. A. Hubbell, H. P. Merkle, and E. Walter. 2003. "Evaluation of pH-dependent membrane-disruptive properties of poly(acrylic acid) derived polymers." *European Journal of Pharmaceutics and Biopharmaceutics* no. 56 (2):237-246. doi: Doi 10.1016/S0939-6411(03)00093-6.

Kwon, GlenS, Masayuki Yokoyama, Teruo Okano, Yasuhisa Sakurai, and Kazunori Kataoka. 1993. "Biodistribution of Micelle-Forming Polymer–Drug Conjugates." *Pharmaceutical Research* no. 10 (7):970-974. doi: 10.1023/a:1018998203127.

Langer, R. 1998a. "Drug delivery and targeting." *Nature* no. 392 (6679):5-10.

Langer, R., and N. A. Peppas. 2003. "Advances in biomaterials, drug delivery, and bionanotechnology." *Aiche Journal* no. 49 (12):2990-3006.

Langer, Robert. 1998b. "Drug Delivery and Targeting." *Nature*:5-10.

Lavasanifar, Afsaneh, John Samuel, and Glen S. Kwon. 2002. "Poly(ethylene oxide)-block-poly(-amino acid) micelles for drug delivery." *Advanced Drug Delivery Reviews* no. 54 (2):169-190.

Lee, A. S., A. P. Gast, V. Butun, and S. P. Armes. 1999. "Characterizing the structure of pH dependent polyelectrolyte block copolymer micelles." *Macromolecules* no. 32 (13):4302-4310.

Lee, Eun Seong, Zhonggao Gao, Dongin Kim, Kyeongsoon Park, Ick Chan Kwon, and You Han Bae. 2008. "Super pH-sensitive multifunctional polymeric micelle for tumor pHe specific TAT exposure and multidrug resistance." *Journal of Controlled Release* no. 129 (3):228-236.

Lee, Eun Seong, Kun Na, and You Han Bae. 2005a. "Doxorubicin loaded pH-sensitive polymeric micelles for reversal of resistant MCF-7 tumor." *Journal of Controlled Release* no. 103 (2):405-418.

———. 2005b. "Super pH-Sensitive Multifunctional Polymeric Micelle." *Nano Letters* no. 5 (2):325-329. doi: 10.1021/nl0479987.

Leobandung, W., H. Ichikawa, Y. Fukumori, and N. A. Peppas. 2003. "Monodisperse nanoparticles of poly(ethylene glycol) macromers and N-isopropyl acrylamide for biomedical applications." *Journal of Applied Polymer Science* no. 87 (10):1678-1684. doi: 10.1002/app.11612.

Leong, K. W., B. C. Brott, and R. Langer. 1985. "Bioerodible Polyanhydrides as Drug-Carrier Matrices .1. Characterization, Degradation, and Release Characteristics." *Journal of Biomedical Materials Research* no. 19 (8):941-955.

Li, Su, and Noah Malmstadt. 2013. "Deformation and poration of lipid bilayer membranes by cationic nanoparticles." *Soft Matter*.

Liechty, W. B., D. R. Kryscio, B. V. Slaughter, and N. A. Peppas. 2010. "Polymers for Drug Delivery Systems." *Annual Review of Chemical and Biomolecular Engineering, Vol 1* no. 1:149-173. doi: DOI 10.1146/annurev-chembioeng-073009-100847.

Liechty, William B., Mary Caldorera-Moore, Margaret A. Phillips, Cody Schoener, and Nicholas A. Peppas. "Advanced molecular design of biopolymers for transmucosal and intracellular delivery of chemotherapeutic agents and biological therapeutics." *Journal of Controlled Release* no. In Press, Corrected Proof. doi: 10.1016/j.jconrel.2011.06.009.

———. 2011. "Advanced molecular design of biopolymers for transmucosal and intracellular delivery of chemotherapeutic agents and biological therapeutics." *Journal of Controlled Release* no. 155 (2):119-127. doi: 10.1016/j.jconrel.2011.06.009.

Liechty, William B., Rongjun Chen, Farzin Farzaneh, Mahvash Tavassoli, and Nigel K. H. Slater. 2009. "Synthetic pH-Responsive Polymers for Protein Transduction." *Advanced Materials* no. 21 (38-39):3910-3914.

Liechty, William B., and Nicholas A. Peppas. 2012. "Expert opinion: Responsive polymer nanoparticles in cancer therapy." *European Journal of Pharmaceutics and Biopharmaceutics* no. 80 (2):241-246. doi: 10.1016/j.ejpb.2011.08.004.

Liechty, William B., Rebekah L. Scheuerle, and Nicholas A. Peppas. 2013. "Tunable, responsive nanogels containing tert-butyl methacrylate and 2-(tert-butylamino)ethyl methacrylate." *Polymer* no. under review.

Liu, Z. H., Z. Y. Zhang, C. R. Zhou, and Y. P. Jiao. 2010. "Hydrophobic modifications of cationic polymers for gene delivery." *Progress in Polymer Science* no. 35 (9):1144-1162. doi: DOI 10.1016/j.progpolymsci.2010.04.007.

Lloyd, J. B., M. K. Pratten, R. Duncan, T. Kooistra, and S. A. Cartlidge. 1984. "Substrate Processing and Selection in Endocytosis." *Biochemical Society Transactions* no. 12 (6):977-978.

Lowman, A. M., M. Morishita, M. Kajita, T. Nagai, and N. A. Peppas. 1999. "Oral delivery of insulin using pH-responsive complexation gels." *Journal of Pharmaceutical Sciences* no. 88 (9):933-937.

Lu, J. J., R. Langer, and J. Z. Chen. 2009. "A Novel Mechanism Is Involved in Cationic Lipid-Mediated Functional siRNA Delivery." *Molecular Pharmaceutics* no. 6 (3):763-771. doi: Doi 10.1021/Mp900023v.

Malmsten, M., and B. Lindman. 1992. "Self-assembly in aqueous block copolymer solutions." *Macromolecules* no. 25 (20):5440-5445.

Manganiello, Matthew J., Connie Cheng, Anthony J. Convertine, James D. Bryers, and Patrick S. Stayton. 2012. "Diblock copolymers with tunable pH transitions for gene delivery." *Biomaterials* no. 33 (7):2301-2309. doi: http://dx.doi.org/10.1016/j.biomaterials.2011.11.019.

Marek, Steve R., Charles A. Conn, and Nicholas A. Peppas. 2010. "Cationic nanogels based on diethylaminoethyl methacrylate." *Polymer* no. 51 (6):1237-1243.

Maruyama, K., N. Takahashi, T. Tagawa, K. Nagaike, and M. Iwatsuru. 1997. "Immunoliposomes bearing polyethyleneglycol-coupled Fab' fragment show

prolonged circulation time and high extravasation into targeted solid tumors in vivo." *Febs Letters* no. 413 (1):177-180.

Mastrobattista, E., and W. E. Hennink. 2012. "Polymers for Gene Delivery Charged for Success." *Nature Materials* no. 11 (1):10-12. doi: Doi 10.1038/Nmat3209.

Mathiowitz, E., J. S. Jacob, Y. S. Jong, G. P. Carino, D. E. Chickering, P. Chaturvedi, C. A. Santos, K. Vijayaraghavan, S. Montgomery, M. Bassett, and C. Morrell. 1997. "Biologically erodable microsphere as potential oral drug delivery system." *Nature* no. 386 (6623):410-414.

Matsumoto, Satoru, R. James Christie, Nobuhiro Nishiyama, Kanjiro Miyata, Atsushi Ishii, Makoto Oba, Hiroyuki Koyama, Yuichi Yamasaki, and Kazunori Kataoka. 2009. "Environment-Responsive Block Copolymer Micelles with a Disulfide Cross-Linked Core for Enhanced siRNA Delivery." *Biomacromolecules* no. 10 (1):119-127. doi: doi:10.1021/bm800985e.

Matsumura, Y., and H. Maeda. 1986. "A New Concept for Macromolecular Therapeutics in Cancer-Chemotherapy - Mechanism of Tumoritropic Accumulation of Proteins and the Antitumor Agent Smancs." *Cancer Research* no. 46 (12):6387-6392.

Mecke, A., I. J. Majoros, A. K. Patri, J. R. Baker, M. M. B. Holl, and B. G. Orr. 2005. "Lipid bilayer disruption by polycationic polymers: The roles of size and chemical functional group." *Langmuir* no. 21 (23):10348-10354. doi: Doi 10.1021/La0506291.

Mellman, I. 1996. "Endocytosis and molecular sorting." *Annual Review of Cell and Developmental Biology* no. 12:575-625.

Moghimi, S. M., A. C. Hunter, and J. C. Murray. 2001. "Long-circulating and target-specific nanoparticles: Theory to practice." *Pharmacological Reviews* no. 53 (2):283-318.

Mok, H., and T. G. Park. 2009. "Functional Polymers for Targeted Delivery of Nucleic Acid Drugs." *Macromolecular Bioscience* no. 9 (8):731-743. doi: DOI 10.1002/mabi.200900044.

Morishita, Mariko, and Nicholas A. Peppas. 2006. "Is the oral route possible for peptide and protein drug delivery?" *Drug Discovery Today* no. 11 (19-20):905-910.

Moriyama, K., and N. Yui. 1996. "Regulated insulin release from biodegradable dextran hydrogels containing poly(ethylene glycol)." *Journal of Controlled Release* no. 42 (3):237-248.

Morse, A. J., D. Dupin, K. L. Thompson, S. P. Armes, K. Ouzineb, P. Mills, and R. Swart. 2012. "Novel Pickering Emulsifiers based on pH-Responsive Poly(tert-butylaminoethyl methacrylate) Latexes." *Langmuir* no. 28 (32):11733-11744. doi: 10.1021/la301936k.

Mukherjee, S., R. N. Ghosh, and F. R. Maxfield. 1997. "Endocytosis." *Physiological Reviews* no. 77 (3):759-803.

Murthy, N., J. R. Robichaud, D. A. Tirrell, P. S. Stayton, and A. S. Hoffman. 1999. "The design and synthesis of polymers for eukaryotic membrane disruption." *Journal of Controlled Release* no. 61 (1-2):137-143.

Nam, H. Y., S. M. Kwon, H. Chung, S. Y. Lee, S. H. Kwon, H. Jeon, Y. Kim, J. H. Park, J. Kim, S. Her, Y. K. Oh, I. C. Kwon, K. Kim, and S. Y. Jeong. 2009. "Cellular uptake mechanism and intracellular fate of hydrophobically modified glycol chitosan nanoparticles." *Journal of Controlled Release* no. 135 (3):259-267. doi: DOI 10.1016/j.jconrel.2009.01.018.

Odian, George. 2004. *Principles of Polymerization*. Fourth ed. Hoboken, New Jersey: John Wiley and Sons.

Oh, Jung Kwon, Daniel J. Siegwart, Hyung-il Lee, Gizelle Sherwood, Linda Peteanu, Jeffrey O. Hollinger, Kazunori Kataoka, and Krzysztof Matyjaszewski. 2007. "Biodegradable Nanogels Prepared by Atom Transfer Radical Polymerization as Potential Drug Delivery Carriers: Synthesis, Biodegradation, in Vitro Release, and Bioconjugation." *Journal of the American Chemical Society* no. 129 (18):5939-5945. doi: 10.1021/ja069150l.

Oncel, S., L. Uzun, B. Garipcan, and A. Denizli. 2005. "Synthesis of phenylalanine-containing hydrophobic beads for lysozyme adsorption." *Industrial & Engineering Chemistry Research* no. 44 (18):7049-7056. doi: Doi 10.1021/Ie0506318.

Owens, D. E., and N. A. Peppas. 2006. "Opsonization, biodistribution, and pharmacokinetics of polymeric nanoparticles." *International Journal of Pharmaceutics* no. 307 (1):93-102. doi: DOI 10.1016/j.ijpharm.2005.10.010.

Owens, Donald E., Yicun Jian, Justin E. Fang, Brandon V. Slaughter, Yi-Hsuan Chen, and Nicholas A. Peppas. 2007. "Thermally Responsive Swelling Properties of Polyacrylamide/Poly(acrylic acid) Interpenetrating Polymer Network Nanoparticles." *Macromolecules* no. 40 (20):7306-7310. doi: 10.1021/ma071089x.

Pack, D. W., A. S. Hoffman, S. Pun, and P. S. Stayton. 2005. "Design and development of polymers for gene delivery." *Nature Reviews Drug Discovery* no. 4 (7):581-593. doi: Doi 10.1038/Nrd1775.

Palermo, Edmund F., Dong-Kuk Lee, Ayyalusamy Ramamoorthy, and Kenichi Kuroda. 2010. "Role of Cationic Group Structure in Membrane Binding and Disruption by Amphiphilic Copolymers." *The Journal of Physical Chemistry B* no. 115 (2):366-375. doi: 10.1021/jp1083357.

Peng, J. L., Y. G. Zhao, J. H. Mai, W. K. Pang, X. H. Wei, P. Z. Zhang, and Y. H. Xu. 2005. "Inhibition of hepatitis B virus replication by various RNAi constructs and their pharmacodynamic properties." *Journal of General Virology* no. 86:3227-3234. doi: DOI 10.1099/vir.0.81171-0.

Peppas, N. A. 2004. "Intelligent therapeutics: biomimetic systems and nanotechnology in drug delivery." *Advanced Drug Delivery Reviews* no. 56 (11):1529-1531. doi: DOI 10.1016/j.addr.2004.07.001.

Peppas, N. A., P. Bures, W. Leobandung, and H. Ichikawa. 2000. "Hydrogels in pharmaceutical formulations." *European Journal of Pharmaceutics and Biopharmaceutics* no. 50 (1):27-46.

Phillips, M. A., M. L. Gran, and N. A. Peppas. 2010. "Targeted nanodelivery of drugs and diagnostics." *Nano Today* no. 5 (2):143-159. doi: DOI 10.1016/j.nantod.2010.03.003.

Pich, A., A. Tessier, V. Boyko, Y. Lu, and H. J. P. Adler. 2006. "Synthesis and characterization of poly(vinylcaprolactam)-based microgels exhibiting temperature and pH-sensitive properties." *Macromolecules* no. 39 (22):7701-7707. doi: Doi 10.1021/Ma060985q.

Plank, C., B. Oberhauser, K. Mechtler, C. Koch, and E. Wagner. 1994. "The Influence of Endosome-Disruptive Peptides on Gene-Transfer Using Synthetic Virus-Like Gene-Transfer Systems." *Journal of Biological Chemistry* no. 269 (17):12918-12924.

Qiu, Y., and K. Park. 2001. "Environment-sensitive hydrogels for drug delivery." *Advanced Drug Delivery Reviews* no. 53 (3):321-339.

Raemdonck, K., J. Demeester, and S. De Smedt. 2009. "Advanced nanogel engineering for drug delivery." *Soft Matter* no. 5 (4):707-715. doi: Doi 10.1039/B811923f.

Randall, G., A. Grakoui, and C. M. Rice. 2003. "Clearance of replicating hepatitis C virus replicon RNAs in cell culture by small interfering RNAs." *Proceedings of the National Academy of Sciences of the United States of America* no. 100 (1):235-240. doi: DOI 10.1073/pnas.0235524100.

Read, E. S., K. L. Thompson, and S. P. Armes. 2010. "Synthesis of well-defined primary amine-based homopolymers and block copolymers and their Michael addition reactions with acrylates and acrylamides." *Polymer Chemistry* no. 1 (2):221-230. doi: Doi 10.1039/B9py00320g.

Rejman, J., V. Oberle, I. S. Zuhorn, and D. Hoekstra. 2004. "Size-dependent internalization of particles via the pathways of clathrin-and caveolae-mediated endocytosis." *Biochemical Journal* no. 377:159-169. doi: Doi 10.1042/Bj20031253.

Rimmer, Stephen, Stacy-Paul Wilshaw, Paul Pickavance, and Eileen Ingham. 2009. "Cytocompatibility of poly(1,2 propandiol methacrylate) copolymer hydrogels and conetworks with or without alkyl amine functionality." *Biomaterials* no. 30 (13):2468-2478. doi: http://dx.doi.org/10.1016/j.biomaterials.2009.01.041.

Ringsdorf, H. 1975. "Structure and properties of pharmacologically active polymers." *Journal of Polymer Science Part C Polymer Symposium* no. 51:135-153.

Rossi, J. J., M. R. Lares, and D. L. Ouellet. 2010. "RNAi and small interfering RNAs in human disease therapeutic applications." *Trends in Biotechnology* no. 28 (11):570-579. doi: DOI 10.1016/j.tibtech.2010.07.009.

Ruel-Gariépy, Eve, and Jean-Christophe Leroux. 2004. "In situ-forming hydrogels--review of temperature-sensitive systems." *European Journal of Pharmaceutics and Biopharmaceutics* no. 58 (2):409-426.

Sanda, F., T. Abe, and T. Endo. 1997. "Syntheses and radical polymerizations of optically active (Meth)acrylamides having amino acid moieties." *Journal of Polymer Science Part a-Polymer Chemistry* no. 35 (13):2619-2629.

Santos, A. F., N. Murthy, P. S. Stayton, O. W. Press, D. Tirrell, and A. S. Hoffman. 1998. "Design of polymers to increase the efficiency of endosomal release of drugs." *Journal of Investigative Medicine* no. 46 (1):91a-91a.

Schild, H. G. 1992. "Poly (N-Isopropylacrylamide) - Experiment, Theory and Application." *Progress in Polymer Science* no. 17 (2):163-249.

Schmaljohann, D. 2006. "Thermo- and pH-responsive polymers in drug delivery." *Advanced Drug Delivery Reviews* no. 58 (15):1655-1670. doi: DOI 10.1016/j.addr.2006.09.020.

Schwarte, L. M., and N. A. Peppas. 1998. "Novel poly(ethylene glycol)-grafted, cationic hydrogels: preparation, characterization and diffusive properties." *Polymer* no. 39 (24):6057-6066.

Schwarz-Barac, S., H. Ritter, and D. Schollmeyer. 2003. "Cyclodextrins in polymer synthesis: Enantiodiscrimination in free-radical polymerization of cyclodextrin-complexed racemic N-Methacryloyl-D,L-phenylalanine methyl ester." *Macromolecular Rapid Communications* no. 24 (4):325-330.

Sethuraman, Vijay A., and You Han Bae. 2007. "TAT peptide-based micelle system for potential active targeting of anti-cancer agents to acidic solid tumors." *Journal of Controlled Release* no. 118 (2):216-224.

Shenoy, D., S. Little, R. Langer, and M. Amiji. 2005a. "Poly(ethylene oxide)-modified poly(beta-amino ester) nanoparticles as a pH-sensitive system for tumor-targeted delivery of hydrophobic drugs. 1. In vitro evaluations." *Molecular Pharmaceutics* no. 2 (5):357-366. doi: 10.1021/mp0500420.

Shenoy, Dinesh, Steven Little, Robert Langer, and Mansoor Amiji. 2005b. "Poly(Ethylene Oxide)-Modified Poly(β-Amino Ester) Nanoparticles as a pH-Sensitive System for Tumor-Targeted Delivery of Hydrophobic Drugs: Part 2. In Vivo Distribution and Tumor Localization Studies." *Pharmaceutical Research* no. 22 (12):2107-2114.

Shibayama, M., and T. Tanaka. 1993. "Volume Phase-Transition and Related Phenomena of Polymer Gels." *Advances in Polymer Science* no. 109:1-62.

Shinichi Kageyama, Shigehisa Kitano, Michiko Hirayama, Yasuhiro Nagata, Hiroshi Imai, Taizo Shiraishi, Kazunari Akiyoshi, Andrew M. Scott, Roger Murphy, Eric W. Hoffman, Lloyd J. Old, Naoyuki Katayama, Hiroshi Shiku,. 2008. "Humoral

immune responses in patients vaccinated with 1-146 HER2 protein complexed with cholesteryl pullulan nanogel." *Cancer Science* no. 99 (3):601-607.

Siegel, R. A., and J. M. Cornejobravo. 1992. "Hydrophobic Polyelectrolytes - Effect of Hydrophobicity on Buffering and Colloid Osmotic-Pressure." *ACS Symposium Series* no. 480:131-145.

Siegel, Ronald A., and Bruce A. Firestone. 1988. "pH-dependent equilibrium swelling properties of hydrophobic polyelectrolyte copolymer gels." *Macromolecules* no. 21 (11):3254-3259. doi: 10.1021/ma00189a021.

Siegwart, D. J., K. A. Whitehead, L. Nuhn, G. Sahay, H. Cheng, S. Jiang, M. L. Ma, A. Lytton-Jean, A. Vegas, P. Fenton, C. G. Levins, K. T. Love, H. Lee, C. Cortez, S. P. Collins, Y. F. Li, J. Jang, W. Querbes, C. Zurenko, T. Novobrantseva, R. Langer, and D. G. Anderson. 2011. "Combinatorial synthesis of chemically diverse core-shell nanoparticles for intracellular delivery." *Proceedings of the National Academy of Sciences of the United States of America* no. 108 (32):12996-13001. doi: DOI 10.1073/pnas.1106379108.

Siegwart, Daniel J., Sidi A. Bencherif, Abiraman Srinivasan, Jeffrey O. Hollinger, and Krzysztof Matyjaszewski. 2008. "Synthesis, characterization, and in vitro cell culture viability of degradable poly(N-isopropylacrylamide-co-5,6-benzo-2-methylene-1,3-dioxepane)-based polymers and crosslinked gels." *Journal of Biomedical Materials Research Part A* no. 87A (2):345-358. doi: 10.1002/jbm.a.31708.

Sklan, Ella H., and Jeffrey S. Glenn. 2007. "The Power of Silence: Application of Small Interfering RNAs to Gastrointestinal Diseases." *Gastroenterology* no. 132 (7):2291-2295.

Slaughter, B. V., S. S. Khurshid, O. Z. Fisher, A. Khademhosseini, and N. A. Peppas. 2009. "Hydrogels in Regenerative Medicine." *Advanced Materials* no. 21 (32-33):3307-3329. doi: DOI 10.1002/adma.200802106.

Song, Erwei, Sang-Kyung Lee, Jie Wang, Nedim Ince, Nengtai Ouyang, Jun Min, Jisheng Chen, Premlata Shankar, and Judy Lieberman. 2003. "RNA interference targeting Fas protects mice from fulminant hepatitis." *Nat Med* no. 9 (3):347-351.

Stachowiak, J. C., C. C. Hayden, and D. Y. Sasaki. 2010. "Steric confinement of proteins on lipid membranes can drive curvature and tubulation." *Proceedings of the*

National Academy of Sciences of the United States of America no. 107 (17):7781-7786. doi: DOI 10.1073/pnas.0913306107.

Standardization, International Organization for. 1996. ISO 13321: Particle Size Analysis - Photon Correlation Spectroscopy.

Stark, G. R., I. M. Kerr, B. R. G. Williams, R. H. Silverman, and R. D. Schreiber. 1998. "How cells respond to interferons." *Annual Review of Biochemistry* no. 67:227-264.

Stuart, M. A. C., W. T. S. Huck, J. Genzer, M. Muller, C. Ober, M. Stamm, G. B. Sukhorukov, I. Szleifer, V. V. Tsukruk, M. Urban, F. Winnik, S. Zauscher, I. Luzinov, and S. Minko. 2010. "Emerging applications of stimuli-responsive polymer materials." *Nature Materials* no. 9 (2):101-113. doi: Doi 10.1038/Nmat2614.

Takigawa, D. Y., and D. A. Tirrell. 1983. "Disruption of Phospholipid Packing by Branched Polyethylenimine Derivatives." *Abstracts of Papers of the American Chemical Society* no. 185 (Mar):81-Poly.

Tamura, Atsushi, Motoi Oishi, and Yukio Nagasaki. 2009. "Enhanced Cytoplasmic Delivery of siRNA Using a Stabilized Polyion Complex Based on PEGylated Nanogels with a Cross-Linked Polyamine Structure." *Biomacromolecules* no. 10 (7):1818-1827. doi: 10.1021/bm900252d.

Tanaka, T. 1978. "Collapse of Gels and Critical Endpoint." *Physical Review Letters* no. 40 (12):820-823.

Tang, Yiqing, Shiyong Y. Liu, Steven P. Armes, and Norman C. Billingham. 2003. "Solubilization and Controlled Release of a Hydrophobic Drug Using Novel Micelle-Forming ABC Triblock Copolymers." *Biomacromolecules* no. 4 (6):1636-1645. doi: 10.1021/bm030026t.

Thomas, M., and A. M. Klibanov. 2002. "Enhancing polyethylenimine's delivery of plasmid DNA into mammalian cells." *Proceedings of the National Academy of Sciences of the United States of America* no. 99 (23):14640-14645. doi: DOI 10.1073/pnas.192581499.

Tijsterman, Marcel, RenÃ© F. Ketting, and Ronald H. A. Plasterk. 2002. "THE GENETICS OF RNA SILENCING." *Annual Review of Genetics* no. 36 (1):489-519. doi: doi:10.1146/annurev.genet.36.043002.091619.

Tokareva, I., S. Minko, J. H. Fendler, and E. Hutter. 2004. "Nanosensors based on responsive polymer brushes and gold nanoparticle enhanced transmission surface plasmon resonance spectroscopy." *Journal of the American Chemical Society* no. 126 (49):15950-15951. doi: Doi 10.1021/Ja044575y.

Tong, R., and J. J. Cheng. 2007. "Anticancer polymeric nanomedicines." *Polymer Reviews* no. 47 (3):345-381. doi: Doi 10.1080/15583720701455079.

Topp, M. D. C., P. J. Dijkstra, H. Talsma, and J. Feijen. 1997. "Thermosensitive Micelle-Forming Block Copolymers of Poly(ethylene glycol) and Poly(N-isopropylacrylamide)." *Macromolecules* no. 30 (26):8518-8520. doi: 10.1021/ma9710803.

Torres-Lugo, M., and N. A. Peppas. 1999. "Molecular design and in vitro studies of novel pH-sensitive hydrogels for the oral delivery of calcitonin." *Macromolecules* no. 32 (20):6646-6651.

———. 2000. "Transmucosal delivery systems for calcitonin: a review." *Biomaterials* no. 21 (12):1191-1196.

Turkmen, D., A. Denizli, N. Ozturk, S. Akgol, and A. Elkak. 2008. "Phenylalanine Containing Hydrophobic Nanospheres for Antibody Purification." *Biotechnology Progress* no. 24 (6):1297-1303. doi: Doi 10.1021/Bp.31.

Ulery, B. D., Y. Phanse, A. Sinha, M. J. Wannemuehler, B. Narasimhan, and B. H. Bellaire. 2009. "Polymer Chemistry Influences Monocytic Uptake of Polyanhydride Nanospheres." *Pharmaceutical Research* no. 26 (3):683-690. doi: DOI 10.1007/s11095-008-9760-7.

van der Aa, M. A. E. M., U. S. Huth, S. Y. Hafele, R. Schubert, R. S. Oosting, E. Mastrobattista, W. E. Hennink, R. Peschka-Suss, G. A. Koning, and D. J. A. Crommelin. 2007. "Cellular uptake of cationic polymer-DNA complexes via caveolae plays a pivotal role in gene transfection in COS-7 cells." *Pharmaceutical Research* no. 24 (8):1590-1598. doi: DOI 10.1007/s11095-007-9287-3.

VanBlarcom, D. S., and N. A. Peppas. 2011. "Microcantilever sensing arrays from biodegradable, pH-responsive hydrogels." *Biomedical Microdevices* no. 13 (5):829-836. doi: DOI 10.1007/s10544-011-9553-3.

Vaupel, P., F. Kallinowski, and P. Okunieff. 1989. "Blood-Flow, Oxygen and Nutrient Supply, and Metabolic Microenvironment of Human-Tumors - a Review." *Cancer Research* no. 49 (23):6449-6465.

Vauthier, C., and P. Couvreur. 2006. "Nanotechnology: Intelligent design to treat complex disease." *Pharmaceutical Research* no. 23 (7):1417-1450. doi: 10.1007/s11095-006-0284-8.

Verwey, E.J.W., and J. T. G. Overbeek. 1999. *Theory of the Stability of Lyophobic Colloids*: Courier Dover Publications.

Vinogradov, S. V., E. Kohli, and A. D. Zeman. 2005. "Cross-linked polymeric nanogel formulations of 5 '-triphosphates of nucleoside analogues: Role of the cellular membrane in drug release." *Molecular Pharmaceutics* no. 2 (6):449-461. doi: Doi 10.1021/Mp0500364.

Vinogradov, Serguei V., Arin D. Zeman, Elena V. Batrakova, and Alexander V. Kabanov. 2005. "Polyplex Nanogel formulations for drug delivery of cytotoxic nucleoside analogs." *Journal of Controlled Release* no. 107 (1):143-157. doi: 10.1016/j.jconrel.2005.06.002.

Weissenboeck, A., E. Bogner, M. Wirth, and F. Gabor. 2004. "Binding and uptake of wheat germ agglutinin-grafted PLGA-nanospheres by Caco-2 monolayers." *Pharmaceutical Research* no. 21 (10):1917-1923. doi: Doi 10.1023/B:Pham.0000045247.09724.26.

White, T. J., L. V. Natarajan, V. P. Tondiglia, T. J. Bunning, and C. A. Guymon. 2007. "Polymerization kinetics and monomer functionality effects in thiol-ene polymer dispersed liquid crystals." *Macromolecules* no. 40 (4):1112-1120. doi: Doi 10.1021/Ma061828u.

Whitehead, K. A., R. Langer, and D. G. Anderson. 2009. "Knocking down barriers: advances in siRNA delivery." *Nature Reviews Drug Discovery* no. 8 (2):129-138. doi: Doi 10.1038/Nrd2742.

Wilson, D. Scott, Guillaume Dalmasso, Lixin Wang, Shanthi V. Sitaraman, Didier Merlin, and Niren Murthy. 2010. "Orally delivered thioketal nanoparticles loaded with TNF-α–siRNA target inflammation and inhibit gene expression in the intestines." *Nature Materials* no. 9 (11):923-928. doi: http://www.nature.com/nmat/journal/v9/n11/abs/nmat2859.html#supplementary-information.

Winter, P. M., K. J. Cai, J. Chen, C. R. Adair, G. E. Kiefer, P. S. Athey, P. J. Gaffney, C. E. Buff, J. D. Robertson, S. D. Caruthers, S. A. Wickline, and G. M. Lanza. 2006. "Targeted PARACEST nanoparticle contrast agent for the detection of fibrin." *Magnetic Resonance in Medicine* no. 56 (6):1384-1388. doi: Doi 10.1002/Mrm.21093.

Xuan, B. Q., Z. K. Qian, J. Hong, and W. D. Huang. 2006. "EsiRNAs inhibit hepatitis B virus replication in mice model more efficiently than synthesized siRNAs." *Virus Research* no. 118 (1-2):150-155. doi: DOI 10.1016/j.virusres.2005.12.005.

Yamanaka, Y. J., and K. W. Leong. 2008. "Engineering strategies to enhance nanoparticle-mediated oral delivery." *Journal of Biomaterials Science-Polymer Edition* no. 19 (12):1549-1570.

Yessine, Marie-Andrée, and Jean-Christophe Leroux. 2004. "Membrane-destabilizing polyanions: interaction with lipid bilayers and endosomal escape of biomacromolecules." *Advanced Drug Delivery Reviews* no. 56 (7):999-1021.

Yokota, T., N. Sakamoto, N. Enomoto, Y. Tanabe, M. Miyagishi, S. Maekawa, L. Yi, M. Kurosaki, K. Taira, M. Watanabe, and H. Mizusawa. 2003. "Inhibition of intracellular hepatitis C virus replication by synthetic and vector-derived small interfering RNAs." *Embo Reports* no. 4 (6):602-608. doi: 10.1038/sj.embor.embor840.

Yuen, K. H. 2010. "The transit of dosage forms through the small intestine." *International Journal of Pharmaceutics* no. 395 (1-2):9-16. doi: DOI 10.1016/j.ijpharm.2010.04.045.

Zhang, Z. Y., and B. D. Smith. 2000. "High-generation polycationic dendrimers are unusually effective at disrupting anionic vesicles: Membrane bending model." *Bioconjugate Chemistry* no. 11 (6):805-814. doi: Doi 10.1021/Bc000018z.

Zhou, J. B., J. Liu, C. J. Cheng, T. R. Patel, C. E. Weller, J. M. Piepmeier, Z. Z. Jiang, and W. M. Saltzman. 2012. "Biodegradable poly(amine-co-ester) terpolymers for targeted gene delivery." *Nature Materials* no. 11 (1):82-90. doi: Doi 10.1038/Nmat3187.

Zhou, Jiehua, Ka-To Shum, John Burnett, and John Rossi. 2013. "Nanoparticle-Based Delivery of RNAi Therapeutics: Progress and Challenges." *Pharmaceuticals* no. 6 (1):85-107.

Zuidam, N. J., G. Posthuma, E. T. J. de Vries, D. J. A. Crommelin, W. E. Hennink, and G. Storm. 2000. "Effects of physicochemical characteristics of poly(2-(dimethylamino)ethyl methacrylate)-based polyplexes on cellular association and internalization." *Journal of Drug Targeting* no. 8 (1):51-+. doi: Doi 10.3109/10611860009009209.

Vita

William B. Liechty was born in Houston, TX. He received a B.S.E. from the University of Iowa. As an undergraduate, he worked with Prof. Allan Guymon on photopolymerization kinetics in holographic polymer dispersed liquid crystals. He later worked with Prof. Mani Subramanian in the isolation and characterization of novel caffeine-degrading enzymes. Upon graduation, he attended the University of Cambridge as a Gates Scholar, where he worked with Prof. Nigel Slater on protein delivery using pH-responsive polymers.

He joined the Department of Chemical Engineering at the University of Texas at Austin as an NSF Graduate Research Fellow and Thrust Fellow. At the University of Texas at Austin, he worked under the direction of Prof. Nicholas Peppas on the work described in this thesis.

Permanent email: william.liechty@gmail.com

This dissertation was typed by the author